BSC

Design Calculation or Analysis Cover Sheet

Complete only applicable items.

3. System	4. Document Identifier
Subsurface Facility/Subsurface Development	800-K0C-SSD0-00400-000-00A

5. Title

Ground Control for Non-Emplacement Drifts for LA

6. Group

Subsurface/Mining/Geotechnical

7. Document Status Designation

☐ Preliminary ☒ Committed ☐ Confirmed ☐ Cancelled/Superseded

8. Notes/Comments

This calculation supersedes the calculation previously issued under DI: 800-KMC-SSD0-00700-000-00A (Rev 00A and ECN 001).

Zorica Radakovic-Guzina and Branko Damjanac of Itasca Consulting Group, Inc. provided technical support and numerical analyses presented in Section 6.

Attachments	Total Number of Pages
Attachment I	28
Attachment II	1 DVD

RECORD OF REVISIONS

9. No.	10. Reason For Revision	11. Total # of Pgs.	12. Last Pg. #	13. Originator (Print/Sign/Date)	14. Checker (Print/Sign/Date)	15. EGS (Print/Sign/Date)	16. Approved/Accepted (Print/Sign/Date)
00A	Revised issue See Notes/Comments in Box 8	253	253	David Tang David T 9/27/07	Jay Cho 9/27/07	Fei Duan 9/27/07	Robert Saunders Robert S. Saunders 9/27/07

DISCLAIMER

The calculations contained in this document were developed by Bechtel SAIC Company, LLC (BSC) and are intended solely for the use of BSC in its work for the Yucca Mountain Project.

CONTENTS

Page

FIGURES

Page

TABLES

Page

ACRONYMS AND ABBREVIATIONS

3DEC	3-Dimensional Distinct Element Code
ANSYS	ANSYS Computer Code
APE	Annual Probability of Exceedance
ASM	American Society for Metals
ASTM	American Society for Testing and Materials
BSC	Bechtel SAIC Company, LLC.
c/c	center to center
DOE	U.S. Department of Energy
DTN	Data Tracking Number
ECRB	Enhanced Characterization of the Repository Block
ESF	Exploratory Studies Facility
ESR	Excavation Support Ratio
FLAC	Fast Lagrangian Analysis of Continua
GRC	Ground Reaction Curve
GSI	Geologic Strength Index
Ko	Horizontal-to-vertical stress ratio
LA	License Application
NGI	Norwegian Geotechnical Institute
NUFT	Nonisothermal Unsaturated-saturated Flow and Transport
Q	Rock Mass Quality Index
QA	Quality Assurance
QARD	Quality Assurance Requirements and Description
PC	Performance Confirmation
RMR	Rock Mass Rating
RQD	Rock Quality Designation
RHH	Repository Host Horizon
SC	Safety category
SCM	Software Configuration Management
SF	Safety factor
SR	Site Recommendation

SRF	Stress Reduction Factor
STN	Software Tracking Number
TBM	Tunnel Boring Machine
TDMS	Technical Data Management Systems
TEV	Transport and emplacement vehicle
Tptpll	Topopah Spring Tuff crystal-poor lower lithophysal zone
Tptpln	Topopah Spring Tuff crystal-poor lower nonlithophysal zone
Tptpmn	Topopah Spring Tuff crystal-poor middle nonlithophysal zone
Tptpul	Topopah Spring Tuff crystal-poor upper lithophysal zone
TSPA	Total System Performance Assessment
TSw2	Topopah Spring welded, lithophysal-poor thermal-mechanical unit
WWF	Welded Wire Fabric
YMP	Yucca Mountain Project

1 PURPOSE

The purpose of this calculation is to analyze the stability of repository non-emplacement drifts during the preclosure period, and to provide a final ground support method for non-emplacement drifts for the License Application (LA). This calculation will provide input for the development of LA documents.

The scope of this calculation is limited to addressing the ground support design for the non-emplacement drifts including access mains, ramps, exhaust mains, turnouts, intersections between access mains and turnouts, and intersections between exhaust mains and emplacement drifts, portals, Tunnel Boring Machine (TBM) launch chambers, and observation drift in the performance confirmation (PC) facilities, etc. The calculation is limited to the non-emplacement drifts subjected to a combined loading of in-situ stress, seismic stress, and thermal stress. Other effects such as hydrological and chemical effects are not considered in this analysis.

2 REFERENCES

2.1 PROCEDURES/DIRECTIVES

2.1.1 EG-PRO-3DP-G04B-00037, Rev. 09. *Calculations and Analyses.* Las Vegas, Nevada: Bechtel SAIC Company. ACC: ENG.20070717.0004.

2.1.2 IT-PRO-0011, Rev. 7. *Software Management.* Las Vegas, Nevada: Bechtel SAIC Company. ACC: DOC.20070905.0007.

2.2 DESIGN INPUTS

2.2.1 3DEC V. 2.01. 2002. WINDOWS 2000/NT 4.0. STN: 10025-2.01-00. [DIRS 161930]

2.2.2 FLAC V. 4.0. 2002. WINDOWS 2000/NT 4.0. STN: 10167-4.0-00. [DIRS 161953]

2.2.3 ACI (American Concrete Institute) 223-98. 1998. *Standard Practice for the Use of Shrinkage-Compensating Concrete.* Farmington Hills, Michigan: American Concrete Institute. TIC: 245440. [DIRS 106849]

2.2.4 ACI 506R-05. 2005. *Guide to Shotcrete.* Farmington Hills, Michigan: American Concrete Institute. TIC: 258596. [DIRS 176319] ISBN: 0-87031-198-0.

2.2.5 ACI 506.2-95. 1995. *Specification for Shotcrete.* Detroit, Michigan: American Concrete Institute. TIC: 226412. [DIRS 118373]

2.2.6 AISC (American Institute of Steel Construction) 1997. *Manual of Steel Construction, Allowable Stress Design.* 9th Edition, 2nd Revision, 2nd Impression. Chicago, Illinois: American Institute of Steel Construction. TIC: 240772. [DIRS 107063] ISBN: 1-56424-000-2.

2.2.7 ASM (American Society for Metals) 1978. *Properties and Selection: Irons and Steels.* Volume 1 of *Metals Handbook.* 9th Edition. Bardes, B.P., ed. Metals Park, Ohio: American Society for Metals. TIC: 209799. [DIRS 102018] ISBN: 0-87170007-7.

2.2.8 ASM International 1990. *Properties and Selection: Irons, Steels, and High-Performance Alloys.* Volume 1 of *Metals Handbook.* 10th Edition. Materials Park, Ohio: ASM International. TIC: 245666. [DIRS 106780] ISBN: 0-87170-377-7.

2.2.9 ASTM (American Society for Testing and Materials) ASTM A 36/A 36M-05. 2005. *Standard Specification for Carbon Structural Steel.* West Conshohocken, Pennsylvania: American Society for Testing and Materials. TIC: 258055. [DIRS 176249]

2.2.10 ASTM A 82-01. 2002. *Standard Specification for Steel Wire, Plain, for Concrete Reinforcement.* West Conshohocken, Pennsylvania: American Society for Testing and Materials. TIC: 253993. [DIRS 168639]

2.2.11 ASTM A 242/A 242M-04. 2005. *Standard Specification for High-Strength Low-Allow Structural Steel.* West Conshohocken, Pennsylvania: American Society for Testing and Materials. TIC: 258681. [DIRS 176405]

2.2.12 ASTM A 276-06. 2006. *Standard Specification for Stainless Steel Bars and Shapes.* West Conshohocken, Pennsylvania: American Society for Testing and Materials. TIC: 258258. [DIRS 176774]

2.2.13 ASTM A 588/A 588M-05. 2005. *Standard Specification for High-Strength Low-Alloy Structural Steel, up to 50 ksi [345 MPa] Minimum Yield Point, with Atmospheric Corrosion Resistance.* West Conshohocken, Pennsylvania: American Society for Testing and Materials. TIC: 258058. [DIRS 176255]

2.2.14 ASTM F 432-95 (Reapproved 2001). 1995. *Standard Specification for Roof and Rock Bolts and Accessories.* West Conshohocken, Pennsylvania: American Society for Testing and Materials. TIC: 253986. [DIRS 165010]

2.2.15 Atlas Copco. 2003. Swellex® – The Engineered Rock Reinforcement System, Extending the Traditional Role of Rock Bolts. [Commerce City, Colorado]: Atlas Copco. TIC: 254198. [DIRS 164868]

2.2.16 Barton, N.; Lien, R.; and Lunde, J. 1974. "Engineering Classification of Rock Masses for the Design of Tunnel Support." *Rock Mechanics, 6,* (4), 189-236. New York, New York: Springer-Verlag. TIC: 219995. [DIRS 101541]

2.2.17 Barton, N. 2002. "Some New Q-Value Correlations to Assist in Site Characterization and Tunnel Design." *International Journal of Rock Mechanics & Mining Sciences, 39,* (2), 185-216. New York, New York: Elsevier. TIC: 252648. [DIRS 160379]

2.2.18 Bieniawski, Z.T. 1984. *Rock Mechanics Design in Mining and Tunneling.* Rotterdam, The Netherlands: A.A. Balkema. TIC: 4281. [DIRS 107731] ISBN: 90-6191-507-4.

2.2.19 Bieniawski, Z.T. 1989. *Engineering Rock Mass Classifications.* New York, New York: John Wiley & Sons. TIC: 226350. [DIRS 101715] ISBN: 0-471-30172-1.

2.2.20 Board, M. 2003. *Resolution Strategy for Geomechanically-Related Repository Design and Thermal-Mechanical Effects (RDTME).* REV 00. Las Vegas, Nevada: Bechtel SAIC Company. ACC: MOL.20030708.0153. [DIRS 165036]

2.2.21 BSC (Bechtel SAIC Company) 2001. *Ground Control for Emplacement Drifts for SR.* ANL-EBS-GE-000002 REV 00 ICN 01. Las Vegas, Nevada: Bechtel SAIC Company. ACC: MOL.20010627.0028. [DIRS 155187]

2.2.22 BSC 2002. *Software Implementation Report for 3DEC Version 2.01.* Document Number: 10025-SIR-2.01-00. Las Vegas, Nevada: Bechtel SAIC Company. ACC: MOL.20021105.0252. [DIRS 168822]

2.2.23 BSC 2002. *Software Implementation Report for FLAC Version 4.0.* Document Number: 10167-SIR-4.0-00. Las Vegas, Nevada: Bechtel SAIC Company. ACC: MOL.20020925.0376. [DIRS 168820]

2.2.24 BSC 2003. *Scoping Analysis on Sensitivity and Uncertainty of Emplacement Drift Stability.* 800-K0C-TEG0-00600-000-000. Las Vegas, Nevada: Bechtel SAIC Company. ACC: ENG.20031125.0002. [DIRS 166183]

2.2.25 BSC 2003. *Underground Layout Configuration.* 800-P0C-MGR0-00100-000-00E. Las Vegas, Nevada: Bechtel SAIC Company. ACC: ENG.20031002.0007. [DIRS 165572]

2.2.26 BSC 2004. *Lithophysal Rock Mass Mechanical Properties of the Repository Host Horizon.* 800-K0C-SS00-00200-000-00A. Las Vegas, Nevada: Bechtel SAIC Company. ACC: ENG.20041111.0001. [DIRS 172334]

2.2.27 BSC 2005. *Q-List.* 000-30R-MGR0-00500-000-003. Las Vegas, Nevada: Bechtel SAIC Company. ACC: ENG.20050929.0008. [DIRS 175539]

2.2.28 BSC 2006. *Basis of Design for the TAD Canister-Based Repository Design Concept.* 000-3DR-MGR0-00300-000-000. Las Vegas, Nevada: Bechtel SAIC Company. ACC: ENG.20061023.0002; ENG.20061121.0005; ENG.20061116.0005; ENG.20061204.0002; ENG.20061218.0003; ENG.20061218.0004; ENG.20070220.0010; ENG.20070220.0011; ENG.20070220.0012; ENG.20070314.0009; ENG.20070412.0002; ENG.20070222.0007; ENG.20070222.0008; ENG.20070221.0010; ENG.20070222.0009; ENG.20070308.0029; ENG.20070501.0009; ENG.20070507.0028; ENG.20070608.0019. [DIRS 177636]

2.2.29 BSC 2006. *Project Design Criteria Document.* 000-3DR-MGR0-00100-000-006. Las Vegas, Nevada: Bechtel SAIC Company. ACC: ENG.20061201.0005; ENG.20070111.0025; ENG.20070111.0026; ENG.20070111.0027; ENG.20070111.0028; ENG.20070112.0001; ENG.20070201.0021; ENG.20070222.0011; ENG.20070222.0012; ENG.20070226.0030; ENG.20070308.0028; ENG.20070412.0001; ENG.20070501.0008; ENG.20070510.0002; ENG.20070516.0030; ENG.20070518.0006; ENG.20070621.0002; ENG.20070627.0009. [DIRS 178308]

2.2.30 BSC 2007. *Ground Control for Emplacement Drifts for LA.* 800-K0C-SSE0-00100-000-00C. Las Vegas, Nevada: Bechtel SAIC Company. ACC: ENG.20070925.0082

2.2.31 BSC 2007. *Ground Support Maintenance Plan.* 800-30R-SSD0-00100-000-00B. Las Vegas, Nevada: Bechtel SAIC Company. ACC: ENG.20070807.0016. [DIRS 179937]

2.2.32 BSC 2007. *IED Geotechnical and Thermal Parameters.* 800-IED-MGR0-00401-000 REV 00G. Las Vegas, Nevada: Bechtel SAIC Company. ACC: ENG.20070601.0020. [DIRS 179928]

2.2.33 BSC 2007. *IED Geotechnical and Thermal Parameters II [Sheet 1 of 1].* 800-IED-MGR0-00402-000-00A. Las Vegas, Nevada: Bechtel SAIC Company. ACC: ENG.20070108.0001. [DIRS 178277]

2.2.34 BSC 2007. *IED Seismic Data.* 800-IED-MGR0-00701-000 REV 00A. Las Vegas, Nevada: Bechtel SAIC Company. ACC: ENG.20070216.0003.

2.2.35 BSC 2007. *Turnout Design and Configuration.* 800-KMC-SSD0-00900-000-00A. Las Vegas, Nevada: Bechtel SAIC Company. ACC: ENG.20070625.0041. [DIRS 182013]

2.2.36 BSC 2007. *Subsurface Geotechnical Parameters Report.* ANL-SSD-GE-000001 REV 00. Las Vegas, Nevada: Bechtel SAIC Company. ACC: ENG.20070115.0006. [DIRS 178693]

2.2.37 BSC 2007. *Underground Layout Configuration for LA.* 800-KMC-SS00-00200-000-00B. Las Vegas, Nevada: Bechtel SAIC Company. ACC: ENG.20070727.0004. [DIRS 179640]

2.2.38 Deere, D.U. and Deere, D.W. 1988. "The Rock Quality Designation (RQD) Index in Practice." *Rock Classification Systems for Engineering Purposes.* Kirkaldie, L., ed. ASTM STP 984. Pages 91-101. Philadelphia, Pennsylvania: American Society for Testing and Materials. TIC: 216484. [DIRS 146611] ISBN: 0-8031-0988-1.

2.2.39 Dowding, C.H. 1979. "Earthquake Stability of Rock Tunnels." *Tunnels & Tunnelling, 11,* 15-20. London, England: Morgan-Grampian Publishing. TIC: 242115. [DIRS 101977]

2.2.40 DSI (Dywidag-Systems International) "DYWIDAG Threadbar." *DSI Ground Support Systems.* Bolingbrook, Illinois: Dywidag-Systems International. TIC: 255197. [DIRS 166160]

2.2.41 Goodman, R.E. 1980. *Introduction to Rock Mechanics.* New York, New York: John Wiley & Sons. TIC: 218828. [DIRS 101966] ISBN: 0-471-04129-7.

2.2.42 Hardy, M.P. and Bauer, S.J. 1991. *Drift Design Methodology and Preliminary Application for the Yucca Mountain Site Characterization Project.* SAND89-0837. Albuquerque, New Mexico: Sandia National Laboratories. ACC: NNA.19910808.0105. [DIRS 102920]

2.2.43 Hoek, E.; Kaiser, P.K.; and Bawden, W.F. 2000. *Support of Underground Excavations in Hard Rock.* Rotterdam, The Netherlands: A.A. Balkema. TIC: 252991. [DIRS 160539] ISBN: 90-5410-186-5.

2.2.44 Hutchinson, D.J. and Diederichs, M.S. 1996. *Cablebolting in Underground Mines.* Richmond, British Columbia, Canada: BiTech Publishers. TIC: 249146. [DIRS 153305] ISBN: 0-921095-37-6.

2.2.45 Itasca Consulting Group. [2002]. *Itasca Software–Cutting Edge Tools for Computational Mechanics.* Minneapolis, Minnesota: Itasca Consulting Group. TIC: 252592. [DIRS 160331]

2.2.46 Jaeger, J.C. and Cook, N.G.W. 1979. *Fundamentals of Rock Mechanics.* 3rd Edition. New York, New York: Chapman and Hall. TIC: 218325. [DIRS 106219] ISBN: 0-41222010-5.

2.2.47 Lama R.D. and Vutukuri, V.S. 1978. "Testing Techniques and Results." In *Handbook on Mechanical Properties of Rocks,* 3. No. 1, Volume IV of *Series on Rock and Soil Mechanics.* Clausthal, Germany: Trans Tech Publications. TIC: 209883. [DIRS 182863] ISBN: 0-87849023-X.

2.2.48 Merritt, F.S., ed. 1983. *Standard Handbook for Civil Engineers.* 3rd Edition. New York, New York: McGraw-Hill. TIC: 206892. [DIRS 106824] ISBN: 0-07041515-3.

2.2.49 MO0306MWDALAFV.000. ANSYS-La-Fine Ventilation. Submittal date: 06/23/2003. [DIRS 163961]

2.2.50 MO0306SDSAVDTH.000. Seismic Design Spectra and Acceleration, Velocity, and Displacement Time Histories for the Emplacement Level at 10^{-4} Annual Exceedance Frequency. Submittal date: 06/26/2003. [DIRS 164033]

2.2.51 MO0407TMHIS104.003. Acceleration, Velocity and Displacement Time Histories for the Emplacement Level (Point B) at 5X10-4 Annual Exceedance Frequency. Submittal date: 07/15/2004. [DIRS 170599]

2.2.52 Onofrei, M.; Gray, M.N.; Pusch, R.; Borgesson, L.; Karnland, O.; Shenton, B.; and Walker, B. 1993. *Sealing Properties of Cement-Based Grout Materials Used in the Rock Sealing Project.* AECL-10815. Pinawa, Manitoba, Canada: Atomic Energy of Canada Limited, Whiteshell Laboratories. TIC: 210964. [DIRS 144334] ISBN: 0-660-15493-5.

2.2.53 Ruest, M. and Martin, L. 2002. *FLAC Simulation of Split-Pipe Tests on an Instrumented Cable Bolt.* CIM Vancouver 2002, Paper No. 287. Montreal, Canada: Canadian Institute of Mining, Metallurgy and Petroleum. TIC: 255291. [DIRS 166251]

2.2.54 SNF37100195002.001. Hydraulic Fracturing Stress Measurements in Test Hole: ESF-AOD-HDFR1, Thermal Test Facility, Exploratory Studies Facility at Yucca Mountain. Submittal date: 12/18/1996. [DIRS 131356]

2.2.55 SNL02030193001.027. Summary of Bulk Property Measurements Including Saturated Bulk Density for NRG-2, NRG-2A, NRG-2B, NRG-3, NRG-4, NRG-5, NRG-6, NRG-7/7A, SD-9, and SD-12. Submittal date: 08/14/1996. [DIRS 108410]

2.2.56 Sun, Y. 2002. *Ground Control Methodology for Emplacement Drifts.* TDR-GCS-GE-000002 REV 00. Las Vegas, Nevada: Bechtel SAIC Company. ACC: MOL.20021118.0097. [DIRS 161697]

2.2.57 Wickham, G.E.; Tiedemann, H.R.; and Skinner, E.H. 1972. "Support Determinations Based on Geologic Predictions." *Proceedings: North American Rapid Excavation and Tunneling Conference, Chicago, Illinois, June 5-7, 1972.* 43-64. New York, New York: American Institute of Mining, Metallurgical, and Petroleum Engineers. TIC: 226274. [DIRS 146617]

It should be noted that the use of Data Tracking Number (DTN): MO0306MWDALAFV.000 (Reference 2.2.49) has been approved by their inclusion on the information exchange drawing, *IED Geotechnical and Thermal Parameters* (Reference 2.2.32). Similarly, DTNs: MO0306SDSAVDTH.000 (Reference 2.2.50) and MO0407TMHIS104.003 (Reference 2.2.51) are included in *IED Seismic Data* (Reference 2.2.34), and SNL02030193001.027 (Reference 2.2.55) is included in *IED Geotechnical and Thermal Parameters II* (Reference 2.2.33). The *Subsurface Geotechnical Parameters Report* (Reference 2.2.36) is owned by BSC Subsurface Organization and is not required to be included on the information exchange drawing. These data are qualified data and therefore are appropriate for use in this document.

2.3 DESIGN CONSTRAINTS

No design constraint.

2.4 DESIGN OUTPUTS

This design calculation is performed to support the information on ground support in non-emplacement drifts in the license application (LA). The final ground support system for non-emplacement drifts is provided in Section 7.3 based on the results of this calculation.

3 ASSUMPTIONS

This section contains assumptions used in this calculation and the rationale for use.

3.1 ASSUMPTIONS THAT REQUIRE VERIFICATION

3.1.1 Vendor Data

Assumption: The following assumptions are made related to ground support components:

- Allowable axial force in fully grouted rock bolts: 264 kN
- Dimension of stainless steel super Swellex-type rock bolt: 54 mm diameter and 3 mm thick

Rationale: The actual data for the above ground support information is not currently available. The above assumption is based on the vendor data (References 2.2.40 and 2.2.15) and is considered appropriate for the purpose of this calculation.

3.1.2 Modulus of Elasticity and Unconfined Compressive Strength of Grout

Assumption: The modulus of elasticity and unconfined compressive strength of grout in fully grouted rock bolts are assumed to be 14 GPa and 90 MPa, respectively.

Rationale: The actual data for the modulus of elasticity and unconfined compressive strength of grout in fully grouted rock bolts is not currently available. The above assumption is based on the data presented in a paper (Reference 2.2.52). It is considered appropriate for the purpose of this calculation.

3.2 ASSUMPTIONS THAT DO NOT REQUIRE VERIFICATION

3.2.1 Initial Ground Relaxation for Rock Bolts

Assumption: An initial ground relaxation value of 60 percent is assumed in the ground support analysis for rock bolts in non-emplacement drifts.

Rationale: The basis for use of this value is provided in the *Ground Control Methodology for Emplacement Drifts* (Reference 2.2.56, Table 6-1). This assumption results in 40 percent of the pre-excavation in situ stresses being imposed on the final ground support. This is conservative since the initial ground relaxation is likely to be completed before the final support system installed. This assumption does not require verification.

Used in Section 6

3.2.2 Initial Ground Relaxation for Final Shotcrete Lining

Assumption: An initial ground relaxation value of 100 percent is assumed and used in the ground support analysis for the final shotcrete lining in non-emplacement drifts.

Rationale: This value is considered to be adequate because the shotcrete lining will usually be installed after the drift excavation. Any rock deformation induced by excavation will most likely be complete well before the application of the shotcrete. This assumption does not require verification.

Used in Section 6.

3.2.3 Average Depth of Repository Host Horizon

Assumption: The average depth of the repository host horizon (RHH) below surface topography is assumed to be 400 m.

Rationale: Depth of emplacement drifts varies from drift to drift, ranging approximately from 215 m to 450 m, and the majority is between 300 to 400 m (Reference 2.2.24. Section 4.2.1). Based on Table 6-67 of Reference 2.2.36, the maximum depth to Tptpll unit is 362.56 m based on the mapping data in Enhanced Characterization of the Repository Block (ECRB) Cross Drift. Note that the elevation of the Exploratory Studies Facility (ESF) main drift in the middle point between Stations 28+04.323 and 56+54.323 is at about 1,085 m (see Figure 3 of Reference 2.2.25) and the elevation of Station 16+02.05 m in ECRB Cross Drift is 1,106 m (Reference 2.2.25, p. 14). It shows that the emplacement drift level (i.e., about the same level of ESF main drift) is about 20 m below the ECRB Cross Drift in the area between Panels 1 and 2. Thus, the maximum depth to Tptpll unit is about 380 m in this emplacement area. In a scoping analysis on emplacement drift stability, it was indicated that the results for the maximum value of 450 m would be similar to those for the bounding case of 400 m (Reference 2.2.24, Section 4.2.1). Since non-emplacement drifts are in the same horizon as that for emplacement drifts, and higher vertical stress will be induced with larger overburden depth, it is therefore, considered adequate to use this assumption, i.e., 400-m overburden depth for the purpose of this calculation. This assumption does not require verification.

Used in Section 6.

3.2.4 Horizontal-To-Vertical In Situ Stress Ratios

Assumption: The horizontal-to-vertical in situ stress ratio (K_o) is assumed to be 0.3 for the two-dimensional modeling.

Rationale: The major horizontal principal stress with a direction of N15^{o}E is 62% of the vertical stress whereas the minor horizontal principal stress with a direction of N75^{o}W is 36% of the vertical stress. This is according to the in situ stress measurement by hydraulic fracturing in a test hole located in the TSw2 unit (Reference 2.2.54). K_o = 0.3 is a lower bound value, which will result in higher stress concentration at the drift wall. It is considered adequate to make this assumption for the purpose of this calculation. This assumption does not require verification.

Used in Section 6.

3.2.5 Tensile Strength in 3DEC Dynamic Simulations

Assumption: To avoid large, unrealistic deformation of zones around the boundary of the excavation that yield in tension due to dynamic simulation, tensile strength in the 3DEC simulations is assumed to be infinitely large.

Rationale: The purpose of this assumption is to facilitate numerical convergence during the modeling for dynamic analysis without sacrificing the drift response. This is considered adequate for the purpose of this calculation. This assumption does not require verification.

Used in Section 6.

3.2.6 Properties of Interface between Shotcrete and Rock

Assumption: The mechanical properties of interface between shotcrete and rock are assumed as follows: cohesion – $1x10^9$ Pa, angle of friction – 45^o, bond stiffness – $2x10^9$ N/m/m, bond shear strength – $2\ x10^9$ N/m, and tensile strength – $1\ x10^9$ Pa.

Rationale: These property values are assumed in 3DEC modeling. Since shotcrete is assumed to be linearly elastic and the interface between shotcrete and rock is intimate and cannot break. These values are assumed to ensure no interfacial breakage between shotcrete and rock. It is considered adequate for the purpose of this calculation. This assumption does not require verification.

Used in Section 6.

3.2.7 Coefficient of Thermal Expansion for Structural Steel

Assumption: The coefficient of thermal expansion for structural steel is assumed to be 11.7×10^{-6} (m/m· ^oC) for temperature range of 0 to 100 ^oC.

Rationale: The coefficient of thermal expansion for structural steel is 11.7×10^{-6} (m/m· ^oC) for temperature range of –46 to 66 ^oC (see the note of Table 9-1 from Reference 2.2.48). The estimated coefficient of thermal expansion for structural steel for temperature of 100 ^oC is 11.71×10^{-6} (m/m· ^oC) based on Equation 9-75 of Reference 2.2.48. The upper temperature limit in non-emplacement drifts is not expected to reach 100 ^oC. It is considered adequate for the purpose of this calculation. This assumption does not require verification.

Used in Section 6.

3.2.8 Temperature Conditions in Exhaust Mains

Assumption: The temperature conditions in exhaust mains are assumed to be the same as those in emplacement drifts.

Rationale: This assumption is used in FLAC modeling for exhaust mains. The exhaust mains are located near (intersecting) the emplacement drifts. After waste emplacement, the exhaust mains will be subjected to the thermal stresses. However, the temperatures in exhaust mains will be

equal to or less than those in emplacement drifts. Assuming the same temperatures as those in emplacement drifts will result in higher thermal stresses in the rock at exhaust mains. It is considered adequate for the purpose of this calculation. This assumption does not require verification.

Used in Section 6.

3.2.9 Friction Angle of Lithophysal Rock

Assumption: A friction angle of 35 degrees is assumed for the lithophysal rock for the assessment of drift stability.

Rationale: The friction angles for typical rocks are generally much higher than 35 degrees based on Table 23 of Reference 2.2.47. Based on friction angles derived from numerical simulations on lithophysal rock mass (see Table 6.5-3 of Reference 2.2.26), the representative friction angle of lithophysal rock mass is about 35 degrees. Therefore, it is considered adequate to assume a friction angle of 35 degrees for the purpose of this calculation because the friction angle of 35 degrees is not only considered low for most rocks, it is also supported by the results of numerical simulations on the lithophysal rock mass. This assumption does not require verification.

Used in Section 6.

3.2.10 Tensile Strength of Lithophysal Rock

Assumption: Tensile strength is assumed to be one-tenth of the unconfined compressive strength of the lithophysal rock.

Rationale: The tensile strength value is typically considered by industry to be about one-tenth of the unconfined compressive strength. It is considered adequate to make this assumption for the lithophysal rock mass for the purpose of this calculation. This assumption does not require verification.

Used in Section 6.

4 METHODOLOGY

4.1 QUALITY ASSURANCE

This calculation has been prepared in accordance with EG-PRO-3DP-G04B-00037, *Calculations and Analyses* (Reference 2.1.1). The Q-List designates the ground control system for non-emplacement drifts as 'not important to waste isolation', and 'not important to safety', and the Safety Category (SC) is 'Non-SC' (Reference 2.2.27, p. A-11). However, this document is prepared with a QA:QA status since the Q-List identifies some of the "Non-emplacement Openings" (North Portal, North Ramp, access main, and turnouts) as Important to Safety and Safety Category "SC" (Reference 2.2.27, Table A-1, p. A-11).

4.2 USE OF SOFTWARE

4.2.1 Level 1 Software

Two level 1 softwares, FLAC (Fast Lagrangian Analysis of Continua) and 3DEC (3-Dimensional Distinct Element Code), are used in this calculation and are identified in Table 4-1. Descriptions of these codes and their qualification status are provided in the following subsections.

Table 4-1 List of Level 1 Software Used in This Calculation

Software Title / Version	Software Tracking Number (STN)	Brief Description of Software Use
FLAC V4.0 Version 4.0	10167-4.0-00	FLAC was used in coupled thermomechanical and dynamic analyses.
3DEC Version 2.01	10025-2.01-00	3DEC was used in mechanical and dynamic analyses.

4.2.1.1 FLAC Computer Software

FLAC Version 4.0 (STN: 10167-4.0-00) is a two-dimensional explicit finite difference code which simulates the behavior of structures built of soil, rock, or other materials subjected to static, dynamic, and thermally-induced loads (Reference 2.2.45). Modeled materials respond to applied forces or boundary restraints according to prescribed linear or non-linear stress/strain laws and undergo plastic flow when a limiting yield condition is reached. FLAC is based upon a Lagrangian scheme that is well suited for large deflections and has been used primarily for analysis and design in mine engineering and underground construction. The explicit time-marching solution of the full equations of motion, including inertial terms, permits the analysis of progressive failure and collapse. A detailed discussion on the general features and fields of the FLAC computer software applications is presented in the user's manual (Reference 2.2.45).

FLAC was used in coupled thermomechanical and dynamic analyses in this calculation. The validation test cases of Test 1, Test 3, Test 4, Test 5, and Test 7 are documented in the Software Implementation Report for FLAC Version 4.0 (Reference 2.2.23, Table 2) and support the application of mechanical, thermomechanical, and dynamic analyses conducted for this

calculation. The input and output files generated by FLAC for the numerical analyses for access mains, exhaust mains and turnouts and the list of input files for observation drift and TBM launch chamber are listed in Attachment I and output files have been archived on one DVD (Attachment II).

FLAC Version 4.0 (Reference 2.2.2) was obtained from the Software Configuration Management (SCM) in accordance with the IT-PRO-0011 (Reference 2.1.2) procedure. FLAC is installed and run on stand- alone PCs with Windows 2000/NT 4.0 operating systems. FLAC Version 4.0 is qualified for use in design in accordance with the IT-PRO-0011 (Reference 2.1.2) procedure. The software was appropriate for the applications used in this analysis, and used only within the range of validation, as specified in the software qualification documentation.

4.2.1.2 3DEC COMPUTER CODE

3DEC Version 2.01 (STN: 10025-2.01-00) is a three-dimensional computer code based on the distinct element method for discontinuum modeling. In 3DEC, the discontinuous medium is presented as an assemblage of discrete blocks. Individual blocks behave as either rigid or deformable material; deformable blocks are subdivided into a mesh of finite difference elements. 3DEC is based on a Lagrangian calculation scheme that is well-suited to model the large deformations of blocks in a system. A detailed discussion on the general features and fields of 3DEC computer software applications is presented in the User's Manual (Reference 2.2.45).

3DEC was used in coupled thermomechanical and dynamic analyses in this calculation. The validation test cases of Test 1 and Test 7 documented in the *Software Implementation Report* for *3DEC Version 2.01* (Reference 2.2.22, Table 2-2) support the application of mechanical and dynamic analyses conducted for this calculation. The input files generated by 3DEC for North portal, intersections between access mains and turnouts and between exhaust mains and emplacement drifts and between observation drift and exhaust mains, and interburden pillar between shaft access and exhaust mains are listed in Attachment I. Output results support the figures presented in the calculation.

3DEC Version 2.01 (Reference 2.2.1) was obtained from the SCM in accordance with the IT-PRO-0011 (Reference 2.1.2) procedure. 3DEC Version 2.01 is installed and run on stand- alone PCs with Windows 2000/NT 4.0 operating systems. 3DEC Version 2.01 is qualified for use in design in accordance with the IT-PRO-0011 (Reference 2.1.2) procedure. The software was appropriate for the applications used in this analysis, and used only within the range of validation, as specified in the software qualification documentation.

4.2.2 Level 2 Software

Microsoft Excel 2000 (STN: 610236-2000-00) was used in displaying some of the FLAC and 3DEC results graphically and to perform simple conversions. In this application, results from the FLAC or 3DEC analyses were used as inputs, and outputs were charts. This is considered Level 2 Usage in accordance with IT-PRO-0011, *Software Management* (Reference 2.1.2).

Microsoft Excel 2000 was performed on personal computers with Windows 2000/NT 4.0 operating systems. The work performed by Excel were confirmed using hand calculations and by visual inspection.

WinZip version 9.0 SR-1 was used on a Dell personal computer, running the Microsoft Windows 2000 operating system to create .zip files on the DVD. These are verified by visual inspection.

4.3 DESIGN METHODOLGY

Both empirical and analytical methods are employed in the design calculations. The empirical methods are primarily used for assessing the needs for ground support of non-emplacement drifts as well as for its selection. A number of hand calculations were performed as part of empirical analysis within this calculation. Design issues such as personnel safety, constructability, and geologic mapping requirements are factored into the design of the ground support system. However, due to the complexity of the problem involved with ground support design for nuclear waste repository, the repository ground control design effort will focus mainly on analytical methods by using computer programs to evaluate the stability of unsupported and supported openings. Applicable thermal and seismic loads will be considered in the design in addition to the in situ loading conditions. Based on empirical estimates, design issues, and computer modeling results, the final ground support system is developed.

4.3.1 Empirical Methods

Two empirical methods used in the design calculation are Rock Mass Rating (RMR) classification system (Reference 2.2.19) and Rock Mass Quality (Q) system of Norwegian Geotechnical Institute (NGI) (Reference 2.2.16).

4.3.1.1 RMR System

The RMR system was developed by Bieniawski (Reference 2.2.19). This engineering classification of rock masses, especially evolved for rock engineering applications, provides a general RMR increasing with rock quality from 0 to 100. It is based upon the following six parameters:

- strength of the rock
- drill core quality or Rock Quality Designation (RQD)
- joint and fracture spacing
- joint conditions
- ground water conditions
- orientation of joints

These parameters not only are measurable in the field but can also be obtained from borings. Joints are the major factor in this classification system; four of the six parameters (RQD, joint spacing, joint conditions, and orientation of joints) are related to joint characteristics. Increments of rock mass rating corresponding to each parameter are summed to determine RMR.

The RMR values for various rock units at the RHH are generally available from the Enhanced Characterization of the Repository Block (ECRB) cross drift. In case these RMR values are not available, empirical correlation can be used to estimate RMR values based on known rock mass modulus. The empirical correlation used in this calculation is shown as follows (Reference 2.2.17, Eq. 8):

$$RMR \quad 40 \log E_m + 10 \qquad \text{(Eq. 4-1)}$$

where E_m = rock mass modulus in GPa

Once the RMR values are determined, the rock mass quality for each rock unit considered can be judged based on the guidelines provided by Bieniawski (Reference 2.2.19, Tables 4.1 and 4.2). Recommendation for the excavation scheme and rock support needs can be made by following the guidelines presented in Table 4-2 (Reference 2.2.19, Table 4.4).

Details on how to apply the RMR classification system to the preliminary design of ground support for rock tunnels such as those in repository emplacement drifts can be found in the *Engineering Rock Mass Classifications* (Reference 2.2.19, Section 4).

Table 4-2 Estimate of Ground Support Needs Based on RMR System

Rock mass class	Excavation	Rock bolts (20 mm diameter, fully grouted)	Shotcrete	Steel sets
I - Very good rock *RMR*: 81-100	Full face, 3 m advance.	Generally no support required except spot bolting.		
II - Good rock *RMR*: 61-80	Full face , 1-1.5 m advance. Complete support 20 m from face.	Locally, bolts in crown 3 m long, spaced 2.5 m with occasional wire mesh.	50 mm in crown where required.	None.
III - Fair rock *RMR*: 41-60	Top heading and bench 1.5-3 m advance in top heading. Commence support after each blast. Complete support 10 m from face.	Systematic bolts 4 m long, spaced 1.5 - 2 m in crown and walls with wire mesh in crown.	50-100 mm in crown and 30 mm in sides.	None.
IV - Poor rock *RMR*: 21-40	Top heading and bench 1.0-1.5 m advance in top heading. Install support concurrently with excavation, 10 m from face.	Systematic bolts 4-5 m long, spaced 1-1.5 m in crown and walls with wire mesh.	100-150 mm in crown and 100 mm in sides.	Light to medium ribs spaced 1.5 m where required.
V – Very poor rock *RMR*: < 20	Multiple drifts 0.5-1.5 m advance in top heading. Install support concurrently with excavation. Shotcrete as soon as possible after blasting.	Systematic bolts 5-6 m long, spaced 1-1.5 m in crown and walls with wire mesh. Bolt invert.	150-200 mm in crown, 150 mm in sides, and 50 mm on face.	Medium to heavy ribs spaced 0.75 m with steel lagging and forepoling if required. Close invert.

Source: Reference 2.2.19, Table 4.4.

4.3.1.2 Q System

The Q system, developed in Norway by Barton et al. (Reference 2.2.16), provides for the design of rock support for tunnels and large underground chambers. The system utilizes the following six factors:

- RQD
- Number of joint sets
- Joint roughness
- Joint alteration
- Joint water condition
- Stress condition

The factors are combined in the following way to determine the rock mass quality (Q) as (Reference 2.2.16, Eq. 1),

$$Q \quad \left(\frac{RQD}{J_n}\right)\left(\frac{J_r}{J_a}\right)\left(\frac{J_w}{SRF}\right) \qquad \text{(Eq. 4-2)}$$

where RQD = rock quality designation
J_n = joint set number
J_r = joint roughness number
J_a = joint alteration number
J_w = joint water reduction factor
SRF = stress reduction factor (dependent on loading conditions)

The three ratios in the Equation 4-2, RQD/Jn, Jr/Ja, and Jw/SRF, represent block size, minimum inter-block shear strength, and active stress, respectively (Reference 2.2.16, p. 202).

Similar to the RMR values, Q indices for various rock units at the RHH are generally available from the ESF and ECRB. In case these Q indices are not available, empirical correlation can be used to estimate Q indices based on given rock mass modulus. The empirical correlation used in this calculation is as follows (Reference 2.2.43, Eqs. 8.16 and 8.19):

$$Q \quad Q' \times \frac{J_w}{SRF} \quad e^{\frac{RMR-44}{9}} \times \frac{J_w}{SRF} \qquad \text{(Eq. 4-3)}$$

where

$$Q' \quad \left(\frac{RQD}{J_n}\right)\left(\frac{J_r}{J_a}\right)$$

The RMR value in Eq. 4-3 is estimated from the given rock mass modulus using Eq. 4-1.

The Q index is used with the Equivalent Dimension, defined as the largest of span, diameter, and height divided by the excavation support ratio (ESR). ESR is roughly analogous to the inverse of the factor of safety used in engineering design. The ESR reflects the degree of safety and ground support required for an excavation as determined by the purpose, presence of machinery, personnel, etc., to meet safety requirements. In essence, the safety factor (SF) of an opening can be increased by reducing the ESR value. The ESR values for various underground openings can be estimated based on Barton et al. (Reference 2.2.16, Table 7). For example, the *ESR* for the access and exhaust mains and the turnouts, classified as "access tunnels", is taken to be 1.3; the intersections are assigned a value of 1.0.

The Equivalent Dimension is plotted against Q on the design chart (Figure 4-1) to determine the required rock support category (Reference 2.2.43, Figure 4.3). Thermal or seismic loads can be included in an implicit way, by increasing the SRF, thereby requiring a higher degree of support.

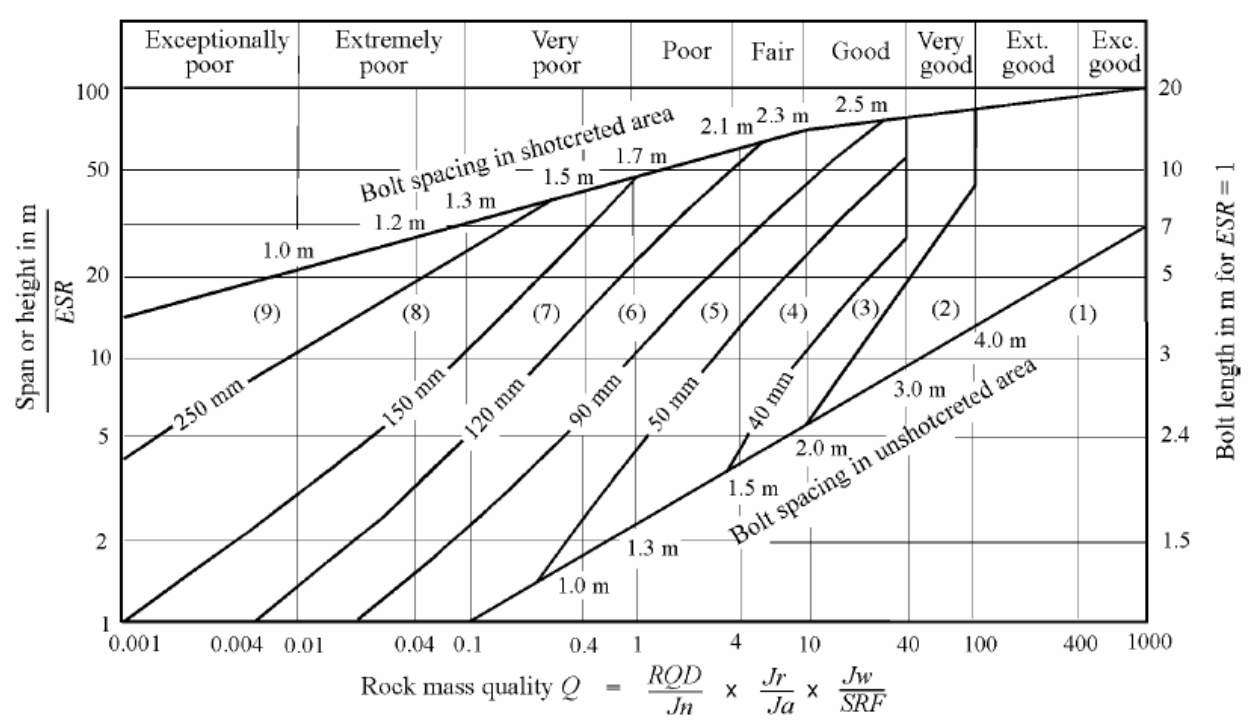

REINFORCEMENT CATEGORIES

1) Unsupported
2) Spot bolting
3) Systematic bolting
4) Systematic bolting with 40-100 mm unreinforced shotcrete
5) Fibre reinforced shotcrete, 50 - 90 mm, and bolting
6) Fibre reinforced shotcrete, 90 - 120 mm, and bolting
7) Fibre reinforced shotcrete, 120 - 150 mm, and bolting
8) Fibre reinforced shotcrete, > 150 mm, with reinforced ribs of shotcrete and bolting
9) Cast concrete lining

Source: Reference 2.2.43, Figure 4.3.

Figure 4-1 Estimate Ground Support Needs Based on Q Index

The NGI rock mass classification system provides guidance on bolt spacing, bolt length, and shotcrete thickness, based on the rock mass quality index (Q) and the opening dimensions. The length L of rockbolts can be estimated from the excavation width B and ESR (Reference 2.2.43, Eq. 4-3):

$$L \quad \frac{2+0.15B}{ESR} \qquad \text{(Eq. 4-4)}$$

4.3.1.3 Applicability of Empirical Methods

Empirical methods are usually applicable to mining or tunneling in jointed rock mass. The nonlithophysal rock which contains joints and fractures of various spacing and trace lengths is certainly a good example of this type of rock. Use of the RMR and Q approaches for non-emplacement drifts in the nonlithophysal rock is considered to be conventional.

For the non-emplacement drifts excavated in the lithophysal rock, however, use of the RMR or Q approach for the ground support design is non-conventional, and there are no sufficient data or field experiences available to support this application. This is primarily due to the fact that the lithophysal rock contains some air-filled large cavities and is hard to be characterized using the RMR or Q index since a RQD value is defined for a rock with fractures not with voids. Therefore, these empirical methods are not used in this calculation for evaluating the requirements of ground support for non-emplacement drifts in the lithophysal rock. Selection of ground support methods for this rock type is based on experiences and observations from the construction of the ESF and the ECRB tunnels, and assessment from numerical analyses.

4.3.2 Analytical Methods

Analytical methods, mainly numerical methods, are used in this calculation to evaluate the stability of non-emplacement openings including ground support analysis.

In general, stability analyses for non-emplacement openings include computer simulation of both unsupported and supported openings. For unsupported openings, stability analysis includes the simulation of excavation of the non-emplacement drifts in a gravity-stressed rock medium, followed by dynamic analysis. For stability analysis of exhaust mains and intersection between them and emplacement drifts, the introduction of thermal loading to simulate the waste emplacement process will follow in situ stress loading and seismic loading. For stability analyses of supported openings, the approach is the same as that for unsupported openings except that the final ground support system is incorporated into the modeling during the excavation process and, therefore, is subjected to in situ, thermal loading (e.g., for intersections between exhaust mains and emplacement drifts, exhaust mains, intersection between exhaust main and observation drift, and interburden area between access to intake shaft #4 and exhaust mains), and seismic loading. Details on numerical modeling of non-emplacement drifts, loading and boundary conditions as well as stability of unsupported and supported non-emplacement drifts will be presented in Section 6.

5 LIST OF ATTACHMENTS

Table 5-1 lists attachments of this calculation.

Table 5-1 List of Attachments

Attachment	Description	Number of Pages
I	File Listing for Attachment II	28
II	One (1) DVD	N/A

6 BODY OF CALCULATION

6.1 GENERAL

6.1.1 Introduction

This calculation provides the technical basis for the design of the ground control systems for non-emplacement drifts for LA. In the design of permanent underground facilities, the ground support needs are determined using several available methods, i.e., empirical methods, observational approach, and analytical methods (Reference 2.2.18, p. 35). The design and construction of an underground high-level nuclear waste repository facility introduce unique challenges that are not commonly experienced with other subsurface facilities. For example, the presence of high level nuclear waste and the resultant thermal loading conditions introduce a series of additional requirements to the overall design and construction of the facility in addition to the waste isolation requirements. In situ (excavation) loads, potential loads from repository operations, and loads due to seismic loading conditions during an earthquake must also be addressed in the design.

The non-emplacement drifts include all other repository underground openings that will not be used for waste emplacement, such as access mains, exhaust mains, ventilation shafts and raises, emplacement drift turnouts, and intersections between turnouts and access mains, etc. For non-emplacement drifts, both the initial and final ground support systems will be developed, but only the final ground support systems will be discussed in this calculation. Also, as indicated in Section 1, the ground support design in this calculation will include access mains, exhaust mains, turnouts, ramps, intersections between access mains and turnouts and between exhaust mains and emplacement drifts, portals, and Tunnel Boring Machine (TBM) launch chambers, observation drift and test alcove in the performance confirmation (PC) facilities, etc. The ground support for ventilation shafts and raises are not included in this calculation.

Unless otherwise indicated, the term “ground support” or “ground control” used in this section is referred to as the final ground support. When the initial ground support is discussed, it will be explicitly indicated.

6.1.2 Input Parameters

6.1.2.1 Rock Mass Mechanical Properties for Lithophysal Rock at RHH

Rock mass mechanical properties for lithophysal rock are listed in Table 6-1, which are primarily obtained from Tables 6-76, 6-77, and 6-70 of *Subsurface Geotechnical Parameters Report* (Reference 2.2.36). The values of bulk modulus (K) and shear modulus (G) are calculated based on values of modulus of elasticity (E) and Poisson’s ratio (ν) in Table 6-1 and from Equations 6-1 and 6-2 (see equations 14 and 13, p. 111 of Reference 2.2.46):

$$K \quad \frac{E}{3(1-2\nu)} \qquad \text{(Eq. 6-1)}$$

$$G \quad \frac{E}{2(1+\nu)} \qquad \text{(Eq. 6-2)}$$

Tensile strength is assumed to be one-tenth of the unconfined compressive strength (Assumption 3.2.10). Values of cohesion (c) corresponding to friction angle of 35 degrees (see Assumption 3.2.9) are estimated based on the unconfined compressive strength (q_u) values for each category identified in Table 6-1 and using the following equation (Reference 2.2.43, Eq. 8.15):

$$c \quad \frac{q_u(1-\sin\phi)}{2\cos\phi} \qquad \text{(Eq. 6-3)}$$

Table 6-1 Rock Mass Mechanical Properties for Lithophysal Rock at RHH

Parameter	Lithophysal Rock				
Rock Mass Category	1	2	3	4	5
Lithophysal Porosity (%)[a]	>30	25-30	15-25	10-15	<10
Poisson's Ratio[b]	0.22	0.22	0.22	0.22	0.22
Modulus of Elasticity (GPa)[c]	1.90	6.40	10.80	15.30	19.70
Bulk Modulus (GPa)	1.13	3.81	6.43	9.11	11.73
Shear Modulus (GPa)	0.78	2.62	4.43	6.27	8.07
Unconfined Compressive Strength (MPa)[c]	10	15	20	25	30
Cohesion (MPa)	2.60	3.90	5.21	6.51	7.81
Friction Angle (degrees)	35	35	35	35	35
Tensile Strength (MPa)	1.0	1.5	2.0	2.5	3.0

Source: Reference 2.2.36, [a] Table 6-70, [b] Table 6-76, [c] Table 6-77.

6.1.2.2 Rock Mass Mechanical Properties for Nonlithophysal Rock at RHH

Rock mass properties for nonlithophysal rock (Tptpmn) are listed in Table 6-2. Note that all data are obtained from Table 6-76 of *Subsurface Geotechnical Parameters Report* (Reference 2.2.36) except that values of bulk modulus and shear modulus are calculated based on values of modulus of elasticity and Poisson's ratio in Table 6-2 and from equations 14 and 13, p. 111 of Reference 2.2.46.

Table 6-2 Rock Mass Mechanical Properties for Nonlithophysal Rock at RHH

Parameter	Nonlithophysal Rock (Tptpmn)				
Rock Mass Category	1	2	3	4	5
Geologic Strength Index (GSI)	51	59	62	68	72
Poisson's Ratio	0.19	0.19	0.19	0.19	0.19
Modulus of Elasticity (GPa)	10.59	16.79	19.95	28.18	35.48
Bulk Modulus (GPa)	5.69	9.03	10.73	15.15	19.08
Shear Modulus (GPa)	4.45	7.05	8.38	11.84	14.91
Global Compressive Strength (MPa)	26.90	32.02	34.28	39.57	43.90
Cohesion (MPa)	7.36	8.33	8.75	9.73	10.52
Friction Angle (degrees)	32.64	35.02	35.91	37.65	38.79
Tensile Strength (MPa)	0.27	0.50	0.63	0.99	1.33

Source: Reference 2.2.36, Table 6-76.

6.1.2.3 Rock Mass Density

A rock mass saturated bulk density of 2,410 kg/m^3 is used to estimate overburden and in situ stress state. This value is the mean saturated density for the rock unit of Tptpln (Reference 2.2.55) at RHH, and is the highest value of lithostratigraphic units, which is conservative for the purpose of this calculation. For the rock at North Portal, use 2,290 kg/m^3, which is the saturated density for TCw unit (Reference 2.2.36, Table 6-67, average saturated bulk density for Tpcpul).

6.1.2.4 Dimensions and Properties for Fully Grouted Rock Bolts

The dimensions and properties of fully grouted rock bolts are shown in Table 6-3. Note that the bond stiffness of grout was calculated based on the following equation (Equation 3 of Reference 2.2.53):

$$K_{bond} \quad \frac{2\pi G}{100\ln\left[1+2t/D\right]} \qquad \text{(Eq. 6-4)}$$

where

K_{bond} = grout shear stiffness, N/m/m
G = Grout shear modulus, Pa
t = annulus thickness, m
D = rock bolt diameter, m

Table 6-3 Dimensions and Properties of Fully Grouted Rock Bolts

Parameter	Value	Source and Remark
Density of Carbon Steel (g/cm^3)	7.859	Reference 2.2.7, p. 145
Diameter of Rock Bolt (m)	0.0254	Converted from a diameter of 1 inch (1 in × 0.0254 m/in = 0.0254 m)
Thickness of Grout Annulus (m)	0.00635	Converted from a thickness of 0.25 in (0.25 in × 0.0254 m/in = 0.00635 m)
Length of Rock Bolts (m)	3 - 5	3 m in typical non-emplacement drifts and 5 m in typical intersection area
Spacing between bolts (m)	1.25	Spacing in both directions
Perimeter of Rock Bolt (m)	0.08	Calculated: p = π D = 3.1415 × 0.0254 = 0.08 m
Allowable Axial Force (kN)	264	Based on the yield strength (force) of 264 kN (Reference 2.2.40, Dywidag threadbar) and Assumption 3.1.1
Modulus of Elasticity of Carbon Steel (GPa)	200	Reference 2.2.6, p. 1-117, (29,000 x1000/(145x 10^6))
Modulus of Elasticity of Grout (GPa)	14	Reference 2.2.52, Figure 33, p. 60 and Assumption 3.1.2
Poisson's Ratio of Grout	0.25	Set to be the same as concrete (Reference 2.2.48, p. 6-8)
Grout Unconfined Compressive Strength (MPa)	90	Reference 2.2.52, Figure 27b, p. 52 and Assumption 3.1.2
Coefficient of Thermal Expansion (m/m·°C) for steel	11.7×10^{-6}	See assumption 3.2.7
Bond Stiffness of Grout (N/m/m)	8.68×10^8	Calculated using Eq. 6-4 (Reference 2.2.53, Eq. 3)
Bond Strength of Grout (cohesion) (10^5 N/m)	2.6 [a], 2.75[b], 2.8[c] 3.0[d], 3.05[e]	Based on recommendation by Reference 2.2.44, Figure 2.6.13. [a] lith. and nonlith. Cat. 1, [b] lith. Cat. 3, [c] nonlith. Cat. 3, [d] lith. Cat. 5, [e] nonlith. Cat. 5

6.1.2.5 Dimension and Properties for Shotcrete

The dimension and properties of shotcrete are shown in Table 6-4.

Table 6-4 Dimension and Properties of Shotcrete

Parameter	Value	Source
Thickness of Shotcrete (m)	0.1	Converted from a thickness of 4 in (4 in × 0.0254 m/in = 0.102 m)
Elastic Modulus *E* (GPa)	29	Based on mean value in Sec. 1.7 of Reference 2.2.4
Poisson's Ratio ν	0.25	Used the same as concrete, Reference 2.2.48,p. 6-8

6.1.2.6 Dimensions and Properties for Stainless Steel Super Swellex Bolts

Stainless steel Super Swellex-type rock bolts are used for emplacement drift turnouts in this calculation. The dimensions and mechanical properties of stainless steel Super Swellex bolts are used in this calculation and are listed in Table 6-5.

Table 6-5 Dimensions and Properties for Stainless Steel Super Swellex-type Rock Bolts

Parameter	Value	Source and Remark
Density (kg/m^3)	8,000	Reference 2.2.8, Table 21, p. 871, for 316 type stainless steel.
Diameter of Rock Bolt (m)	0.054	Reference 2.2.15, p. 10 and Assumption 3.1.1
Thickness of (m)	0.003	Reference 2.2.15, p. 10 and Assumption 3.1.1
Length of Rock Bolts (m)	3	Typical bolt length in emplacement drifts
Young's Modulus of Stainless Steel (GPa)	193	The value is 193 GPa for 316 type stainless steel based on Reference 2.2.8 (Table 21, p. 871).
Tensile Strength (MPa)	620	Reference 2.2.12, Table 2, p. 4, for 316 type stainless steel.
Limit Axial Force (kN)	298	Calculated from $620\times10^6\times\pi/4\times(0.054^2-0.048^2)/1000$=298 kN.
Coefficient of Thermal Expansion (m/m·°C)	15.9×10^{-6}	Reference 2.2.8, Table 21, p. 871, for 316 type stainless steel at a temperature range of 0 to 100°C.
Bond Stiffness (N/m/m)	3×10^8	See Table 6-6 of Reference 2.2.30.
Bond Strength (N/m)	2.75×10^5	See Table 6-6 of Reference 2.2.30.

6.1.2.7 Seismic Velocity History

Seismic velocity histories for the mean annual probability exceedance of 5 x 10^{-4} (2,000-year return period) is shown in Figure 6-1 (Reference 2.2.51). This seismic velocity history is used in all the numerical analyses in Section 6 except in Section 6.6, in which seismic velocity history with an APE of 1 x 10^{-4} (10,000-year return period) as shown in Figure 6-2 (Reference 2.2.50) is used for the sensitivity analysis. Details on how these seismic velocity histories are applied in numerical calculations are discussed in Section 6.5.2.3.

6.1.2.8 Rock Mass Thermal Properties

The coefficients of thermal expansion for lithophysal and nonlithophysal rocks at RHH are shown in Table 6-6 (Reference 2.2.36, Table 6-86).

Table 6-6 Coefficients of Thermal Expansion for Lithophysal and Nonlithophysal Rocks at RHH

Temperature Range (°C)	Value (10^{-6}/°C)[a]
25 - 50	7.34
50 - 75	8.99
75 - 100	9.73
100 - 125	10.22
125 - 150	10.91
150 - 175	12.20
175 - 200	14.74
200 - 225	22.31

Source: Reference 2.2.36, Table 6-86. [a] Values from heating cycle.

Table 6-7 shows the thermal conductivity and specific heat values for the lithophysal and nonlithophysal rocks at RHH (Reference 2.2.36, Tables 6-90 and 6-94). Note that Tptpmn and Tptpll units are used for nonlithophysal and lithophysal rock, respectively, since they are the major units in which non-emplacement drifts are located (see Section 6.2)

Table 6-7 Thermal Conductivity and Specific Heat for Lithophysal and Nonlithophysal Rocks at RHH

Litho-Stratigraphic Unit	Thermal Conductivity (W/m·K)		Specific Heat (J/kg·K)		
	Wet	Dry	25 - 94°C	95 - 114°C	115 - 325°C
Tptpmn	2.07	1.42	910	3000	990
Tptpll	1.89	1.28	930	3300	990

Source: Thermal conductivity from Table 6-90 and specific heat from Table 6-94 of Reference 2.2.36.

6.1.2.9 Time Histories of Rock Temperatures at Emplacement Drifts

Time histories of rock temperatures at emplacement drifts are listed in Table 6-8. These values reflect the effect of forced continuous ventilation at 15 m^3/s during the 50-year period, and are obtained from the ANSYS output files associated with the ventilation model (Reference 2.2.49). The rock temperatures at 50 m above and below the drift center are obtained from two neighboring points by linear interpolation as shown in Equation 6-5 from the source reference. Note that this simple linear interpolation applies to Table 6-8. These ANSYS output files were downloaded from the Technical Data Management Systems (TDMS) under Reference 2.2.49.

$$T(y) \quad T_u + ((y - y_u)/(y_l - y_u))(T_l - T_u) \qquad \text{(Eq. 6-5)}$$

where T is for temperature, y for elevation, *u* and *l* for upper and lower elevations, respectively.

Table 6-8 Time Histories of Rock Temperatures at Emplacement Drifts

Time (years)	Temperatures (°C)		
	Drift Wall	50-m Above Drift Center[a]	50-m Below Drift Center[a]
0	22.28	21.68	23.08
0.01	36.64	21.68	23.08
1	71.80	21.68	23.08
2	72.22	21.68	23.08
5	70.42	21.71	23.10
7	68.63	21.81	23.19
10	66.32	22.09	23.45
20	59.88	23.42	24.72
30	54.32	24.68	25.96
50	46.78	26.53	27.81

Source: Reference 2.2.49, ANSYS-LA-Fine.xls, and la600c24.rth. Note: [a] Temperature data at the exact locations were obtained by linear interpolation between two neighboring points from the source reference.

6.1.2.10 Rock Mass Mechanical Properties of TCw Thermal Mechanical Unit

Table 6-9 lists the rock mass mechanical properties for the TCw thermal mechanical unit (Reference 2.2.36, Table 6-76). Note that the bulk modulus and shear modulus values are derived based on values of modulus of elasticity (E) and Poisson's ratio (ν) in Table 6-9 using Equations 6-1 and 6-2.

Table 6-9 Rock Mass Mechanical Properties of TCw Unit

Thermal Mechanical Unit	TCw	
Density (kg/m^3)	2290	
Rock Mass Quality (RMQ)	1	5
Modulus of Elasticity (GPa)	8.78	45.97
Bulk Modulus (GPa)	5.06	26.68
Shear Modulus (GPa)	3.63	18.97
Poisson's Ratio	0.21	0.21
Cohesion (MPa)	6.78	11.51
Friction Angle (degrees)	29.98	38.04
Tensile Strength (MPa)	0.26	2.23

Source: Values are averaged based on data from Reference 2.2.36, Table 6-76.

6.1.2.11 Horizontal-to-vertical In Situ Stress Ratios

The horizontal-to-vertical in situ stress ratio (K_o) is assumed to be 0.3 for the two-dimensional modeling (see Assumption 3.2.4). The horizontal-to-vertical in situ stress ratios (K_os) are 0.62 and 0.36 for the major and minor horizontal principal stress directions, respectively, which are

used for the 3-dimensional modeling. This is according to the in situ stress measurement by hydraulic fracturing in a test hole located in the TSw2 unit (Reference 2.2.54).

6.1.2.12 Configuration and Dimensions of Non-Emplacement Drifts

- The diameter of emplacement drift is 5.5 m (Reference 2.2.37, Table 3) and the diameter of access mains is 7.62 m (Reference 2.2.37, Table 5).
- The diameter of exhaust mains is 7.62 m in all panels (Reference 2.2.37, Tables 4 to 6) except that it is 5.5 m in panel 1 (Reference 2.2.37, Table 3).
- The diameter of TBM excavated emplacement drift turnout is 5.5 m (Reference 2.2.35).
- Both observation drift and test alcove have a horseshoe shape in cross-section (5 m wide and 5 m high). The observation drift is parallel to the emplacement drift in the plan view and the horizontal spacing, center-to-center, between them is 20 m. Along most of its length the vertical distance between the crown of the observation drift and the floor of the emplacement drift is 10 m. The test alcove is below the emplacement drift with a minimum of 10 m from crown to invert (Reference 2.2.25, Section 8.5).
- The TBM launch chamber at the portal area is a horseshoe-shaped underground excavation. It is 11 m × 11 m in cross-section and 20-m long (Reference 2.2.25, Section 8.3). For TBM launch chambers adjacent to turnouts, they are 7.0 m (wide) × 6.25 m (high) in cross-section and about 12 m long (Reference 2.2.35, Section 6.2).

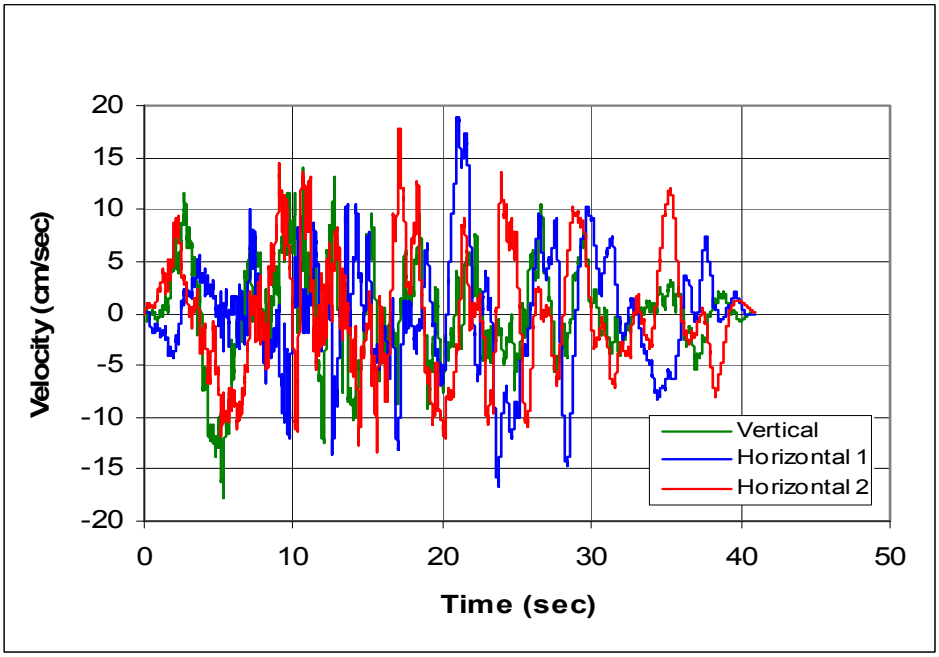

Source: Reference 2.2.51, V.vth, H1.vth, H2.vth

Figure 6-1 Time Histories of Velocity Components of Seismic Motion for APE of 5×10^{-4}

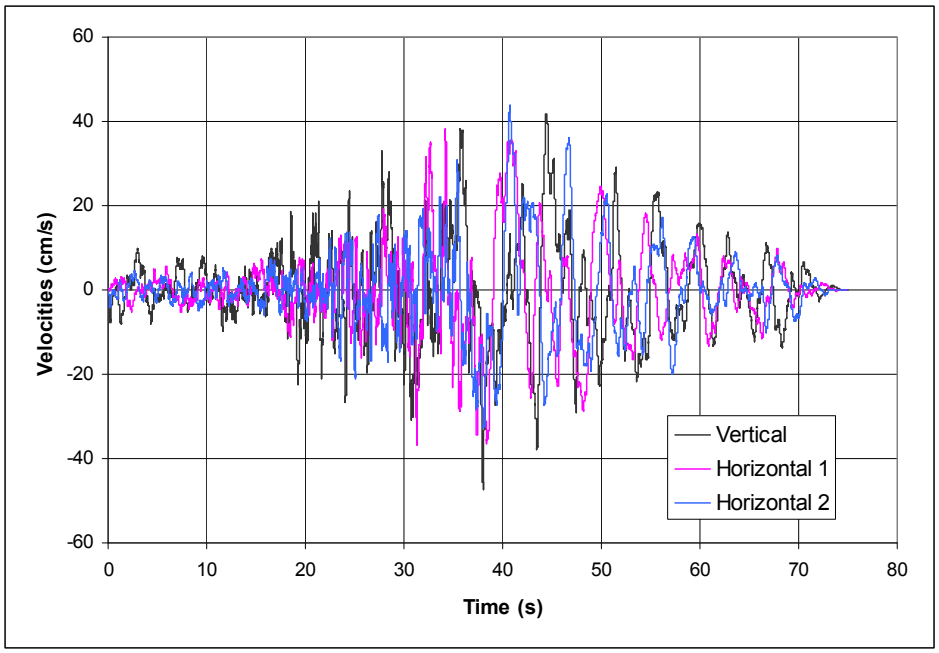

Source: Reference 2.2.50, MatH1.vth, MatH2.vth, and MatV.vth.

Figure 6-2 Time Histories of Velocity Components of Seismic Motion for APE of 1×10^{-4}

6.2 REPOSITORY HOST HORIZON AND GEOTECHNICAL CHARACTERIZATION

In order to design the ground support system in non-emplacement drifts, it is important to understand the environment in which these drifts will be located.

According to the *Underground Layout Configuration* calculation (Reference 2.2.25, Section 7.1.7), the RHH will be located in the lower part of the lithophysal zone of the densely welded devitrified lithophysal-rich tuff unit and the entire densely welded devitrified lithophysal-poor tuff unit of the Topopah Spring Tuff. The RHH contains four lithostratigraphic units, namely the upper lithophysal unit (Tptpul), the middle non-lithophysal unit (Tptpmn), the lower lithophysal unit (Tptpll), and the lower nonlithophysal unit (Tptpln). The underground layout is shown in Figure 6-3 (Reference 2.2.37, Figure 11). Of the total emplacement areas, approximately 85% will lie within the Tptpll and Tptpul units combined and the rest 15% will be located in the Tptpmn and Tptpln units. In the lithophysal rock, 95% of the emplacement area lies in the Tptpll unit whereas in the nonlithophysal rock, 83% of the emplacement area lies in the Tptpmn unit (Reference 2.2.25, Table II-2). Note that both emplacement drifts and non-emplacement drifts are located within the same boundary for the underground repository. In other words, among the area for non-emplacement drifts, the primary tuff rock units for lithophysal and nonlithophysal rocks are Tptpll and Tptpmn units, respectively.

Geological mapping was conducted in the ESF tunnel and the ECRB drift to characterize the rock units within the RHH. The data collected were analyzed using two empirical rock mass classification systems, the Geomechanics RMR system (Reference 2.2.19) and the Rock Mass Quality (Q) system of Norwegian Geotechnical Institute (NGI) (Reference 2.2.16). The geotechnical characteristics of the Tptpll and Tptpmn units are summarized as follows (Reference 2.2.20, Section 3.4):

Tptpll Unit. The Tptpll unit has a horizontal RQD rating of 42 (poor), a Q rating of 7.9 (fair), and a RMR value of 57 (fair). Its content of lithophysae varies from 5 to 30 percent by volume, with a size ranging from 5 to 130 cm. The larger lithophysal cavities tend to be irregular or ellipsoidal features that exhibit prismatic fracturing. The unit has an average of two plus random joint sets; however no keyblock problems are expected. Typical lithophysae and fracturing in the Tptpll unit are shown in Figure 6-4.

Tptpmn Unit. The Tptpmn unit has a mean horizontal RQD rating ranging from 60 to 62 (fair to good), and a RMR value of 60 (fair). It is characterized by less than 3 percent lithophysae by volume. This unit has an average of three to three plus random joint sets, with predominately two vertical joint sets and one horizontal joint set. The horizontal joint set, or vapor-phase partings, is the primary cause of potential formation of keyblocks. A typical fracture pattern in the Tptpmn unit is shown in Figure 6-5.

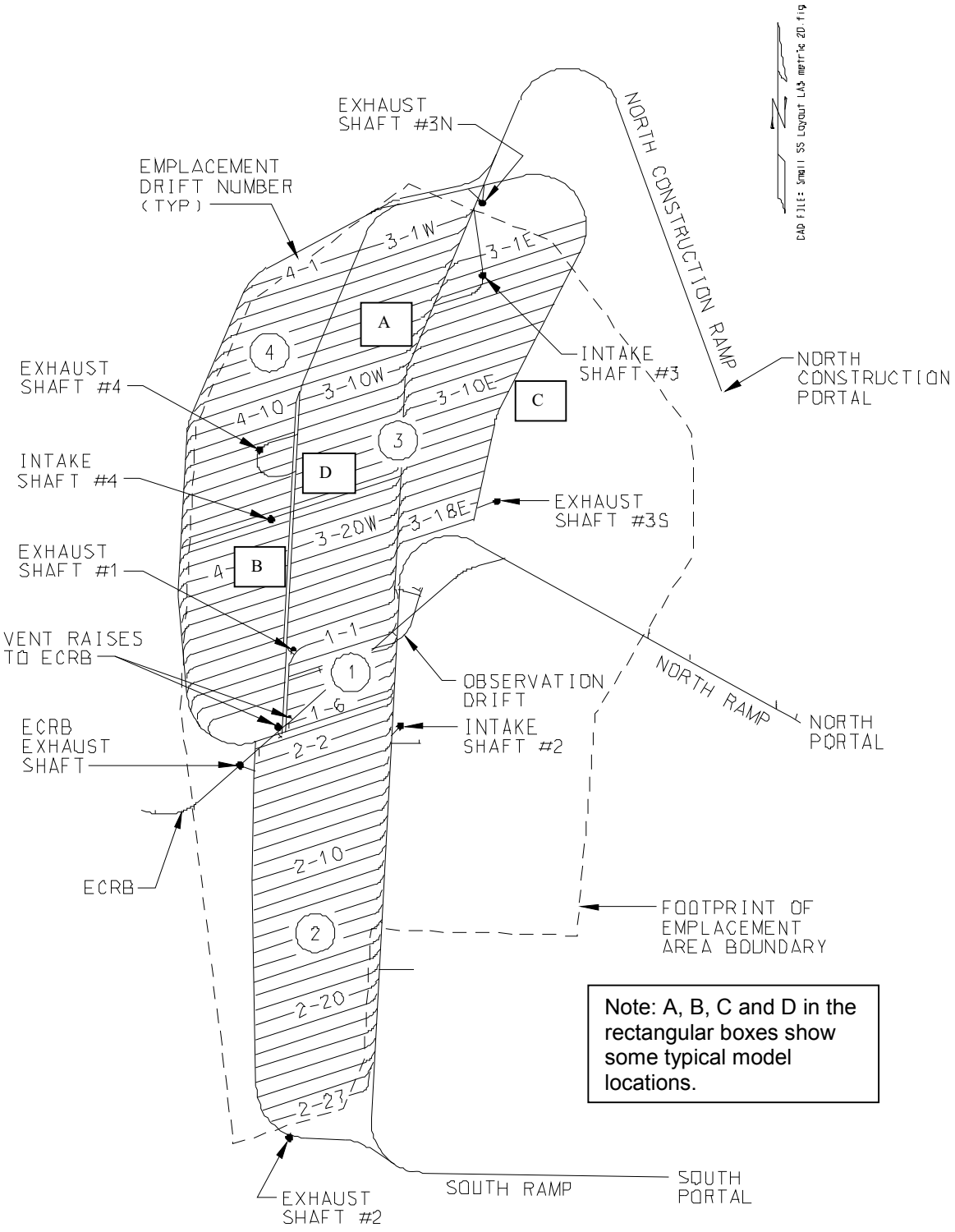

Source: Reference 2.2.37, Figure 11.

Figure 6-3 Underground Layout and Panel Configuration

Source: Reference 2.2.20, Figure 10(b)

Figure 6-4 Lithophysae and Fracturing in the Tptpll Unit

Source: Reference 2.2.20, Figure 8

Figure 6-5 Fractures in the Wall of the ECRB Cross Drift in the Tptpmn Unit

6.3 GROUND SUPPORT FUNCTIONAL REQUIREMENTS

Ground support design for non-emplacement drifts has the following functional and performance requirements:

- Ensure the stable conditions for personnel and environmental safety during construction and throughout the preclosure period (Reference 2.2.20, Section 7.3)
- Account for the appropriate worst possible case in terms of combinations of in situ, thermal, seismic, construction, and operation loads (Reference 2.2.29, Section 4.5.2.1)
- Prevent for rock falls that could potentially result in personnel injury (Reference 2.2.29, Section 4.5.2.2)
- Interface with TSPA to ensure general acceptance of committed ground support materials (Reference 2.2.29, Section 4.5.2.12)
- Accommodate the maintenance of accessible non-emplacement openings (Reference 2.2.29, Section 4.5.2.14)
- For non-accessible non-emplacement areas, ground support is to be designed to function without planned maintenance during the operational life, while providing for the ability to perform unplanned maintenance on as-needed basis (Reference 2.2.29, Section 4.5.2.13)
- Use the site-specific geotechnical data that are obtained from rock at Yucca Mountain (Reference 2.2.29, Section 4.5.2.7)
- Interface with the subsurface development and emplacement drift subsystems to accommodate opening orientation, configuration, and excavated opening sizes (Reference 2.2.29, Section 4.5.2.11).

6.4 EMPIRICAL METHODS

6.4.1 Introduction

Empirical methods are usually applicable to designing tunnels in mining and civil engineering. The empirical approach relies on rock mass classification systems. To date, many rock mass classification systems have been proposed, such as systems by Deere and Deere (Reference 2.2.38), Wickham et al. (Reference 2.2.57), Bieniawski (Reference 2.2.19), Barton et al. (Reference 2.2.16), and Barton (Reference 2.2.17). Two common classification systems were recommended in the *Drift Design Methodology and Preliminary Application for the Yucca Mountain Site Characterization Project* (Reference 2.2.42, p. 6-6) and in the *Support of Underground Excavations in Hard Rock* (Reference 2.2.43, p. 44). These two classification systems are the RMR value developed by Bieniawski (Reference 2.2.19), and the Q value developed by Barton (Reference 2.2.17). Both methods incorporate geological, geometric and design/engineering parameters in arriving at quantitative value of their rock mass quality

(Reference 2.2.43, p. 44). The latter system was used in designing the ESF, and the successful performance of that facility has lead to adoption of this system for analysis of ground control elements for SR (Reference 2.2.21, p. 50). These two classification systems are briefly described in the following sections. A detailed description of them can be found in Bieniawski (Reference 2.2.19) and Barton et al. (Reference 2.2.16), respectively.

6.4.2 Empirical Analysis of Ground Support Needs

Results of the empirical analysis based on the RMR and Q approaches for non-emplacement drifts in the nonlithophysal rock are presented in the following paragraph. Note that the empirical analysis is only considered for access/exhaust mains, turnouts, intersections between access mains and emplacement drift turnouts, and intersections between exhaust mains and emplacement drifts, which comprise the majority of non-emplacement drifts; observation drift, TBM launch chambers, and portals are not included in empirical analysis. The methods used are described in Sections 4.3.1.1 and 4.3.1.2.

Based on the RMR approach, the ground support needs for the nonlithophysal rock in non-emplacement drifts can be estimated based on Table 4-2. First, RMR values are calculated from E_m (elastic modulus) values shown in Table 6-10 based on Eq. 4-1. It needs to be noted that RMR values are not available, so the correlation between RMR and E_m is used. Table 6-10 shows the RMR values (under third column) for rock mass categories 1 to 5.

By comparing RMR values for various rock mass categories shown in Table 6-2 with those in Table 4-2, the following ground support needs are estimated: bolt lengths range from 3 m in the good rock (categories 3-5) to 4 m in the fair rock (categories 1-2). Bolt spacing ranges from 2.5 m in the good rock to 1.5 - 2 m in the fair rock. In the good rock, 50-mm of shotcrete is recommended in crown where required. In the fair rock, 50-100 mm of shotcrete in crown with 30-mm in the sides is recommended. It should be noted that Bieniawski's recommendations for ground support shown in Table 4-2 was based on a 10-m wide, horseshoe-shaped tunnel (Reference 2.2.18, Table 6.11). Because this span is larger than those of the excavations outside the intersection, and because the support was designed for a civil application, the estimated ground support needs are considered very conservative for use at Yucca Mountain.

For the NGI Rock Mass Classification approach, Q values for various rock mass categories need to be calculated. The following steps are needed for estimating the Q values:

- Calculate the RMR values (note that RMR values are already calculated, see Table 6-10).
- Determine the unconfined compressive strength (σ_c) of intact nonlithophysal rock (Tptpmn), which is about 165 MPa (Reference 2.2.36, Table 6-9).
- Estimate the major principal stress (σ_1) of rock adjacent to non-emplacement drifts, which is estimated to be about 20 to 53 MPa (Section 6.5.3.1).
- Calculate the ratio σ_c/σ_1 to be in the ranges of 3 to 8.

- Assign SRF value according to Table 4.6 of the *Support of Underground Excavations in Hard Rock* (Reference 2.2.43, p. 43). A SRF value ranging from 0.5 to 2 is considered adequate for the purpose of empirical analysis.

Based on Eq. 4-3 and *Jw* of 1, Q values are calculated for rock mass categories 1 to 5 and listed in Table 6-10 (under fifth column). The lengths of rock bolts calculated based on Eq. 4-4 for various roof spans and ESR values are shown in Table 6-11. Note that equivalent dimension, D_e, is obtained by dividing the span, B, by ESR (Reference 2.2.43, p. 39).

Table 6-10 RMR and Q Values for Nonlithophysal Rock

Category	E_m (GPa)	RMR	SRF	Q
1	10.59	51	0.5 – 2.0	1.09 – 4.35
2	16.79	59	0.5 – 2.0	2.65 – 10.59
3	19.95	62	0.5 – 2.0	3.69 – 14.78
4	28.18	68	0.5 – 2.0	7.20 – 28.78
5	35.48	72	0.5 – 2.0	11.22 – 44.89

Table 6-11 Equivalent Dimension D_e and Bolt Length for Various Openings

Opening Types	Span (m)	ESR	D_e (m)	Bolt Length (m)
Access and Exhaust Mains	7.62	1.3	5.9	2.4
Turnout	5.5	1.3	4.2	2.2
Intersection between Access Main and Turnout	22.0	1.0	22.0	5.3
Intersection between Exhaust Main and Emplacement Drift	12.7	1.0	12.7	3.9

Figure 6-6 through Figure 6-9 are plots of ground support needs for various rock mass categories for access/exhaust mains, turnouts, intersection between access main and turnout, and intersection between exhaust main and emplacement drift, respectively. These plots are derived based on Q and D_e values listed in Table 6-10 -and Table 6-11, respectively.

Based on these figures, the estimated ground support needs can be summarized as follows:

- For access and exhaust mains: bolt length - 2.4 m, bolt spacing - 1.8 m to 2.5 m, unreinforced shotcrete - 40 to 50 mm thick for category 1 rock whereas none to 45 mm thick for categories 2 to 4 rock, and no shotcrete for category 5 rock.

- For turnouts: bolt length - 2.2 m, bolt spacing - 1.8 m to 2.5 m, unreinforced shotcrete - 40 to 50 mm thick for category 1 rock whereas none to 45 mm thick for categories 2 to 3 rock, and no shotcrete for category 4 and 5 rock.

- For intersections between access mains and turnouts: bolt length – 5.3 m, bolt spacing - 1.8 m to 2.7 m, fiber-reinforced shotcrete - 40 to 120 mm thick for categories 1 to 3 rock whereas unreinforced shotcrete none to 90 mm thick for categories 4 and 5 rock.

- For intersections between exhaust mains and emplacement drifts: bolt length – 3.9 m, bolt spacing - 1.8 m to 2.7 m, fiber-reinforced shotcrete - 40 to 90 mm thick for

categories 1 to 3 rock whereas unreinforced shotcrete none to 90 mm thick for categories 4 and 5 rock.

As discussed in Section 6.2, typical rock conditions in nonlithophysal rock (Tptpmn) are approximately close to fair and good (Geomechanics RMR approach, see Table 4-2) or support categories 3 and 4 (NGI Q approach, see Figure 4-1). Therefore, by comparing the recommendations made by both RMR and Q approaches, use of pattern bolting with 3 m long, spaced at 1.25 to 1.5 m, in conjunction with 30 to 50 mm thick shotcrete is considered adequate for access and exhaust mains. Note that since use of shotcrete is only designed for intersections in non-emplacement drifts, use of shotcrete in access and exhaust mains is replaced by the heavy duty welded wire fabric. For ground support in turnouts, which are inaccessible non-emplacement openings with potential high radiation due to the passage of the waste package loaded transport and emplacement vehicle (TEV), stainless steel friction-type rock bolts and stainless steel welded wire fabric (WWF) are considered adequate. For ground support needs at intersections, use of pattern bolting with bolt length of 5 m, spaced at 1.25 to 1.5 m, and in conjunction with 100 mm thick steel fiber-reinforced shotcrete is considered adequate.

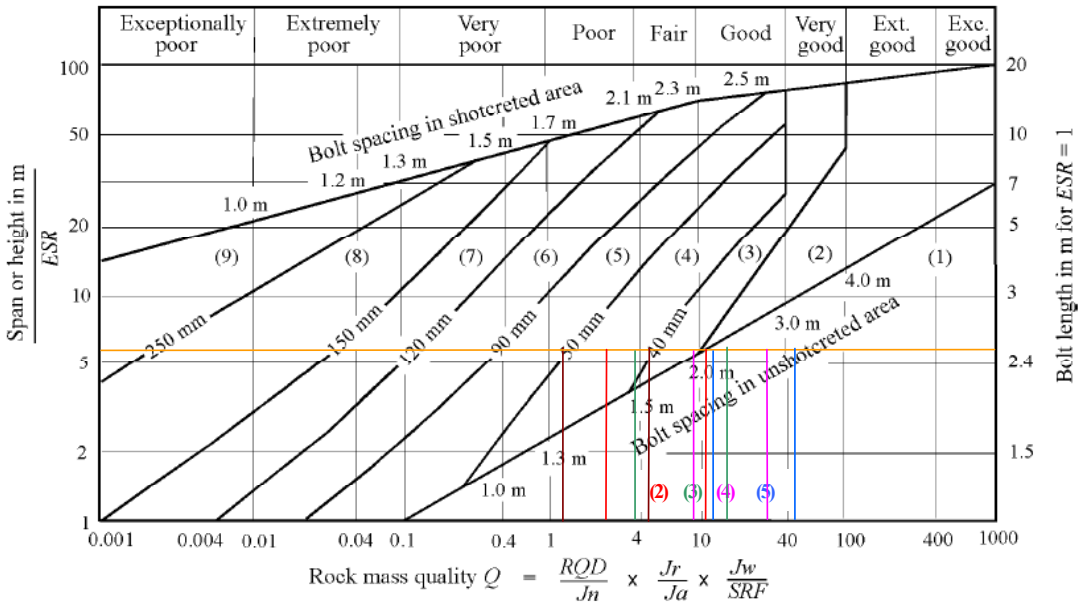

REINFORCEMENT CATEGORIES

1) Unsupported
2) Spot bolting
3) Systematic bolting
4) Systematic bolting with 40-100 mm unreinforced shotcrete
5) Fibre reinforced shotcrete, 50 - 90 mm, and bolting
6) Fibre reinforced shotcrete, 90 - 120 mm, and bolting
7) Fibre reinforced shotcrete, 120 - 150 mm, and bolting
8) Fibre reinforced shotcrete, > 150 mm, with reinforced ribs of shotcrete and bolting
9) Cast concrete lining

Figure 6-6 Ground Support Needs for Access and Exhaust Mains

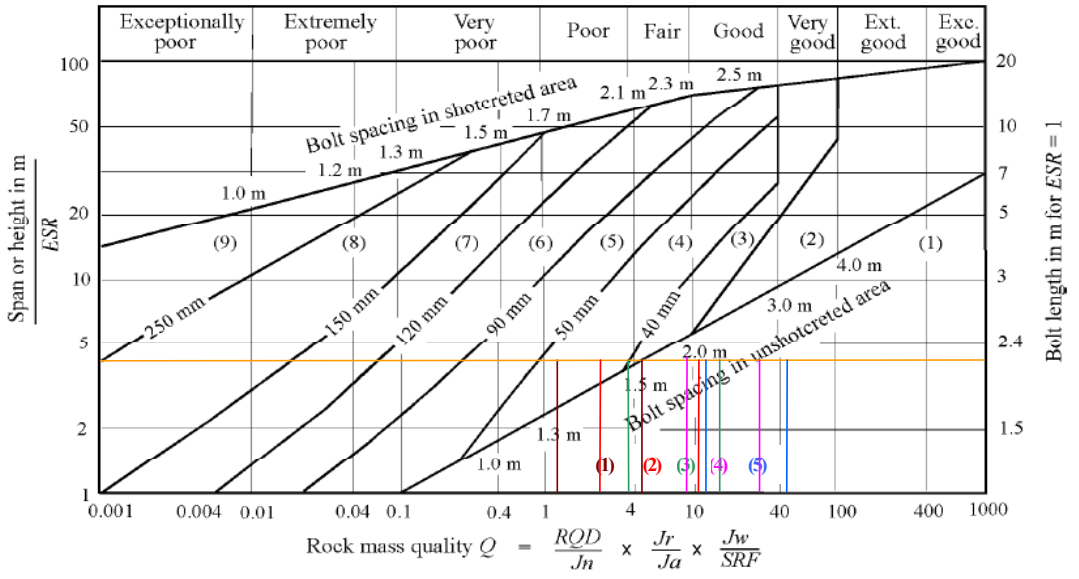

REINFORCEMENT CATEGORIES

1) Unsupported
2) Spot bolting
3) Systematic bolting
4) Systematic bolting with 40-100 mm unreinforced shotcrete
5) Fibre reinforced shotcrete, 50 - 90 mm, and bolting
6) Fibre reinforced shotcrete, 90 - 120 mm, and bolting
7) Fibre reinforced shotcrete, 120 - 150 mm, and bolting
8) Fibre reinforced shotcrete, > 150 mm, with reinforced ribs of shotcrete and bolting
9) Cast concrete lining

Figure 6-7 Ground Support Needs for Turnouts

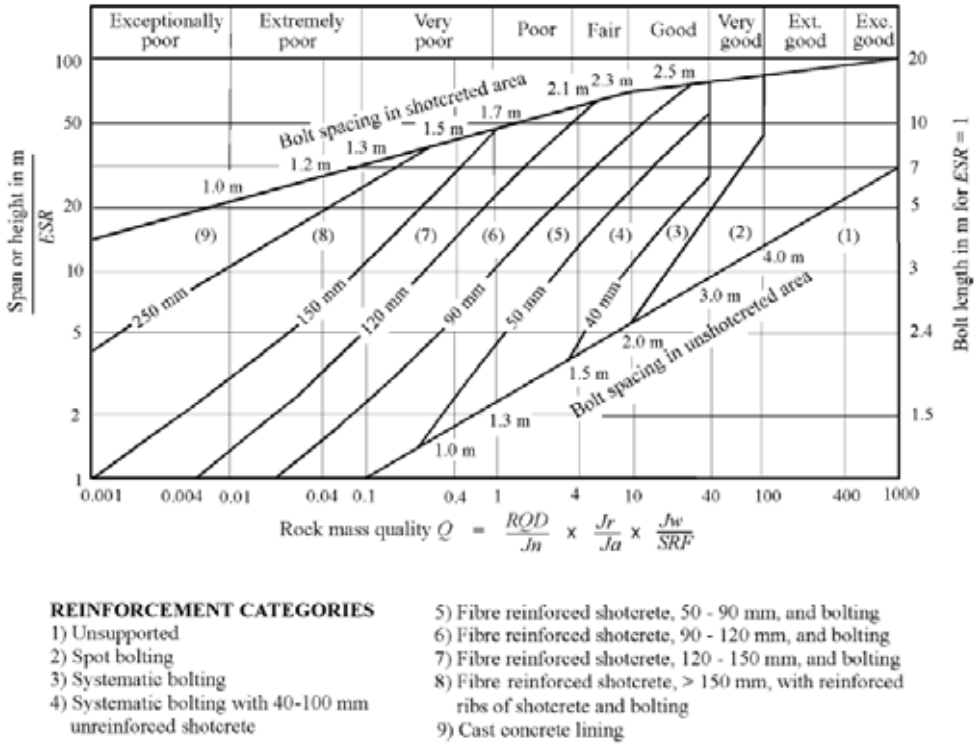

REINFORCEMENT CATEGORIES

1) Unsupported
2) Spot bolting
3) Systematic bolting
4) Systematic bolting with 40-100 mm unreinforced shotcrete
5) Fibre reinforced shotcrete, 50 - 90 mm, and bolting
6) Fibre reinforced shotcrete, 90 - 120 mm, and bolting
7) Fibre reinforced shotcrete, 120 - 150 mm, and bolting
8) Fibre reinforced shotcrete, > 150 mm, with reinforced ribs of shotcrete and bolting
9) Cast concrete lining

Figure 6-8 Ground Support Needs for Intersection between Access Main and Turnout

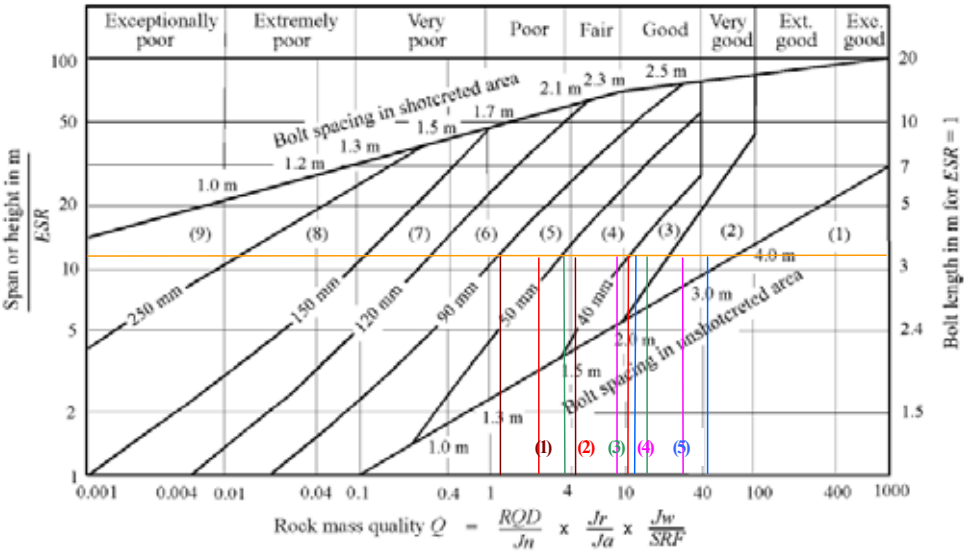

REINFORCEMENT CATEGORIES

1) Unsupported
2) Spot bolting
3) Systematic bolting
4) Systematic bolting with 40-100 mm unreinforced shotcrete
5) Fibre reinforced shotcrete, 50 - 90 mm, and bolting
6) Fibre reinforced shotcrete, 90 - 120 mm, and bolting
7) Fibre reinforced shotcrete, 120 - 150 mm, and bolting
8) Fibre reinforced shotcrete, > 150 mm, with reinforced ribs of shotcrete and bolting
9) Cast concrete lining

Figure 6-9 Ground Support Needs for Intersection between Exhaust Main and Emplacement Drift

6.5 ANALYTICAL METHODS

The computer modeling techniques serve as an analytical basis for assessing the opening shape and determining the general stress distribution around the tunnel opening in underground design. In repository ground support design, numerical analyses will play an important role in determining and evaluating the effects of the seismic and thermal loading conditions.

For the non-emplacement drift ground support analysis, a series of computer analyses are conducted and presented here to simulate the in situ, seismic, and/or thermal loading conditions. An in situ thermal test has been completed in the ESF to provide an experimental basis for evaluating the thermal-hydrological-geomechanical-geochemical behavior at the site. The response of the host rock and ground support components to temperatures higher than the anticipated operating temperature in the repository provides knowledge about the response of the surrounding rock and the ground support components when subjected to high temperatures. A summary of observations and discussions from the drift scale test is given in the Ground Support Maintenance Plan (Reference 2.2.31, Section 6.1.3)

The methodology on analytical methods for non-emplacement drift stability was presented in Section 4.3.2. This section presents the details on modeling, boundary and loading conditions, and the results of analyses.

6.5.1 Modeling of Non-Emplacement Drifts

6.5.1.1 Modeling of Access and Exhaust Mains and Turnouts

For non-emplacement drifts such as access mains, exhaust mains, and turnouts, which have relatively large distance in the longitudinal axis compared to its cross-sectional area, a two-dimensional computer modeling is appropriate. A two-dimensional continuum approach will be used for the ground support design calculation for these openings. This is considered adequate and consistent with the conventional practice in mining or tunneling industry.

In a continuum modeling approach, the geologic features, such as fractures or lithophysae, in the rock mass are “lumped” into a thermomechanical constitutive model that represents the overall equivalent effect of these features. In a discontinuum modeling approach, fractures or lithophysae are modeled explicitly as interfaces or cavities. The difference between these techniques is therefore the level of detail that is necessary in the model to adequately capture the deformation and failure mechanisms (Reference 2.2.20, Section 5.3.1). From a ground support design perspective, stability of non-emplacement drifts is judged by overall rock mass displacements and stresses. Two-dimensional continuum approach that uses equivalent rock mass properties and constitutive model may provide good tools for bounding analyses and also allow ease of parametric examination and model interpretation. Therefore, it is appropriate for use in ground support design related analyses.

The FLAC computer code is employed in the two-dimensional analyses. In FLAC models, rock mass properties that reflect the effects of lithophysae and fractures on rock mass properties are used. These property values are presented in Table 6-1 and Table 6-2 for the lithophysal and nonlithophysal rocks, respectively. The behavior of rock mass is judged using the Mohr-Coulomb yield criterion. Figure 6-10 illustrates the configuration of a FLAC model for access

and exhaust mains. The vertical dimension of the model is 100 m, and the horizontal is 60 m. Figure 6-11 shows the FLAC model for turnouts with rock bolts installed. Determination of the model dimension depends on requirements on accuracy and computational efforts. In general, the boundary effect is negligible if the model dimension is at least five times the size of an opening to be analyzed.

6.5.1.2 Modeling of Intersections between Access Mains and Turnouts and between Exhaust Mains and Emplacement Drifts

Because the geometry of the intersections is three-dimensional, the numerical analysis was conducted using the three-dimensional code 3DEC. Note that 3DEC is a discontinuum code, but in the simulations of intersections, the blocks were glued together to behave effectively as a continuum. Thus, the local stability of blocks created by joints around the excavation was not considered.

The geometries of typical intersections of access mains and turnouts, such as at location A and hereinafter called as intersection A as represented in the 3DEC model (showing the tunnels only, i.e., the surrounding rock mass is hidden) is shown in Figure 6-12. The locations of the vertical section planes and profiles in which some of the results are presented are indicated in the figures. The access main has a circular cross-section with a diameter of 7.62 m. The turnout has a horseshoe shape in the cross-section of 8 m wide and 7 m high. The floors of the two tunnels are at the same elevation. The dimensions of the entire model for both locations are 200 m × 200 m in plan and 100 m in height. The geometry of the entire 3DEC model for intersection A is shown in Figure 6-13.

It should be noted that the current turnout layout configuration is slightly different from what was shown in Figure 6-12 and Figure 6-13. The so-called “turnout” has been divided into various segments, such as TEV alignment segment, turnout curve, launch chamber, turnout bulkhead segment, and rail turnout segment (Reference 2.2.35, Table 5). In this calculation, it is still referred to as turnouts in general to simplify the discussion, unless noted otherwise. In addition, the orientations of access mains and their intersecting turnouts remain the same as in the past. Although the size of a major portion of turnout, i.e., TEV alignment segment and turnout curve, is smaller and circular-shaped (5.5-m diameter), the opening sizes and shapes at the intersections and their immediate vicinity in the current layout remain very similar to those presented in Figure 6-13. Using the model with layout configurations as shown in Figure 6-12 and Figure 6-13 will generate conservative results.

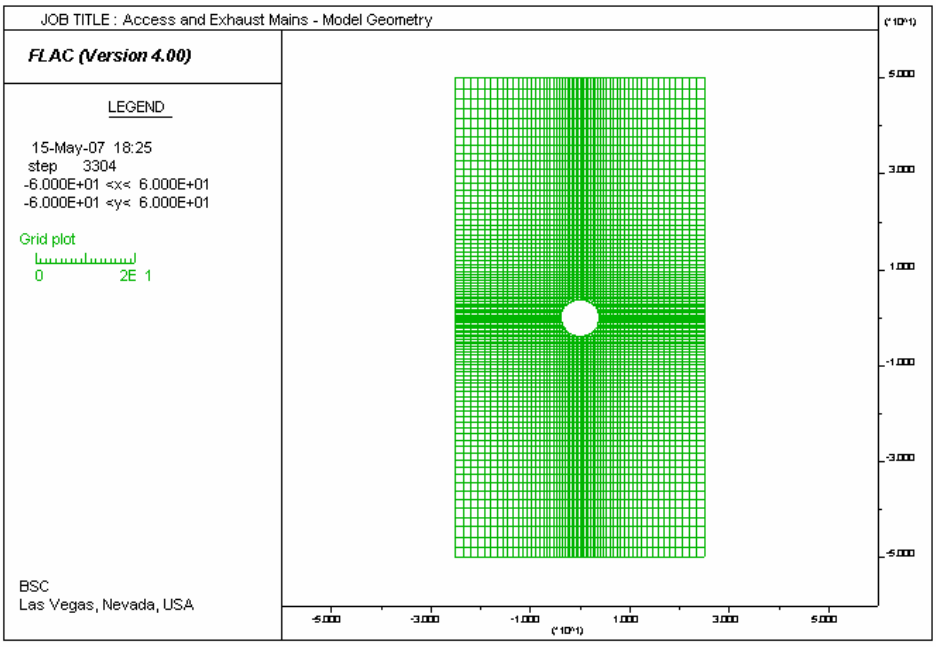

Figure 6-10 FLAC Model of Access and Exhaust Mains

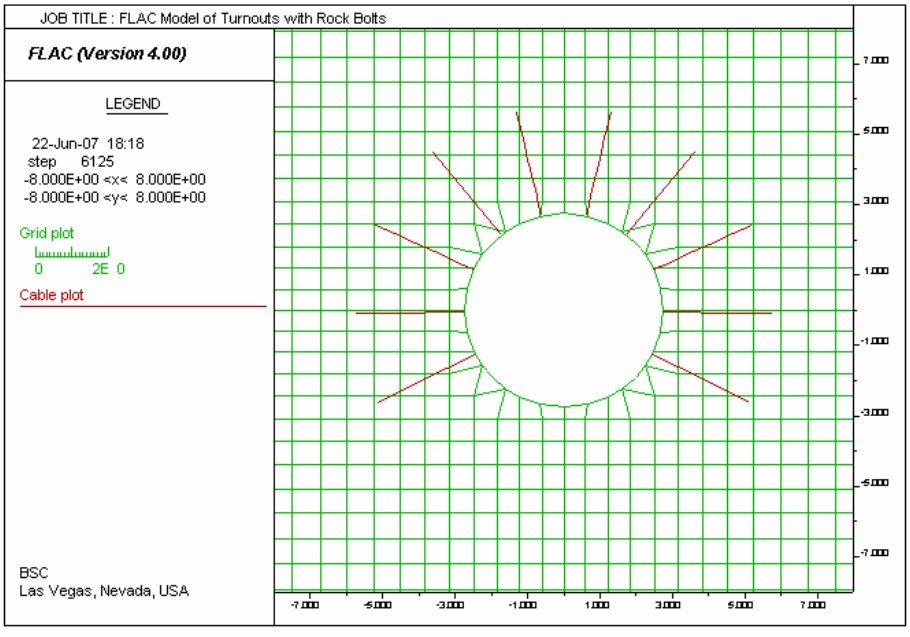

Figure 6-11 A Close-up of the FLAC Model of Turnouts with Rock Bolts

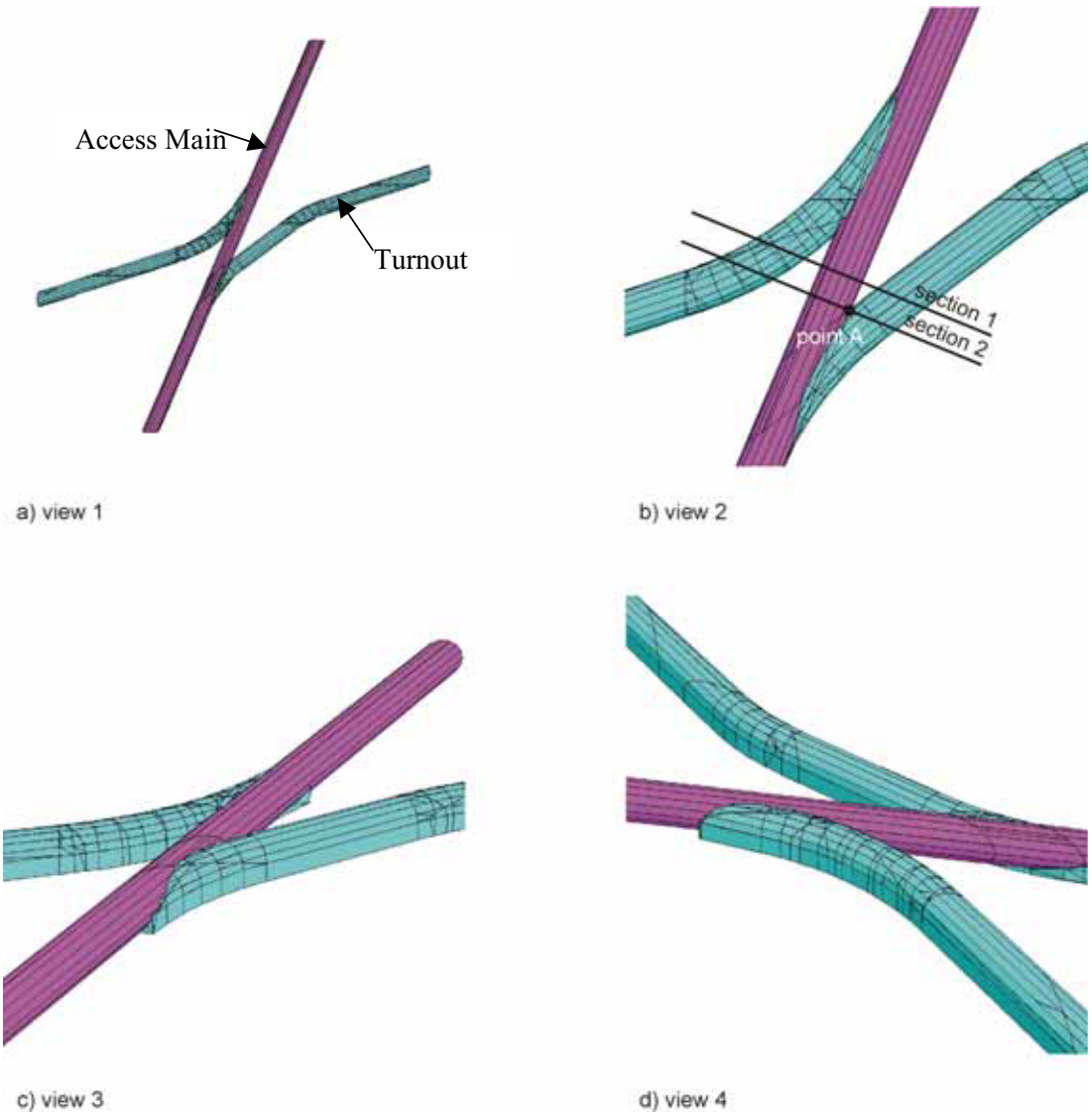

Note: The distance between sections 1 and 2 is 6.2 m.

Figure 6-12 3DEC Model Representation of Intersection A

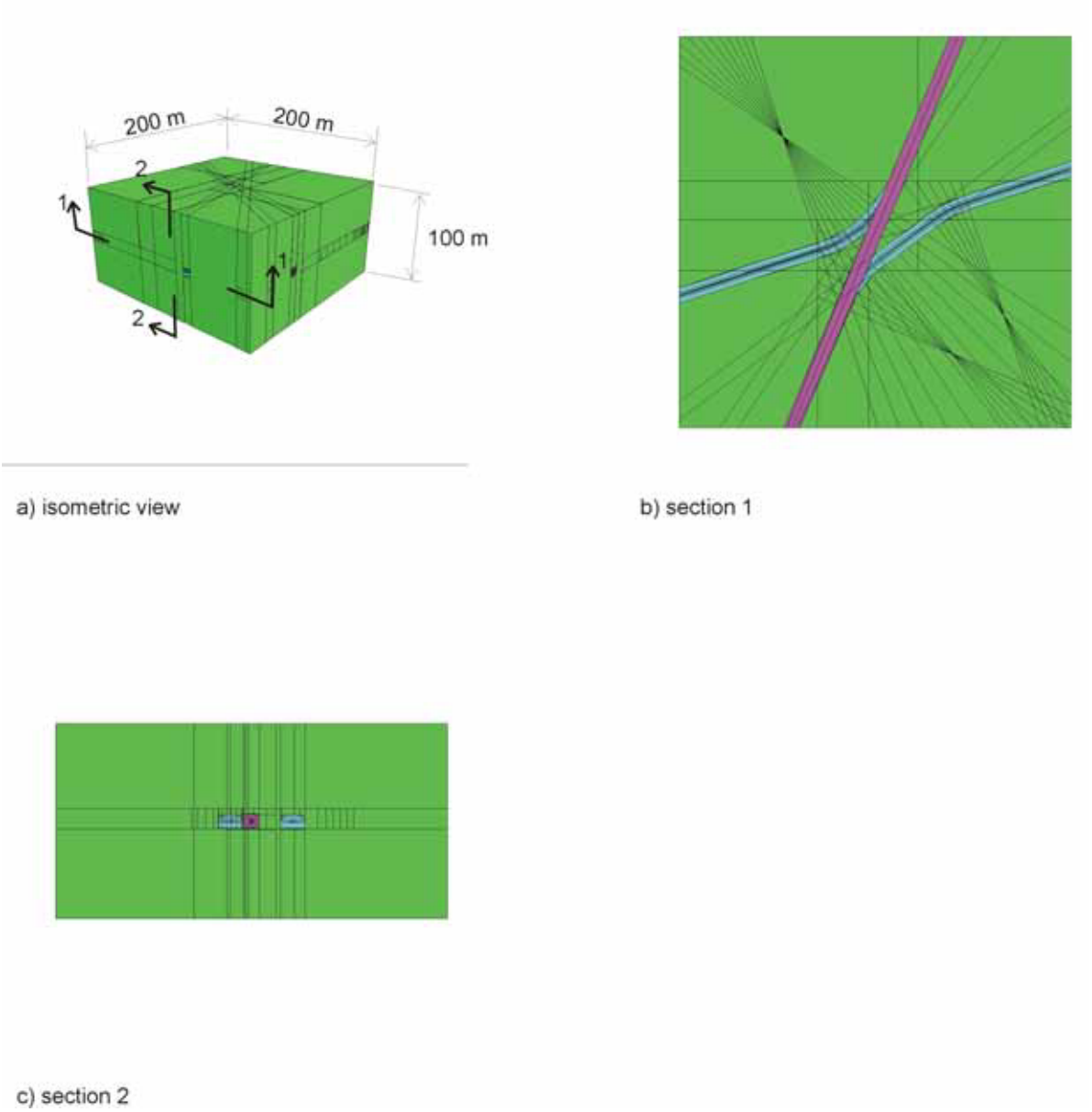

Figure 6-13 3DEC Model Geometry and Dimension for Intersection A

The model geometries for locations B and C (See Figure 6-3, referred hereafter as intersections B and C, respectively) for intersections of exhaust mains and the emplacement drifts are shown in Figure 6-14 and Figure 6-15. In both cases, the model size is 200 m × 81 m in plan and 100 m in height. The typical dimension for exhaust main is 7.62m except in Panel 1 of the repository, where it is 5.5 m. However, throughout the analyses, the diameter of the exhaust main used in the model is 7.62 m, which is conservative (resulting in larger spans) with regard to stability of the excavations.

6.5.1.3 Modeling of Observation Drift

Two geometrical configurations of the observation drift were analyzed. A typical cross-section when the observation drift is parallel to the emplacement drift is analyzed using a two-dimensional FLAC model. The geometry of the model and computational mesh are shown in Figure 6-16 and Figure 6-17. The intersection of the observation drift with the exhaust main, accounting also for the interaction with the nearest emplacement drift, is analyzed in a three-dimensional 3DEC model. The geometry of the observation drift in the intersection with exhaust main and the geometry of the 3DEC model are shown in Figure 6-18 and Figure 6-19.

6.5.1.4 Modeling of TBM Launch Chamber

The TBM launch chamber was analyzed using a two-dimensional FLAC model. Figure 6-20 shows the geometry and grid of the model in a cross-section normal to the chamber axis. Note that the stability analysis for the TBM launch chamber is only performed for the large opening as shown in this figure. The results of analysis on this large opening is conservative for the smaller TBM launch chamber adjacent to turnouts.

6.5.1.5 Modeling of North Portal

Figure 6-21 shows isometric and plan views of the 3DEC model of the North Portal. The model was constructed based on available topographical information and cross-sections of the portal region. Cross-sections C_1-C_1' and L-L', indicated in Figure 6-21, are shown in Figure 6-22(a) and Figure 6-22(b).

6.5.1.6 Modeling of Interburden Pillar between Shaft Access and Exhaust Mains

The location of the 3DEC model for interburden pillar between shaft access and exhaust mains is shown in location D in Figure 6-3. At this location, the access drift to #4 intake shaft overlies the two parallel exhaust mains. In plan view, the first drift intersects with the two exhaust mains. From three-dimensional viewpoint, these three drifts are not intersecting. The interburden between the first drift and the latter two drifts is about 10 m and the diameter of each of these drifts is 7.62 m. The model size is 200 m × 81 m in plan and 100 m in height. Figure 6-23 and Figure 6-24 show the configuration and geometry of the 3DEC model. Note that only unsupported drifts were modeled for this case.

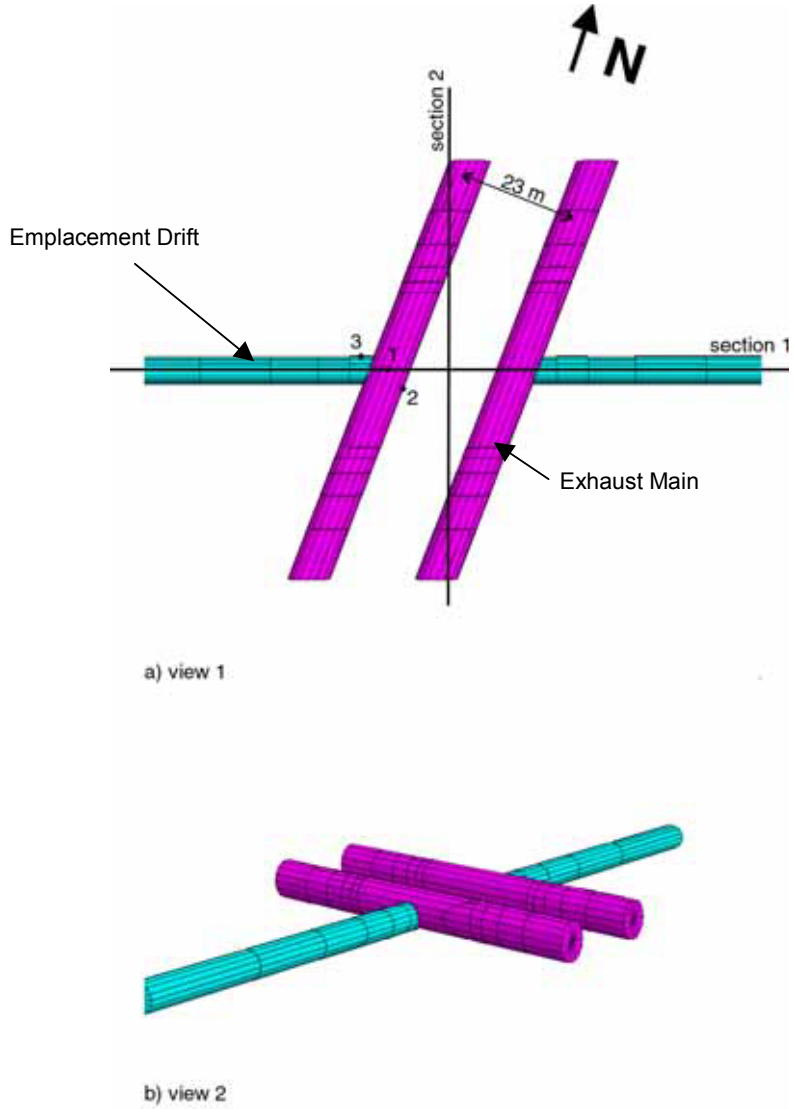

Figure 6-14 Geometry of 3DEC Model for Intersection B

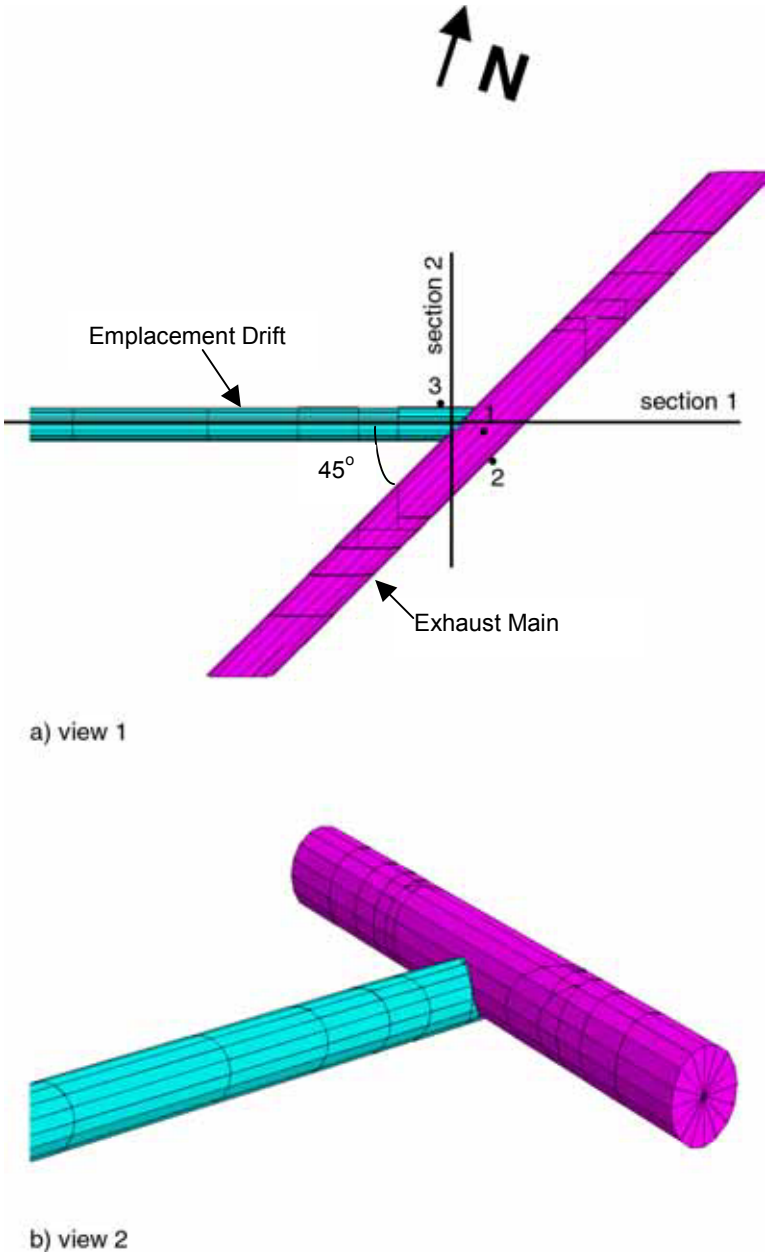

Figure 6-15 Geometry of 3DEC Model for Intersection C

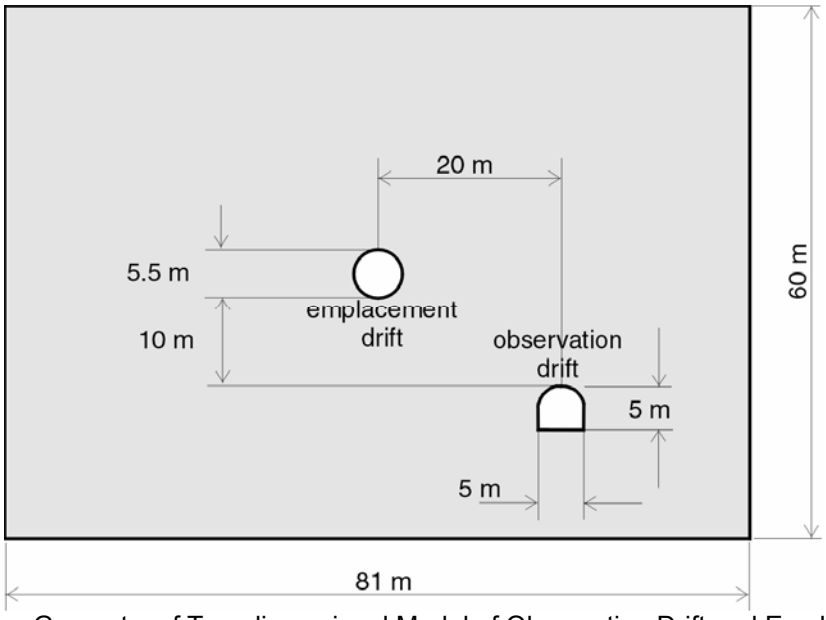

Figure 6-16 Geometry of Two-dimensional Model of Observation Drift and Emplacement Drift

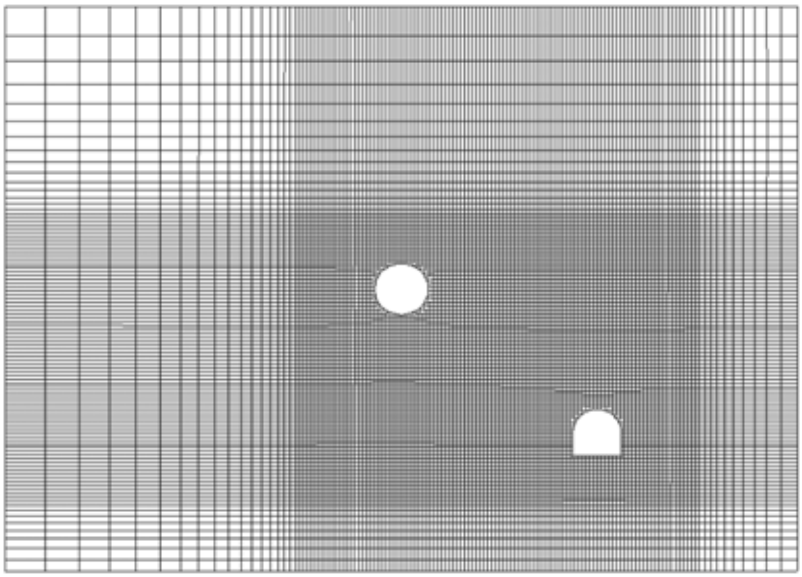

Figure 6-17 Mesh of Two-dimensional Model of Observation Drift and Emplacement Drift

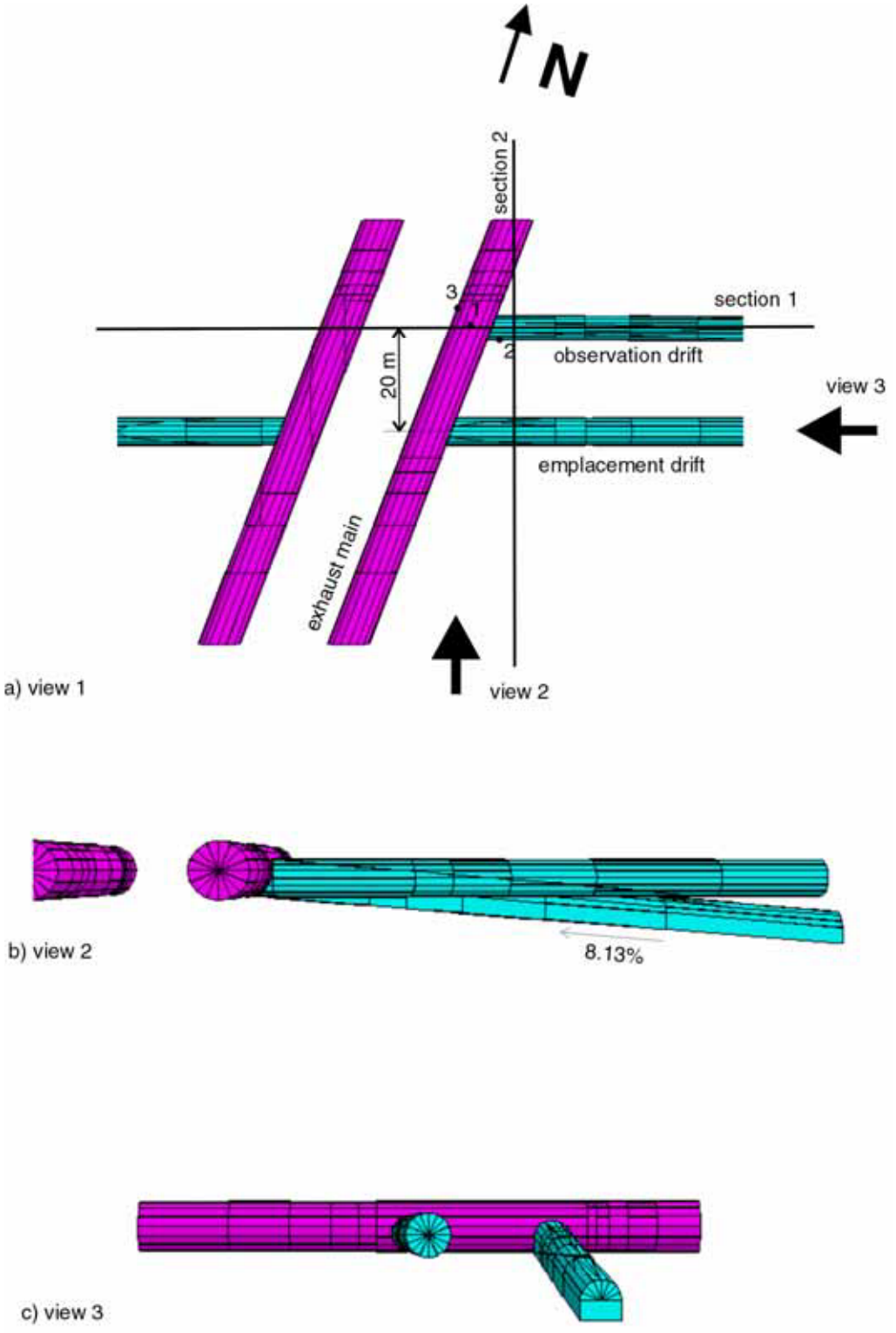

Figure 6-18 Geometry of Intersection of Observation Drift with Exhaust Main

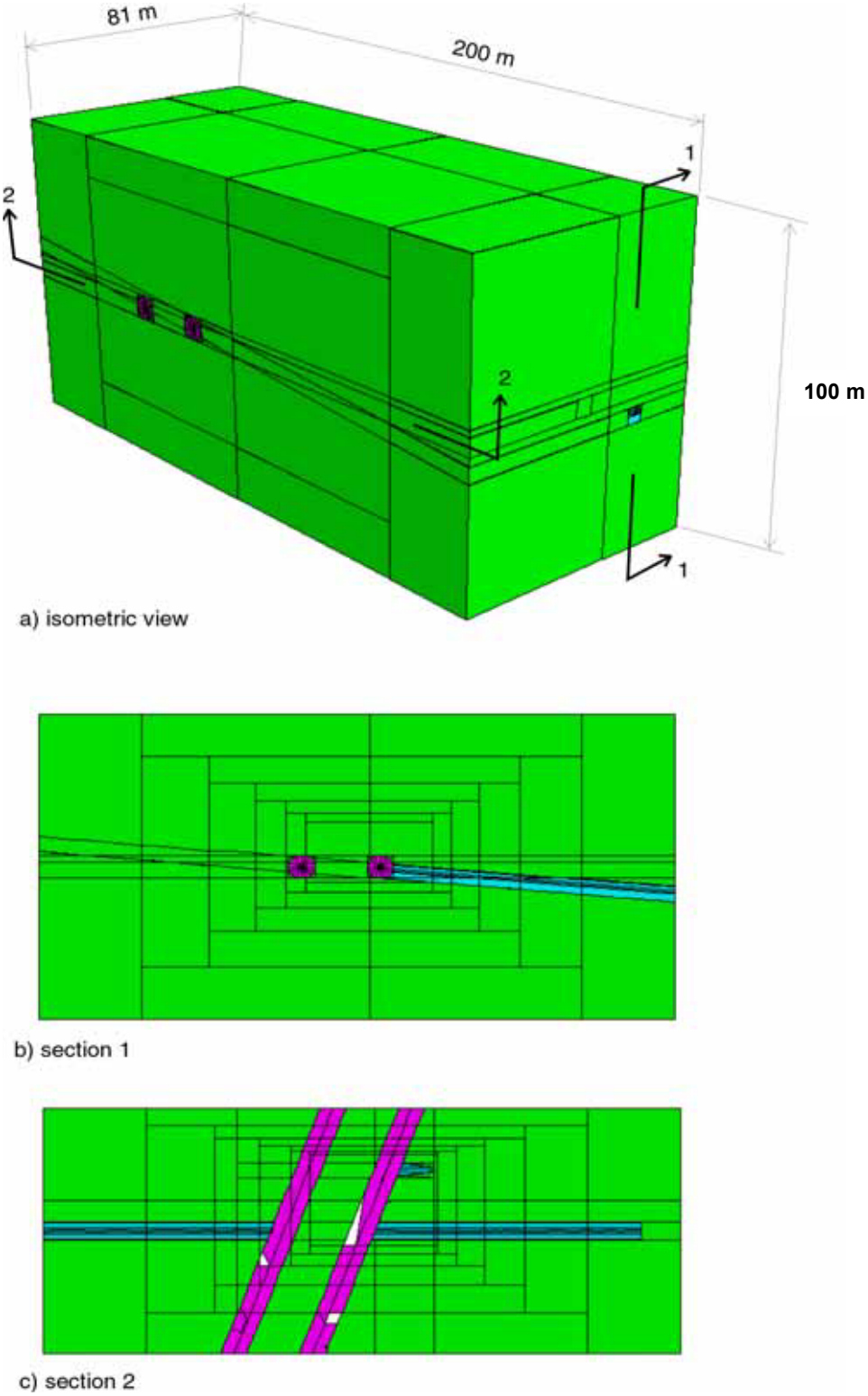

Figure 6-19 Geometry of 3DEC Model for Intersection between Observation Drift and Exhaust Main

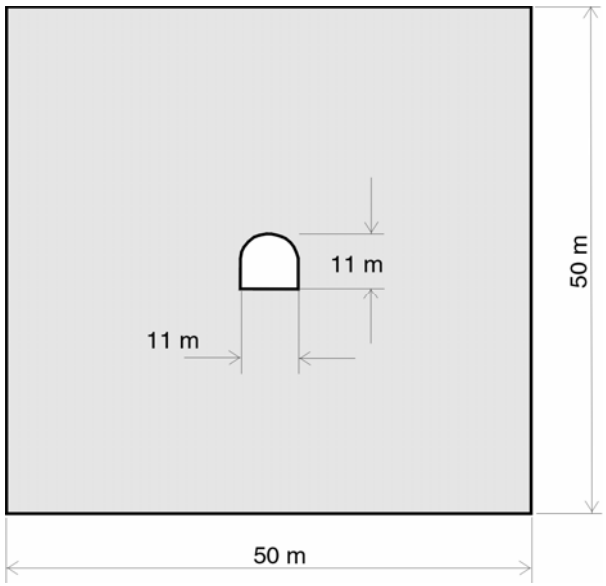

Figure 6-20 Geometry of Two-dimensional Model of TBM Launch Chamber

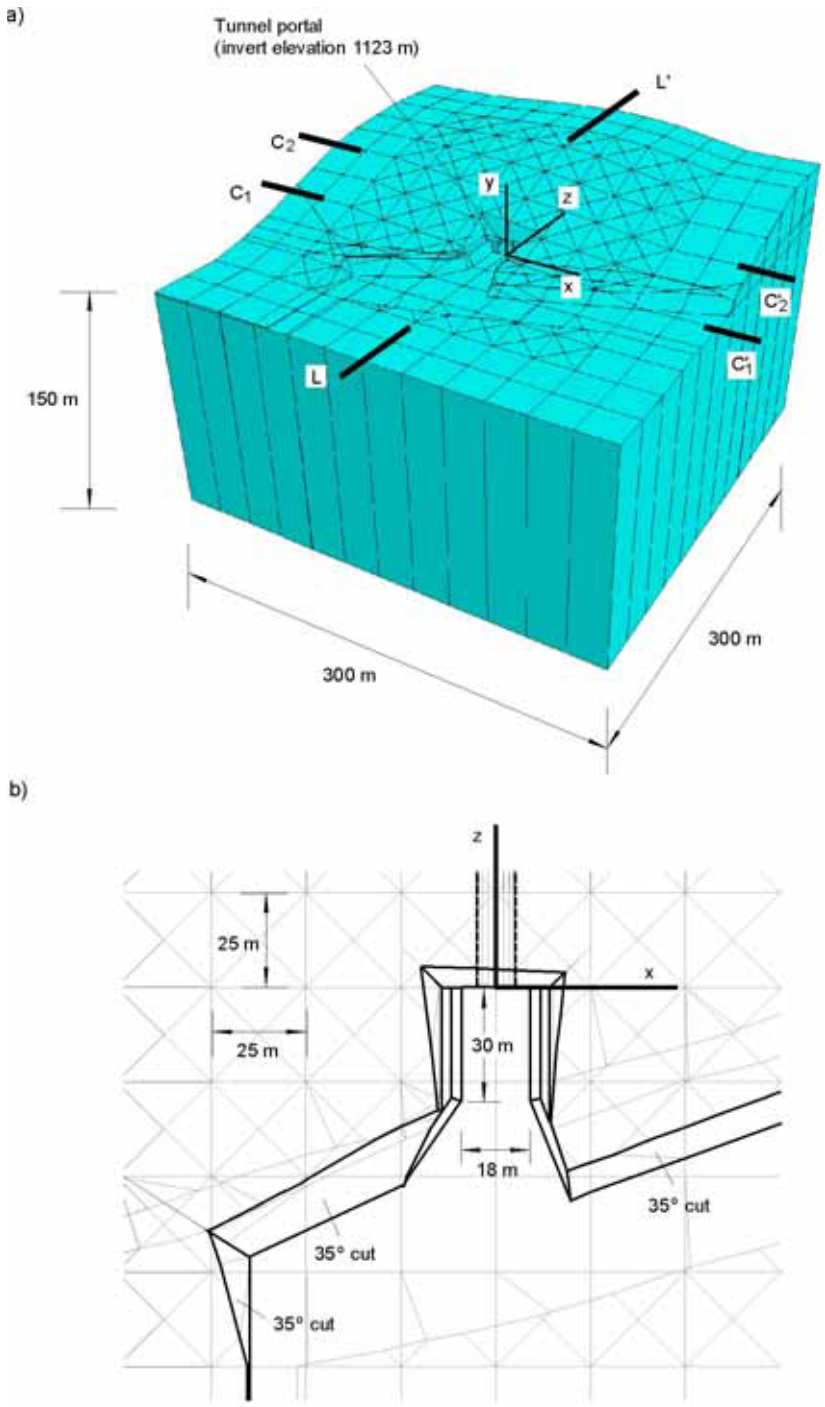

Figure 6-21 a) Isometric and b) Plan Views of North Portal Model

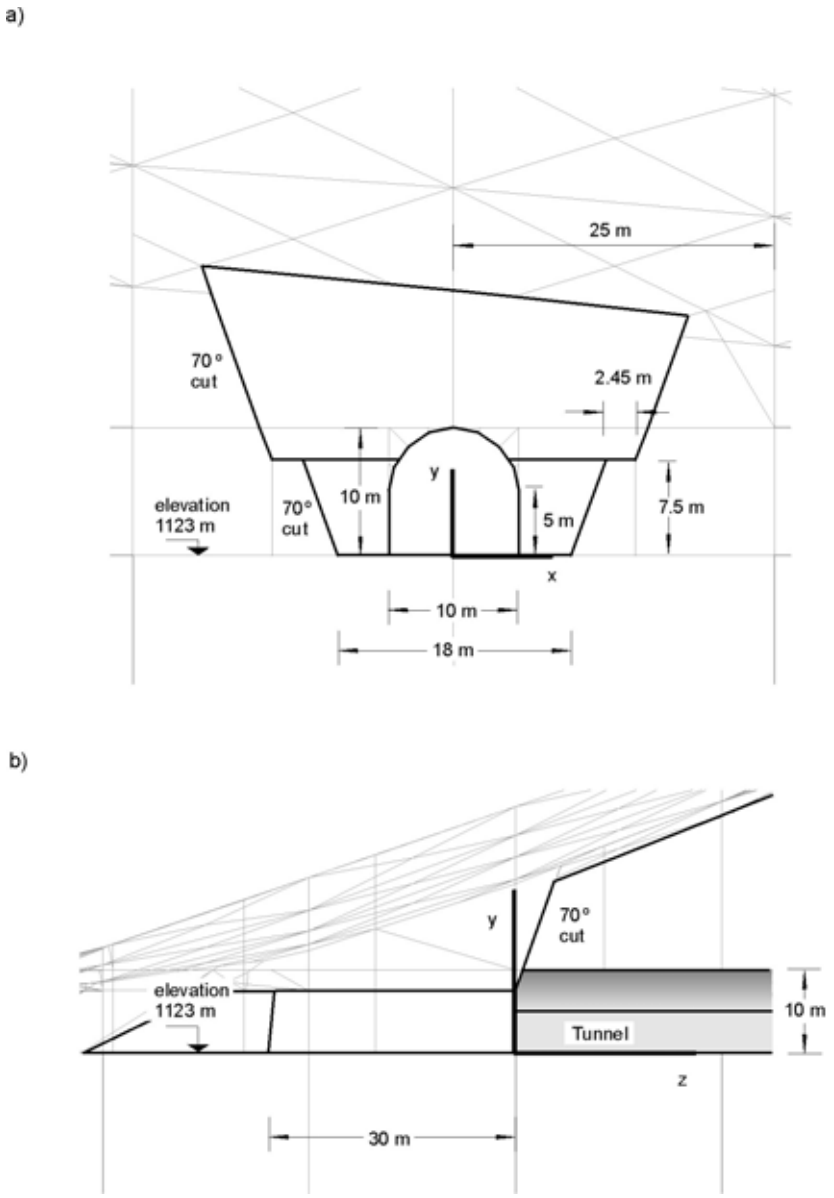

Figure 6-22 a) Frontal Cross-sectional (C1-C1') and b) Longitudinal Cross-sectional (L-L') Views of North Portal Model

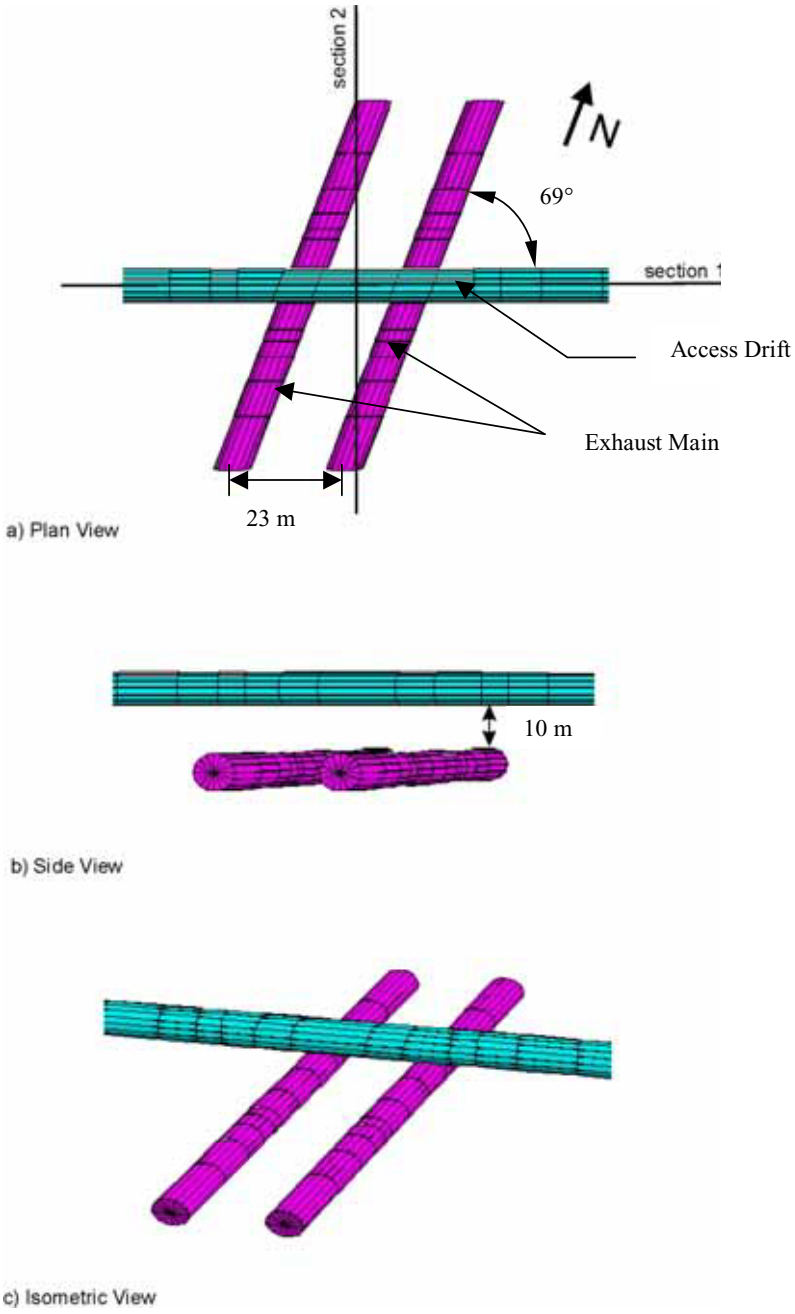

Figure 6-23 Configuration of 3DEC Model for Interburden Pillar between Access Drift to Intake Shaft #4 and Exhaust Mains

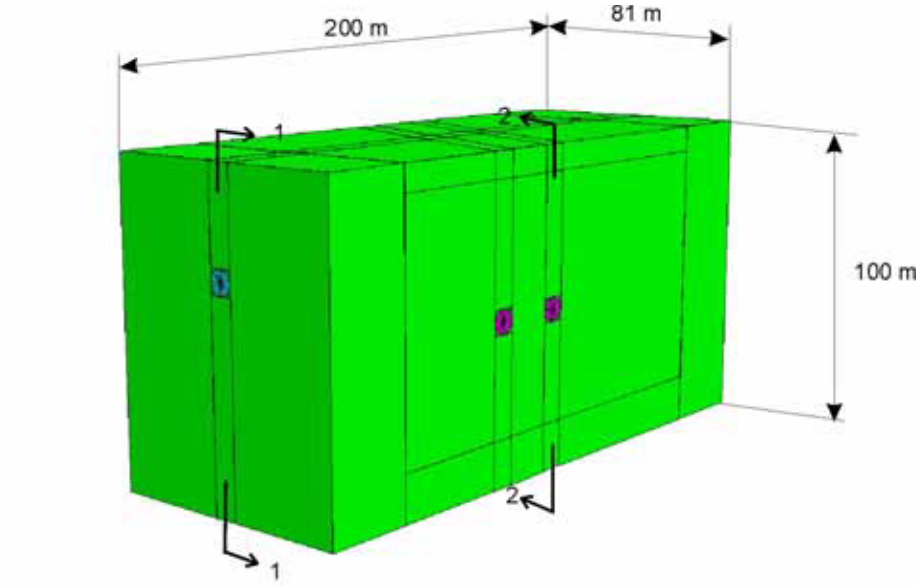

a) isometric view

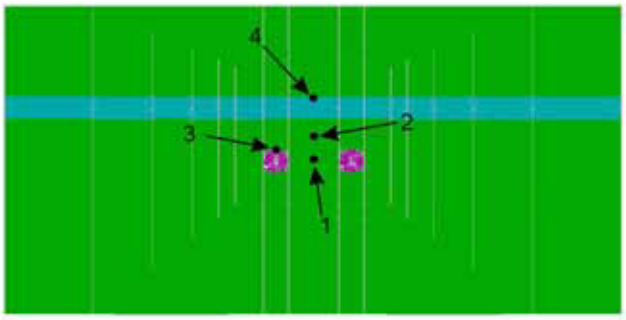

b) section 1

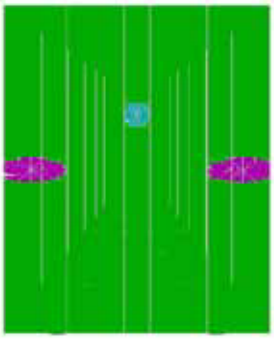

c) section 2

Figure 6-24 Geometry of 3DEC Model for Interburden Pillar between Access Drift to Intake Shaft #4 and Exhaust Mains

6.5.2 Loading and Boundary Conditions

Design loads considered in the evaluation of stability of non-emplacement drifts include in situ, thermal, and seismic stresses.

In designing the repository openings, stresses resulting from various sources are considered: in situ (including excavation effects), construction and operation activities, thermal (nuclear waste), and seismic. In situ stresses exist prior to drift excavation and will be redistributed in the vicinity of openings during repository excavation. The applicability and magnitude of some of the design loads will vary depending on the type of ground support system. Some of the loads, such as thermal loads, will only apply to the final ground support system. In the following sections, a description for each design load type is presented.

6.5.2.1 In Situ Loads

The virgin stress field existing before excavation is the in situ or geostatic state of rock stress. Excavation of repository openings will disturb the surrounding in situ stress field. The stability of the opening will depend on the concentrations of excavation-induced stress and rock mass deformation behavior. For repository openings, computer simulation of the excavation process will be used to assess the stability. In situ stress estimates, opening dimensions, rock mass bulk density, rock mass elastic moduli, and rock mass strength parameters for the failure or yield criteria are required to perform the analyses.

The in situ stress state at the repository has not been measured directly and will vary from location to location. For the initial state of stress, the vertical stress (σ_v) at some point is caused by the overburden weight and is estimated in the following expression (Reference 2.2.41, Eq. 4.1):

$$\sigma_v \quad - \sum_{i\ 1}^{n} \rho_i g h_i \qquad \text{(Eq. 6-6)}$$

where ρ_i (kg/m^3) is average bulk density of the ith layer of rock mass, h_i (m) is thickness of the ith layer of rock mass above an opening, g (m/s^2) is the gravitational acceleration, and n is the total number of overlaying layers of rock mass.

Average initial horizontal stress (σ_h) at the same location is estimated as:

$$\sigma_h \quad K_0 \sigma_v \qquad \text{(Eq. 6-7)}$$

where K_o = horizontal-to-vertical stress ratio, dimensionless.

The vertical in-situ stress is gravitational, and it is the major principal stress. In this calculation, the average rock density of 2,410 kg/m^3 (Section 6.1.2.3) is used to estimate the overburden and in situ stress state for modeling all non-emplacement drifts. For 3DEC modeling, the major horizontal principal stress is 62% of the vertical stress whereas the minor horizontal principal stress is 36% of the vertical stress (Assumption 3.2.4). This is according to the in situ stress measurement by hydraulic fracturing in a test hole located in the TSw2 unit (Reference 2.2.54).

For FLAC modeling, the horizontal-to-vertical stress ratio is 0.3 (Assumption 3.2.4). The overburden weight is applied as a stress boundary condition at the top of the model.

In evaluation of the stresses induced by excavation in the ground support components for the non-emplacement drifts, an initial ground relaxation value of 60 percent is used. This results in 40 percent of the pre-excavation in situ stress being imposed on the ground support system (Assumption 3.2.1). This value is considered to be conservative to account for the effect of face advance and stand-off between the face and the installed rock bolts. Also, as discussed in Assumption 3.2.2, an initial ground relaxation value of 100 percent is assumed and used in the ground support analysis for the final shotcrete lining in non-emplacement drifts. In other words, there will be no pre-excavation in situ stress being imposed on the shotcrete system.

6.5.2.2 Operation Loads

Operational loads, such as waste package weight and invert material weight, are not considered in this calculation due to the preliminary nature of the design. Exclusion of these loads was believed to result in an overestimate of the inward rock displacements (particularly below the springline) since these loads are expected to offset some of the displacements caused by excavation and heating (note that heating is only considered for those areas in the proximity of emplacement drifts and exhaust mains or directly connected with them).

6.5.2.3 Seismic Loads

Ground motions associated with earthquakes are required to be considered in the design of the repository underground openings. The critical ground motions for subsurface design are ground velocity and acceleration.

In contrast to surface structures, underground structures such as tunnels and their lining or reinforcement systems are constrained by the surrounding medium and do not move independently of the surrounding rock. In reality, the underground structures display significantly greater degrees of redundancy due to the confinement from the ground compared to surface structures, which are generally unsupported above their foundation. Therefore, for underground openings, the surrounding rock acts as a support during a seismic event. Case history studies of underground openings, which have been subjected to seismic activities, are generally used in practice to provide a basis for ground support design. Forty-one (out of seventy-one) cases of observed damage to rock tunnels from earthquake movements were compared to calculate peak surface motions to determine damage thresholds (Reference 2.2.39). The tunnels were built between late 1800s and the 1960s, and, thus, represent a wide variety of construction methods. It is shown that peak surface accelerations which cause heavy damage to surface structures, cause only minor damage to tunnels. For accelerations up to 0.19g and velocities up to 20 cm/s, no damage was experienced even for unsupported openings. Minor damage (new cracks and minimal rock fall) was observed for accelerations up to 0.5g and velocities up to about 90 cm/s.

Other than case history studies, there are no empirical or closed-form solutions available to assess seismic effects on underground openings. Limited progress has been made in seismic design methodology for underground tunnels, possibly because of favorable performance data.

The lack of applicable codes in the past has led to widely varied measures of precaution taken by different engineers. Moreover, the development of pertinent computer codes, as well as vast improvements in computational capacities of hardware, provides effective tools for seismic design of underground openings. For ground support analysis for LA, fully dynamic analyses will be performed to simulate seismic effects and assess opening stability.

Dynamic loading was applied at the bottom of the model, propagating vertically upwards. Although the dynamic loading was specified as velocity time histories, it was numerically applied at the bottom model boundary as stress boundary condition by using formulas developed for plane waves in elasto-dynamics with the direct relation between velocity and stress given as follows (Reference 2.2.45, Manuals/3DEC/Optional Features/Section 2: Dynamic Analysis, Section 2.6):

$$\begin{matrix} \sigma_y & 2\rho C_p v_v \\ \sigma_{xy} & 2\rho C_s v_{h1} \\ \sigma_{zy} & 2\rho C_s v_{h2} \end{matrix} \qquad \text{(Eq. 6-8)}$$

where ρ is material density; C_p and C_s are P and S wave velocity, respectively; and v_v and v_{h1} and v_{h2} are vertical and horizontal particle velocity components. The factor 2 in Equation 6-8 is to account for quiet boundaries. probability of exceedance of 5×10^{-4} (2,000-year return period) as mentioned in Section 6.1.2.7. Seismic load is considered in both FLAC and 3DEC models by applying seismically-induced stresses to the lower boundary of a model. Both P- and S-waves are applied simultaneously. In order to reduce computer computational time, only the dominant portion of the velocity time histories that cover 5 to 95% of energy bracket is used. Note that below and beyond this bracket dynamic amplitudes are significantly low. The duration corresponding to this portion of velocity time histories for the 2,000-year return period is from 3.46 to 28.67 seconds (Reference 2.2.51).

6.5.2.4 Thermal Loads

Thermally induced stresses are generated by thermal expansion of the rock mass due to the thermal energy released from the stored nuclear waste. Thermal stresses at any location depend on the proximity and timing of waste emplacement, the waste heat generation, the age of the waste, packaging and emplacement configuration, and the thermomechanical properties of the rock mass.

Heat transfer process due to heat decay of the waste packages in the emplacement drift is a complicated thermal process. During the preclosure period, the heat transfer process is dictated by the thermal radiation from the waste package to the drift wall, convection due to the preclosure ventilation, and the thermal conduction of heat into the rock mass around the drift. The convective heat transfer occurs due to the temperature difference between the airflow and surfaces of the waste package and the drift wall. The temperature difference was originated by the thermal radiation from the waste package to drift wall.

It should be noted that thermal loading is considered in evaluating the stability analysis for intersections between exhaust mains and emplacement drifts, exhaust mains, observation drift, intersection between observation drift and exhaust main, and interburden pillar between access to

intake shaft #4 and exhaust mains. There are some other areas in the non-emplacement areas that are also subjected to thermal loading, such as the areas in the proximity of ECRB exhaust shaft and intake shaft #3, etc., however, the impact of the thermal loading on the stability of these non-emplacement openings are expected to be less significant.

The exhaust mains are located near (intersecting) the emplacement drifts. After waste emplacement, the exhaust mains and the intersections between the exhaust mains and the emplacement drifts will be subjected to the thermal stresses. The temperature change and thermal stresses will be different around the intersection B (see Figure 6-3) and C (see Figure 6-3). The evolution of the temperature field around the intersections (see Figure 6-3) was calculated by the NUFT code. Temperature changes at the edge of the repository (intersection C) are overpredicted by NUFT's two-dimensional results (because emplacement drift is considered to be infinitely long in 2-D model whereas there is no emplacement drift on the other side of exhaust main at intersection C), resulting in conservative estimate of stress increase (and more unfavorable stability conditions). The temperature fields from the NUFT code (Reference 2.2.24, Section 6.4.1) were imported into 3DEC in order to calculate the thermal stress around the excavations, according to the following formula (Reference 2.2.45, Manuals/3DEC/Optional Features/Section 1: Thermal Option, Section 1.2.3):

$$\Delta\sigma_{ij} \quad \delta_{ij} 3K\alpha(T)\Delta T \qquad \text{(Eq. 6-9)}$$

where $\Delta\sigma_{ij}$ is the stress change, δ_{ij} is the Kronecker delta, K is the bulk modulus of the rock mass, $\alpha(T)$ is the coefficient of the linear thermal expansion as a function of temperature (as listed in Table 6-6), and ΔT is the temperature change.

3DEC was used to model the effects of the thermal stress on stability and deformation of the intersections between emplacement drifts and exhaust mains, observation drift, intersection between observation drift and exhaust main, and interburden pillar between access to intake shaft #4 and exhaust mains.

FLAC was used to model the effects of the thermal stress on stability and deformation of the exhaust mains. In the FLAC model, time histories of temperatures on the model boundaries are applied as time-dependent boundary conditions. The time-dependent rock temperatures at 50 m above and below the drift center and at the drift wall are the same as those for emplacement drifts (see Assumption 3.2.8) (see Table 6-1 of Reference 2.2.30). Two lateral boundaries are adiabatic due to a thermal symmetry, meaning that there is no heat flow across these boundaries. The temperature distributions within rock are calculated based on these thermal boundary conditions and the thermal conductivity and specific heat values using thermal analysis logic built in FLAC code. Thermally-induced stresses within rock at a given time are then estimated from the changes in temperature and rock mass coefficient of thermal expansion through a thermomechanical analysis.

6.5.2.5 Boundary Conditions

The boundary conditions for 3DEC computer analysis are presented in Table 6-12. At the in situ loading stage and the later thermal loading period, fixed velocity at lateral and bottom

boundaries were used to ensure boundary effect does not affect the stress distribution around the opening. The prescribed temperatures generated from NUFT at various time periods were incorporated into 3DEC model to evaluate the thermomechanical behavior. For the dynamic analysis, non-reflecting boundary is used for both the top and bottom of the model, whereas free-field boundary is imposed at the lateral perimeter of the model. The free-field boundaries ensure that plane waves propagating upward suffer no distortion at the boundary. At the dynamic loading stage, the seismic load is considered in the 3DEC models by applying seismically induced stresses (both normal and shear tractions) to the lower boundary of a model. FLAC is used for static analysis in this calculation. The boundary conditions for FLAC models are the same as those for 3DEC models.

Table 6-12 Boundary Conditions for 3DEC Analysis

Boundary	Static Analysis Stage	Dynamic Analysis Stage
Lateral	Fixed at the direction normal to the face	Free-Field boundary
Bottom	Fixed at the vertical direction	Non-reflecting boundary
Top	Applied pressure at the vertical direction	Non-reflecting boundary
Drift Wall	Free	Free

6.5.3 Stability of Unsupported Non-Emplacement Drifts

This section presents the results of assessment of stability of unsupported non-emplacement drifts. The assessment is based on numerical analysis using the FLAC and 3DEC computer codes. The analysis evaluates displacement and stress in the vicinity of an unsupported non-emplacement drift, SF, ground reaction curves (GRC), and temperature increases in rock following waste emplacement.

6.5.3.1 In Situ Stress Loading Condition

The effect of the rock mass quality variability within the lithophysal and nonlithophysal units at the repository level was accounted for by considering different rock mass categories. There are five categories in the lithophysal unit and five categories in the nonlithophysal units. The rock mass properties for different categories listed in Table 6-1 and Table 6-2 for the lithophysal and nonlithophysal rock mass, respectively, are determined by rock mass characterization based on laboratory and in-situ testing. In this calculation, the computer simulations for access mains, exhaust mains, turnouts, and intersections between access mains and turnouts and between exhaust mains and emplacement drifts were carried out for category 1 rock (the poorest quality rock mass), category 3 rock (the medium quality rock mass), and category 5 rock (the strongest quality rock mass) both in lithophysal and nonlithophysal units. For other non-emplacement openings, category 1 and 3 rocks were simulated in the models. A Mohr-Coulomb, elastic-plastic constitutive model was used for all simulations.

6.5.3.1.1 Access and Exhaust Mains and Turnouts

Table 6-13 summarizes the results of unsupported access and exhaust mains for drift displacement and rock stresses induced by excavation. Note that under in situ stress loading condition, the displacement and stress results for access main and exhaust main are the same since they are of the same shape and cross sectional areas and were modeled under the same rock conditions. For access and exhaust mains, the horizontal displacements range from 0.1 mm for category 5 (lithophysal and nonlithophysal) rock to 1.8 mm for lithophysal category 1 rock at springline. The vertical displacements are estimated to range from 2.1 mm for category 5 nonlithophysal rock to 41.6 mm for lithophysal category 1 rock at crown. The largest displacement occurs at the crown. The results also show the effect of rock mass quality on the drift deformation, i.e., the deformation decreases with increase of Young's modulus of rock.

Table 6-13 Unsupported Access Mains – FLAC Results for In Situ Stress Loading Condition

Items	Access/Exhaust Mains		Access/Exhaust Mains		Access/Exhaust Mains	
	L. Cat. 1	NL. Cat. 1	L. Cat. 3	NL. Cat. 3	L. Cat. 5	NL. Cat. 5
Horizontal Displacement (mm)	-1.8	0.4	0.3	0.2	0.1	0.1
Vertical Displacement (mm)	-41.6	-7.0	-6.6	-3.7	-3.6	-2.1
Major Principal Stress near Crown (MPa)	-2.1	-2.2	-2.2	-2.3	-1.8	-2.1
Minor Principal Stress near Crown (MPa)	-0.3	-0.4	-0.4	-0.4	-0.5	-0.5
Major Principal Stress near Springline (MPa)	-12.0	-23.8	-23.0	-23.7	-23.8	-23.7
Minor Principal Stress at Springline (MPa)	-0.6	-1.0	-0.9	-1.0	-1.0	-1.0

Note: a) L – Lithophysal, NL – nonlithophysal, b) The vertical displacement occurs at crown whereas horizontal displacement at springline.

The major principal stresses for access and exhaust mains under in situ loading vary from about 24 MPa in compression occurring near the skin of springline to about 1.8 MPa in compression occurring near the skin of crown. The stresses at the crown are much smaller than those at the springline. The minor principal stresses are about 1 MPa or lower, which are much lower than those of the major principal stresses.

Figure 6-25 to Figure 6-27 show the contours of SF against Mohr-Coulomb shear failure around the unsupported access/exhaust mains for categories 1, 3, and 5 rock in lithophysal units, respectively. The SF in this case is defined as the ratio of shear strength to the shear stress on the potential failure plane. For lithophysal category 1 rock (poorest rock mass category), a narrow zone adjacent to wall (about 1.0 m into wall) is shown with potential yield. For lithophysal category 3 rock (median rock mass category), a very narrow zone adjacent to wall (about 0.4 m into wall) is shown with potential yield. At distance of about 1 m into wall SF increases to 2. For lithophysal category 5 rock (strongest rock mass category), no potential yield zone is identified. At distance of about 0.5 m into wall SF increases to 2.

Figure 6-28 to Figure 6-30 show the contours of SF against Mohr-Coulomb failure criteria around the unsupported access/exhaust mains for categories 1, 3, and 5 rock in nonlithophysal units, respectively. Similar stability conditions as those for lithophysal rock are observed for nonlithophysal rock, except that the stability condition is a little better. For example, for nonlithophysal category 1 rock, a very narrow zone adjacent to wall (about 0.4 m into wall) is shown with potential yield. At distance of about 1 m into wall SF increases to 2.

Figure 6-31 shows the displacements around the unsupported turnouts for lithophysal category 1 rock. The largest displacement of 28.5 mm occurs at the crown. Figure 6-32 shows the stresses of the unsupported turnouts for lithophysal category 1 rock. The maximum compressive stress of 19 MPa occurs at the springline. Similar stability conditions as those for access and exhaust mains.

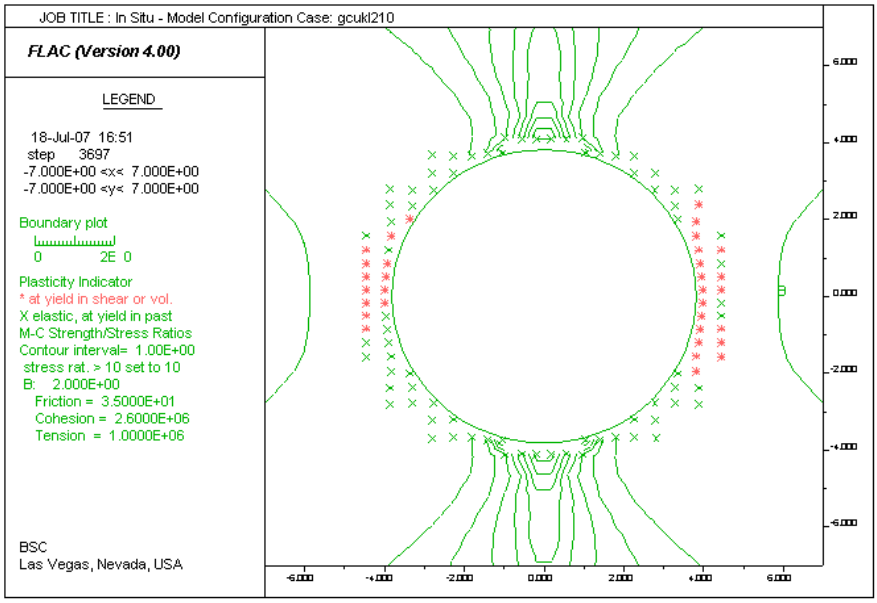

Figure 6-25 Contours of SF around Unsupported Access/Exhaust Main for Lith. Cat. 1 Rock

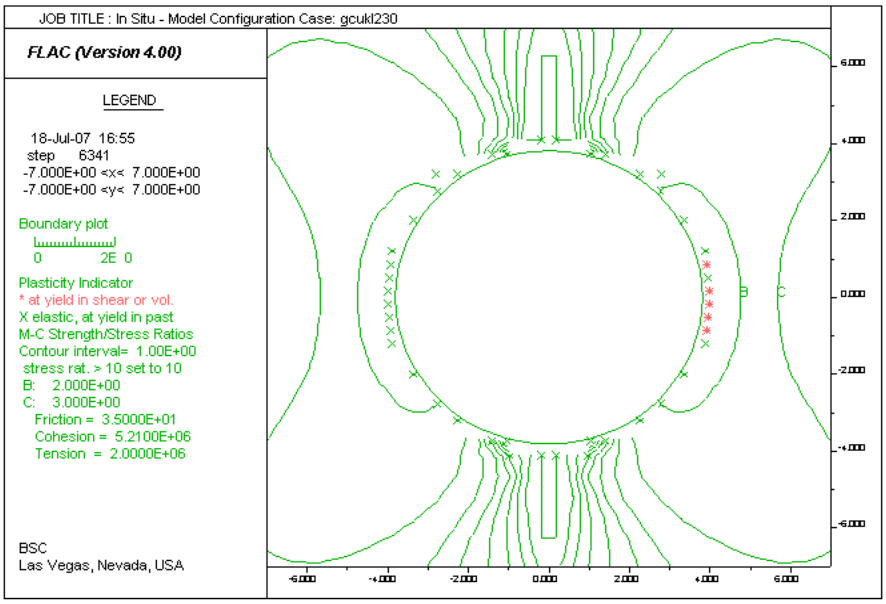

Figure 6-26 Contours of SF around Unsupported Access/Exhaust Main for Lith. Cat. 3 Rock

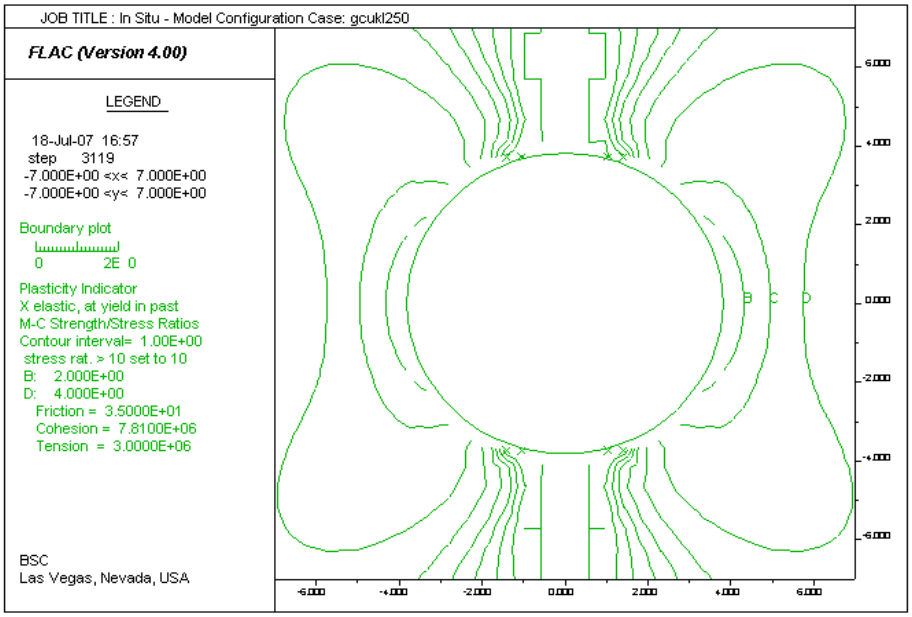

Figure 6-27 Contours of SF around Unsupported Access/Exhaust Main for Lith. Cat. 5 Rock

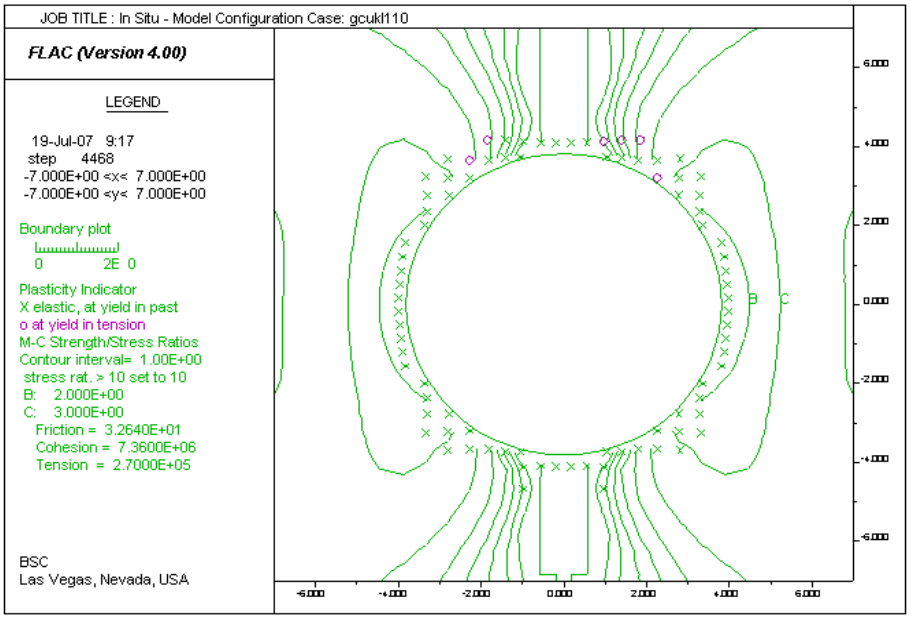

Figure 6-28 Contours of SF around Unsupported Access/Exhaust Main for N. Lith. Cat. 1 Rock

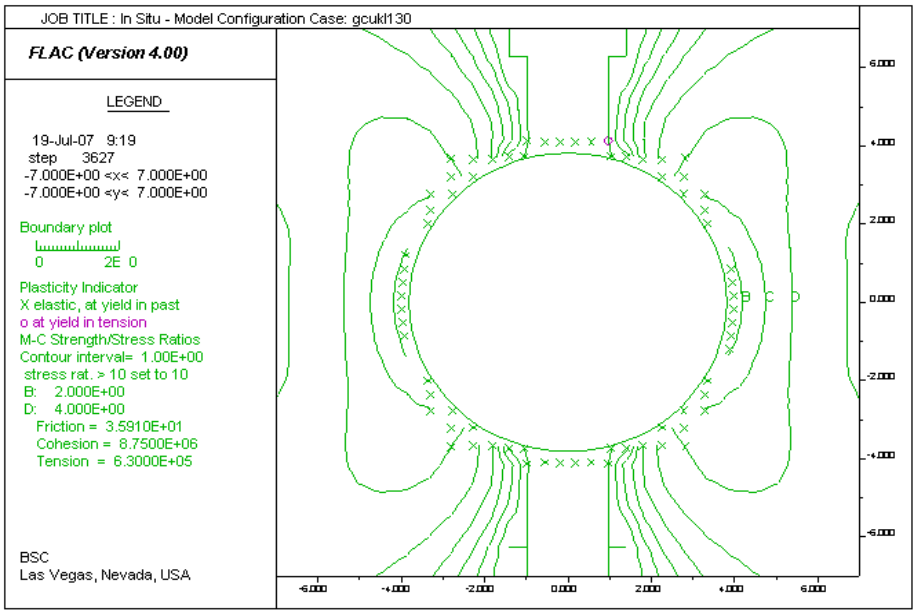

Figure 6-29 Contours of SF around Unsupported Access/Exhaust Main for N. Lith. Cat. 3 Rock

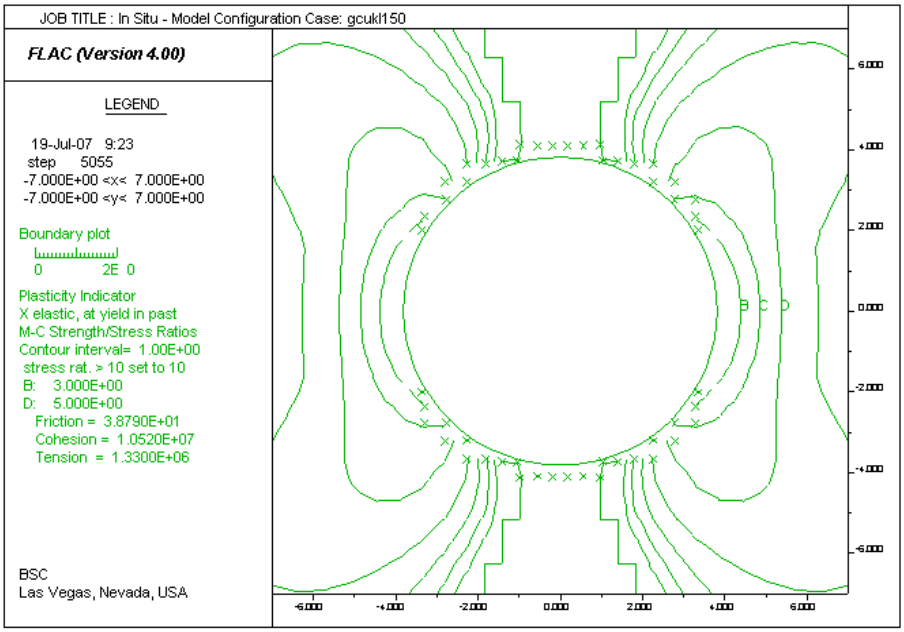

Figure 6-30 Contours of SF around Unsupported Access/Exhaust Main for N. Lith. Cat. 5 Rock

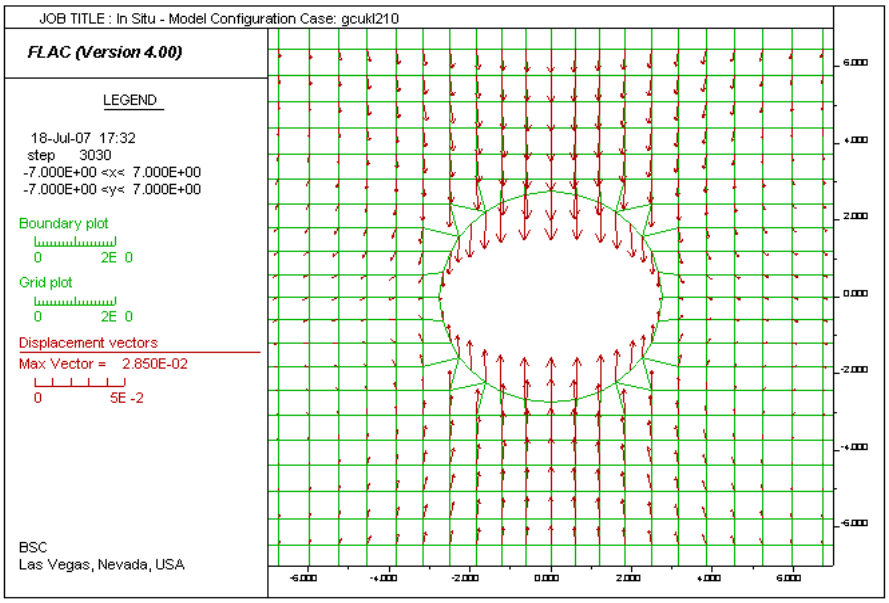

Figure 6-31 Displacement Vectors around Unsupported Turnout for Lith. Cat. 1 Rock

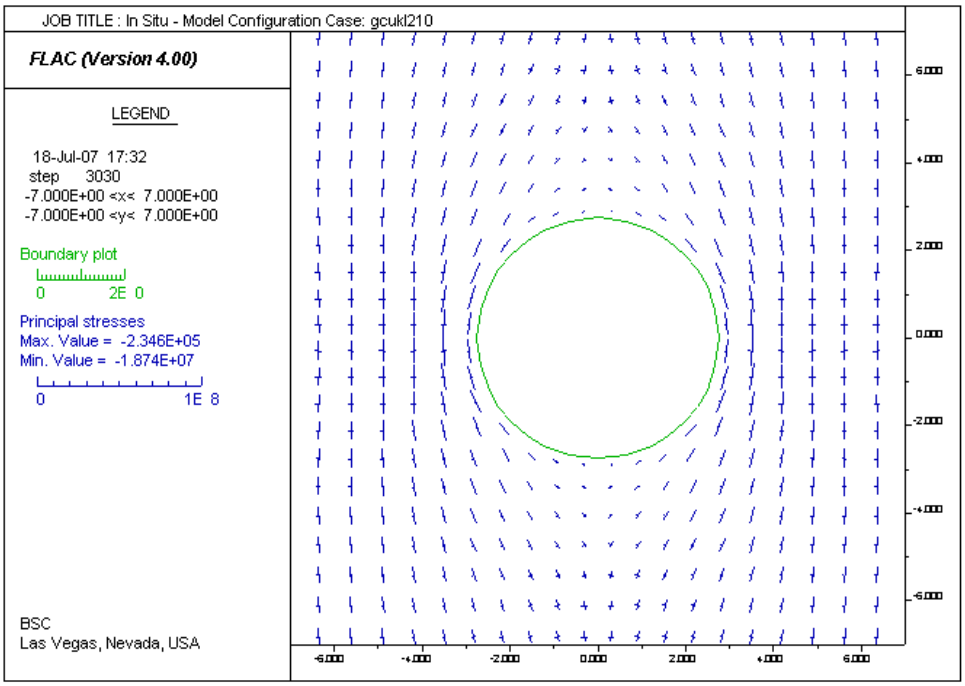

Figure 6-32 Stress Tensors around Unsupported Turnout for Lithophysal Cat. 1 Rock

6.5.3.1.2 Intersection between Access Main and Turnout

Stability of the unsupported intersections in the lithophysal and nonlithophysal rock mass for in-situ stress conditions is analyzed for layout at intersection A, which represents the critical conditions with respect to the maximum span of the roof and stress concentrations in the pillars.

To avoid large, unphysical deformation of zones around the boundary of the excavation that yield in tension, tensile strength in the 3DEC simulations was assumed to be infinitely large (Assumption 3.2.5).

The results for the intersection A are shown in Figure 6-33 through Figure 6-48. For both units (lithophysal and nonlithophysal), the figures include the plots of:

1. Displacement fields in two vertical sections 1 and 2 (see section location in Figure 6-12);
2. Displacement profile along the vertical line though the point A (see Point A location in Figure 6-12);
3. Stress fields in the same vertical sections as for the displacement fields;
4. Average pillar stress as a function of the distance from the tip (see Point A in Figure 6-12). The stresses were averaged over the entire pillar width and height for a 2-m long segments measured radially from the pillar tip; and
5. Potential yield zones in the horizontal and the vertical sections.

Rock Mass Displacements

Figure 6-33 and Figure 6-34 show displacement fields in vertical section 1 at intersection A (see Figure 6-12) for the category 1 rock of lithophysal and nonlithophysal units, respectively. For the same intersection, Figure 6-35 and Figure 6-36 show displacement fields in vertical section 2 for the category 1 rock of lithophysal and nonlithophysal units, respectively. Note that vertical section 1 cuts across two turnouts and one access main as well as two very narrow pillars. Vertical section 2 cuts through the intersecting access main and turnout, one narrow pillar, and another turnout. The important features of these two sections are: section 1 cuts through very narrow pillar whereas section 2 cuts through an opening with large roof span. The results show that the maximum displacement of 72 mm in lithophysal rock occurs at the intersection area with large roof span. The maximum displacement in the nonlithophysal rock at the same location is 11 mm. Relatively large displacements for the lithophysal category 1 rock mass result from the very low elastic modulus assigned to the lithophysal category 1 rock mass. These observations are confirmed with plots of the rock mass regions of potential yield zones, as shown in Figure 6-37 and Figure 6-38. The potential yield zone extends to approximately 1 m from the drift walls in the lithophysal, category 1 rock mass, the poorest rock mass category. There is practically no plastic deformation around the drifts in the nonlithophysal rock mass.

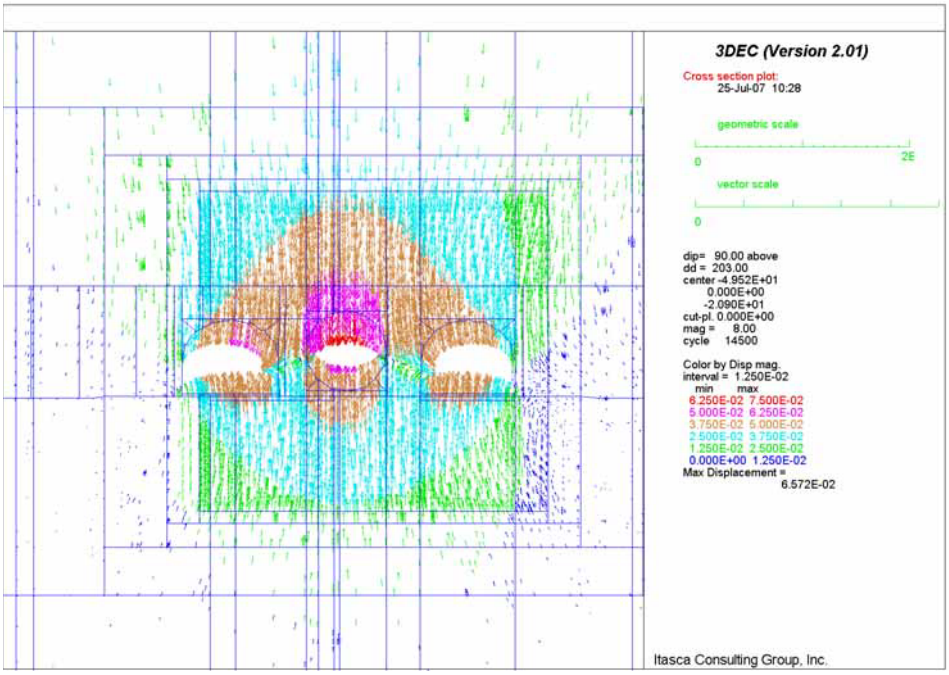

Figure 6-33 Intersection A: Displacement Field in Vertical Section 1 for Lith. Cat. 1 Rock

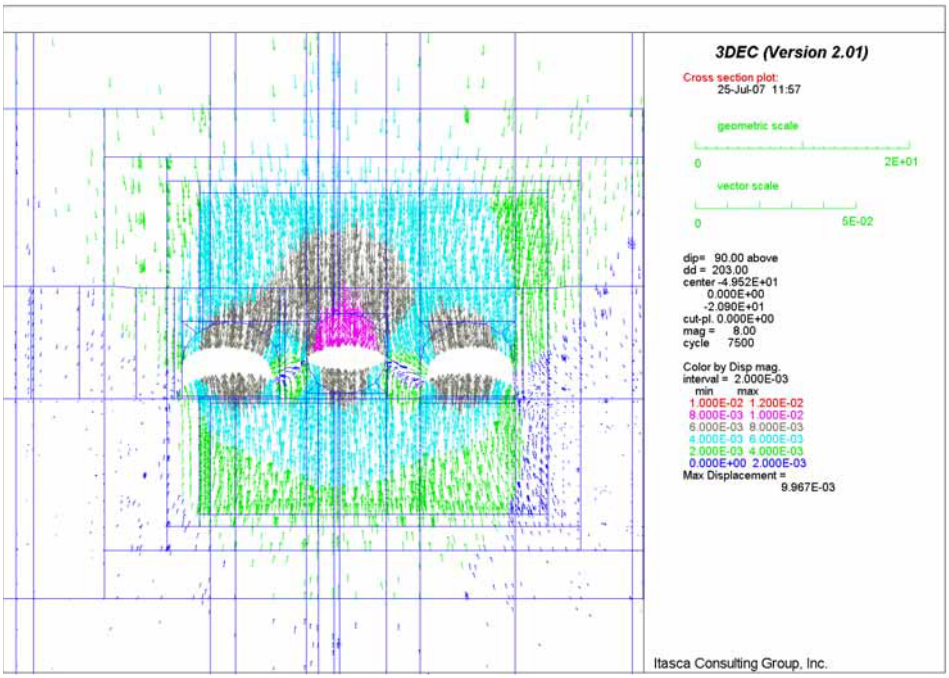

Figure 6-34 Intersection A: Displacement Field in Vertical Section 1 for N. Lith. Cat. 1 Rock

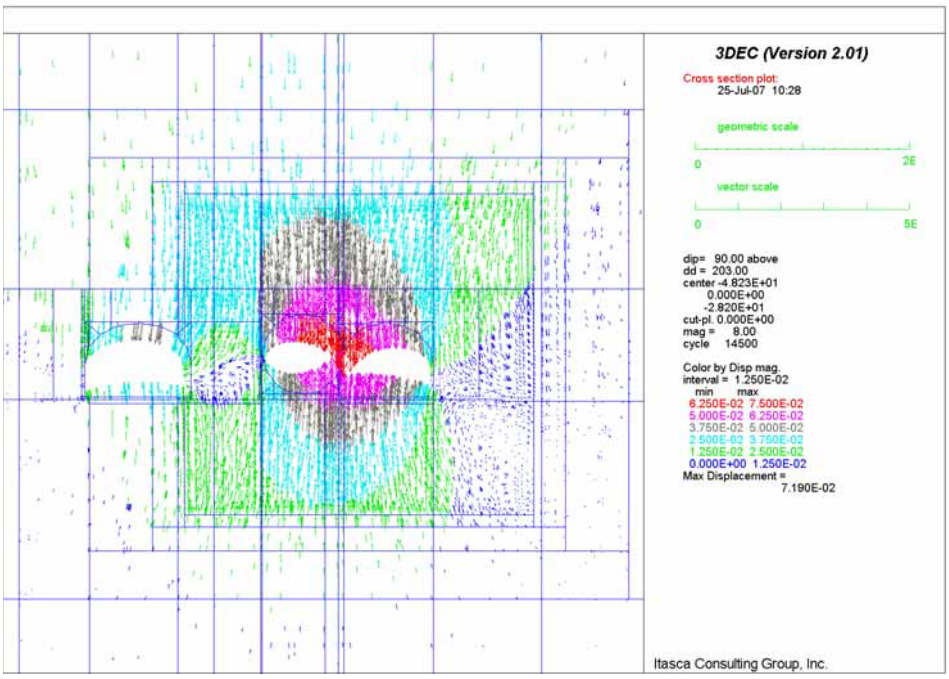

Figure 6-35 Intersection A: Displacement Field in Vertical Section 2 for Lith. Cat. 1 Rock

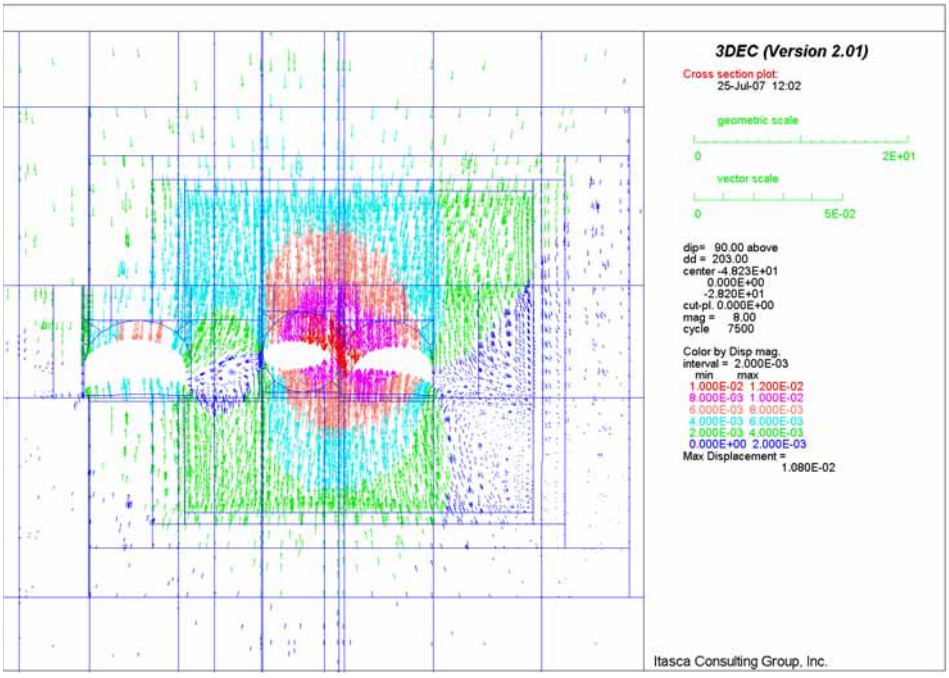

Figure 6-36 Intersection A: Displacement Field in Vertical Section 2 for N. Lith. Cat. 1 Rock

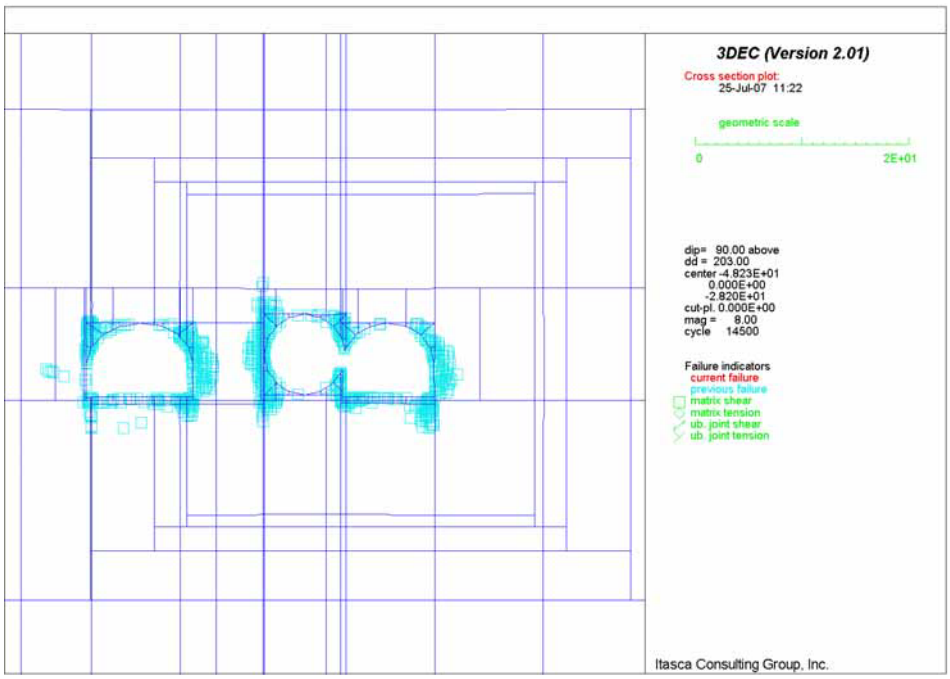

Figure 6-37 Intersection A: Potential Yield Zone in Vertical Section 2 for Lith. Cat. 1 Rock

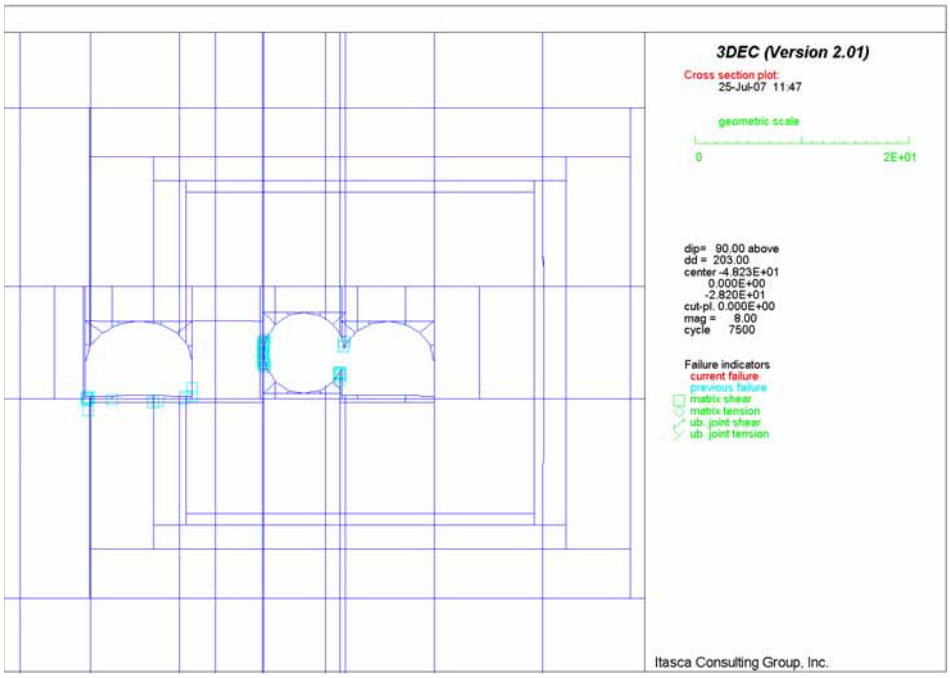

Figure 6-38 Intersection A: Potential Yield Zone in Vertical Section 2 for Nonlith. Cat. 1 Rock

Stresses in Rock Mass Adjacent to Openings

Figure 6-39 and Figure 6-40 show stress fields in vertical section 1 at intersection A (see Figure 6-12) for category 1 rock of lithophysal and nonlithophysal rock, respectively. For the same intersection, Figure 6-41 and Figure 6-42 show stress fields in vertical section 2 (see Figure 6-12) for category 1 rock of lithophysal and nonlithophysal rock, respectively. The results indicate that the maximum compressive stress occurs near the sidewall or in the pillar between adjacent openings and slight destressing above crown and below invert. The highest compressive stress of 53 MPa occurs near the sidewall of the opening at intersection area with large roof span in the nonlithophysal category 1 rock (see Figure 6-42). Note that this stress value is larger than the unconfined compressive strength of the rock mass (see Table 6-2). This result does not mean that rock will fail at that location since the rock mass in situ is under some confinement. Yet, it does indicate that there is a potential for rock spalling near the sidewall, which is also revealed in Figure 6-43 and Figure 6-44. In these two figures, the contours of SFs ranging from 1 to 1.4 are observed along the sidewalls of the openings, especially more evident for the lithophysal rock. Figure 6-46 shows the stress field with indication of tensile stresses in vertical section 2 for lithophysal category 1 rock. A very narrow region of tensile stress is observed in the crown and the invert area. There are no indications of instability of the roof even in category 1, lithophysal rock mass. It is possible that a limited volume of the rock mass becomes unstable due to local structures unaccounted for in this analysis (continuum approach) if the intersections are unsupported. The ground support system analyzed for the intersection will be able to prevent any such rockfall.

Stability of the pillar between the access main and the turnout is assessed based on a plot of average pillar stress (shown in Figure 6-45) and plots of regions of plastic deformation (i.e., potential yield zone) shown in the horizontal section in Figure 6-47 and Figure 6-48 (note that the similar plots in vertical section are shown in Figure 6-37 and Figure 6-38). The stress concentrations may cause damage and rock fracturing in the pillar. The extent of the damage will depend on the quality of the rock mass. The calculations predict pillar damage to extend 8 m from the tip in the lithophysal rock mass, category 1. In good quality lithophysal rock mass and nonlithophysal rock mass the pillar will be damaged to a distance of approximately 3 m from the tip. However, in reality, the pillars will be rounded to a distance from the tip where the major damage is observed. It is not needed (and probably impossible) to create the pillar tip. If rounding of the pillars is not performed during excavation, it will take place naturally by broken ground falling off. The pillars will eventually attain the stable geometry. It seems, based on the numerical results, that the rounding length does not need to be larger than 5 m in the poorest quality lithophysal rock mass. If the additional ground support is used the pillar rounding length could be reduced even more.

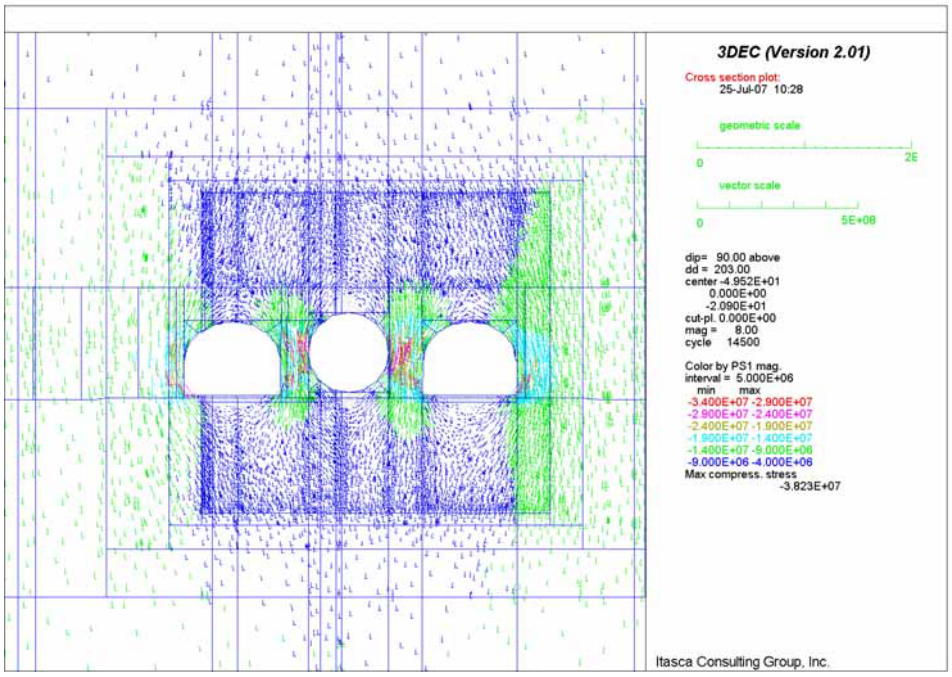

Figure 6-39 Intersection A: Stress Field in Vertical Section 1 for Lith. Cat. 1 Rock

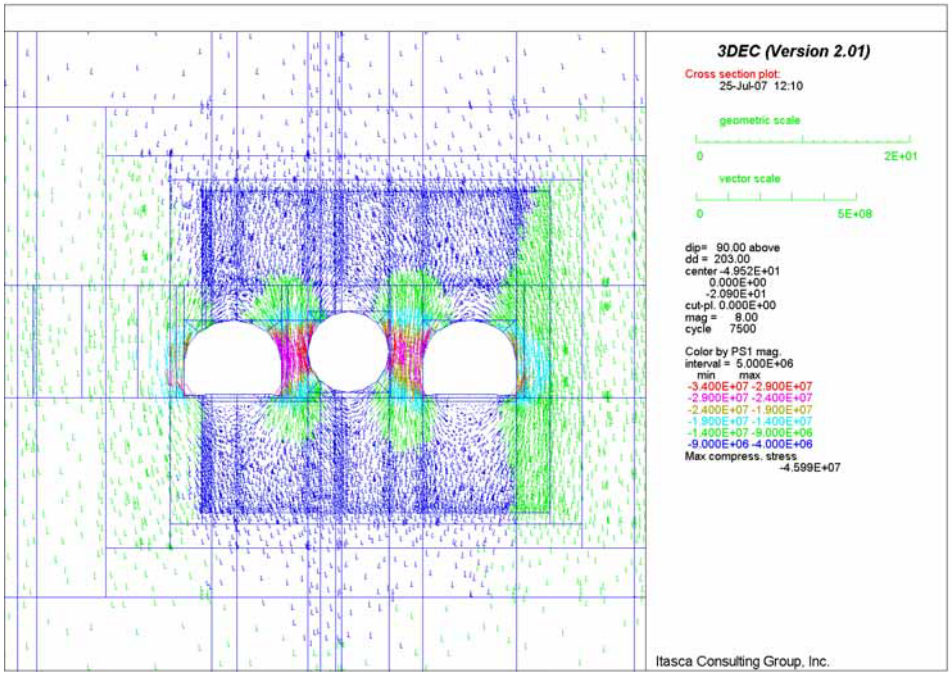

Figure 6-40 Intersection A: Stress Field in Vertical Section 1 for Nonlith. Cat. 1 Rock

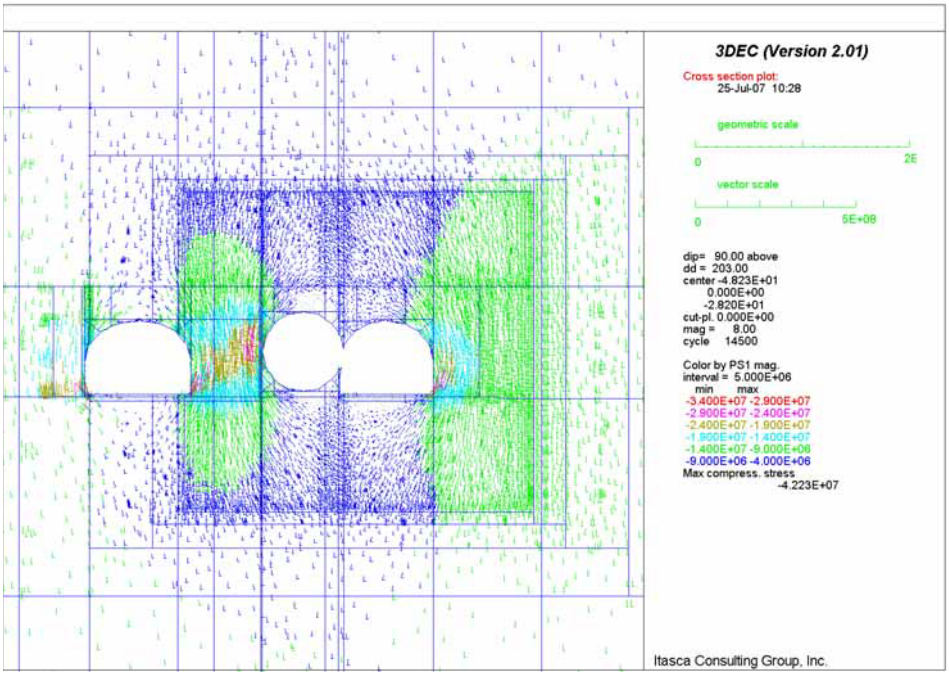

Figure 6-41 Intersection A: Stress Field in Vertical Section 2 for Lith. Cat. 1 Rock

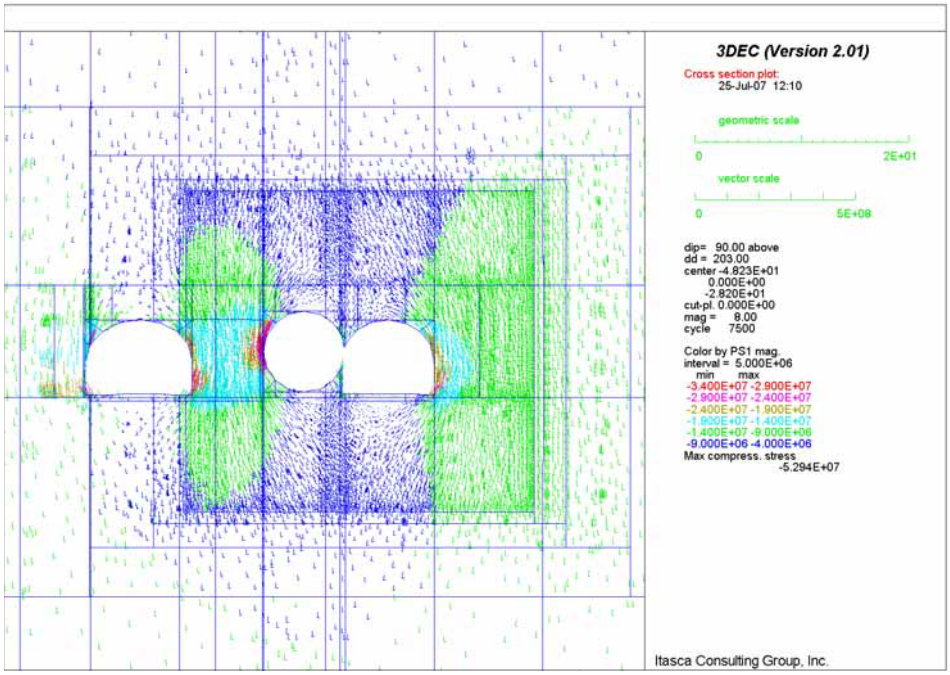

Figure 6-42 Intersection A: Stress Field in Vertical Section 2 for Nonlith. Cat. 1 Rock

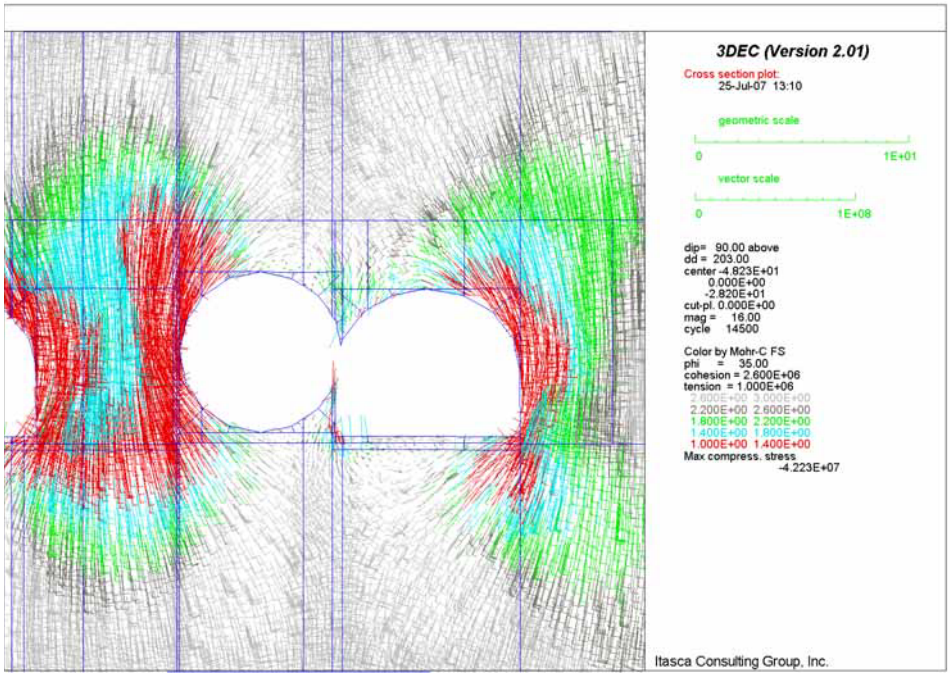

Figure 6-43 Intersection A: Factor of Safety in Vertical Section 2 for Lith. Cat. 1 Rock

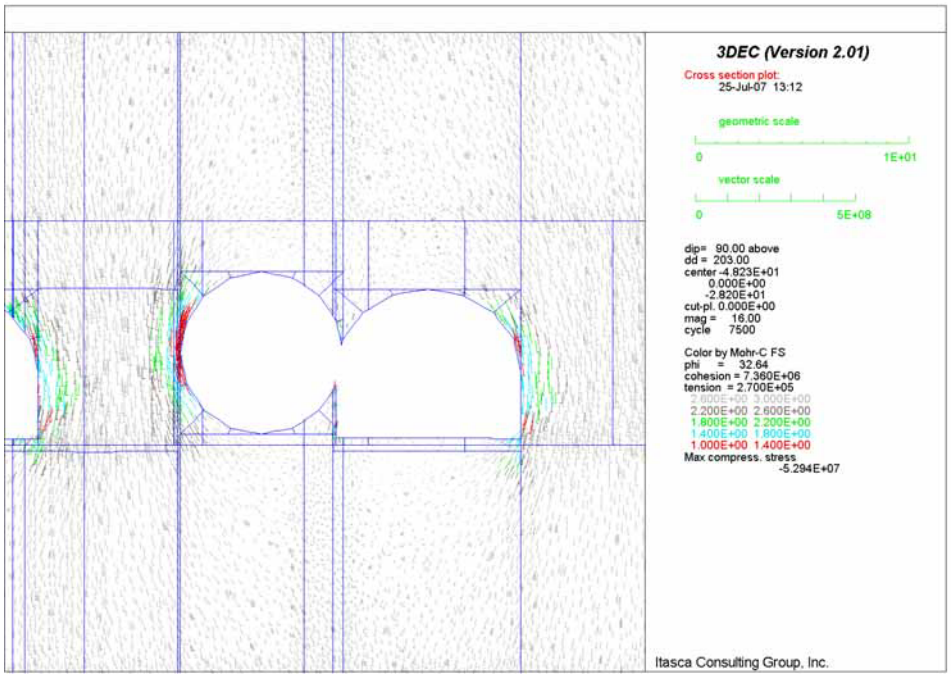

Figure 6-44 Intersection A: Factor of Safety in Vertical Section 2 for N. Lith. Cat. 1 Rock

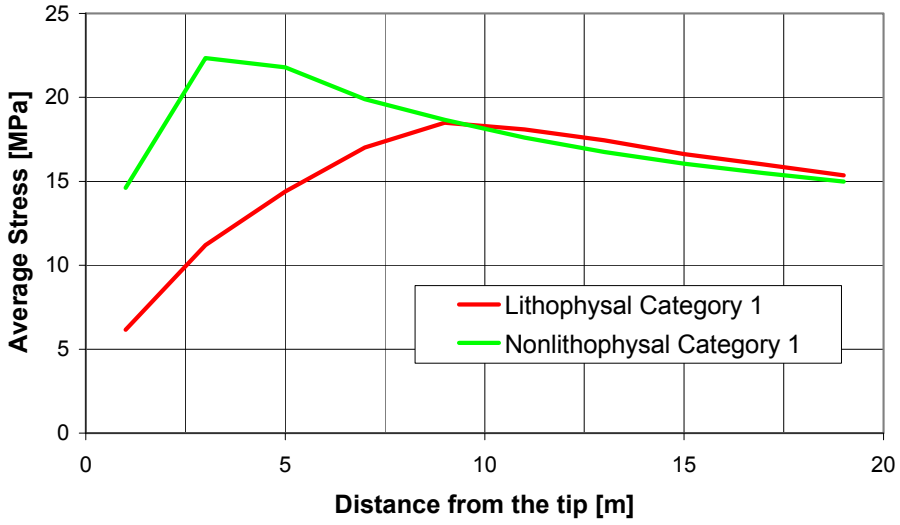

Figure 6-45 Intersection A: Average Pillar Stress vs. Distance from the Pillar Tip

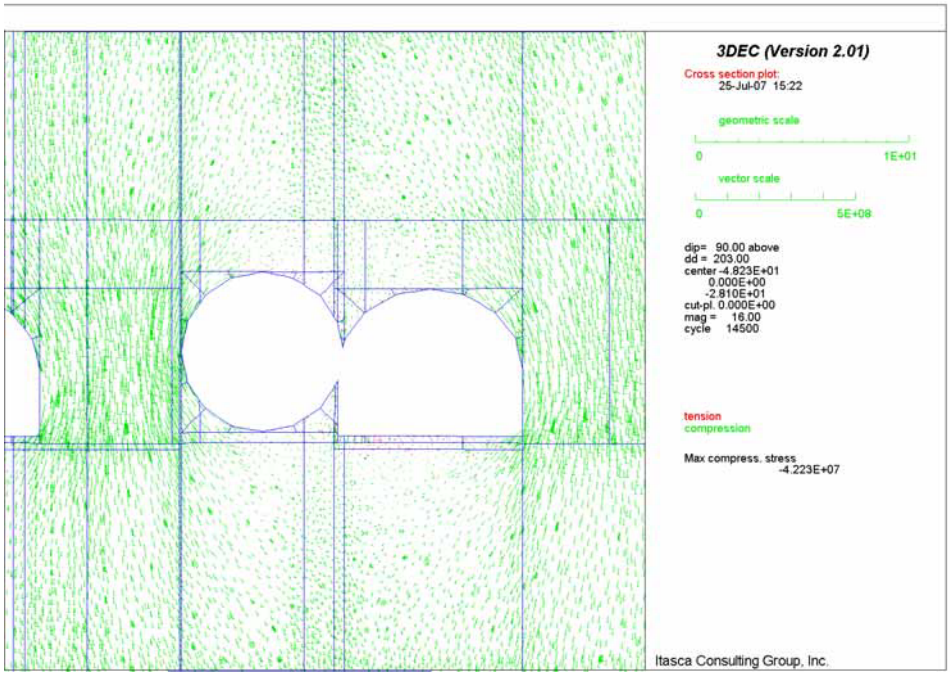

Figure 6-46 Intersection A: Compressive and Tensile Stresses in Vertical Section 2 for Lith. Cat. 1 Rock

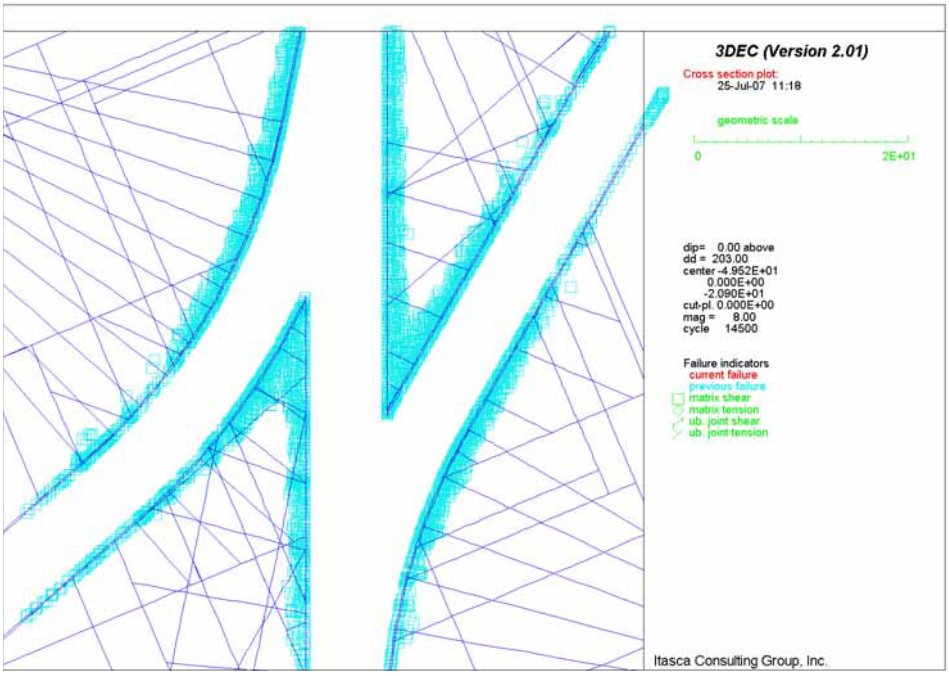

Figure 6-47 Intersection A: Potential Yield Zone in Horizontal Section for Lith. Cat. 1 Rock

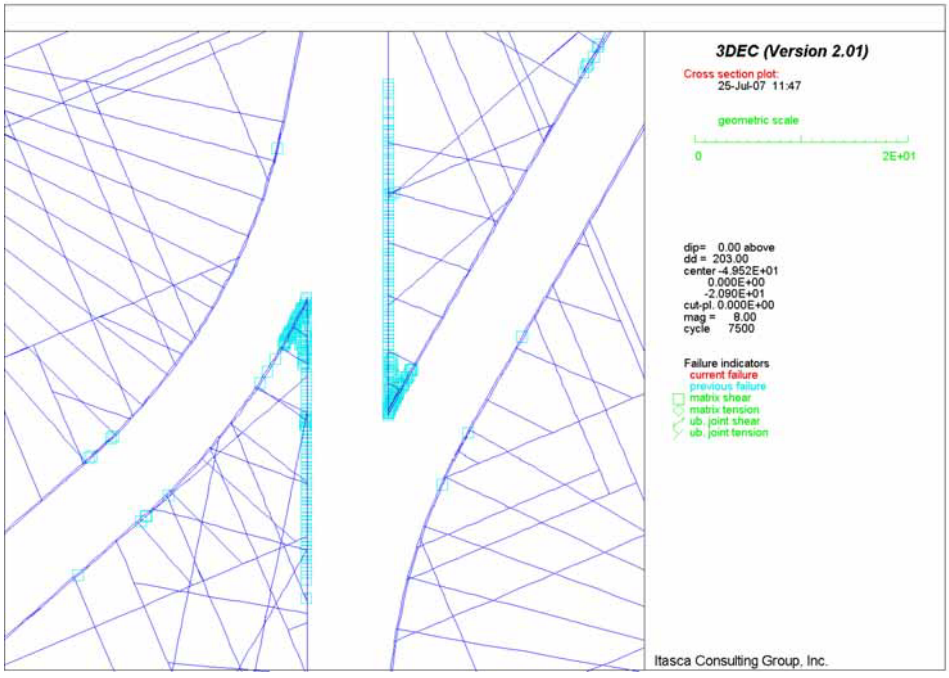

Figure 6-48 Intersection A: Potential Yield Zone in Horizontal Section for Nonlith. Cat. 1 Rock

Discussion

The rock mass deformation around intersections are shown to be largely elastic. The potential yield zones extend approximately 1 m from the drift walls into the rock mass for the poorest quality rock mass. A relatively large displacement of 70 mm predicted for the lithophysal, category 1 rock mass (see Figure 6-35), is a consequence of the low Young's modulus used. There are no indications of loosening and instability of the rock mass in the crown for any of the analyzed cases. Numerical results show that the roof in the intersections is stable, even for the largest spans.

The tips of the pillars between the access main and the turnouts will be damaged due to stress concentrations. The extent of this damage from the pillar tip will depend on the rock mass quality. Rounding of the pillars and additional ground support will resolve the problem of pillar instability.

6.5.3.1.3 Intersection between Exhaust Main and Emplacement Drift

Two intersection layouts, B and C, were analyzed as being representative of the extreme conditions existing in the exhaust main intersections from the perspective of excavation stability. The diameter of the exhaust main is 7.62 m — except in Panel 1 of the repository, where it is 5.5 m. Throughout the analyses presented in this calculation, the diameter of 7.62 m was used for the exhaust main, which is conservative with regard to stability of the excavations.

The results of the stability analysis of unsupported intersections B and C are shown in Figure 6-49 through Figure 6-58. The analysis was carried out for categories 1, 3, and 5 in lithophysal (intersection B) and 1 and 3 in nonlithophysal (intersection C) rock masses, representing the variability of rock mass quality at the repository horizon. The results are presented here for category 1 only. The rock mass around the intersections in category 5 deforms elastically. The modeling sequence followed the expected construction sequence: the exhaust mains were excavated prior to excavation of the emplacement drifts. The presented results are for the final stage of the excavation.

The maximum vertical displacement in the roof is 44 mm in the lithophysal category 1 rock mass (Figure 6-49). The maximum displacements in the nonlithophysal rock mass are predicted to be less than 10 mm (Figure 6-50) for all categories. The intersections cause stress concentrations of about 25MPa (see Figure 6-51 and Figure 6-52) in the walls of the exhaust main. However, stress tensors colored by the factor-of-safety with respect to a Mohr-Coulomb yield condition (shown in Figure 6-53 and Figure 6-54), and the extent of the rock mass that undergoes plastic deformation in the vertical and horizontal sections (shown in Figure 6-55 through Figure 6-58) indicate that deformation of the rock mass around the intersections will be predominantly elastic. There is a narrow (less than 1 meter) region of the rock mass around the exhaust main at intersection B for category 1 that yields (Figure 6-55). However, the effect of the interaction between the exhaust main and the emplacement drift on the extent of rock mass yielding is negligible. The sharp angle between the exhaust main and the emplacement drift creates a pillar (Figure 6-58) between these two excavations. At most, the rock mass yields 1 m from the tip of the pillar, indicating that rounding the pillar tip would resolve any potential problems.

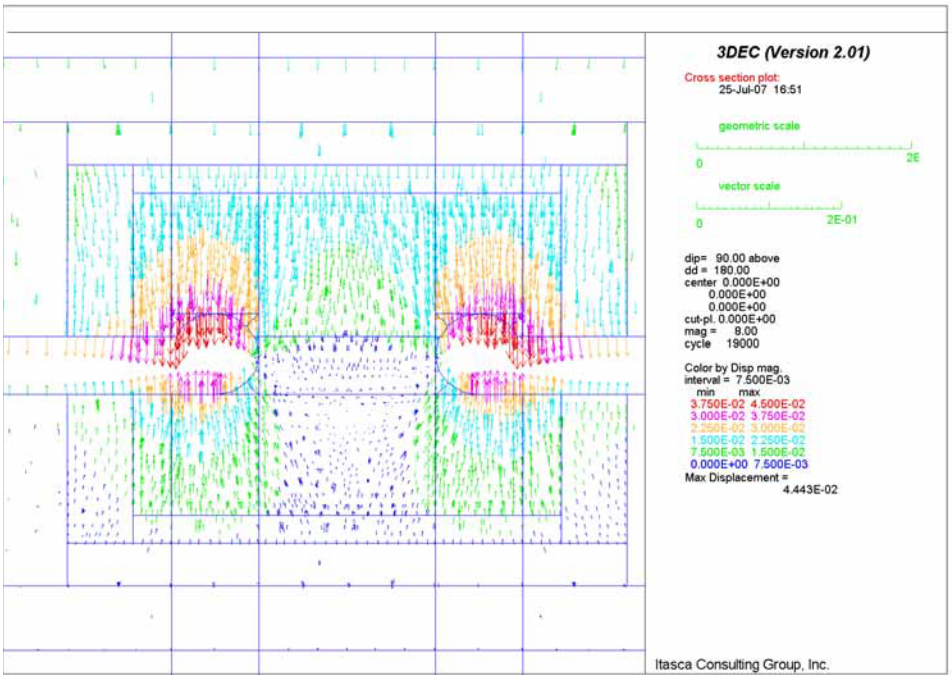

Figure 6-49 Intersection B: Displacement Field in Vertical Section 1 for Lith. Cat. 1 Rock

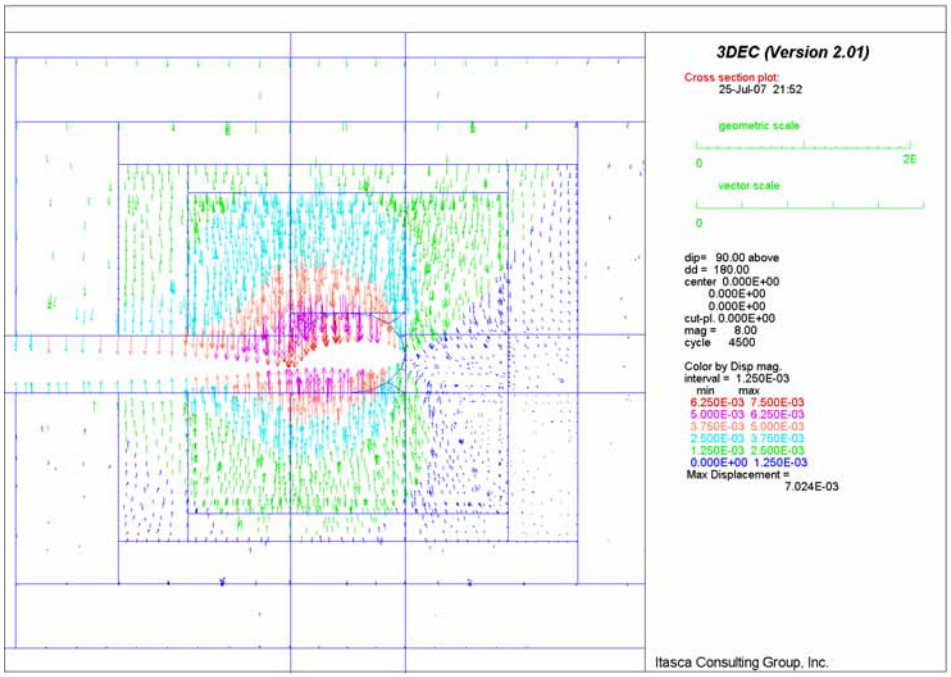

Figure 6-50 Intersection C: Displacement Field in Vertical Section 1 for N. Lith. Cat. 1 Rock

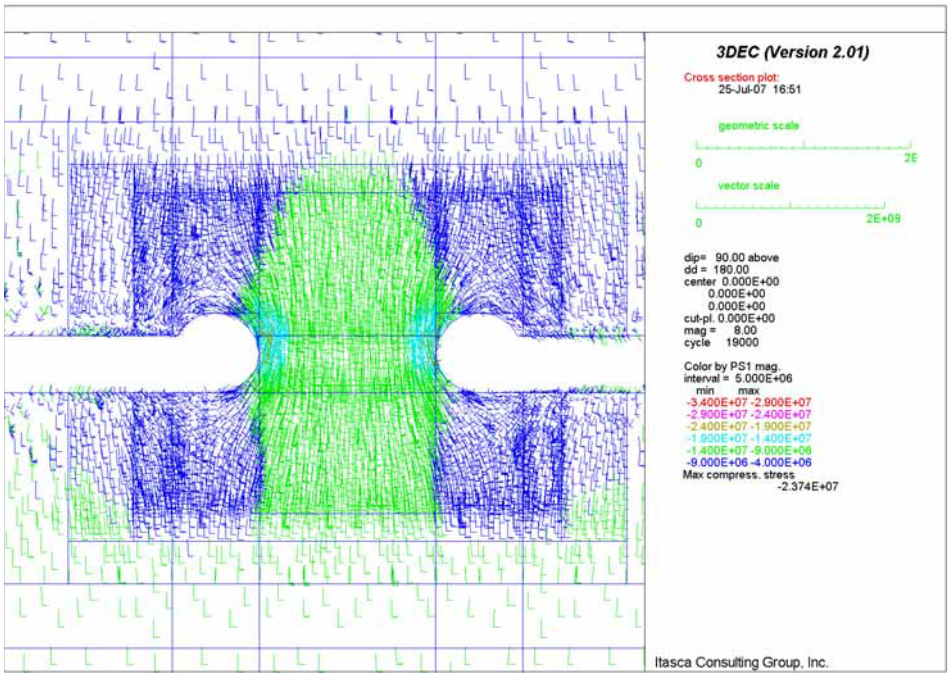

Figure 6-51 Intersection B: Stress Field in Vertical Section 1 for Lith. Cat. 1 Rock

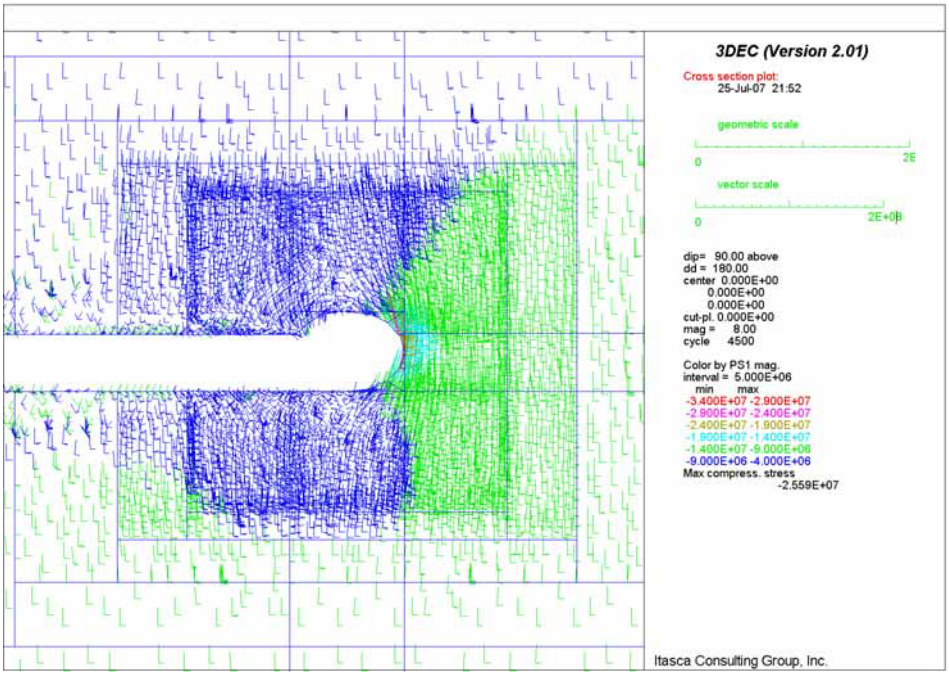

Figure 6-52 Intersection C: Stress Field in Vertical Section 1 for N. Lith. Cat. 1 Rock

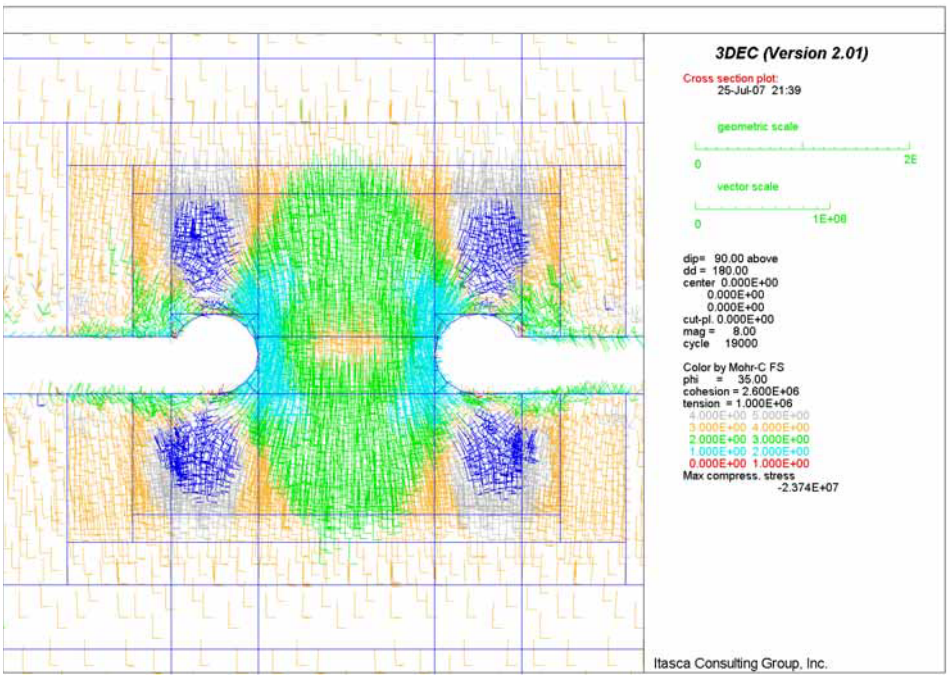

Figure 6-53 Intersection B: Factor of Safety in Vertical Section 1 for Lith. Cat. 1 Rock

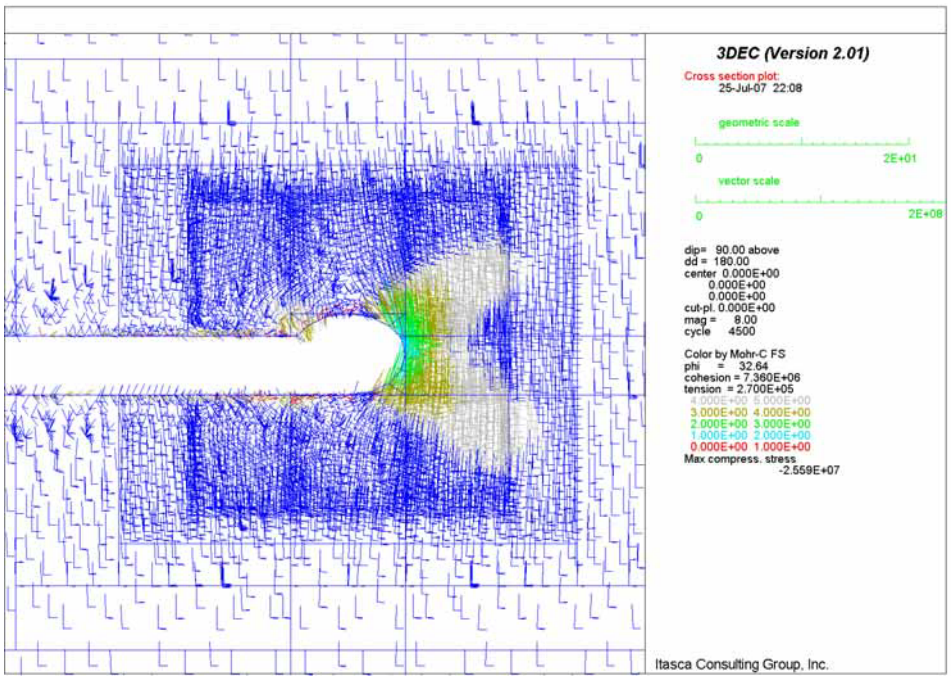

Figure 6-54 Intersection C: Factor of Safety in Vertical Section 1 for N. Lith. Cat. 1 Rock

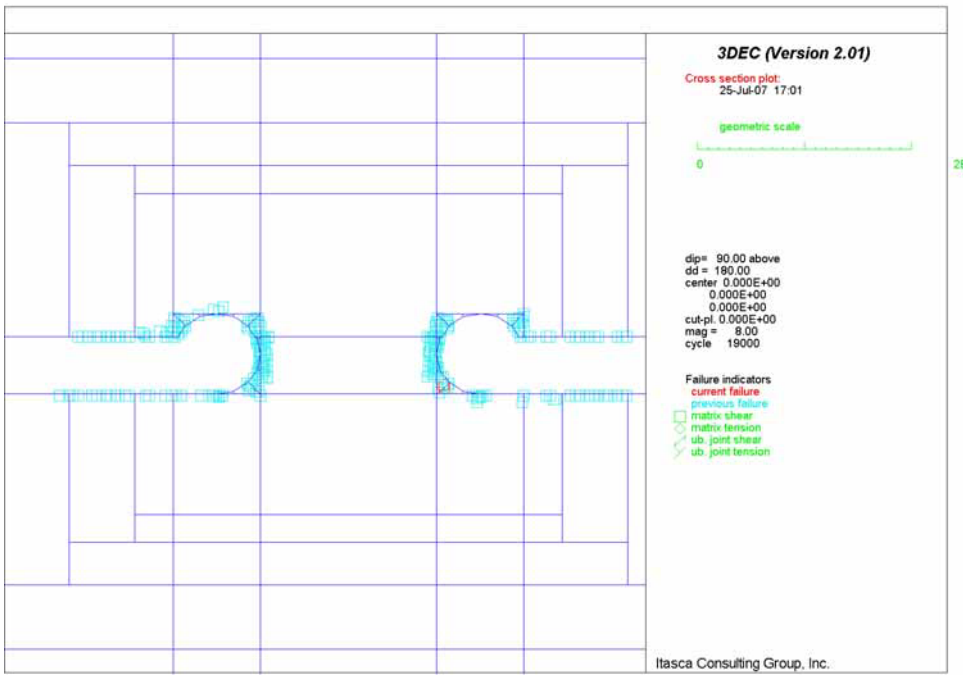

Figure 6-55 Intersection B: Potential Yield Zone in Vertical Section 1 for Lith. Cat. 1 Rock

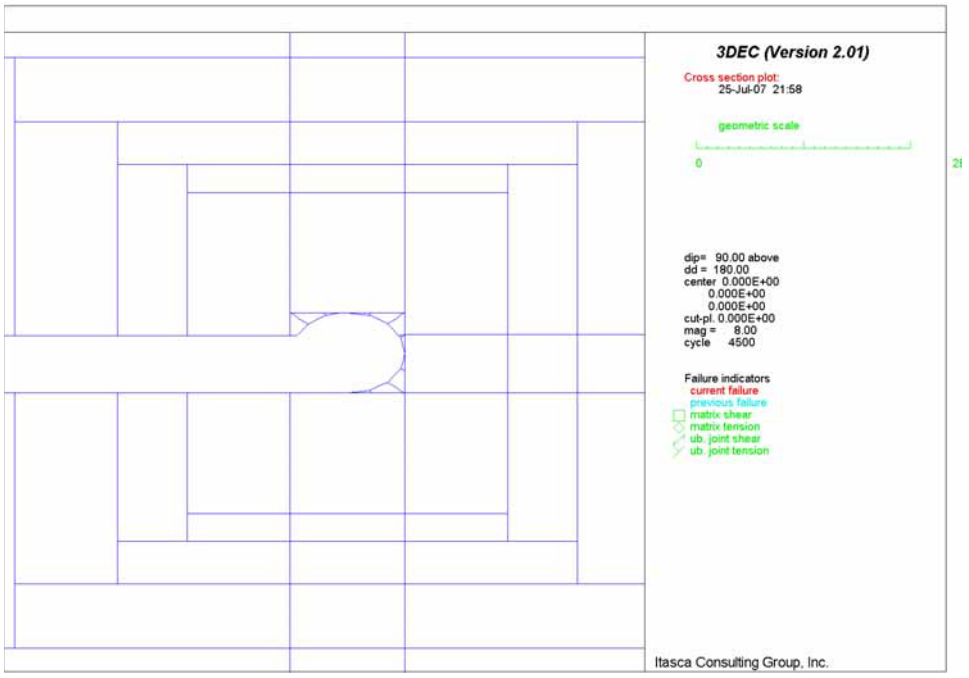

Figure 6-56 Intersection C: Potential Yield Zone in Vertical Section 1 for N. Lith. Cat. 1 Rock

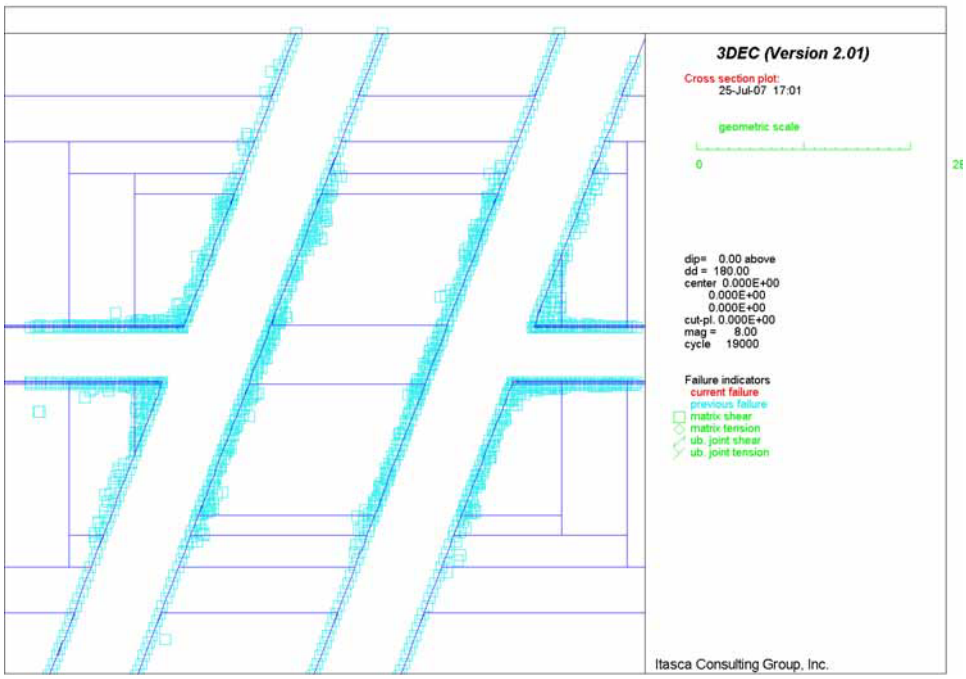

Figure 6-57 Intersection B: Potential Yield Zone in Horizontal Section for Lith. Cat. 1 Rock

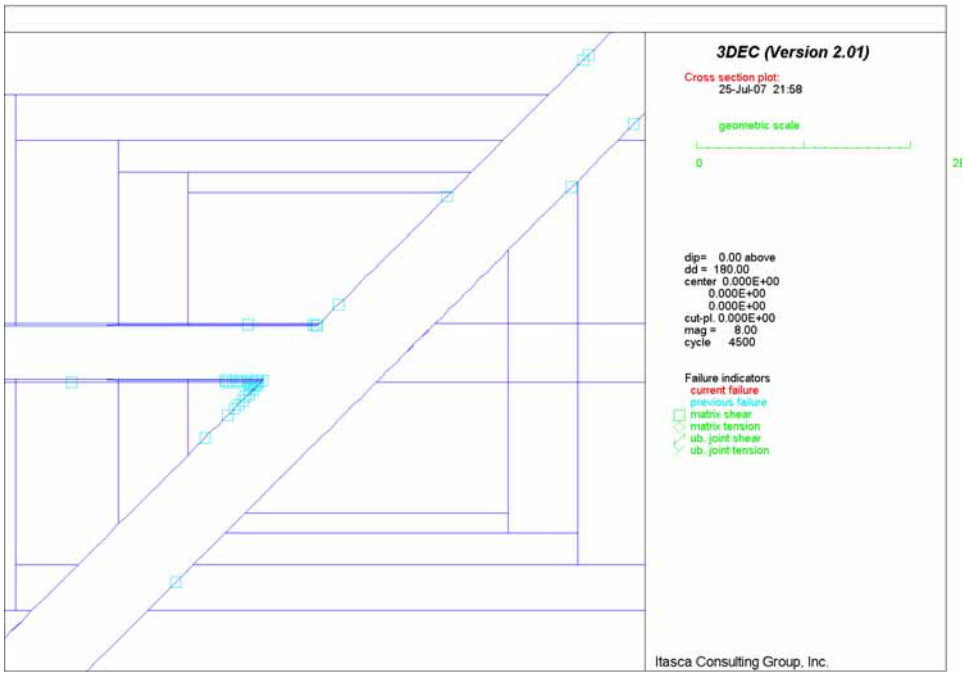

Figure 6-58 Intersection C: Potential Yield Zone in Horizontal Section for N. Lith. Cat. 1 Rock

6.5.3.1.4 Observation Drift

The model results for the typical cross-section perpendicular to the observation drift axis are shown in Figure 6-59 to Figure 6-62. The maximum displacements predicted for the observation drift are similar to those for the emplacement drift (for the same rock-mass quality), of the order of 0.03 m, because the sizes of both tunnels are similar. The plot of the contours of the major principal stress (Figure 6-60) shows that, for a given distance, the level of interaction between two excavations (the emplacement drift and the observation drift) is minimal. The predicted extent of the damage of the rock mass (Figure 6-61) surrounding the observation drift and the emplacement drift is similar. There is a little more damage in the walls and the floor of the observation drift because of mechanically less-favorable shape (i.e., flat walls and corners). The factor-of-safety with respect to Mohr-Coulomb shear failure (Figure 6-62) increases quickly as a function of distance from the drift boundary; the factor-of-safety is larger than 2 only a couple of meters from the drift walls except along the line connecting two openings where factor-of-safety becomes larger than 2 after about 10 m.

The results of modeling for the intersection between the observation drift and the exhaust main are presented in Figure 6-63 to Figure 6-68. The maximum displacements (Figure 6-63 and Figure 6-64) are comparable to predictions of the two-dimensional model because of the larger span of the exhaust main (7.62 m). For the analyzed conditions, there are no indications of instability in the intersection. The regions of the potential yield zones are confined to the vicinity of the excavations (Figure 6-65 and Figure 6-66). The extent of damage does not increase in the intersection, and it does not seem that the excavations interact with each other. The pillar between the observation drift and the exhaust main appears (in the vertical section 2) (see Figure 6-18) to have some damage. Factor-of-safety with respect to Mohr-Coulomb shear failure criteria is greater than 2 (Figure 6-67 and Figure 6-68) except in close vicinity of the excavations and in the pillar.

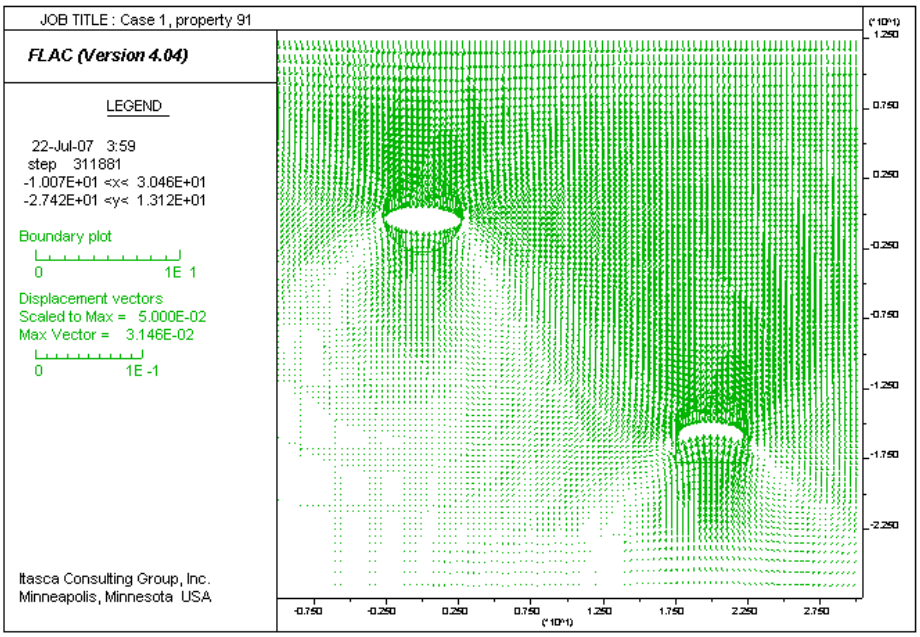

Figure 6-59 Displacements due to Excavations of Observation Drift and Emplacement Drift

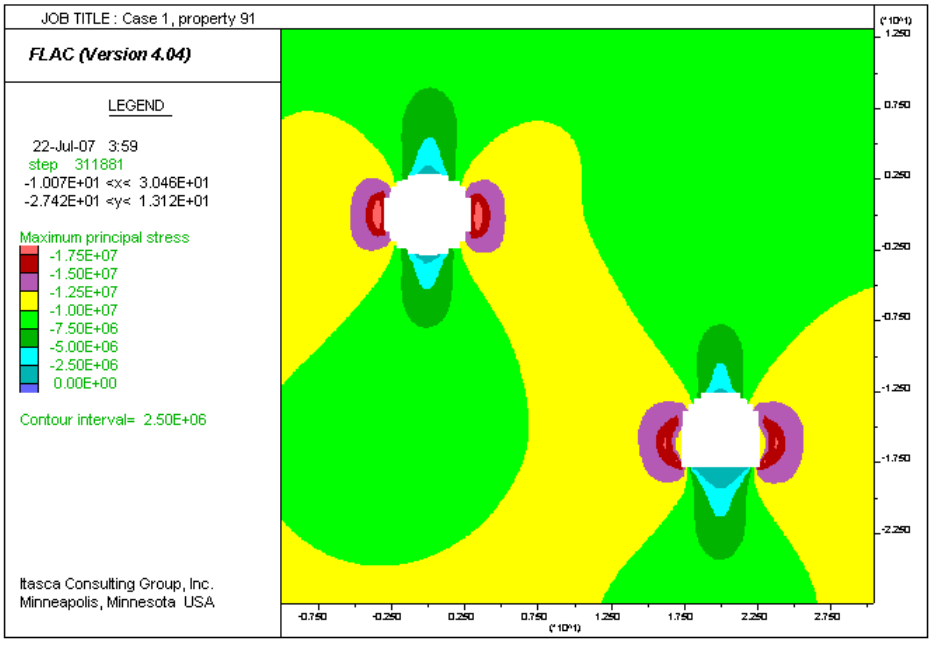

Figure 6-60 Contours of Major Principal Stress after Excavation of Observation Drift and Emplacement Drift

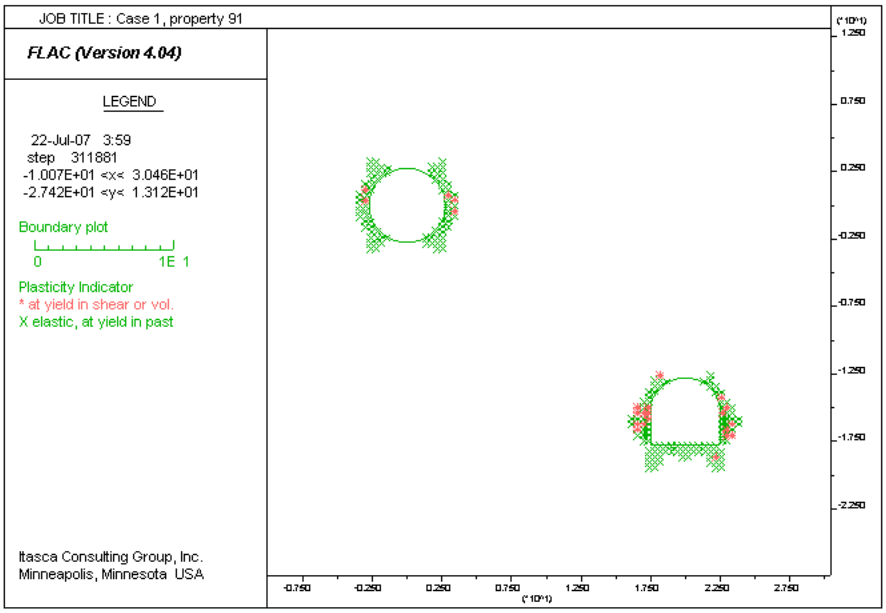

Figure 6-61 Potential Yield Zone after Excavation of Observation Drift and Emplacement Drift

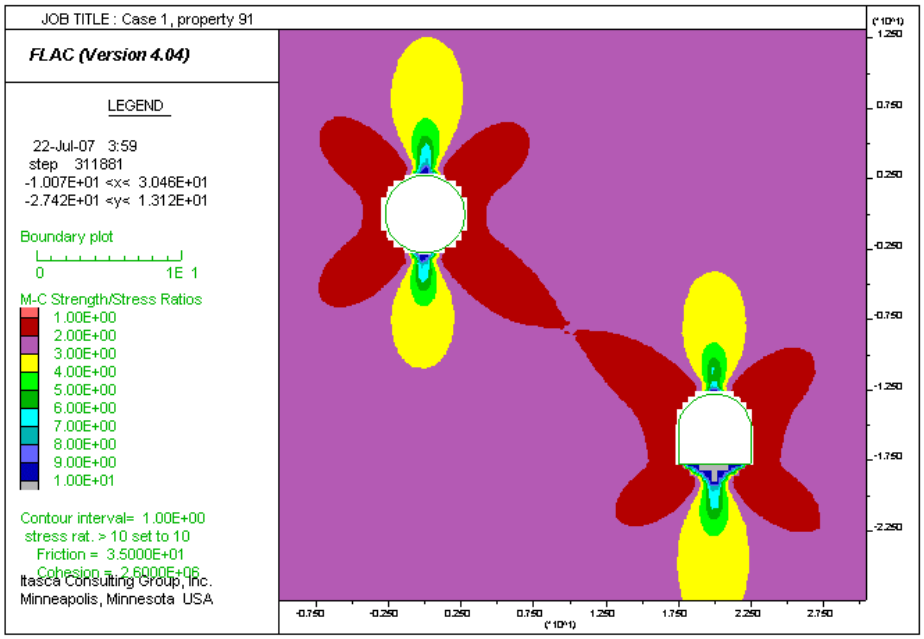

Figure 6-62 Factor of Safety after Excavation of Observation Drift and Emplacement Drift

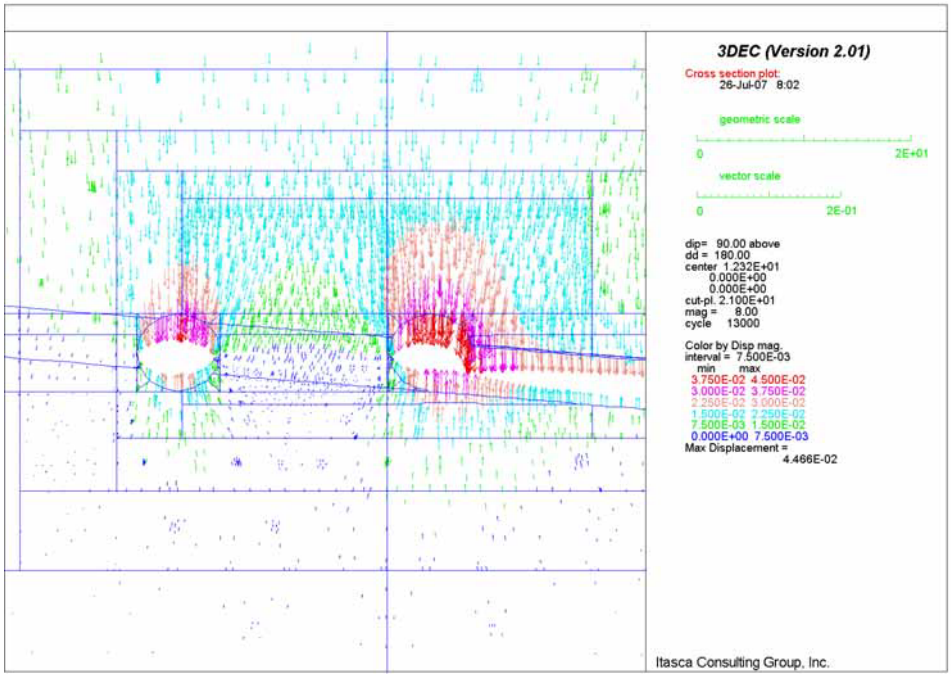

Figure 6-63 Displacement Field in Vertical Section 1 at Intersection between Observation Drift and Exhaust Main

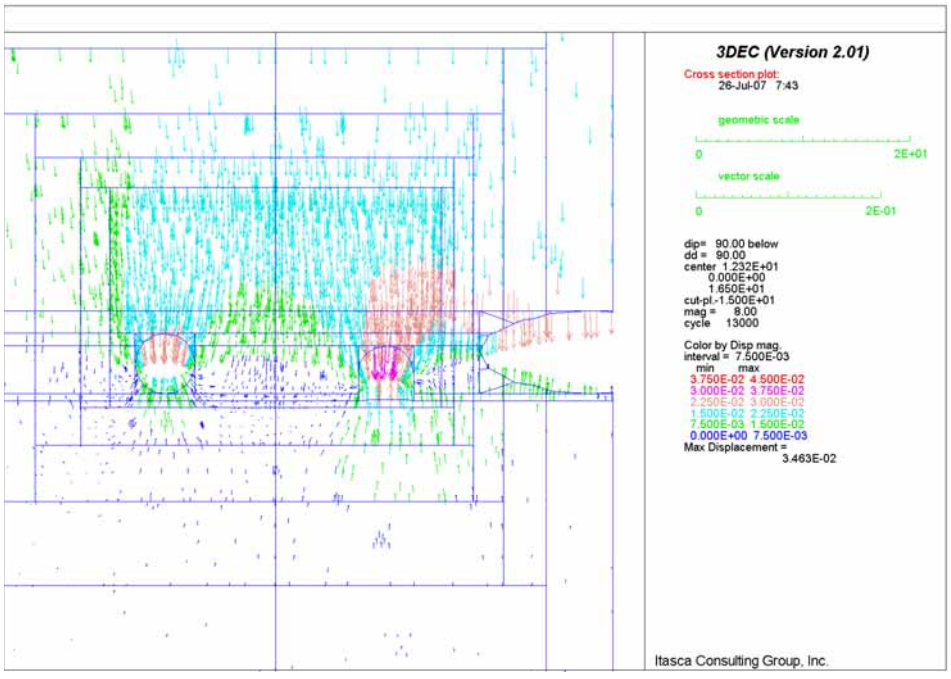

Figure 6-64 Displacement Field in Vertical Section 2 at Intersection between Observation Drift and Exhaust Main

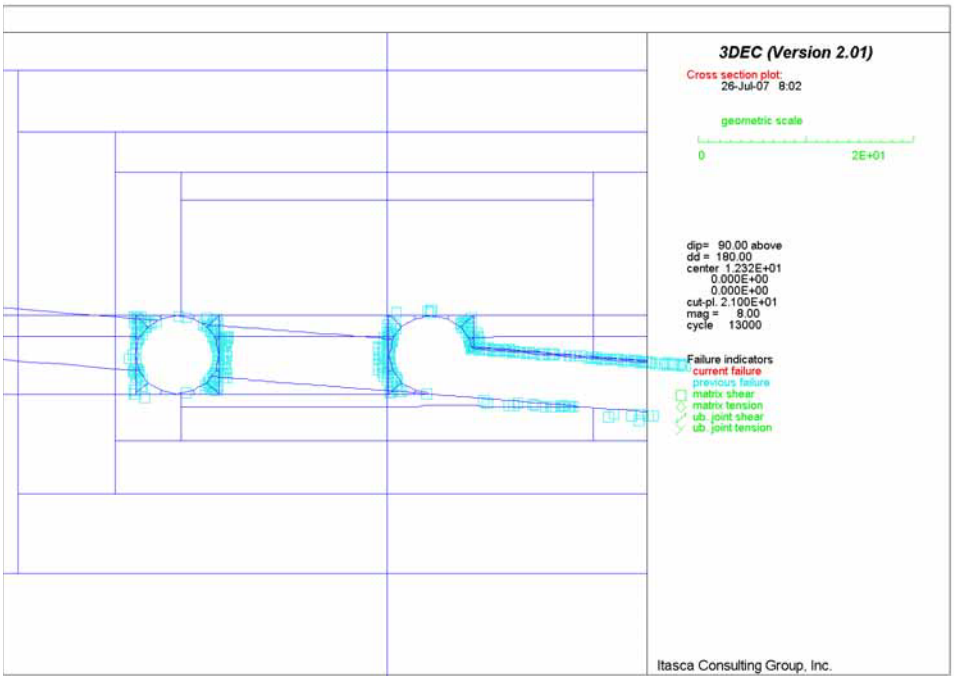

Figure 6-65 Potential Yield Zone in Intersection between Observation Drift and Exhaust Main in Section 1

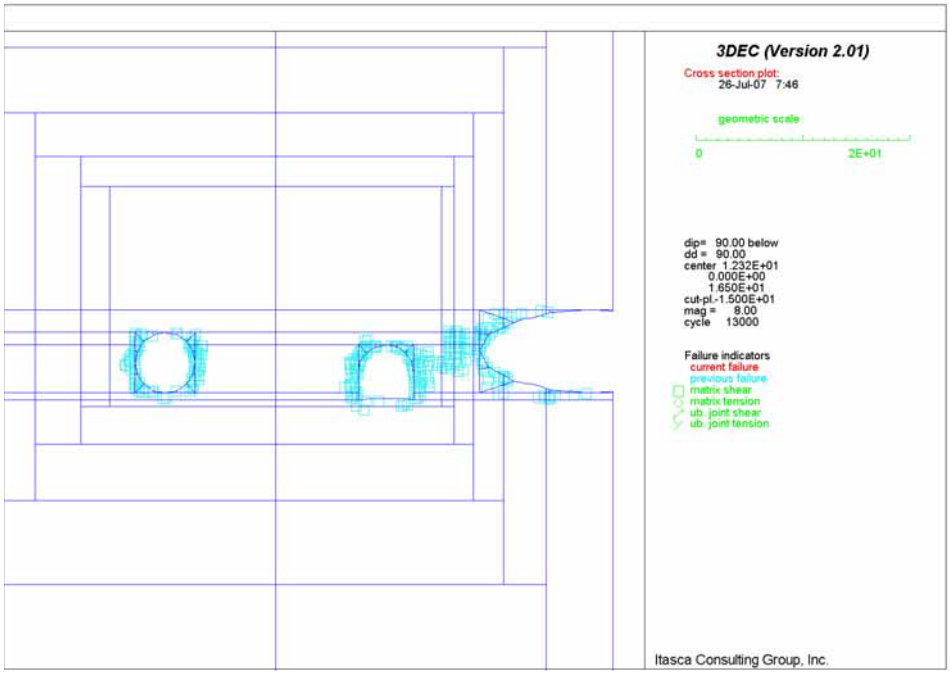

Figure 6-66 Potential Yield Zone in Intersection between Observation Drift and Exhaust Main in Section 2

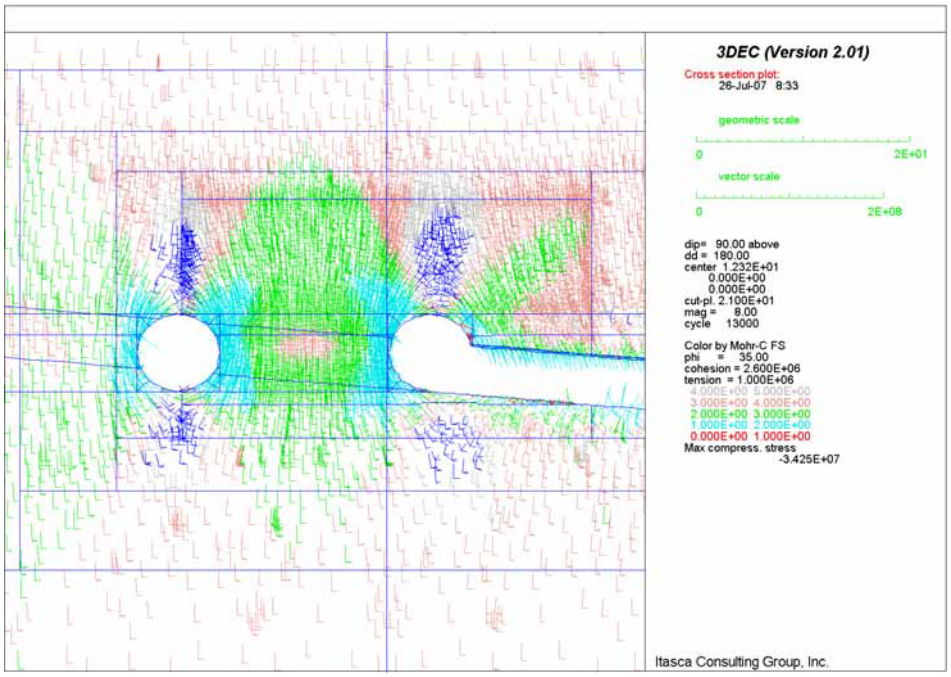

Figure 6-67 Factor of Safety in Intersection between Observation Drift and Exhaust Main in Section 1

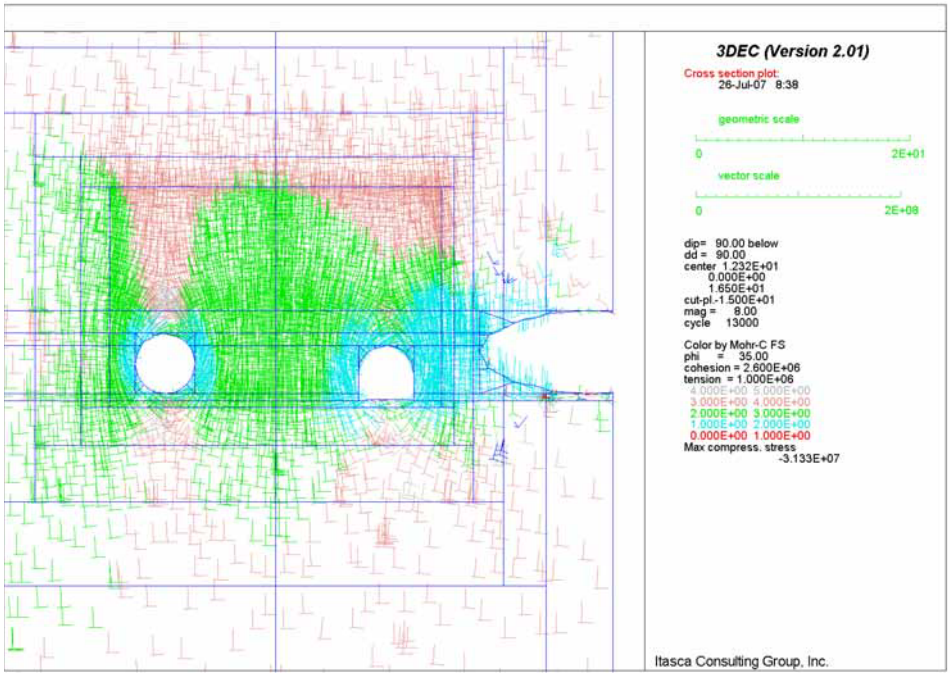

Figure 6-68 Factor of Safety in Intersection between Observation Drift and Exhaust Main in Section 2

6.5.3.1.5 TBM Launch Chamber

The larger span of the TBM launch chamber (11 m) compared to other openings considered (i.e., access mains and exhaust mains) results in larger displacements due to excavation and relaxation of the in situ stresses. The maximum displacement is 0.061 m (Figure 6-69). The stress state around the chamber (

Figure 6-70) is similar to the stress state around the observation drift (Figure 6-60), because two excavations have the same shape. Consequently, the size of the region of the rock mass undergoing inelastic deformation (

Figure 6-71), when scaled with characteristic dimension of the excavation, is the same for the launch chamber as for the observation drift. Because the span (or height) of the launch chamber is approximately two times of the span of the observation drift, the depth of the damaged rock in the wall of the launch chamber is about 2 m, compared to the depth of about 1 m predicted in the wall of the observation drift. Outside the yielded region, the factor-of-safety to shear failure increases rapidly as a function of distance from the drift wall (Figure 6-72), indicating overall stability of the excavation.

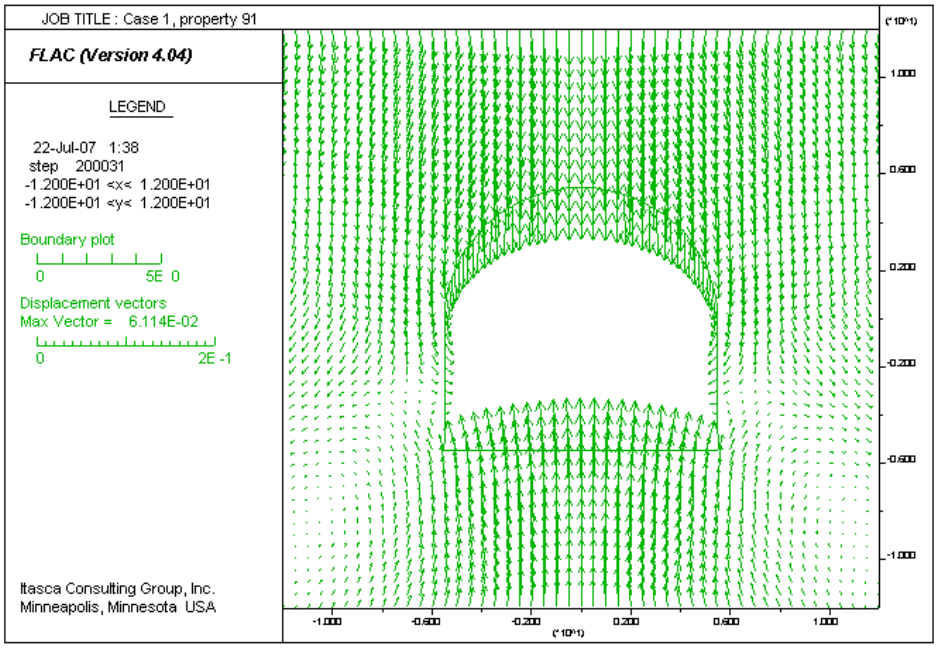

Figure 6-69 Displacements due to Excavation of TBM Launch Chamber

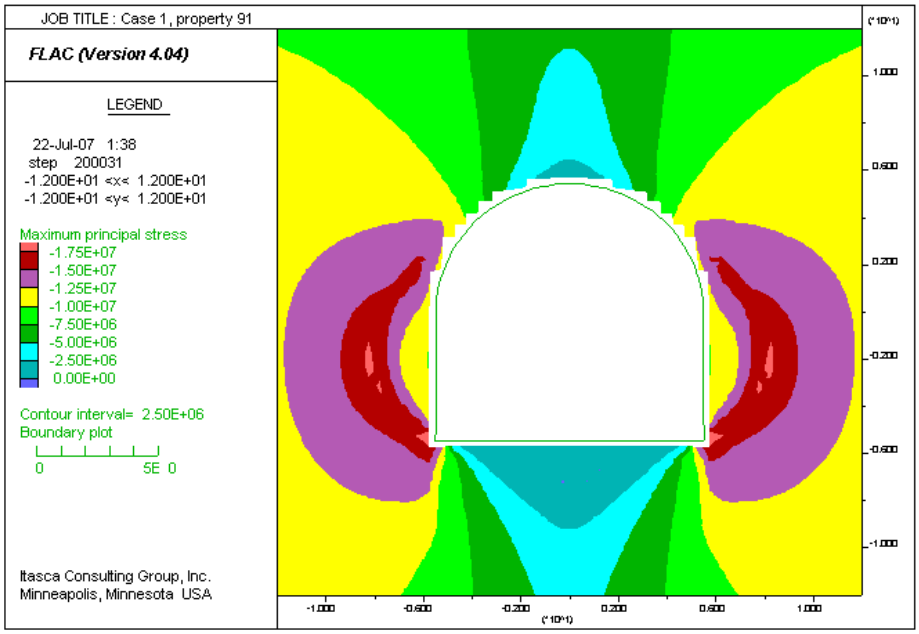

Figure 6-70 Contours of Major Principal Stress after Excavation of TBM Launch Chamber

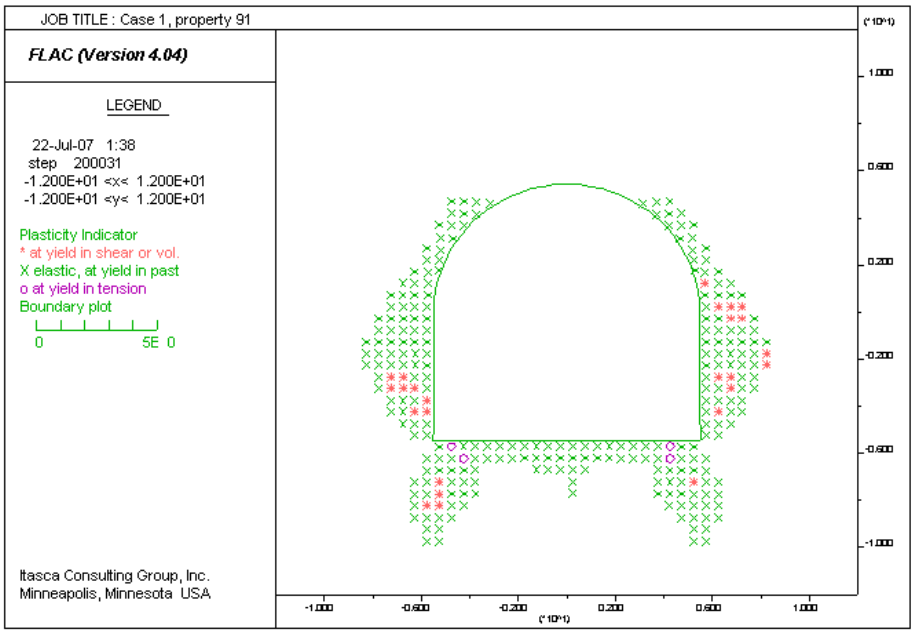

Figure 6-71 Potential Yield Zone after Excavation of TBM Launch Chamber

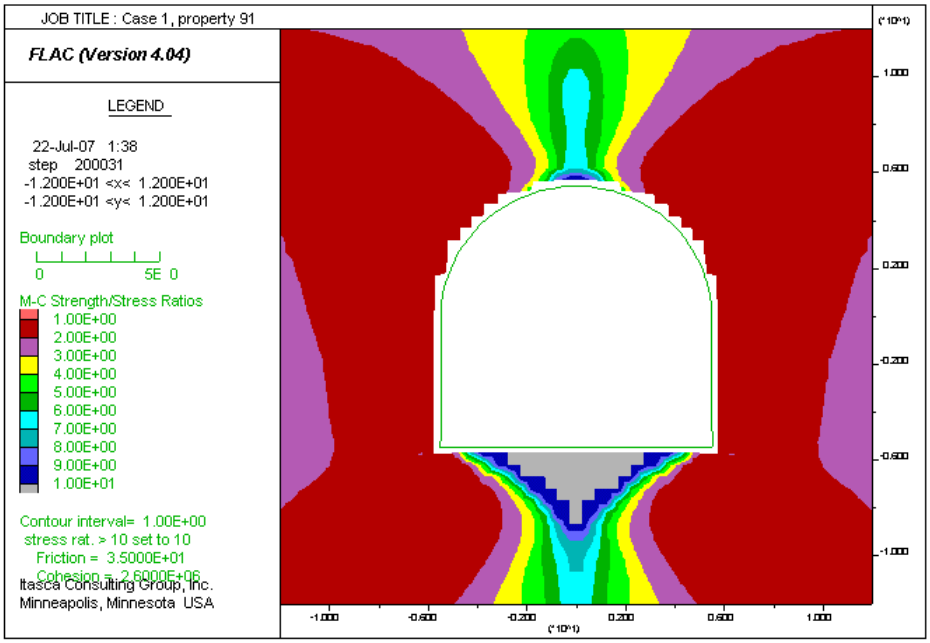

Figure 6-72 Factor of Safety after Excavation of TBM Launch Chamber

6.5.3.1.6 North Portal

The model results under static in situ conditions after both the slope and the starter tunnel are excavated are shown in Figure 6-73 to Figure 6-75. The stress state is completely elastic. Small overburden and slope heights result in stresses (Figure 6-74) that are small compared to cohesion, even in the case of the poorest-quality rock mass, category 1, which was considered in the calculation. The factor-of-safety with respect to Mohr-Coulomb shear failure is quite large (approximately 5) throughout the entire model (see Figure 6-73). The displacement field shown in Figure 6-75 is due to the excavation of the starter tunnel only. The magnitude of the displacements is very small, of the order of 0.0015 m or less. It appears from the results of the numerical modeling that the North Portal and the starter tunnel would be stable for the considered mechanical properties of the rock mass even if no ground support was used.

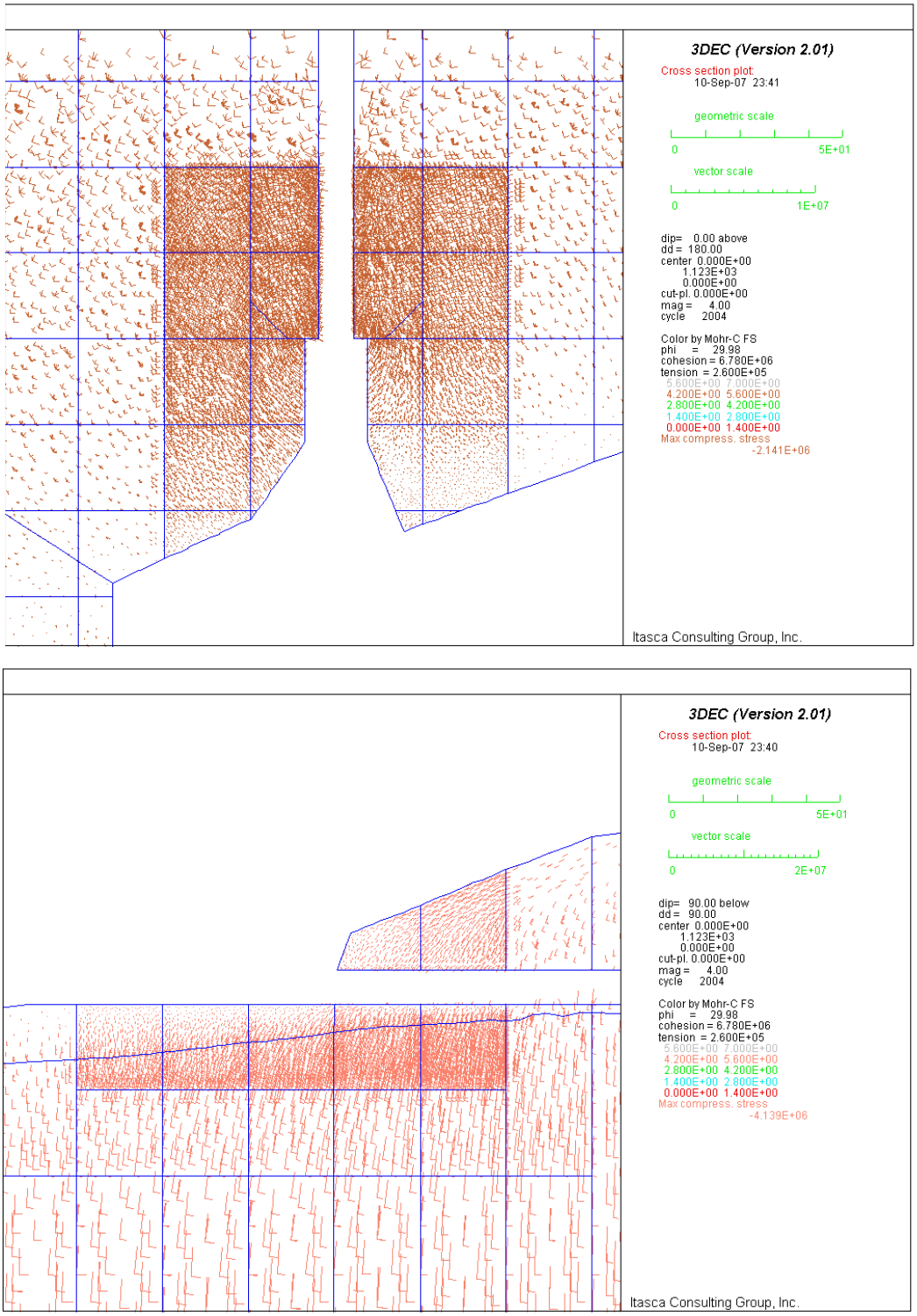

Figure 6-73 Factor of Safety after Excavation of North Portal Starter Tunnel: top) Horizontal Cross-section at Elevation 1123 m, and bottom) Longitudinal Cross-section L-L'

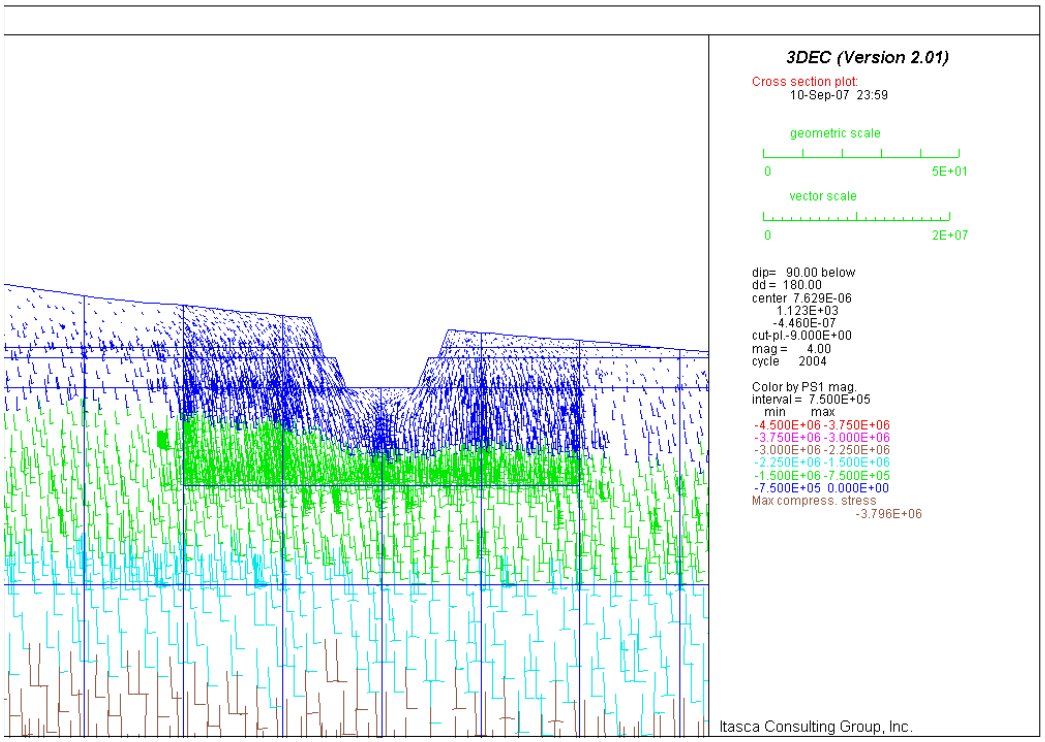

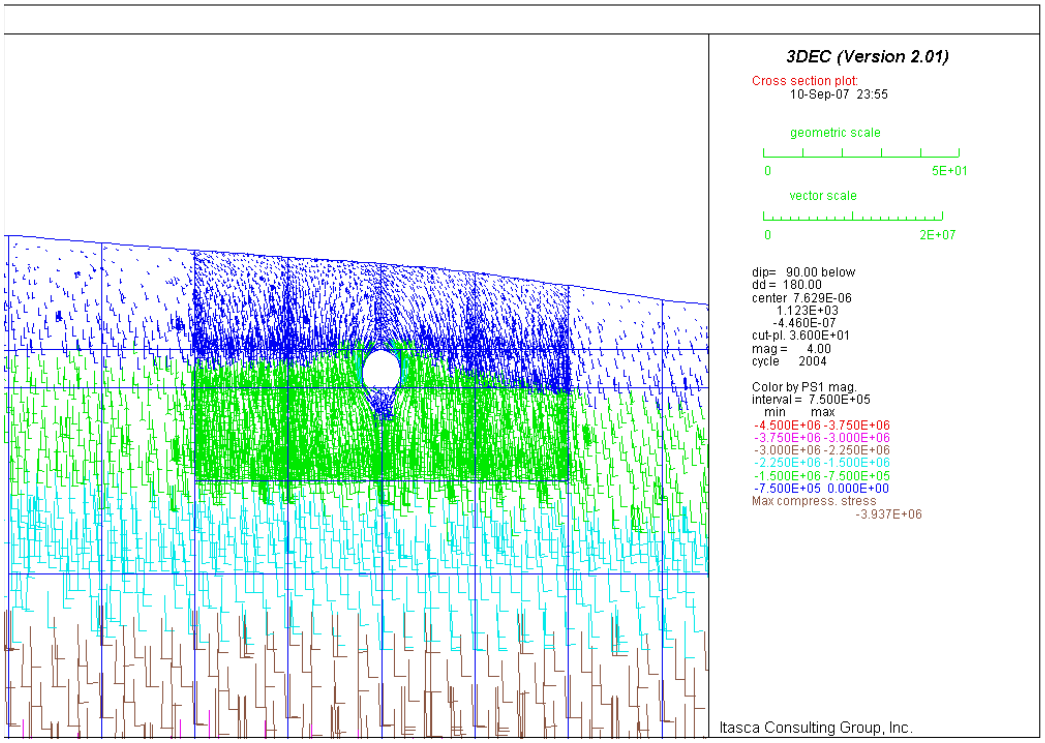

Figure 6-74 Principal Stresses after Excavation of North Portal Starter Tunnel for Cross-sections: top) C1-C1' and bottom) C2-C2'

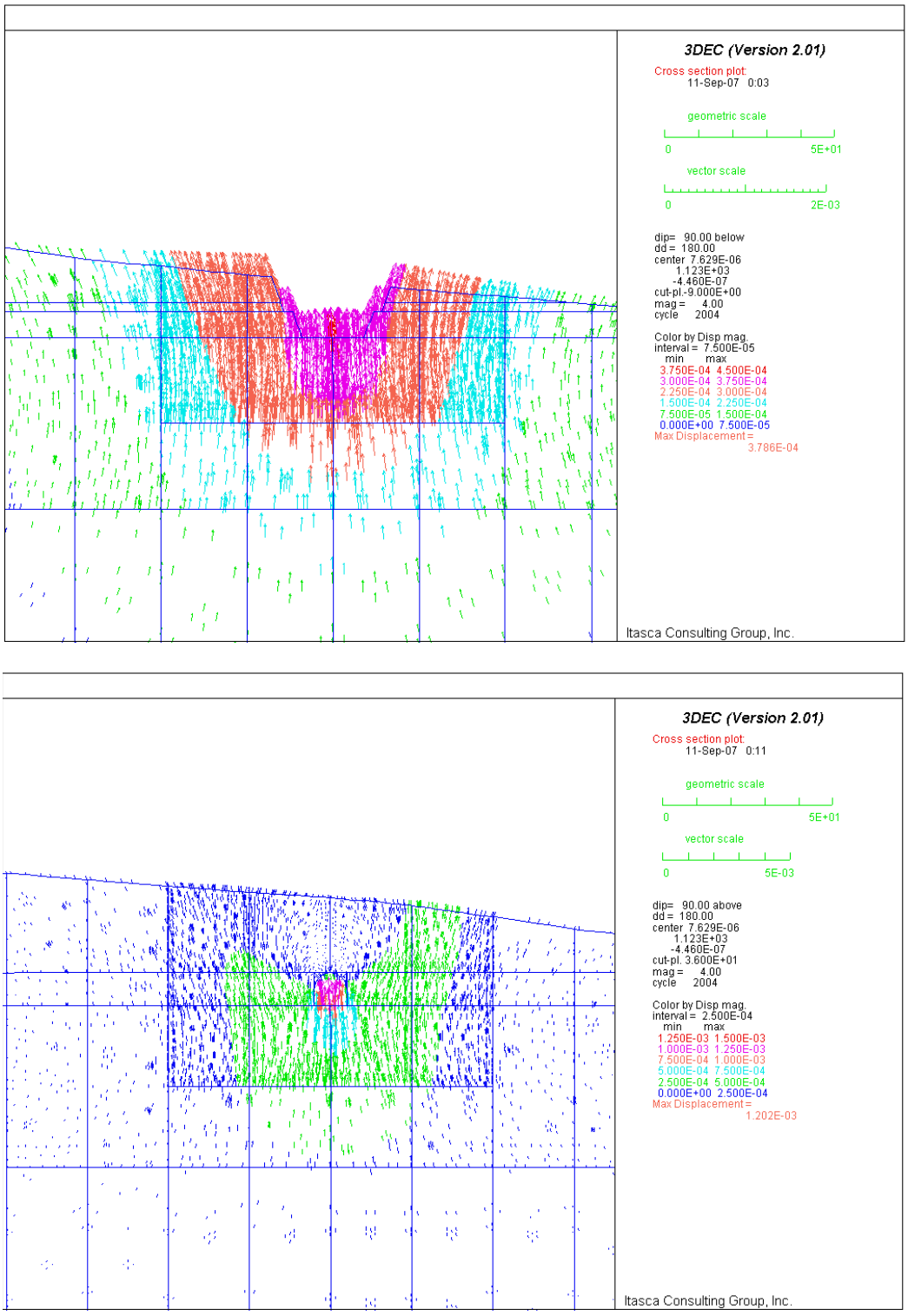

Figure 6-75 Displacement Field after Excavation of North Portal Starter Tunnel for Cross-sections: top) C1-C1' and bottom) C2-C2'

6.5.3.1.7 Interburden Pillar between Shaft Access and Exhaust Mains

The results of the interburden pillar stability analysis are shown in Figure 6-76 through Figure 6-83. The results are for the final stage of the excavation. The maximum vertical displacement in the exhaust mains (crown and floor) is less than 37.5 mm. In the access drift, the maximum vertical displacement of 45 mm (Figure 6-76 and Figure 6-77) occurs in the crown of drift.

The excavation of drifts causes maximum stress concentrations of approximately 25 and 24 MPa (see Figure 6-78 and Figure 6-79) in the walls of the exhaust mains and access drift, respectively. However, SFs with respect to the Mohr-Coulomb yield condition averaging 1 to 3 are shown for the rock immediately surrounding the drifts (shown in Figure 6-80 and Figure 6-81 In addition, a limited extent of the rock mass yielding is shown in Figure 6-82 and Figure 6-83. Therefore, the results indicate that deformation of the rock mass around the drifts and in the pillar between the drifts will be predominantly elastic.

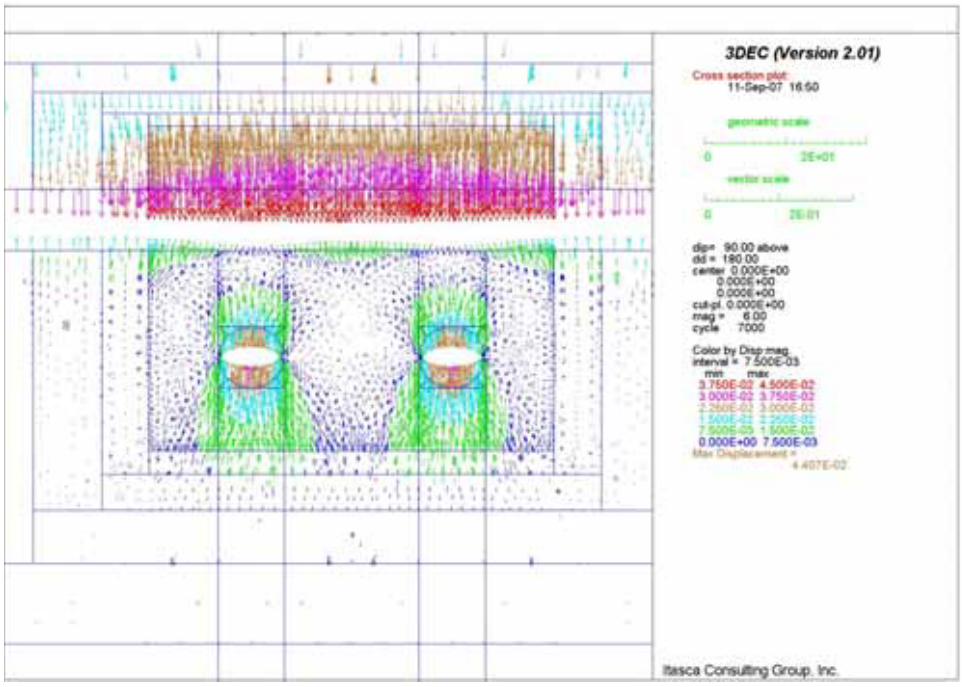

Figure 6-76 Displacement Field in Vertical Section 1 for Lith. Cat. 1 Rock at Interburden Area

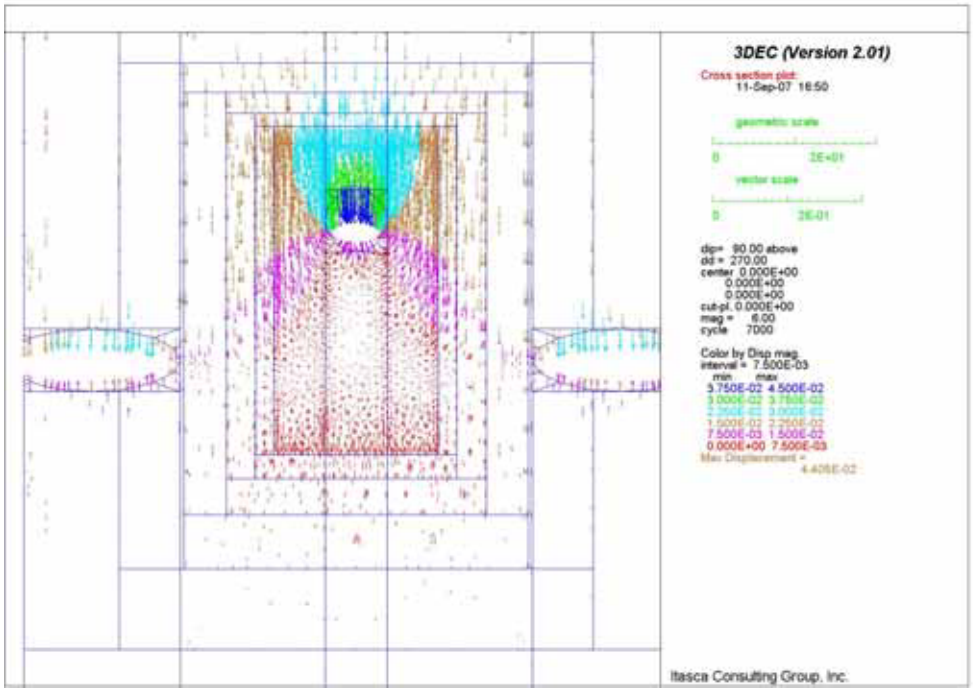

Figure 6-77 Displacement Field in Vertical Section 2 for Lith. Cat. 1 Rock at Interburden Area

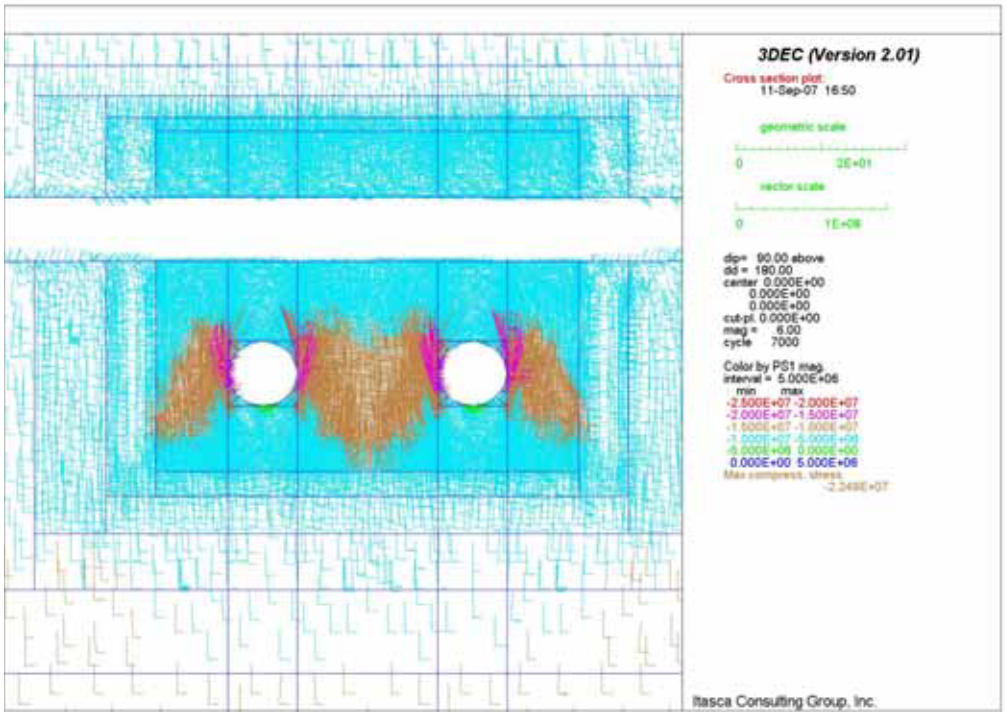

Figure 6-78 Stress Field in Vertical Section 1 for Lith. Cat. 1 Rock at Interburden Area

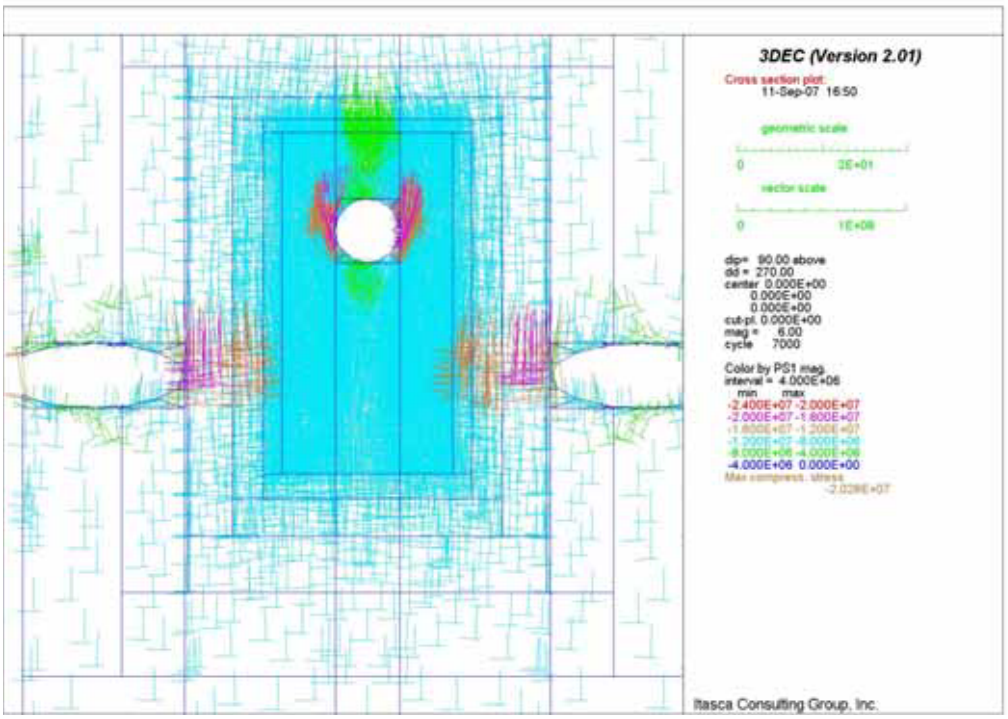

Figure 6-79 Stress Field in Vertical Section 2 for Lith. Cat. 1 Rock at Interburden Area

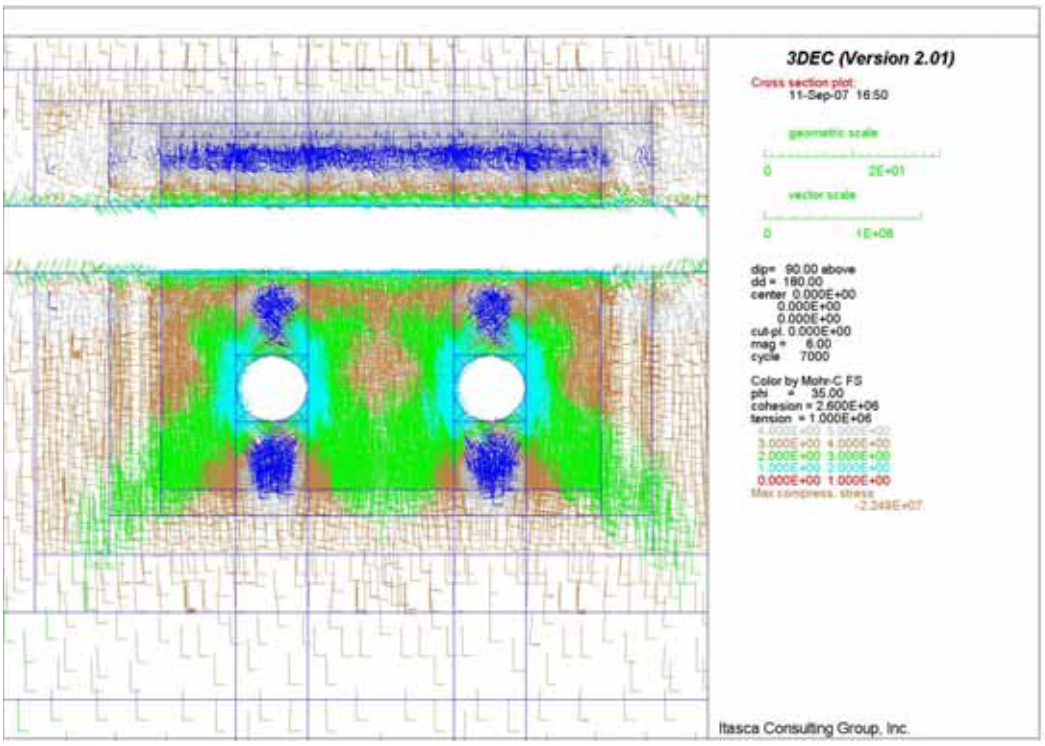

Figure 6-80 Factor of Safety in Vertical Section 1 for Lith. Cat. 1 Rock at Interburden Area

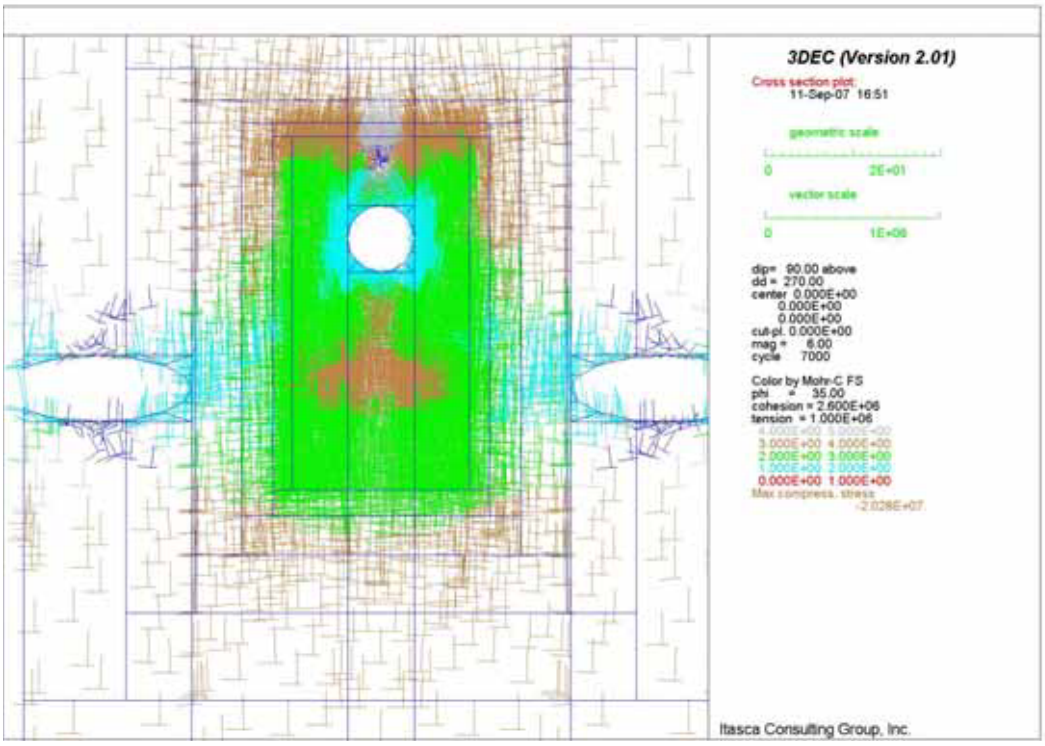

Figure 6-81 Factor of Safety in Vertical Section 2 for Lith. Cat. 1 Rock at Interburden Area

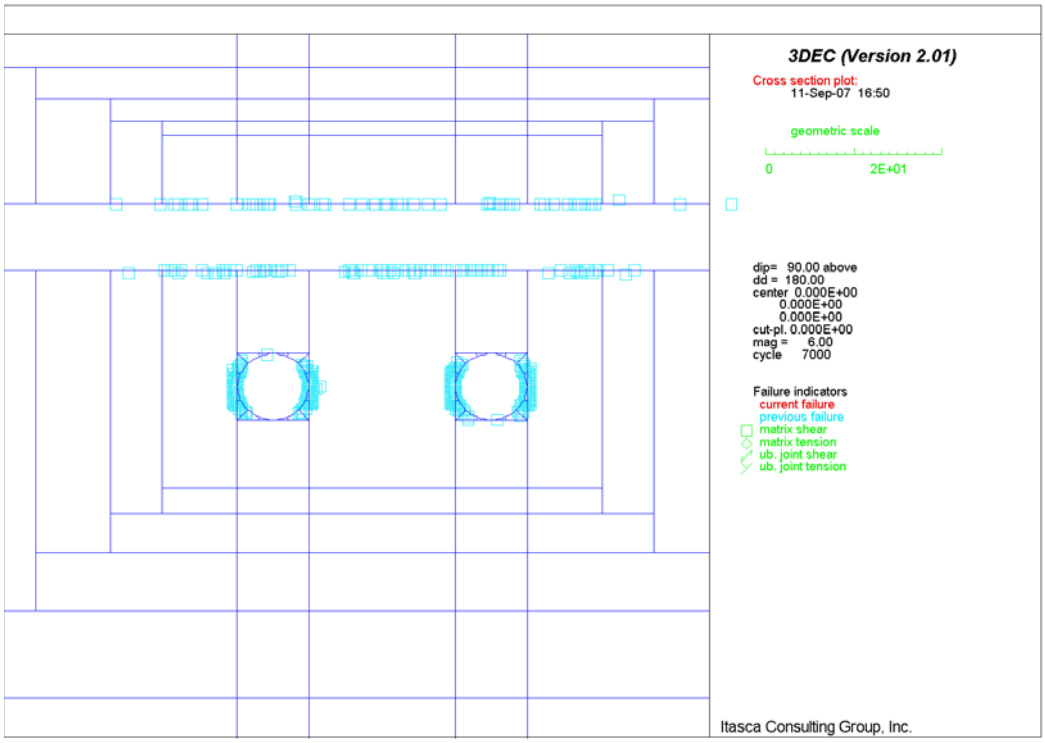

Figure 6-82 Potential Yield Zone in Vertical Section 1 for Lith. Cat. 1 Rock at Interburden Area

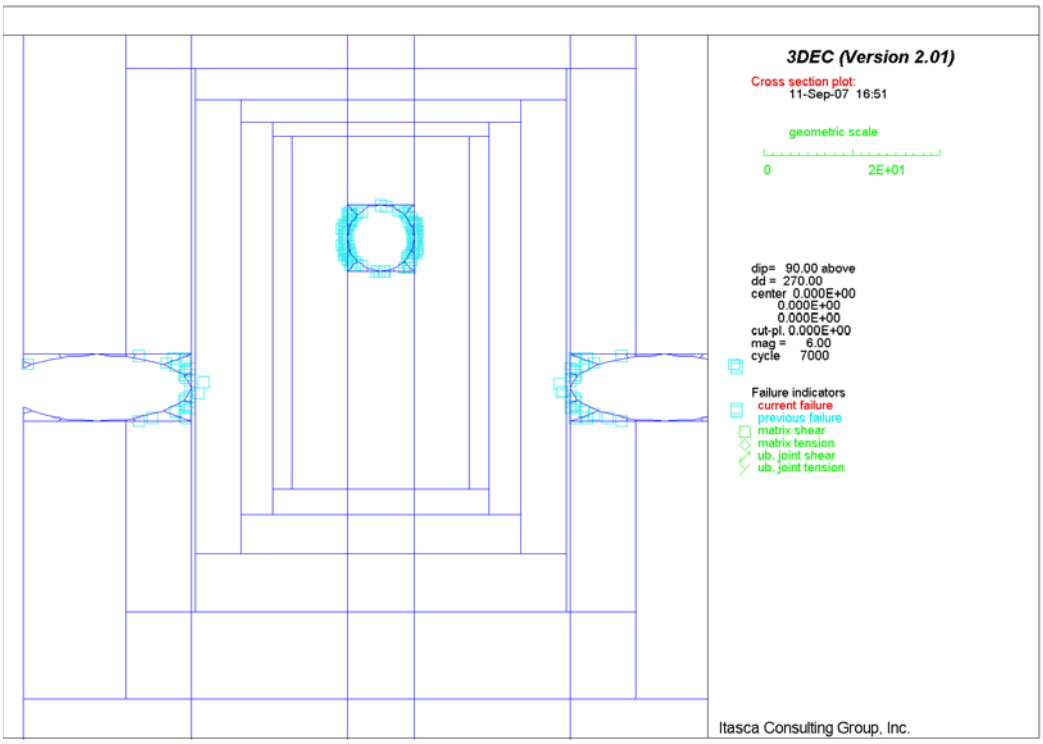

Figure 6-83 Potential Yield Zone in Vertical Section 2 for Lith. Cat. 1 Rock at Interburden Area

6.5.3.2 Thermal Loading Condition

It should be noted the thermal loading condition is only applied to intersections of exhaust mains with emplacement drifts, exhaust mains, observation drift, intersection of observation drift with exhaust main, and interburden pillar between access to intake shaft #4 and exhaust mains. The discussion in this section is limited to these areas.

6.5.3.2.1 Intersection between Exhaust Main and Emplacement Drift

The temperature fields in intersection B, as calculated in NUFT and imported into 3DEC, after 3 and 20 years of heating are shown in Figure 6-84 and Figure 6-85. The temperature histories at points 1 and 3 (indicated in Figure 6-14 and Figure 6-15) are shown in Figure 6-86 and Figure 6-87 for intersections B and C, respectively. As indicated in Figure 6-88, thermally induced variation of major principal stress in the preclosure period is relatively small, i.e., about a few percent with respect to the initial stress state before heating began.

The thermal stress changes, shown (at points 1 and 3 at intersections B and C) are much larger in better quality and stiffer rock masses (comparing Figure 6-88 and Figure 6-90 with Figure 6-89 and Figure 6-91). The increase in the maximum major principal stress is about 25 MPa in category 5 of the lithophysal and non-lithophysal rock masses. However, the stress change does not change factor-of-safety with respect to the Mohr-Coulomb yield condition throughout the rock mass (Figure 6-92 through Figure 6-95) nor cause significant additional yielding of the rock mass (comparing Figure 6-96 and Figure 6-97 with Figure 6-55 and Figure 6-56). The extent of plastic deformation for both intersections, and for the different rock-mass categories remains practically unchanged after 50 years of heating. The heating causes movement of the entire model vertically upward. The change in displacement in the vertical direction of the excavation in the intersection (at point 1) due to temperature change is not significant (Figure 6-98 and Figure 6-99). For intersections B and C, it appears that displacement in the vertical direction at point 1 is reduced.

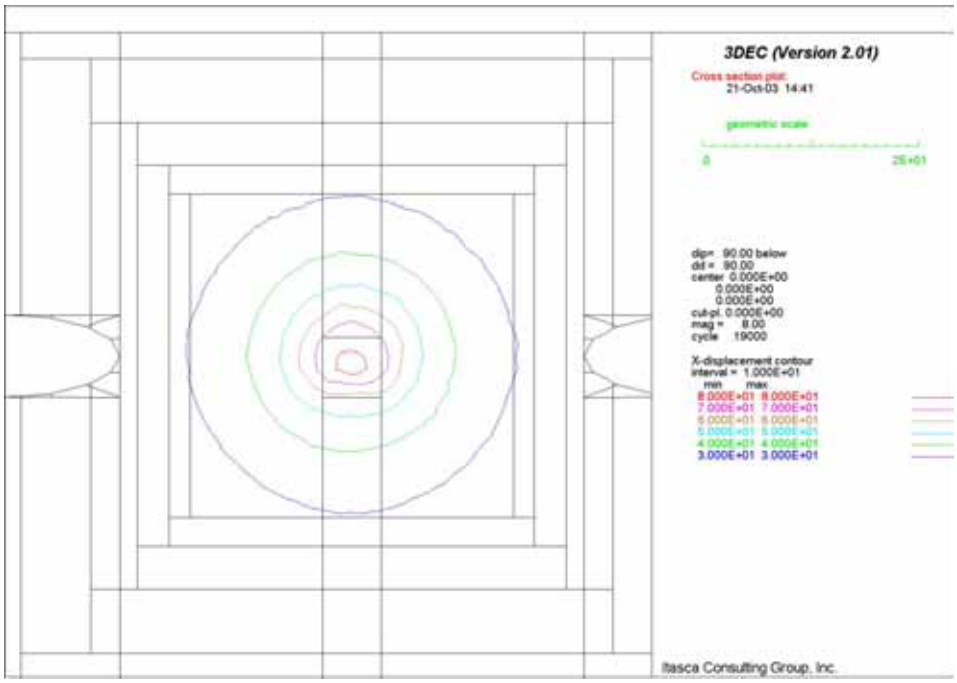

Figure 6-84 Intersection B: Temperature Field in Vertical Section 1 after 3 Years of Heating

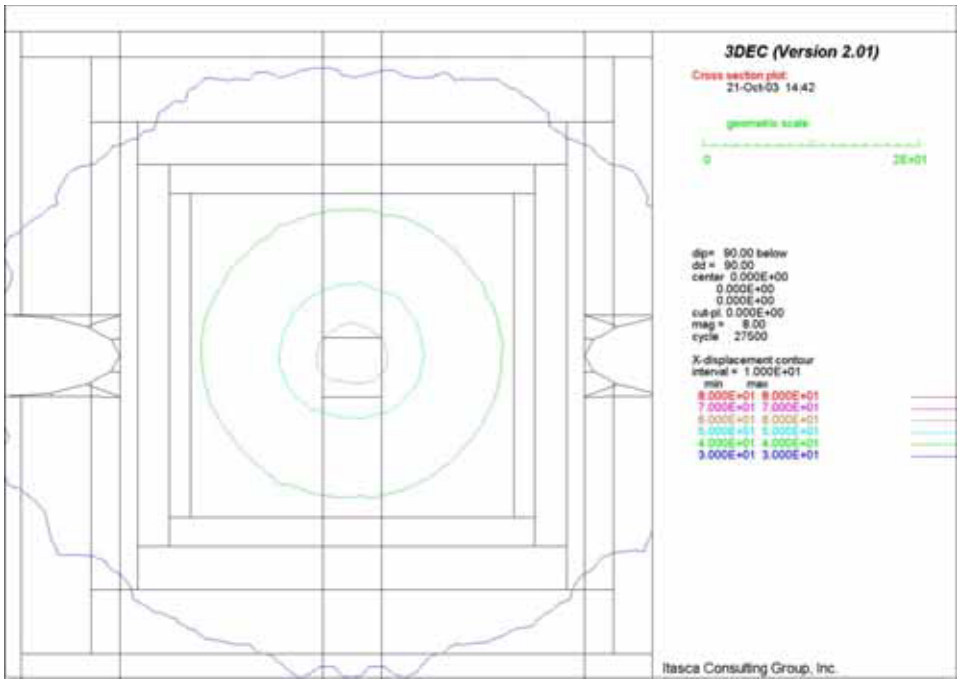

Figure 6-85 Intersection B: Temperature Field in Vertical Section 1 after 20 Years of Heating

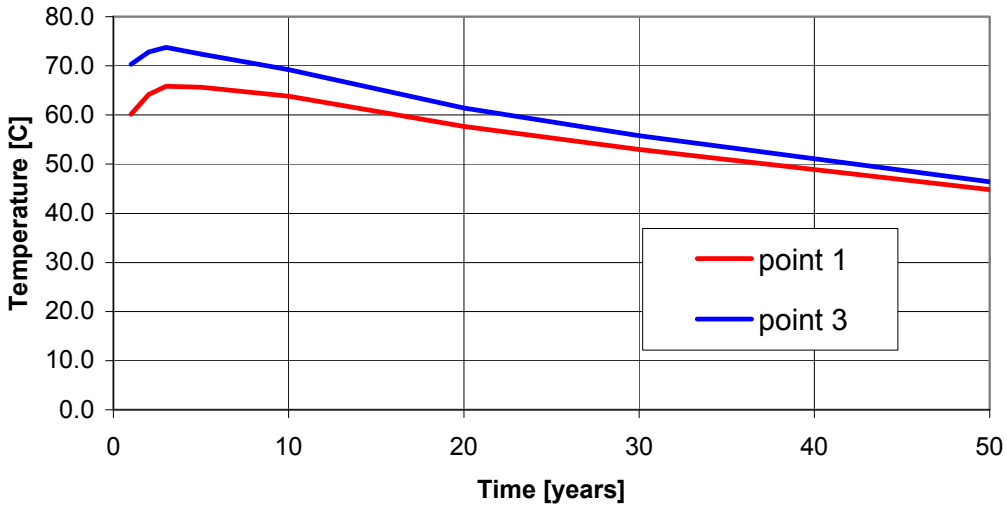

Figure 6-86 Intersection B: Temperature History at Points 1 and 3

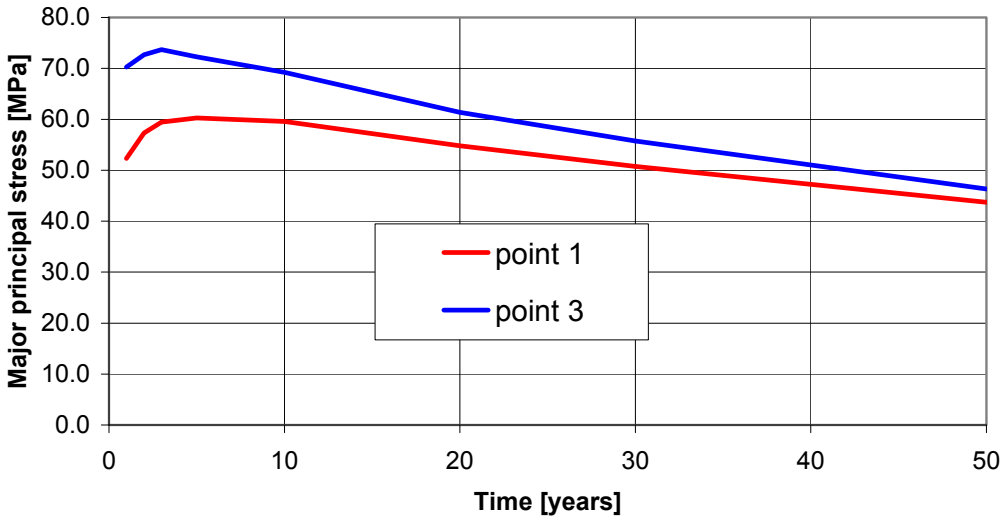

Figure 6-87 Intersection C: Temperature History at Points 1 and 3

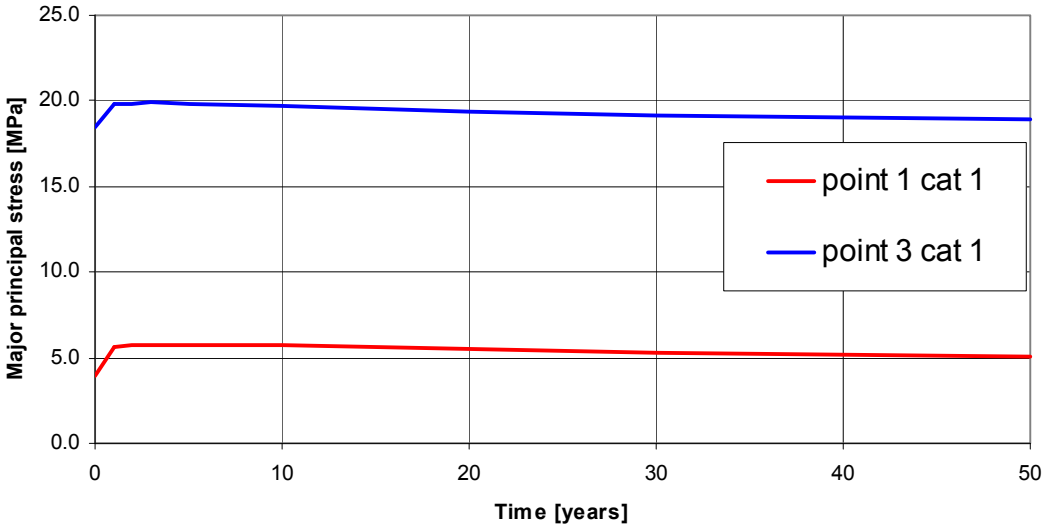

Figure 6-88 Intersection B: Time History of Major Principal Stresses for Lith. Cat. 1 Rock

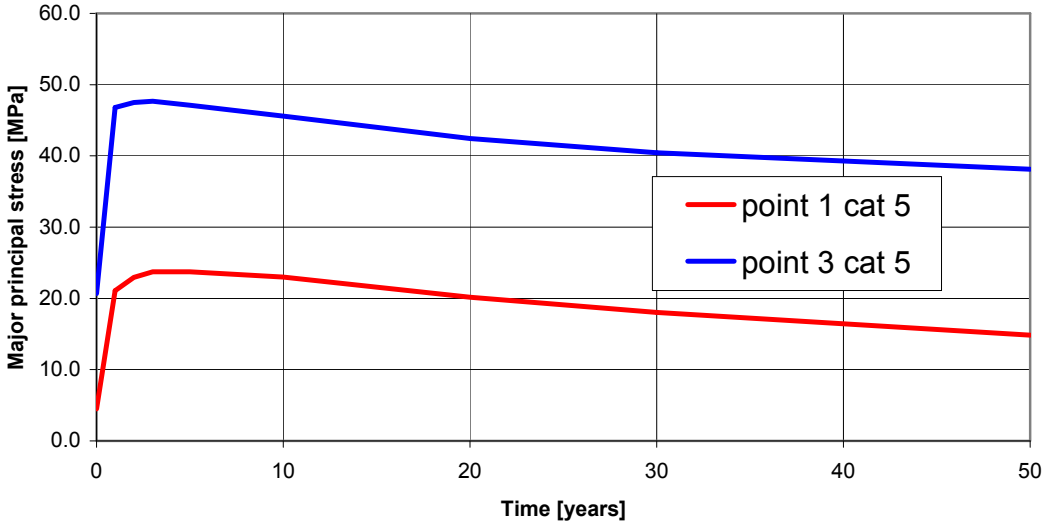

Figure 6-89 Intersection B: Time History of Major Principal Stresses for Lith. Cat. 5 Rock

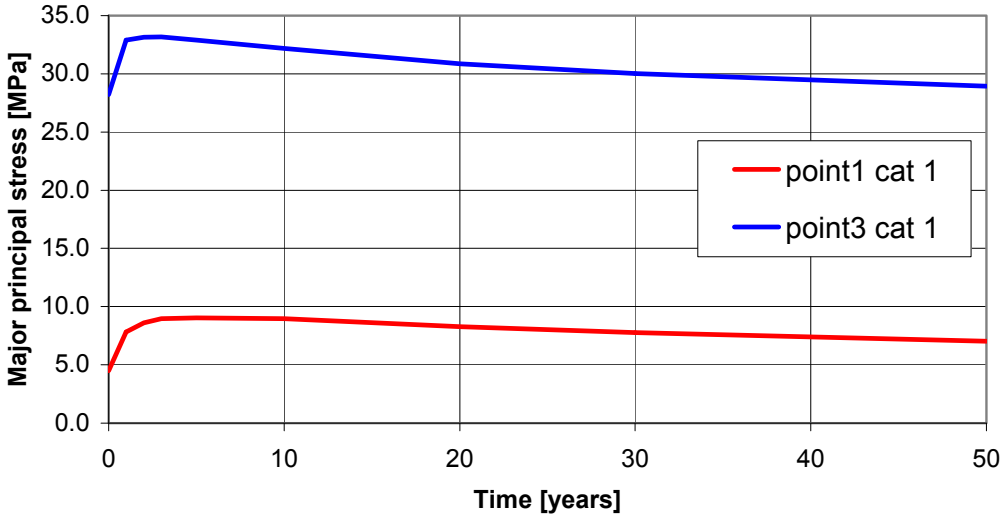

Figure 6-90 Intersection C: Time History of Major Principal Stresses for Nonlith. Cat. 1 Rock

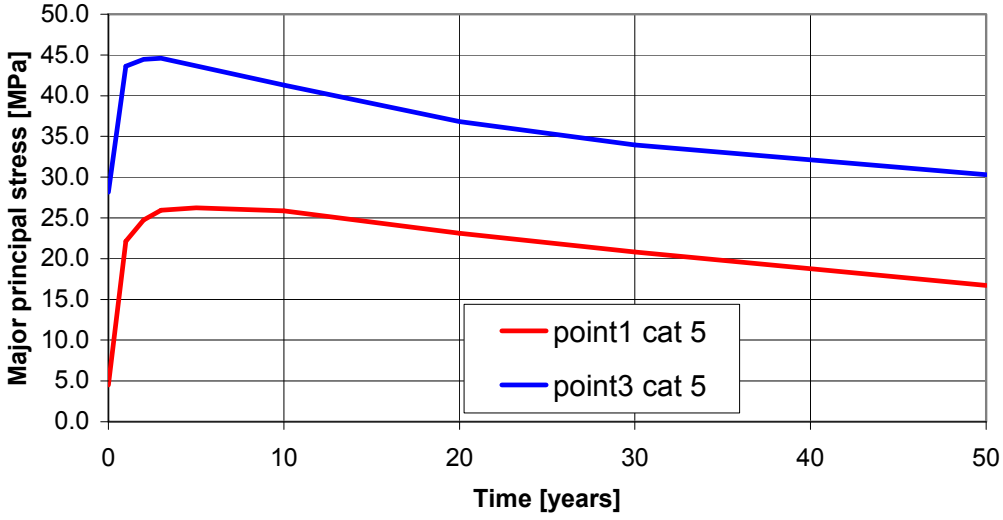

Figure 6-91 Intersection C: Time History of Major Principal Stresses for Nonlith. Cat. 5 Rock

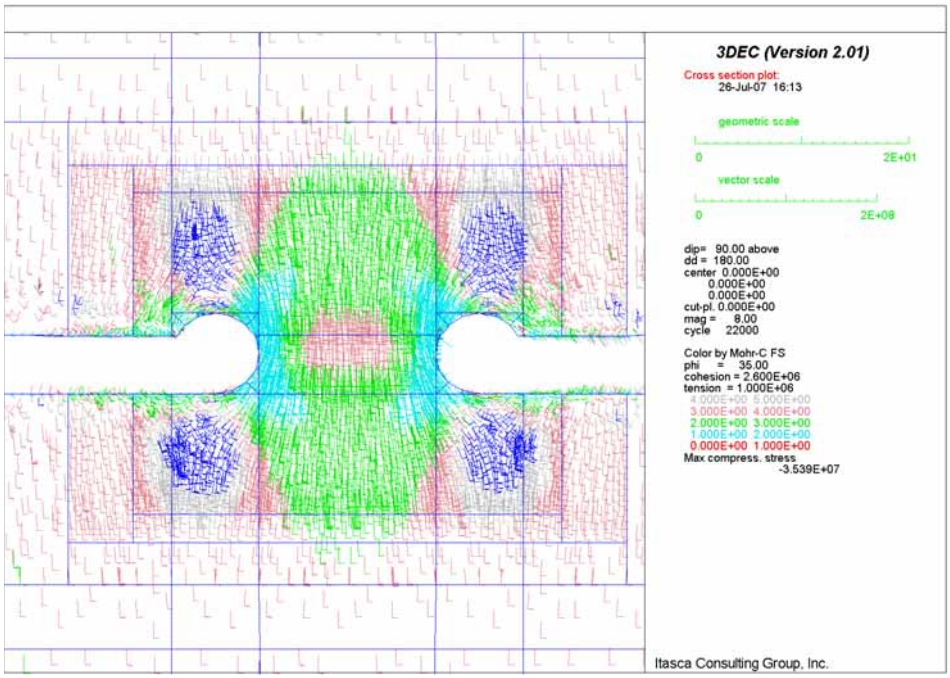

Figure 6-92 Intersection B: Factor of Safety in Vertical Section 1 for Lith. Cat. 1 Rock after 1 Year of Heating

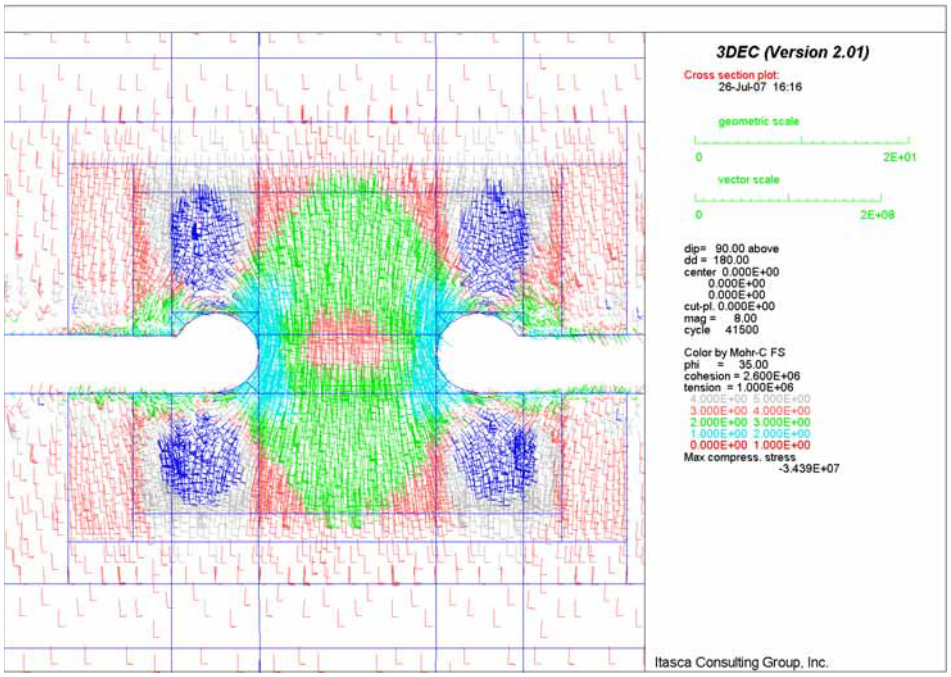

Figure 6-93 Intersection B: Factor of Safety in Vertical Section 1 for Lith. Cat. 1 Rock after 50 Years of Heating

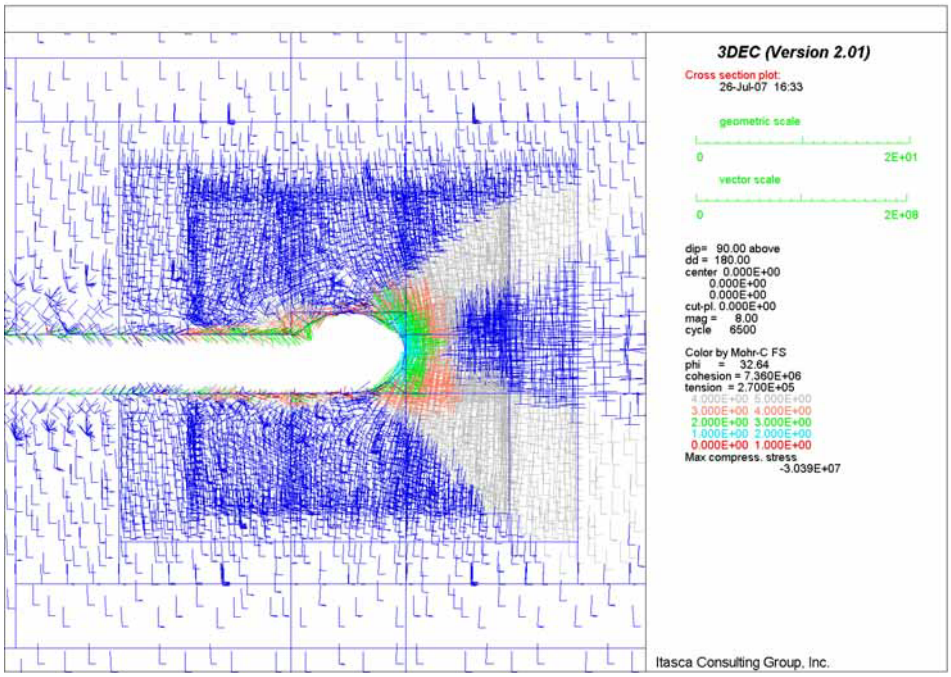

Figure 6-94 Intersection C: Factor of Safety in Vertical Section 1 for Nonlith. Cat. 1 Rock after 1 Year of Heating

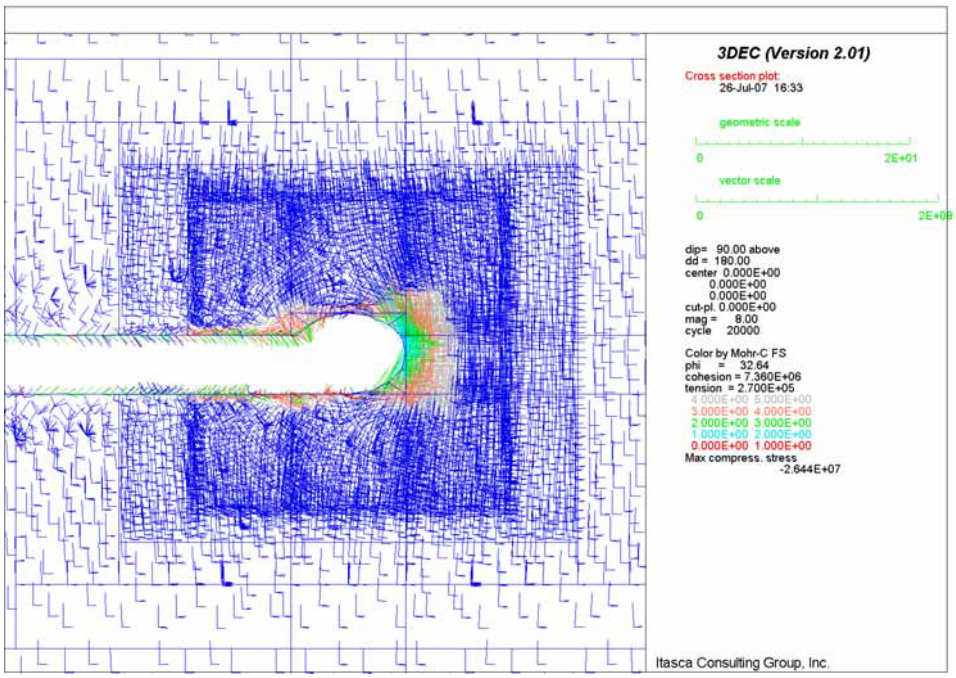

Figure 6-95 Intersection C: Factor of Safety in Vertical Section 1 for Nonlith. Cat. 1 Rock after 50 Years of Heating

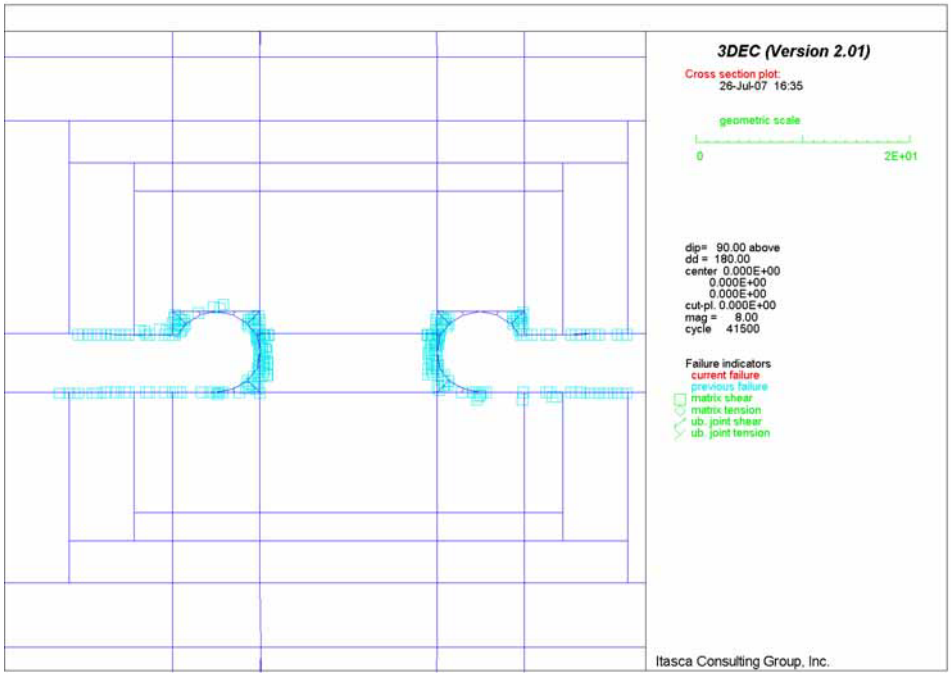

Figure 6-96 Intersection B: Potential Yield Zone in Vertical Section 1 for Lith. Cat. 1 Rock after 50 Years of Heating

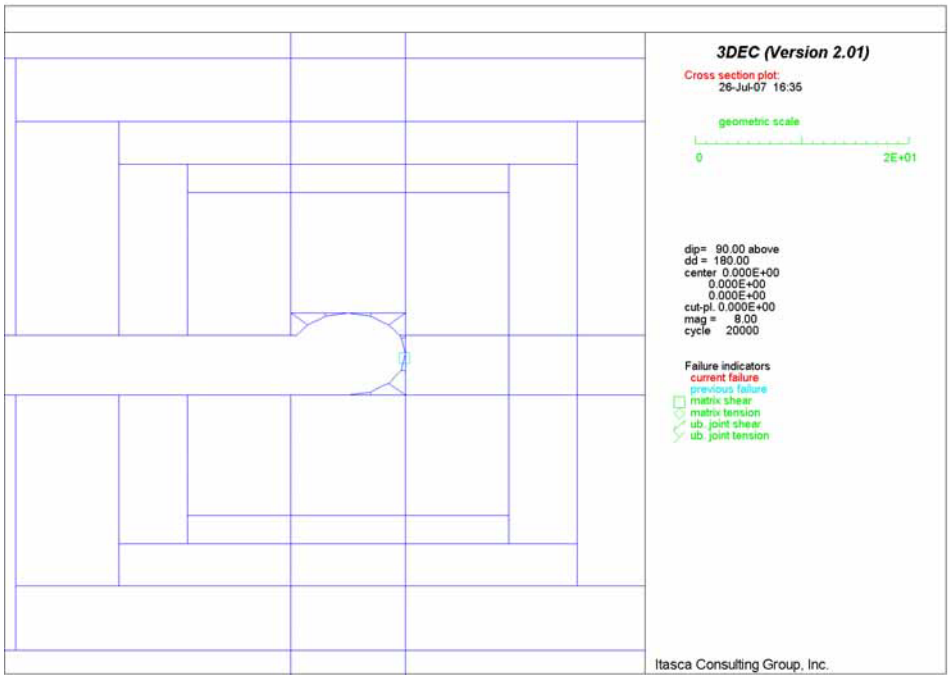

Figure 6-97 Intersection C: Potential Yield Zone in Vertical Section 1 for Nonlith. Cat. 1 Rock after 50 Years of Heating

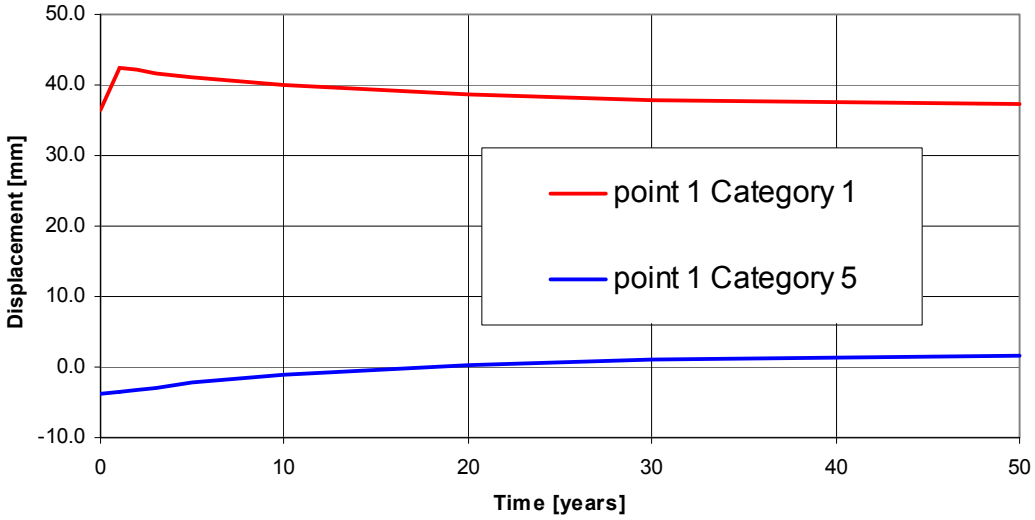

Figure 6-98 Intersection B: Time History of Vertical Displacement at Point 1 for Lith. Rock

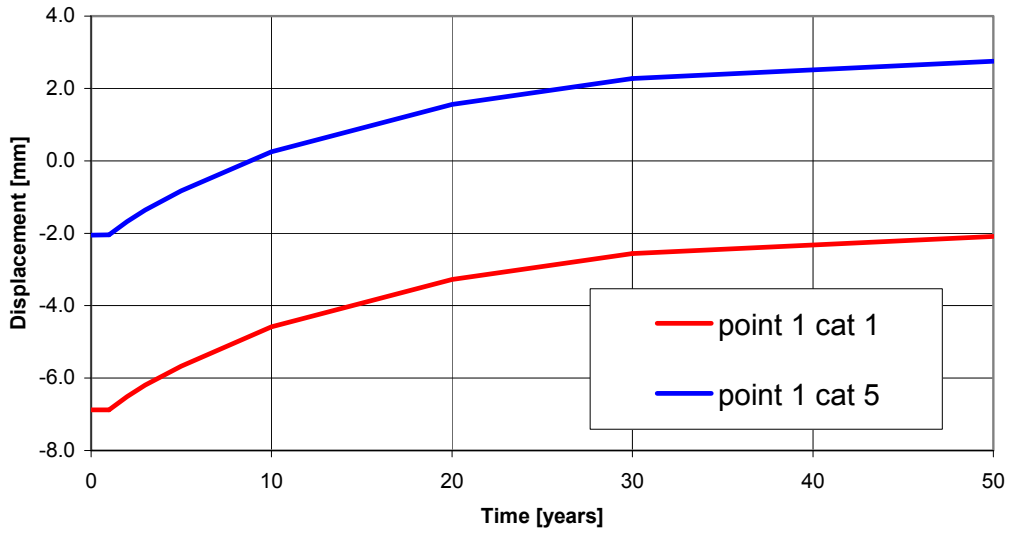

Figure 6-99 Intersection C: Time History of Vertical Closure at Point 1 for Nonlith. Rock

6.5.3.2.2 Exhaust Mains

The temperature field after 50 years of heating around the exhaust mains is shown in Figure 6-100. It should be noted that the temperature conditions shown in this figure are the same as those for rock temperatures in the emplacement drifts based on Assumption 3.2.8. As discussed in Assumption 3.2.8, the exhaust mains are located near (intersecting) the emplacement drifts. After waste emplacement, the exhaust mains will be subjected to the thermal stresses. However, the temperatures in exhaust mains will not exceed those in emplacement drifts. By assuming the same temperatures as those in emplacement drifts will result in higher thermal stresses in the rock at exhaust mains.

Time histories of the drift vertical and horizontal closures are illustrated in Figure 6-101 for unsupported exhaust mains subjected to in situ and thermal loads in the lithophysal and nonlithophysal rock corresponding to the initial horizontal-to-vertical stress ratio (K_o) of 0.3.

For category 1 rock with K_o = 0.3, the maximum vertical closures due to in situ and thermal loads are about 73 mm and 12 mm for the lithophysal and nonlithophysal rock, respectively. The maximum horizontal closures are about 8 and 2 mm for the lithophysal and nonlithophysal rock, respectively.

Category 5 rock mass shows smaller deformations. The maximum vertical closures due to in situ and thermal loads are about 6 mm and 4 mm for the lithophysal and nonlithophysal rock, respectively. The maximum horizontal closures are about 3 mm for both lithophysal and nonlithophysal rocks. The rock deformation is induced primarily by in situ stress during excavation. Thermally-induced deformation is minimal (a maximum of about 3 mm for all cases analyzed) because the increase in temperature during the preclosure ventilation period is very small.

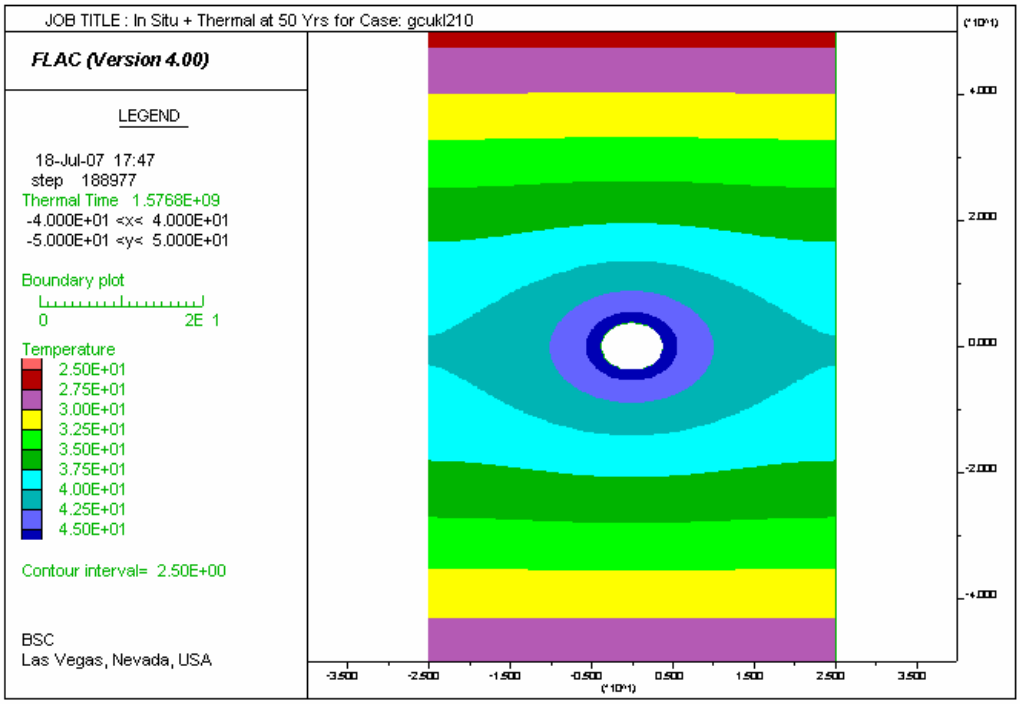

Figure 6-100 Temperature Contours around Exhaust Main after 50 Years of Heating in FLAC Model

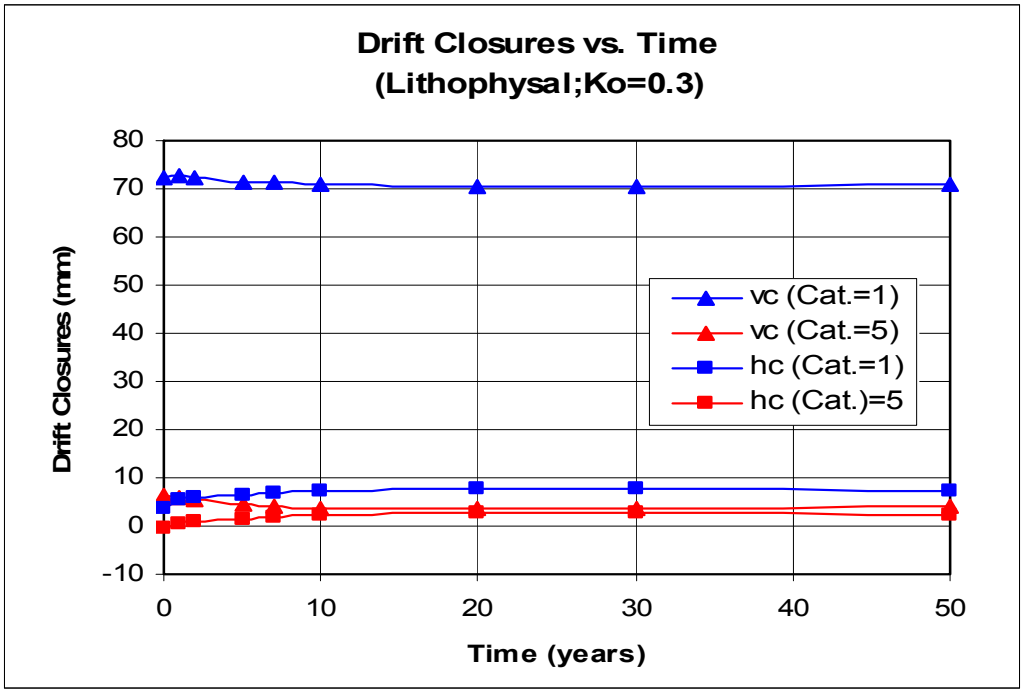

(a)

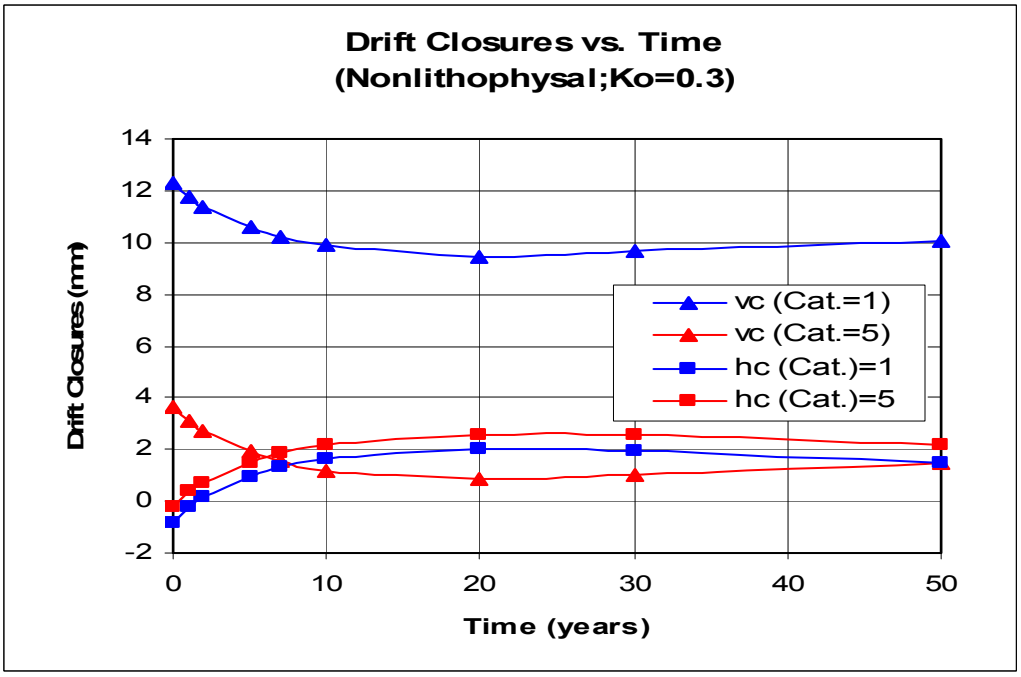

(b)

Figure 6-101 Time Histories of closures of Exhaust Mains under In Situ and Thermal Loads in (a) Lithophysal; (b) Nonlithophysal Rock

Time histories of the major principal stresses at the crown and the springline are shown in Figure 6-102 for unsupported exhaust mains subjected to in situ and thermal loads corresponding to the initial horizontal-to-vertical stress ratio (K_o) of 0.3 in the lithophysal and nonlithophysal rock. It is indicated that stresses change with temperature, especially in category 5 rock mass, though the magnitude of change is not substantial for category 1 rock mass. The maximum major principal stresses for category 1 rock are predicted to be about 12 and 27 MPa for lithophysal and nonlithophysal rock, respectively.

For category 5 rock, similar to what is observed for the category 1 rock, stresses change with temperature, however, with larger magnitude. The maximum major principal stresses are predicted to be about 28 and 37 MPa for the lithophysal and nonlithophysal rock, respectively.

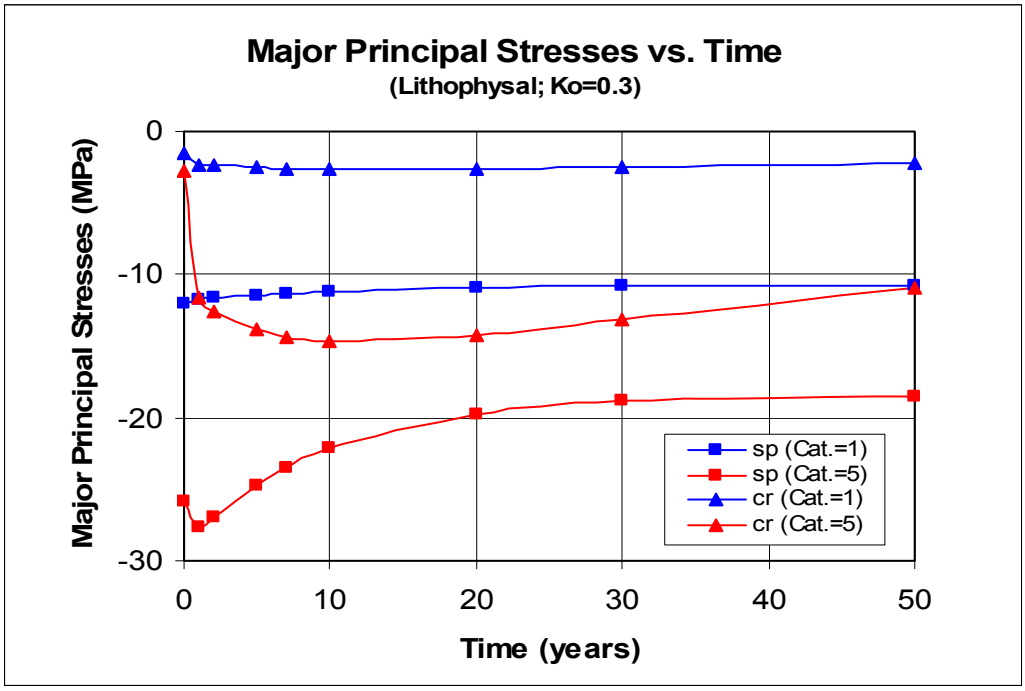

(a)

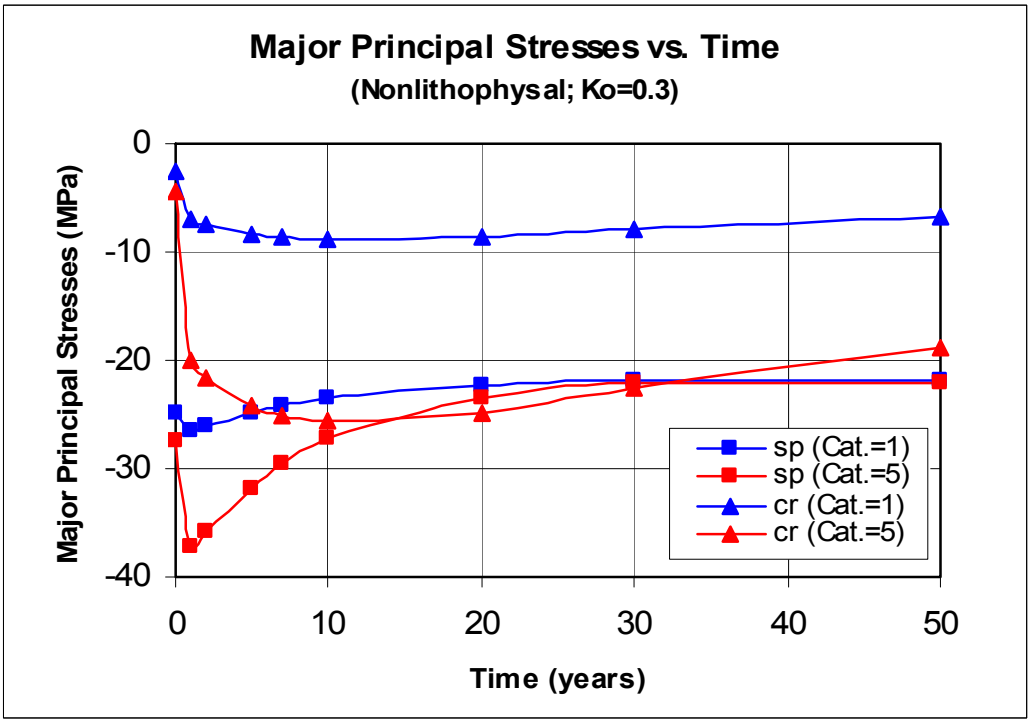

(b)

Figure 6-102 Time Histories of Major Principal Stresses near Crown and Springline of Exhaust Mains under In Situ and Thermal Loads in (a) Lithophysal; (b) Nonlithophysal Rock

6.5.3.2.3 Observation Drift

The temperature field after 50 years of heating around the observation drift is shown in Figure 6-103. The observation drift does not significantly affect heat transport or the predicted temperature fields. This simplification is conservative, resulting in overestimation of the temperatures around the observation drift.

It is predicted that the maximum temperature increase around the observation drift during the 50-yr period after waste emplacement is approximately 13^{o}C. It does not appear that this temperature change causes any additional damage around the observation drift (Figure 6-104 and Figure 6-105). Figure 6-106 to Figure 6-109 indicate that thermal loads do not affect the stability conditions of the rock mass around the intersection between the observation drift and the exhaust main.

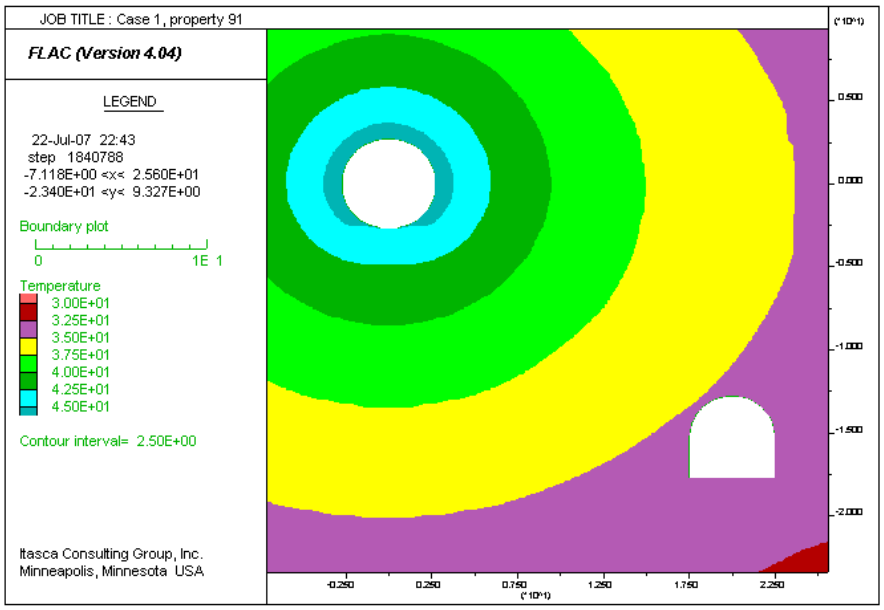

Figure 6-103 Temperature Contours around Observation Drift after 50 Years of Heating

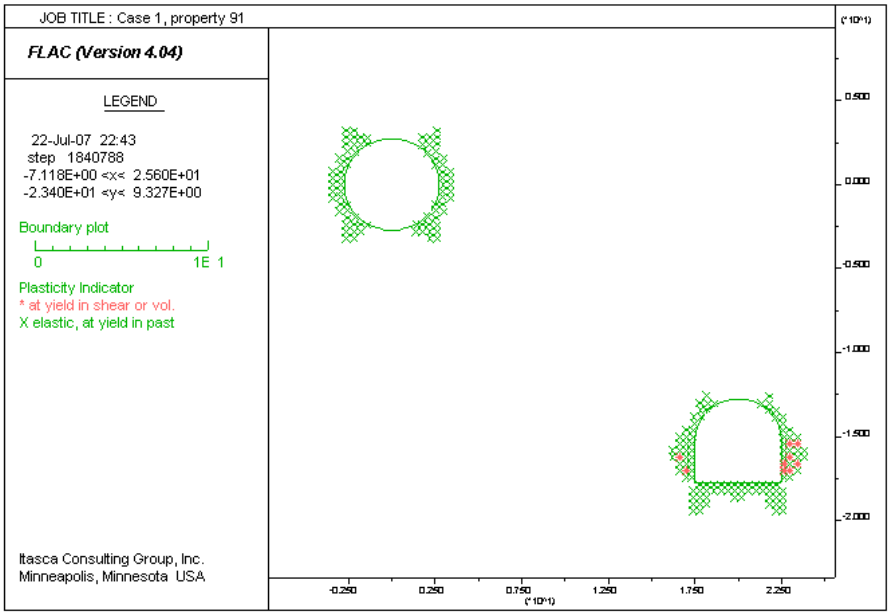

Figure 6-104 Potential Yield Zone around Observation Drift after 50 Years of Heating

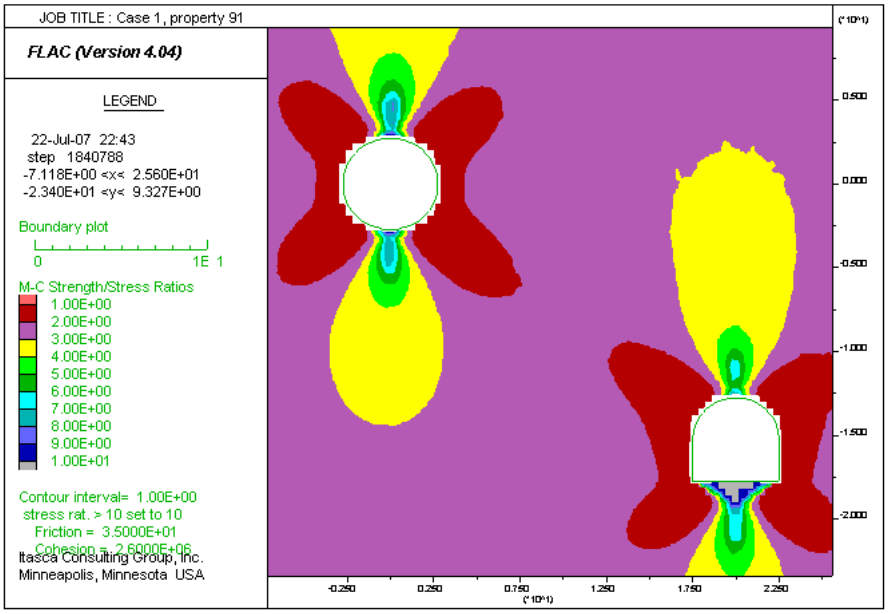

Figure 6-105 Factor of Safety around Observation Drift after 50 Years of Heating

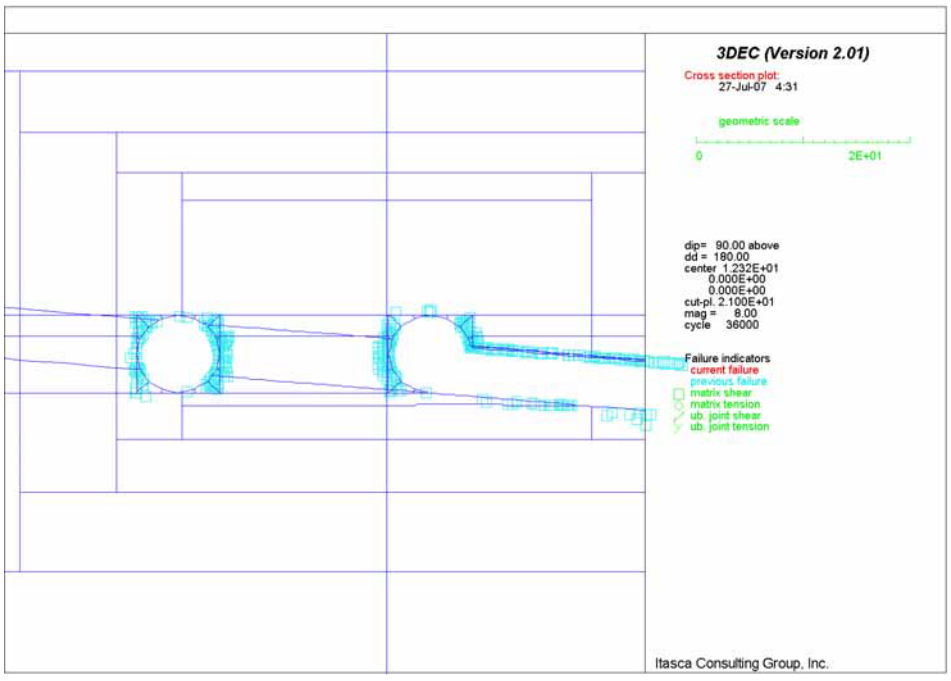

Figure 6-106 Potential Yield Zone at Intersection between Observation Drift and Exhaust Main in Vertical Section 1 after 50 Years of Heating

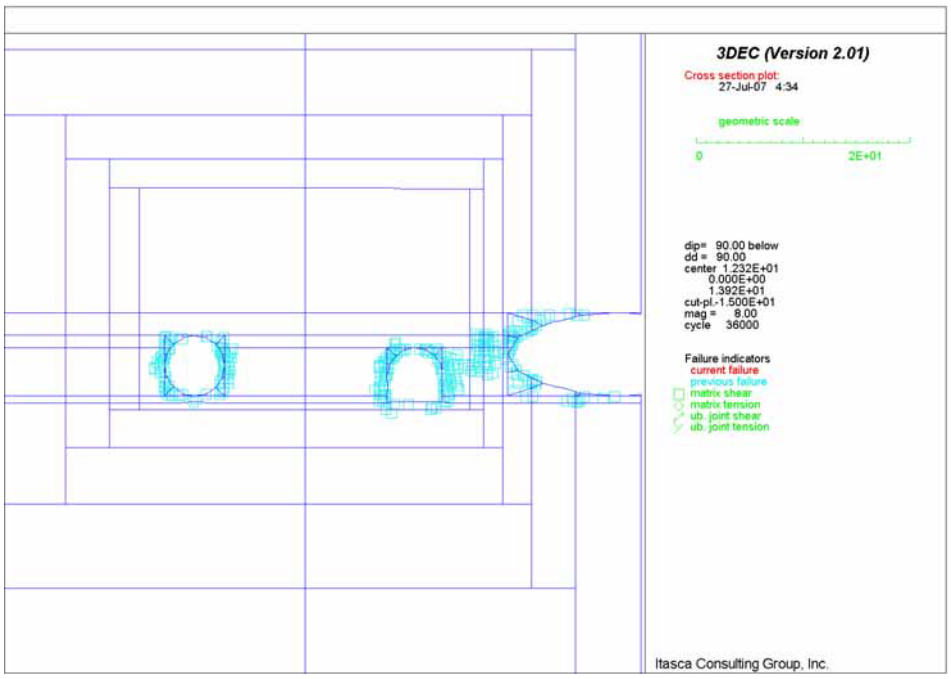

Figure 6-107 Potential Yield Zone at Intersection between Observation Drift and Exhaust Main in Vertical Section 2 after 50 Years of Heating

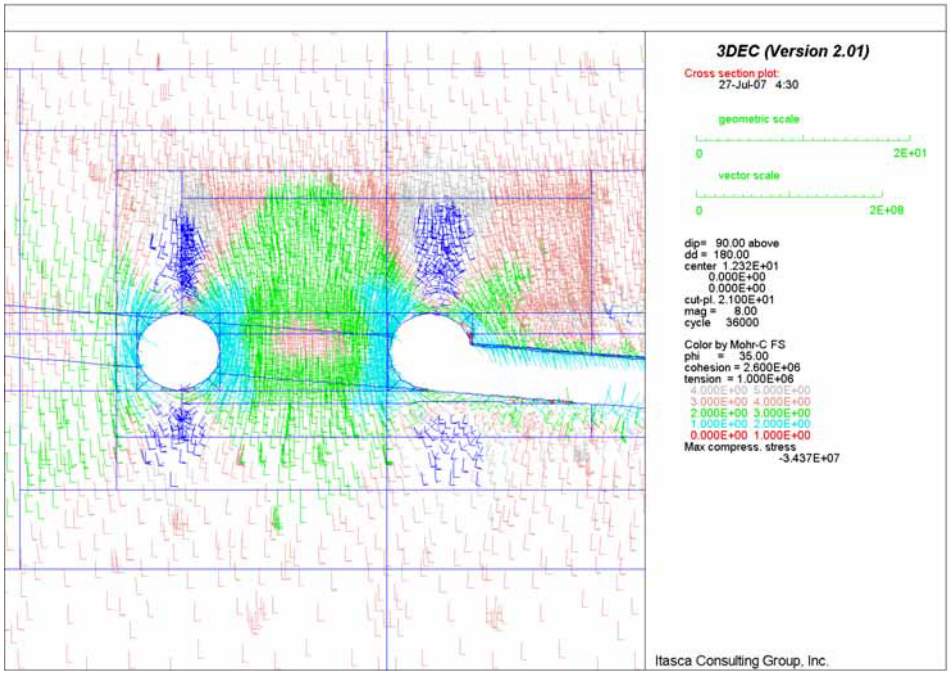

Figure 6-108 Factor of Safety at Intersection between Observation Drift and Exhaust Main in Vertical Section 1 after 50 Years of Heating

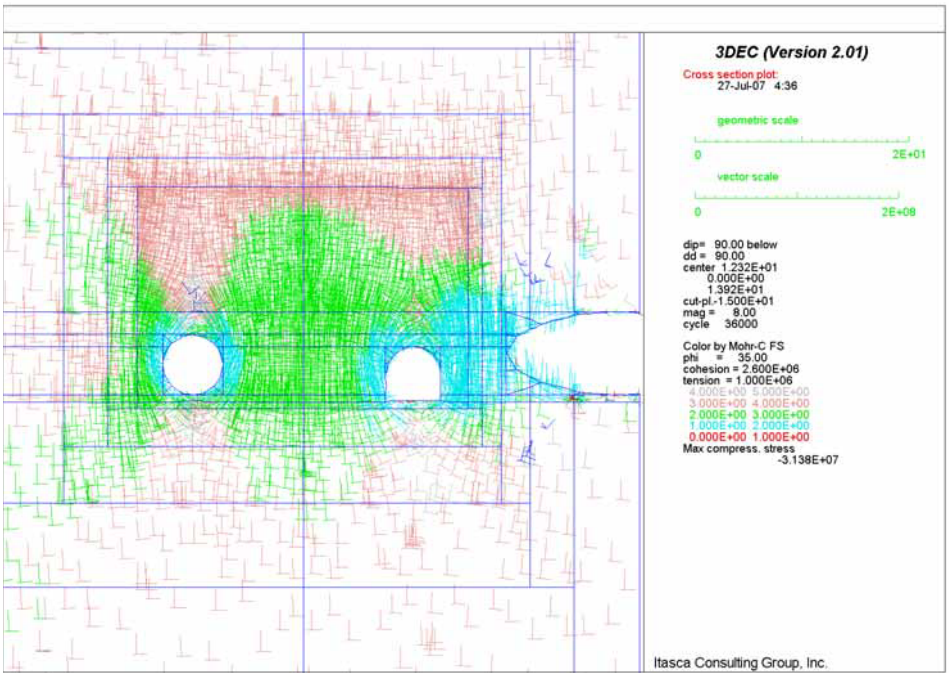

Figure 6-109 Factor of Safety at Intersection between Observation Drift and Exhaust Main in Vertical Section 2 after 50 Years of Heating

6.5.3.2.4 Interburden Pillar between Shaft Access and Exhaust Mains

After waste emplacement, the exhaust mains and the pillar between the exhaust mains and the access drifts drift to the ventilation shaft will be subjected to the thermal stresses. The evolution of the temperature field around the pillar was calculated by the NUFT code. The temperature fields (at 1, 2, 3, 5, 10, 20, 30 and 50 years) from the NUFT code were imported into 3DEC in order to calculate the thermal stress around the excavations, according to Equation 6-9.

The temperature fields, as calculated in NUFT and imported into 3DEC, after 3 and 20 years of heating are shown in Figure 6-110 and Figure 6-111, respectively. As shown in these two figures, the temperatures at the middle of pillar are lower than those near the exhaust mains. Stress change due to the thermal load does not change the level of factor-of-safety with respect to the Mohr-Coulomb yield condition due to in situ stress (comparing Figure 6-80 with Figure 6-112 and Figure 6-113) nor cause significant additional yielding of the rock mass (comparing Figure 6-82 with Figure 6-114).

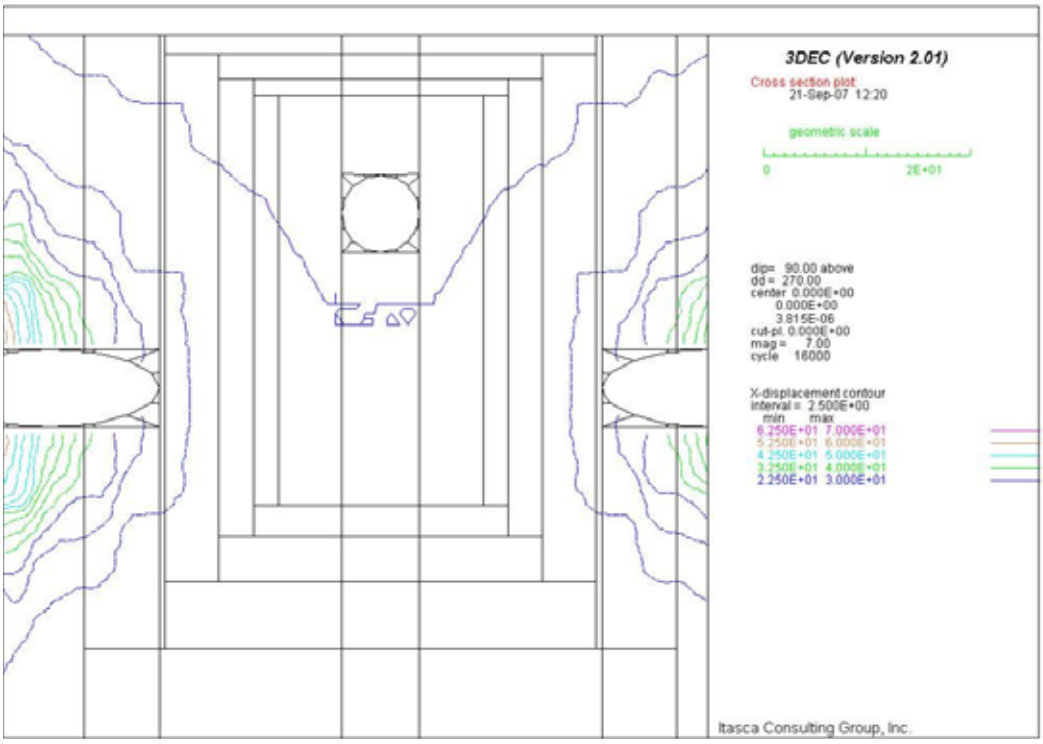

Figure 6-110 Temperature Field in Vertical Section 2 after 3 Years of Heating at Interburden Area

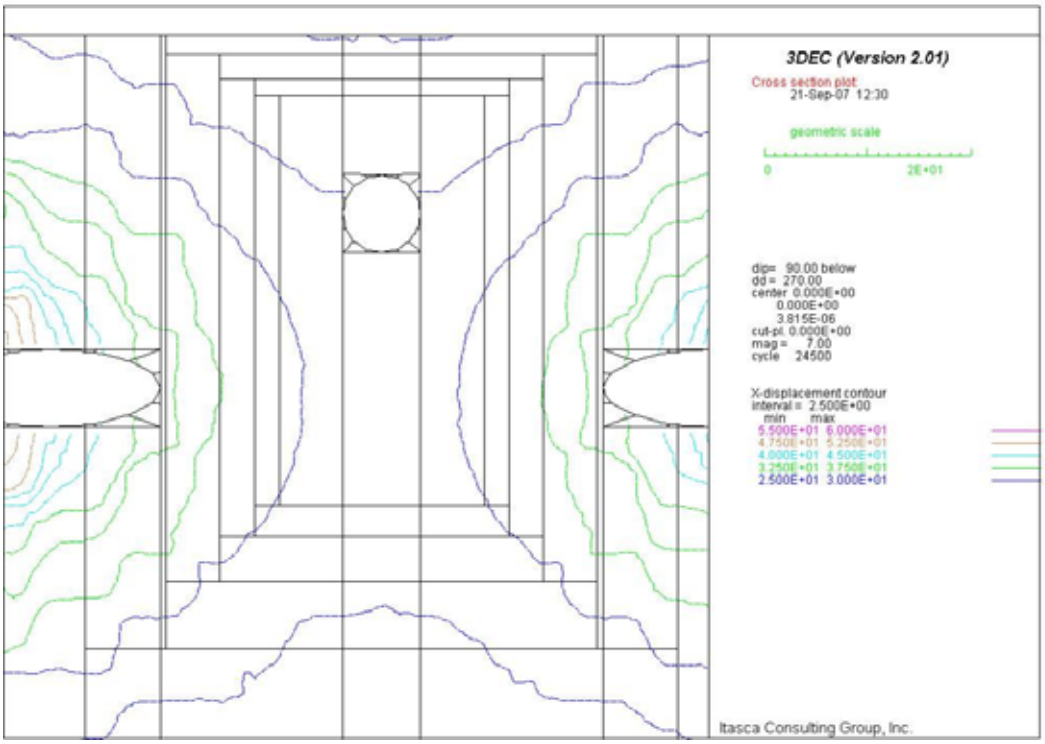

Figure 6-111 Temperature Field in Vertical Section 2 after 20 Years of Heating at Interburden Area

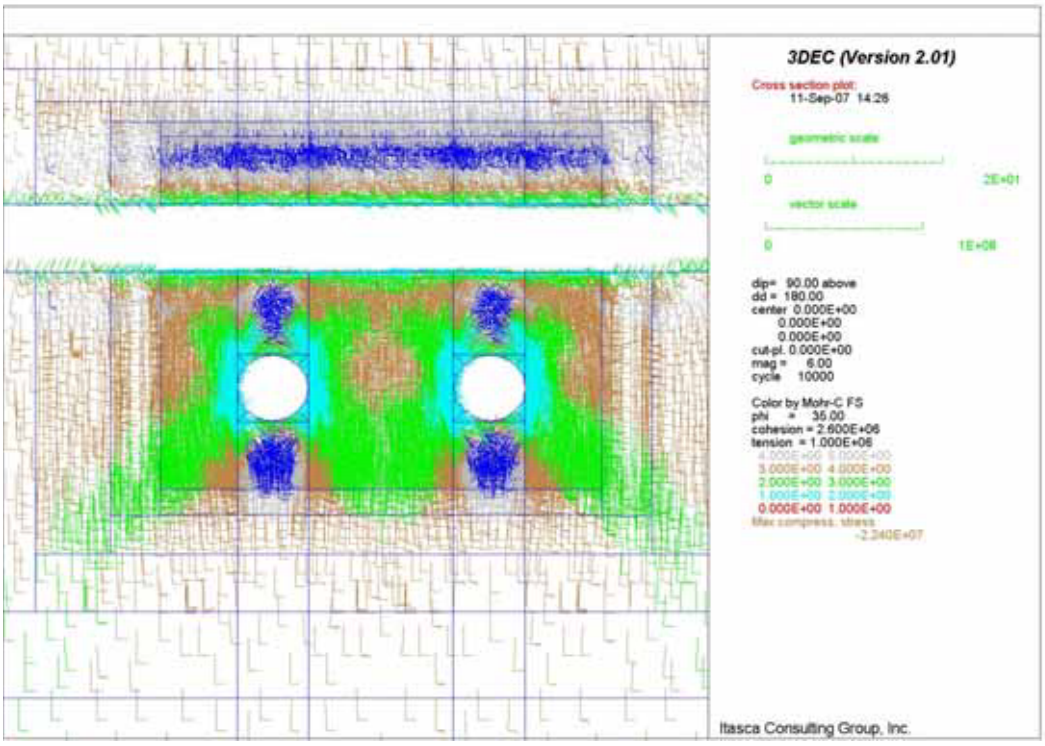

Figure 6-112 SF in Vertical Section 1 for Lith. Cat. 1 Rock after 1 Year of Heating at Interburden Area

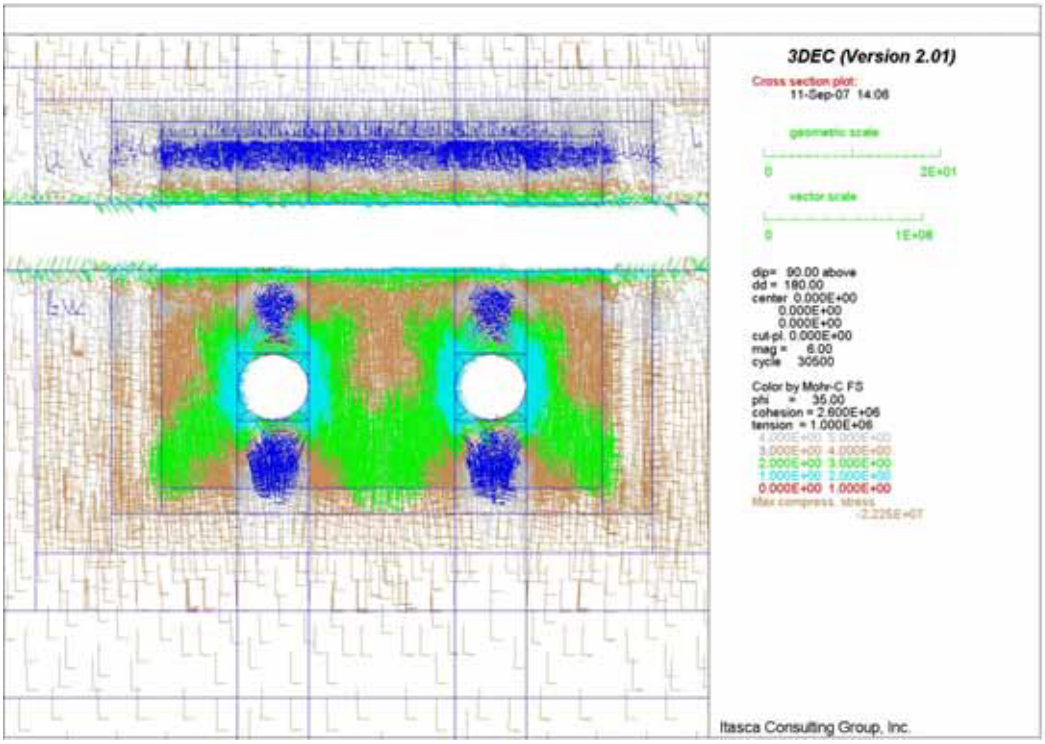

Figure 6-113 SF in Vertical Section 1 for Lith. Cat. 1 Rock after 50 Years of Heating at Interburden Area

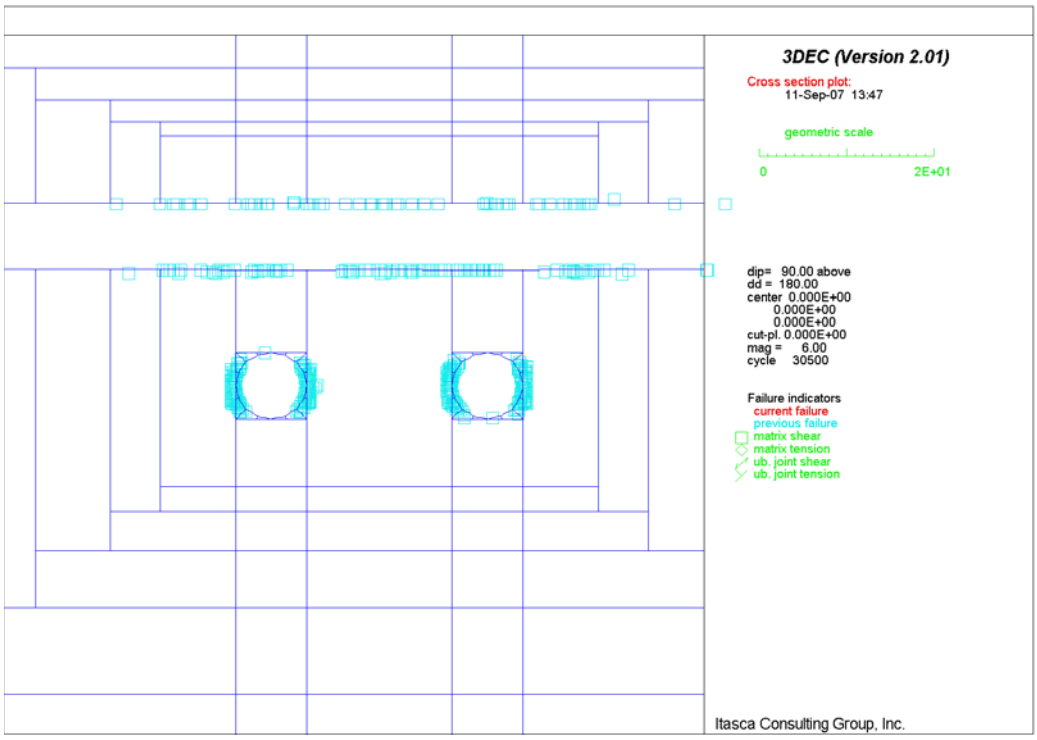

Figure 6-114 Potential Yield Zone in Vertical Section 1 for Lith. Cat. 1 after 50 Years of Heating

6.5.3.3 Seismic Loading Condition

6.5.3.3.1 Intersection between Access Main and Turnout

The non-emplacement excavations including the access main, the turnout and their intersections will be subject to seismic loading during the preclosure period. The stability condition for these underground openings was analyzed for ground motion with an APE of 5×10^{-4} (Section 6.1.2.7). The dynamic analysis was carried out for the intersection A (the most critical regarding the length of the span) for category 1 rock mass (poorest quality) of both the lithophysal and nonlithophysal units.

The results of dynamic analysis are shown in Figure 6-115 through Figure 6-124. Clearly the level of ground shaking due to an earthquake with a 2,000 year return period is not expected to cause significant damage to access mains, turnouts, and intersections between access mains and turnouts. The continuum analysis indicates that the extent of inelastic deformation in the surrounding rock mass and, particularly, in the pillar between the two openings, does not increase with respect to the extent of the rock mass yielded under static conditions. During the passage of the seismic waves, the stresses in the rock oscillate. The maximum transient stress change caused by an earthquake with a 2,000 year return period is approximately 0.5 MP and 1 MPa for the lithophysal and nonlithophysal units, respectively. Note that the stress changes are calculated based on Eq. 6-8, without multiplier 2, and the velocity amplitude to be 0.2 m/s. However, at the end of the simulation, when oscillations die out, the stresses return to the state that existed prior to the shaking. Figure 6-119 and
Figure 6-120 indicate that there is no permanent stress change, or stress redistribution, indicating loosening or instability of a portion of the rock mass. The stress fields at the end of simulation in

the lithophysal rock mass are colored by: a) the factor-of-safety with respect to the Mohr-Coulomb yield condition; and b) indication of tensile and compressive stresses, as shown in Figure 6-121 and Figure 6-122, respectively.

By comparing dynamic results with static ones, it can be concluded that an earthquake with a 2,000 year return period does not: a) cause significant, permanent change in the factor-of-safety with respect to the Mohr-Coulomb yield condition throughout the rock mass; b) increase the volume of the rock mass subject to tensile stresses. The average stresses in the pillar between the drifts are almost unchanged as shown in Figure 6-123. All three components of the velocity histories were monitored during the simulations at points in the roof and the walls of the intersection. The histories at point A in the roof (see Figure 6-12), shown in Figure 6-124, are almost the same (offset for traveling time from the boundary to the history point) as applied velocities at the bottom boundary (see Figure 6-1). The accumulation of permanent displacement due to inelastic deformation cannot be detected.

Seismic load due to an earthquake with a 2,000-year return period does not result in a significant increase in damage of the rock mass around the drifts, nor an increase in the permanent displacements. The dynamic analysis of global stability of the intersections was carried out using the continuum models.

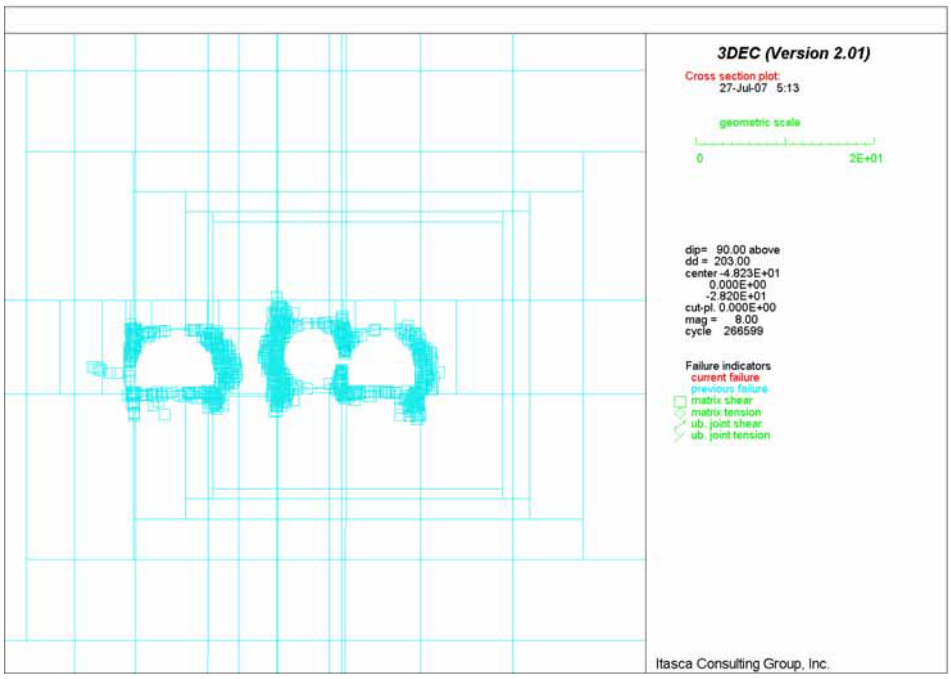

Figure 6-115 Intersection A: Potential Yield Zone in Vertical Section 2 for Lith. Cat. 1 Rock under In Situ and Seismic Loads

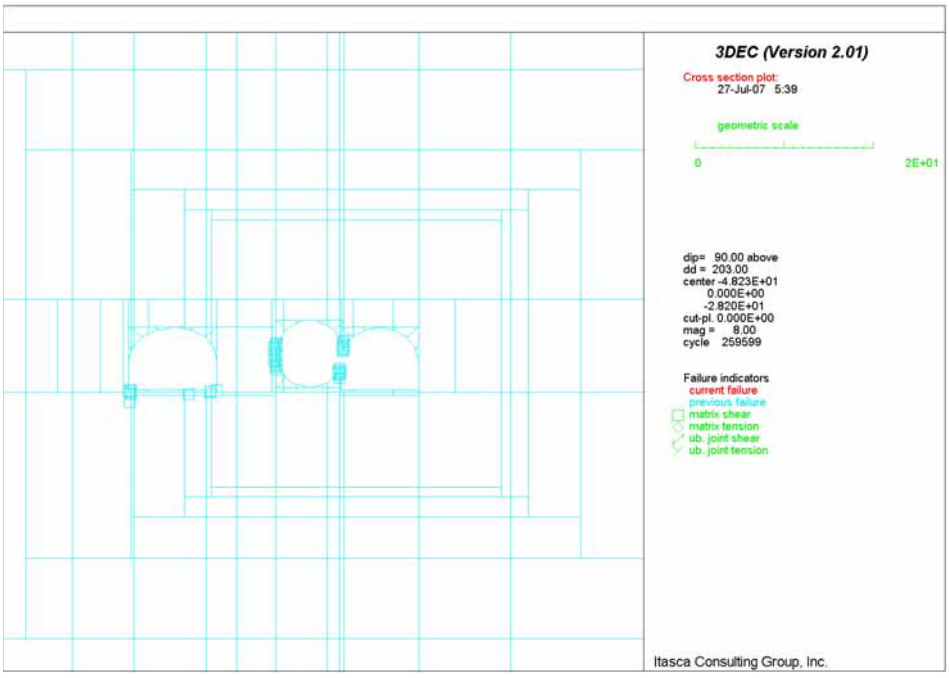

Figure 6-116 Intersection A: Potential Yield Zone in Vertical Section 2 for Nonlith. Cat. 1 Rock under In Situ and Seismic Loads

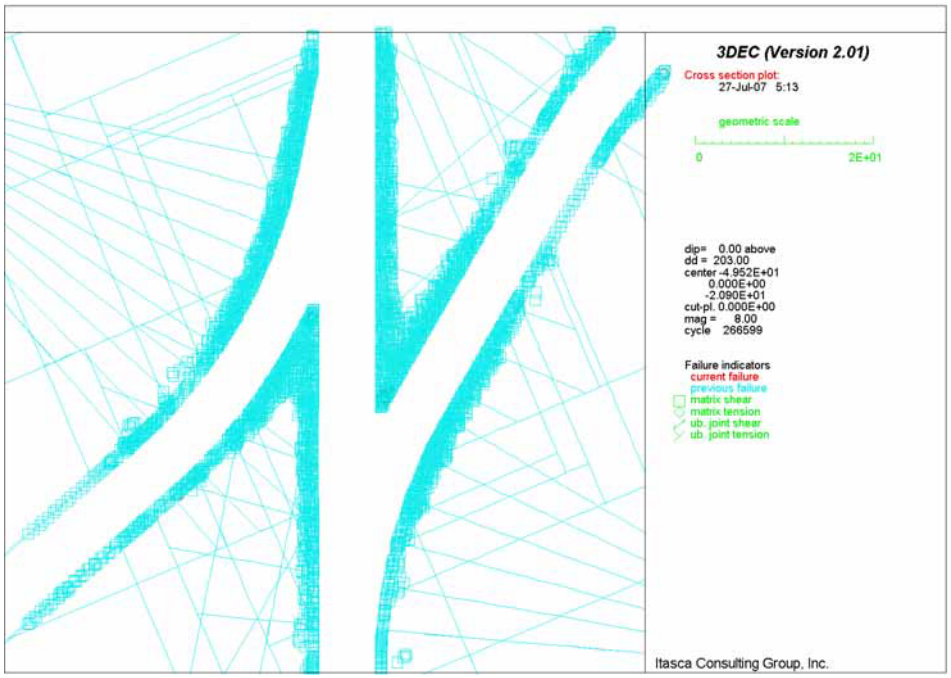

Figure 6-117 Intersection A: Potential Yield Zone in Horizontal Section for Lith. Cat. 1 Rock under In Situ and Seismic Loads

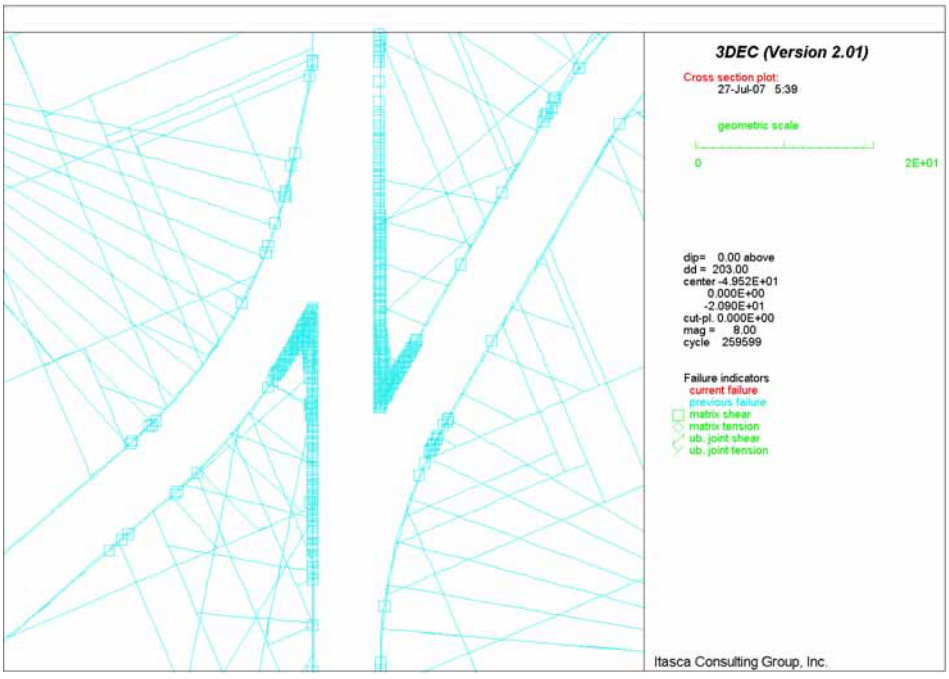

Figure 6-118 Intersection A: Potential Yield Zone in Horizontal Section for Nonlith. Cat. 1 Rock under In Situ and Seismic Loads

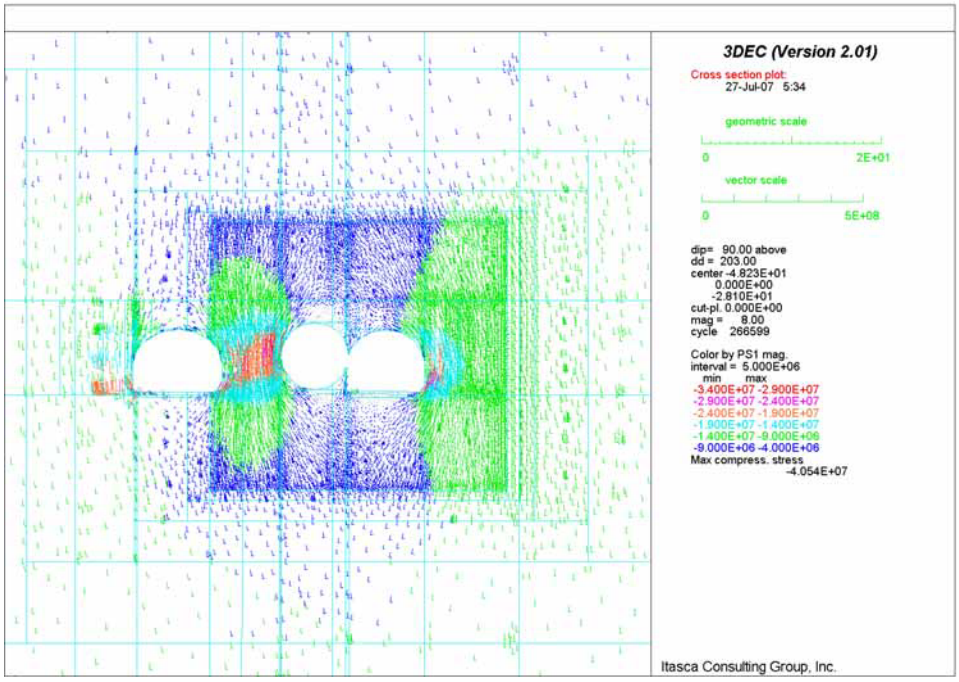

Figure 6-119 Intersection A: Stress Field in Vertical Section 2 for Lith. Cat. 1 Rock under In Situ and Seismic Loads

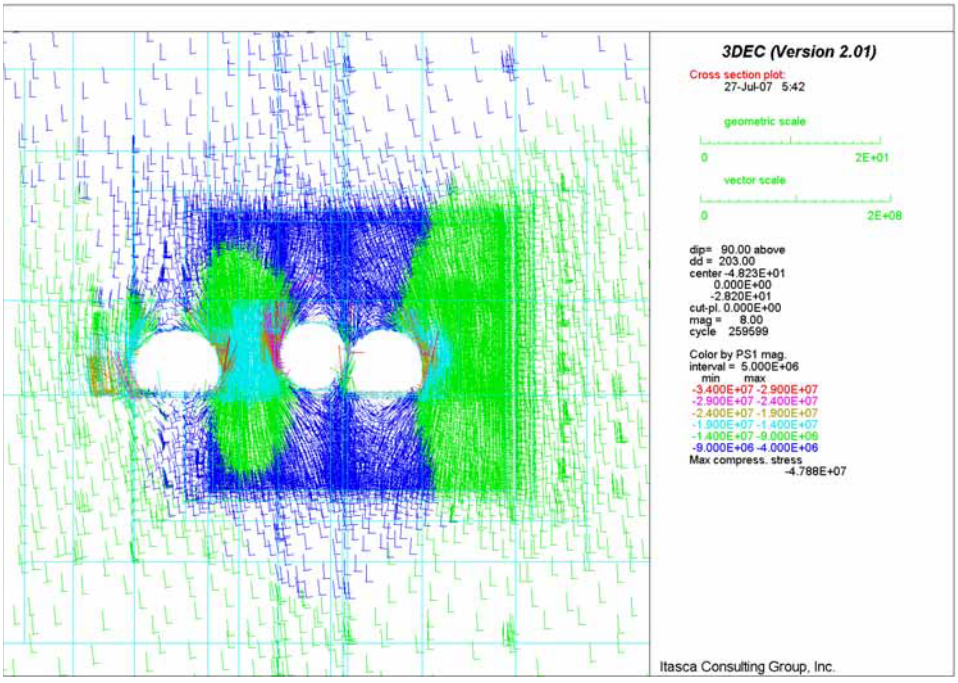

Figure 6-120 Intersection A: Stress Field in Vertical Section 2 for Nonlith. Cat. 1 Rock under In Situ and Seismic Loads

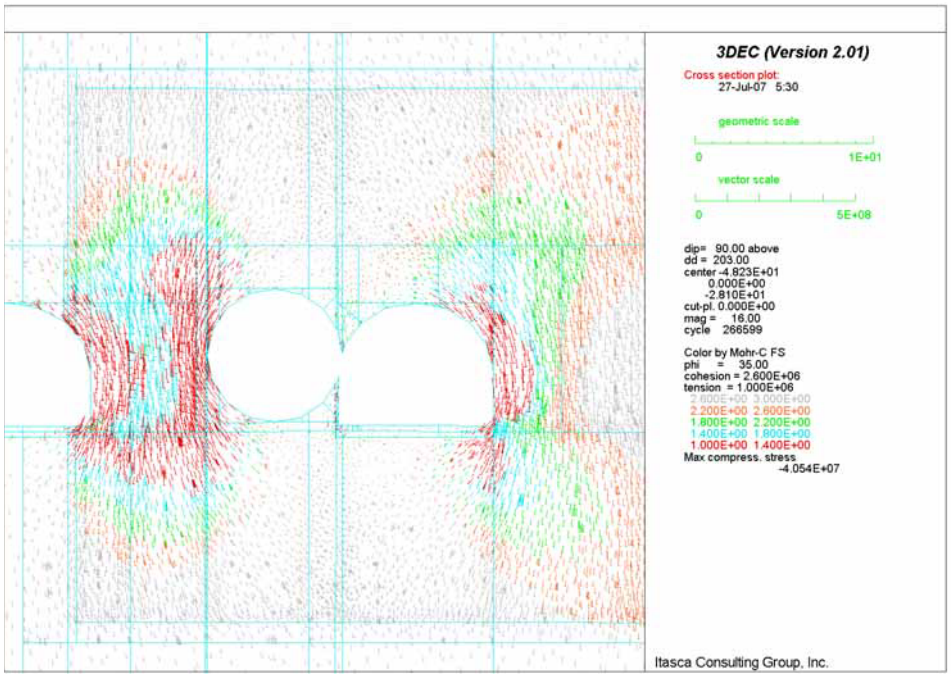

Figure 6-121 Intersection A: Factor of Safety in Vertical Section 2 for Lith. Cat. 1 Rock under In Situ and Seismic Loads

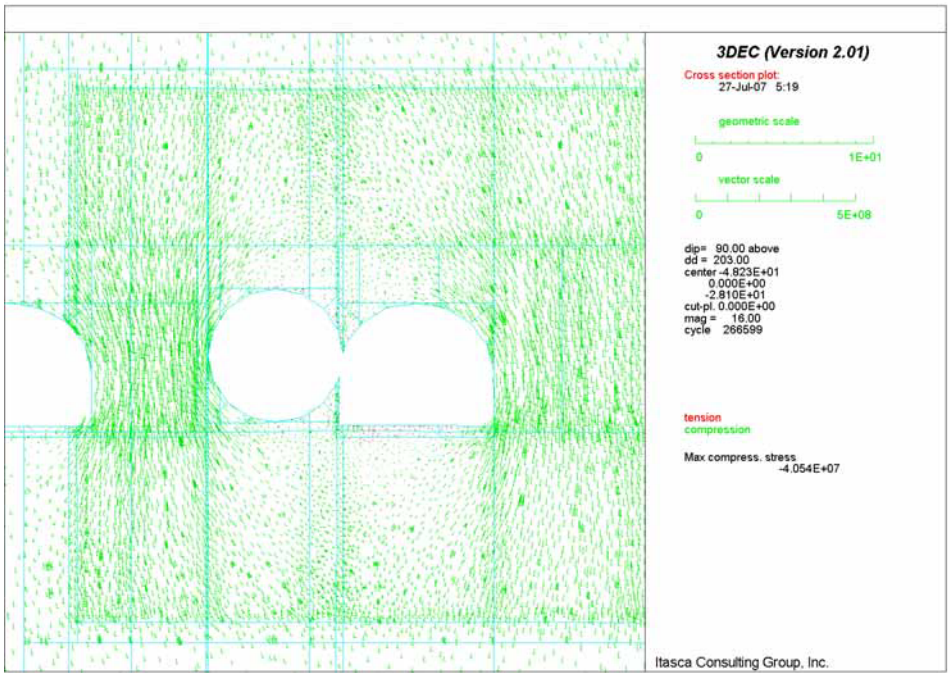

Figure 6-122 Intersection A: Compressive and Tensile Stresses in Vertical Section 2 for Lith. Cat. 1 Rock under In Situ and Seismic Loads

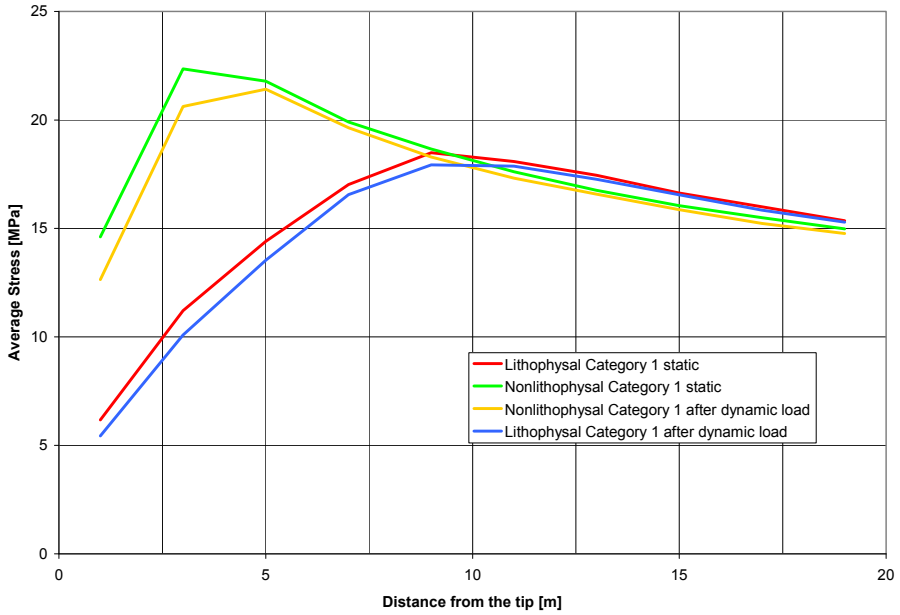

Figure 6-123 Intersection A: Average Pillar Stress vs. Distance from Pillar Tip under In Situ and Seismic Loads

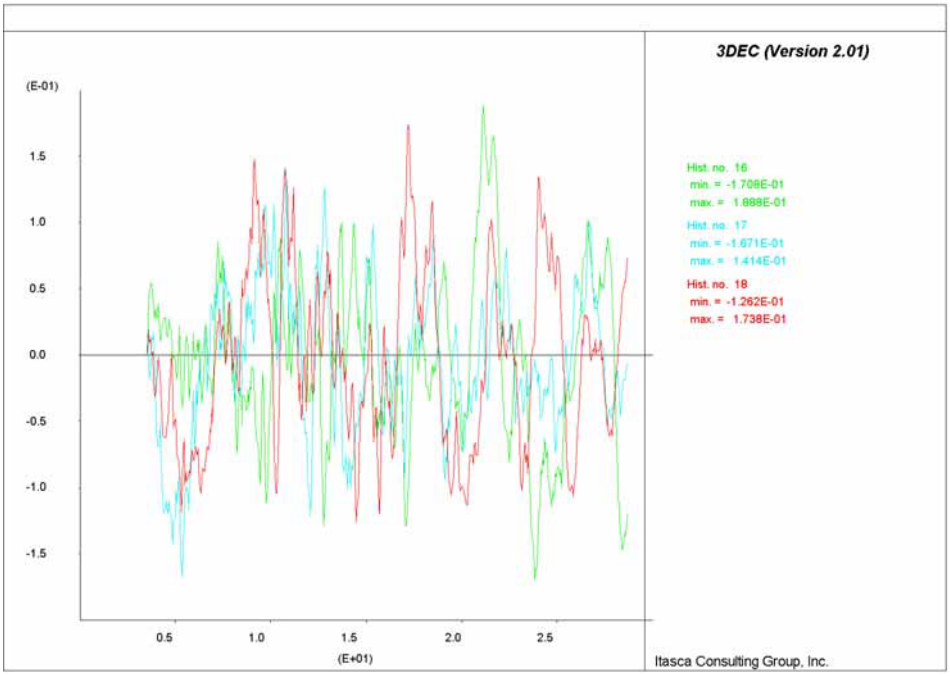

Note: Y axis-Velocity (m/sec); X axis-Time (sec)

Figure 6-124 Intersection A: Velocity Histories in x, y and z Direction near Point A for Lith. Cat. 1 Rock

6.5.3.3.2 Intersections between Exhaust Mains and Emplacement Drifts

The results of dynamic simulation of the intersections between exhaust mains and emplacement drifts for seismic ground motion with a 2,000 year return period are shown in Figure 6-125 through Figure 6-132. Seismic loading was applied on the model at the initial state, after excavation of the drifts but before heating (due to waste emplacement) began.

The results are presented for category 1 in both lithophysal (intersection B) and non-lithophysal (intersection C) rock masses. The dynamic load causes insignificant additional yielding, which was caused by stress oscillations. After completion of the dynamic simulation, the models for all simulated cases are stable. There is no indication of permanent stress redistribution or destressing of portions of rock mass indicating grounds prone to rockfall. Velocity histories were recorded during the simulations at a number of points throughout the model, particularly at the wall and roof of the intersection. The velocity histories near point 1 (located at the intersection of longitudinal axes of exhaust main and emplacement drift, see Figure 6-14 and Figure 6-15) in the intersections B and C are shown in Figure 6-125 and Figure 6-126, respectively. These histories are almost identical to the velocity histories applied at the base of the model due to the vertically propagating seismic wave. Thus, the model deforms elastically under seismic load. There is no indication of accumulation of irreversible, plastic deformation.

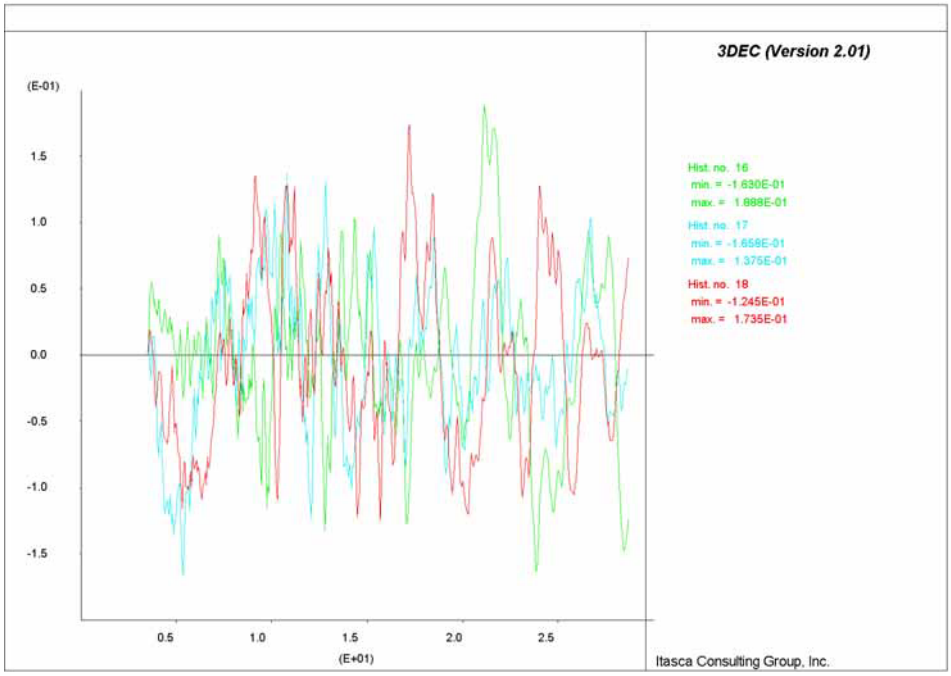

Note: Y axis-Velocity (m/sec); X axis-Time (sec)

Figure 6-125 Intersection B: Velocity Histories in X, Y and Z Directions near Point 1for Lith. Cat. 1 Rock

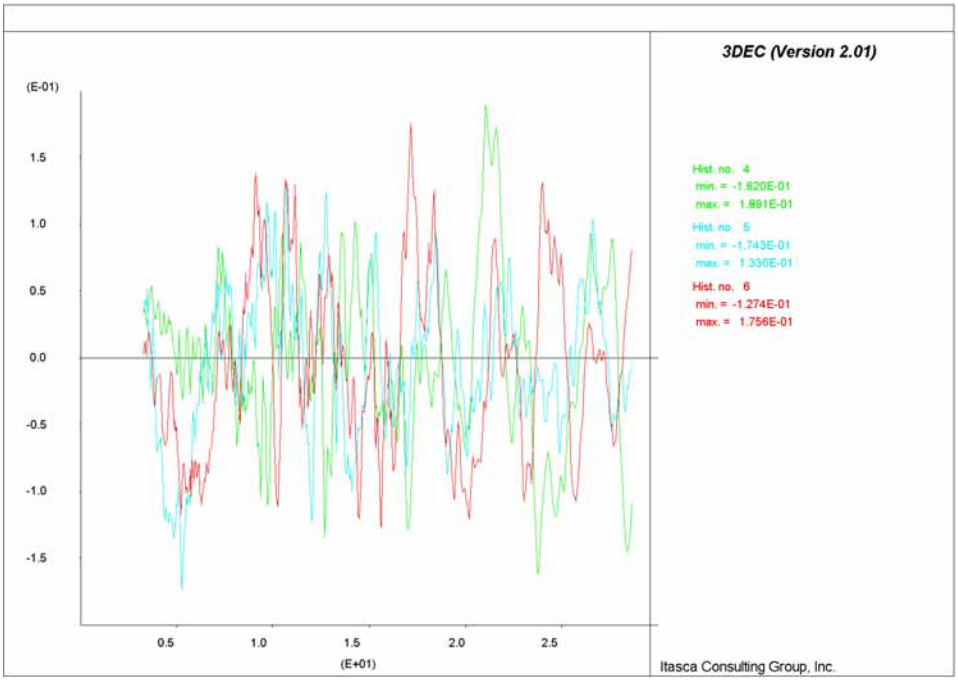

Note: Y axis-Velocity (m/sec); X axis-Time (sec)

Figure 6-126 Intersection C: Velocity Histories in X, Y and Z Directions near Point 1for Nonlith. Cat. 1 Rock

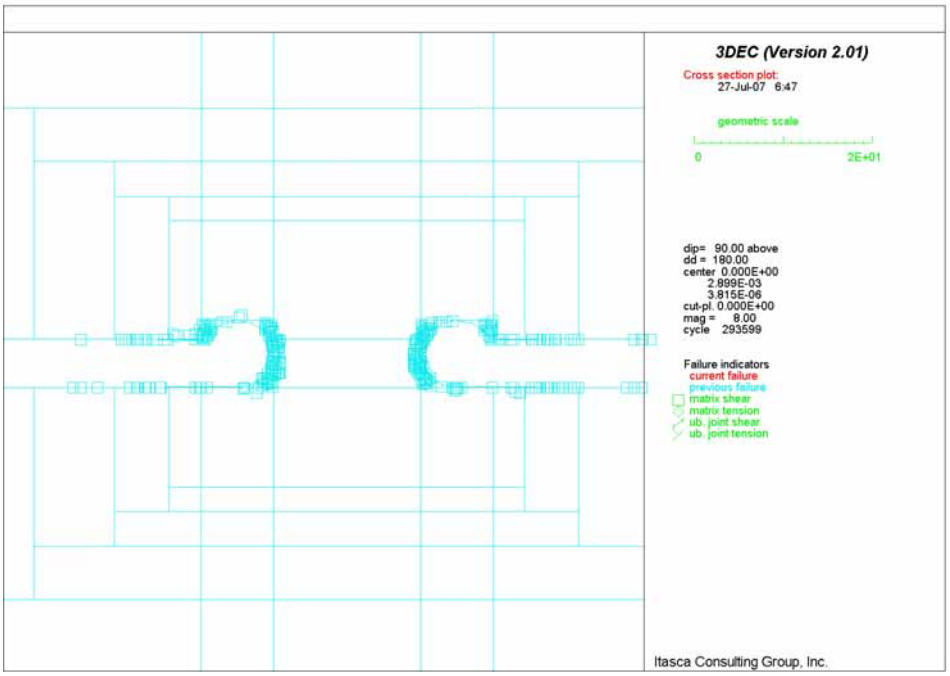

Figure 6-127 Intersection B: Potential Yield Zone in Vertical Section 1 for Lith. Cat. 1 Rock under In Situ and Seismic Loads

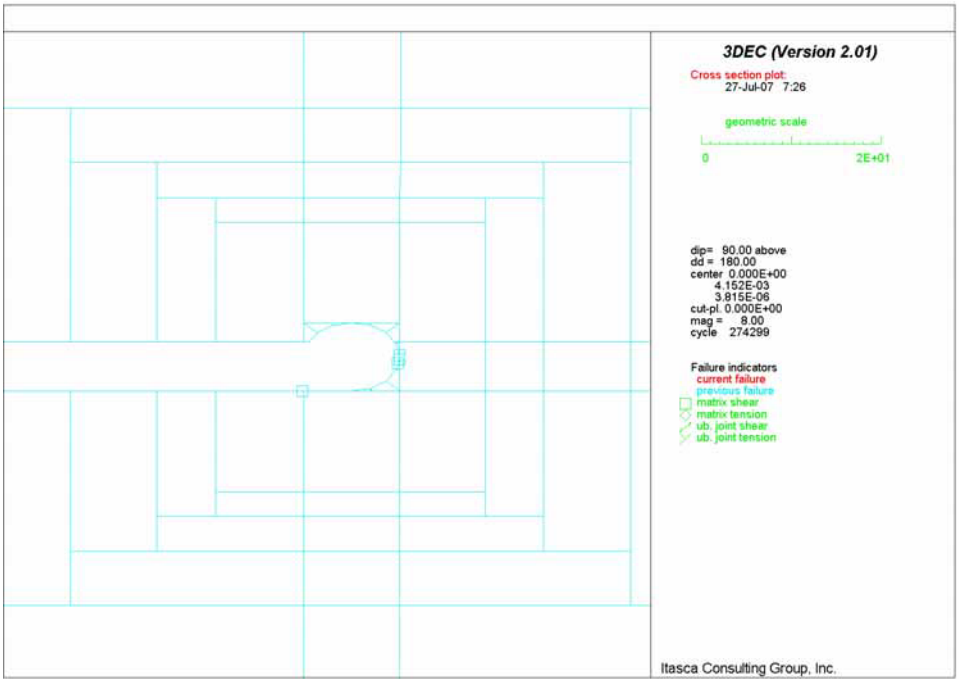

Figure 6-128 Intersection C: Potential Yield Zone in Vertical Section 1 for Nonlith. Cat. 1 Rock under In Situ and Seismic Loads

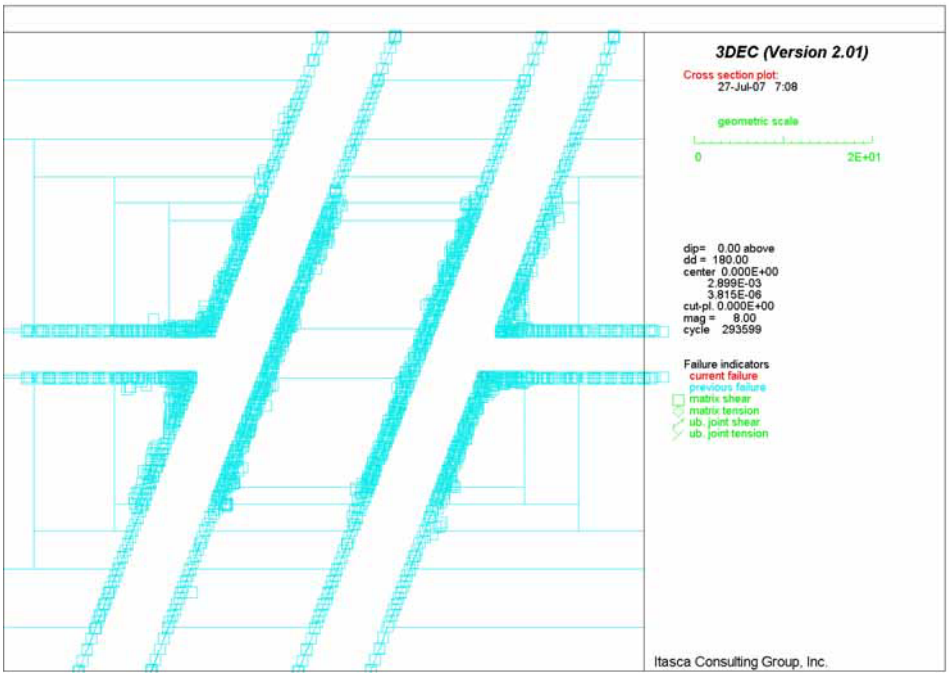

Figure 6-129 Intersection B: Potential Yield Zone in Horizontal Section 1 for Lith. Cat. 1 Rock under In Situ and Seismic Loads

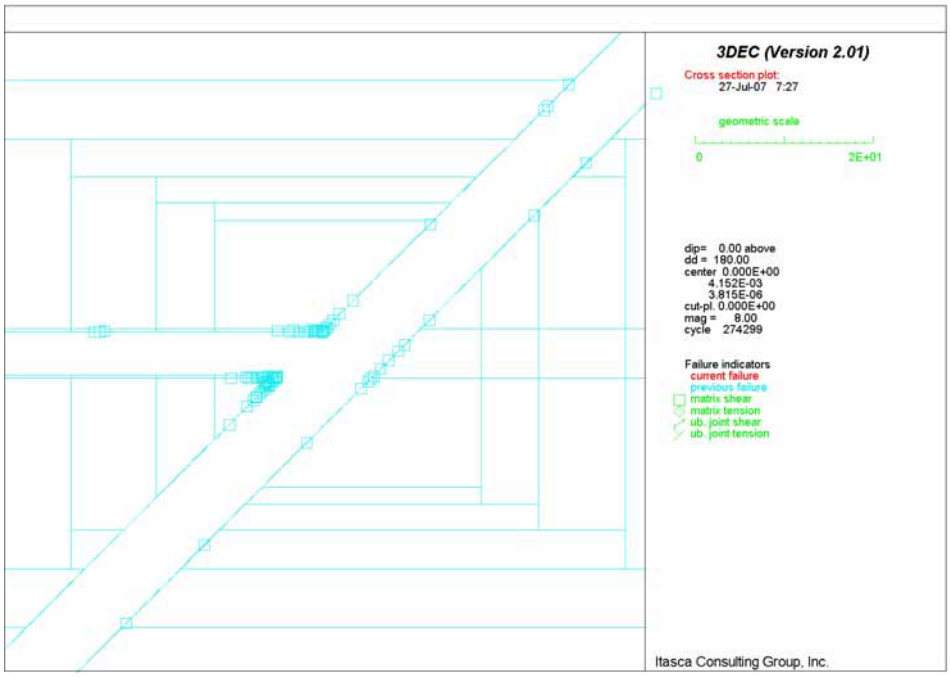

Figure 6-130 Intersection C: Potential Yield Zone in Horizontal Section 1 for Nonlith. Cat. 1 Rock under In Situ and Seismic Loads

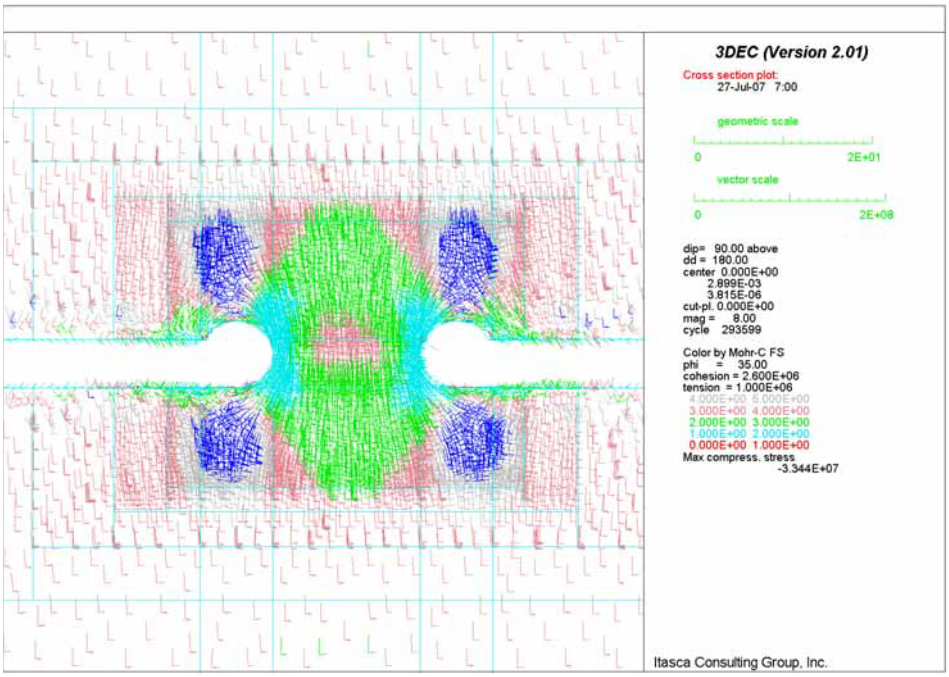

Figure 6-131 Intersection B: Factor of Safety in Vertical Section 1 for Lith. Cat. 1 Rock under In Situ and Seismic Loads

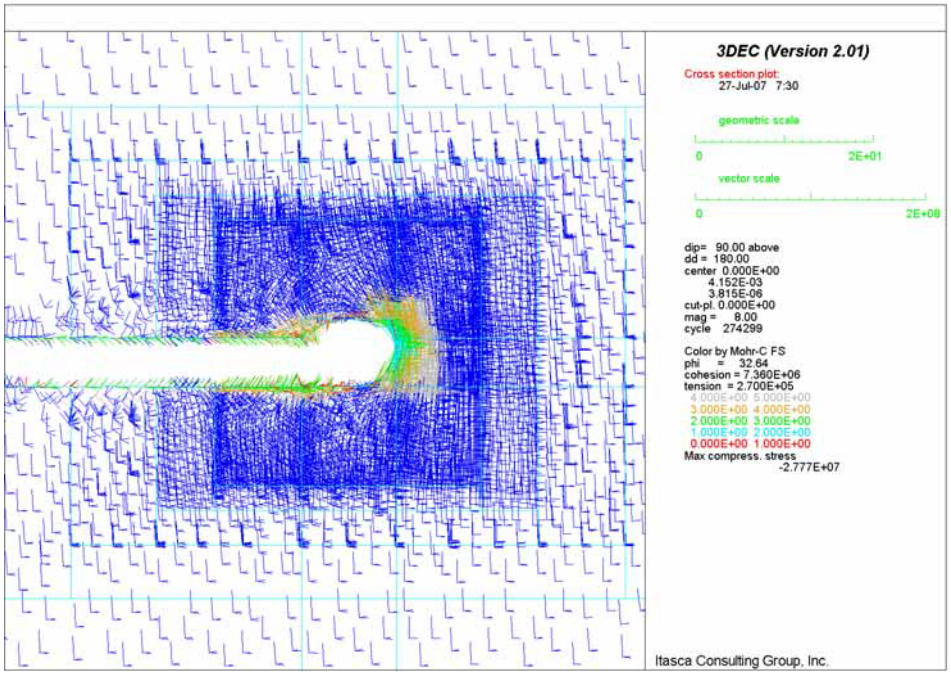

Figure 6-132 Intersection C: Factor of Safety in Vertical Section 1 for Nonlith. Cat. 1 Rock under In Situ and Seismic Loads

6.5.3.3.3 Exhaust Mains

Drift closures induced by seismic ground motions were calculated for exhaust mains in both the lithophysal and nonlithophysal rocks, and are presented in Figure 6-133 and Figure 6-134. It is indicated that seismically-induced rock deformation using FLAC, i.e., a continuum model, is not significant. The maximum closures due to seismic loadings are predicted to vary from less than 4 mm for the category 1 lithophysal rock to less than 2 mm for the category 1 nonlithophysal rock. The results also indicate that the rock is not expected to behave much differently if the seismic ground motions occur at the beginning of waste emplacement (year=0) or at 50 years following waste emplacement. This is because that the effect of heating by waste on rock mass behavior is minimized by the use of continuous ventilation during the preclosure period.

By combining the rock displacements induced by in situ and thermal loads (see Section 6.5.3.2.2) with those caused by seismic load, the maximum drift closures are about 77 mm for the poorest lithophysal rock (category=1) and about 14 mm for the poorest nonlithophysal rock (category=1).

During a seismic event, dynamically induced stresses fluctuate with seismic velocities, as illustrated in Figure 6-135 and Figure 6-136 for the lithophysal rock and the nonlithophysal rock, respectively. The magnitude of fluctuation in stresses varies with locations. Near the crown of exhaust mains, the variations are small, while near the springlines, the changes are larger. The maximum fluctuation in the major principal stresses near the springline is predicted to vary from about 2 MPa for category 1 lithophysal rock to about 5 MPa for category 5 lithophysal rock. For exhaust mains in the nonlithophysal rock, the maximum fluctuation is predicted to vary from about 3 MPa for category 1 rock to about 6 MPa for category 5 rock. These results suggest that the stronger the rock is, the greater the variations in stress will be.

Combining the stresses induced by in situ and thermal loads (see Section 6.5.3.2.2) with those caused by seismic loads, the maximum major principal stresses in the lithophysal rock are expected to vary from about 14 MPa for the category 1 rock to about 33 MPa for the category 5 rock. In the nonlithophysal rock, the maximum major principal stresses are shown to vary from about 30 MPa for category 1 rock to about 43 MPa for category 5 rock. For the lithophysal rock, the maximum principal stresses induced by the combined loads are slightly higher than the corresponding strengths in category 1 and 5 rock (see Table 6-1 and Table 6-2). These induced stress concentrations are either slightly higher or lower than the corresponding unconfined compressive strengths, indicating the potential for the drift skin rock to yield. However, yielding will be rather shallow because of confinement, and the proposed ground support system will be capable of controlling the spalling of the openings but will not affect the overall stability of the openings. This result indicates the need of ground support to provide the confinement and prevent the potential rock spalling.

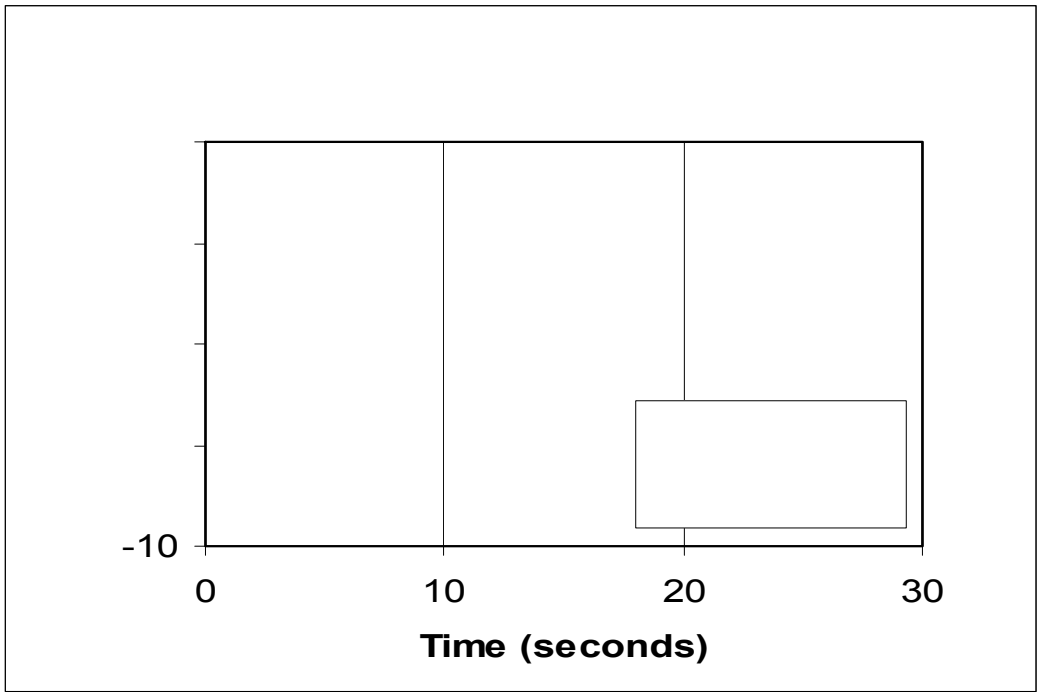

(a)

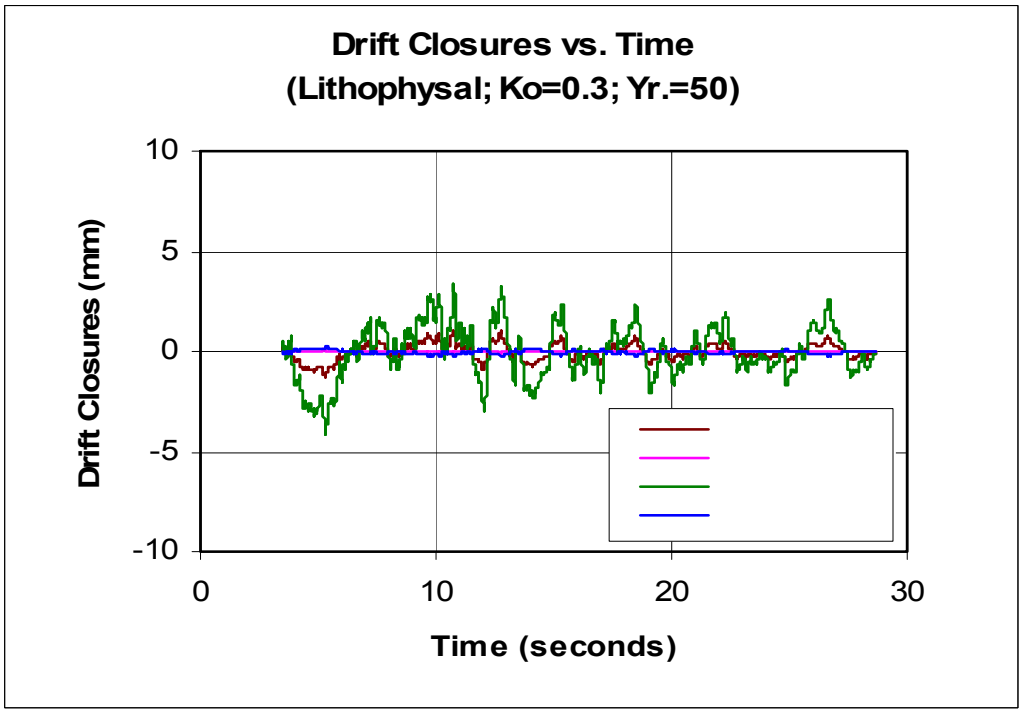

(b)

Figure 6-133 Time Histories of Closures of Exhaust Mains under Seismic Loads in Lithophysal Rock at (a) year 0; (b) Year 50.

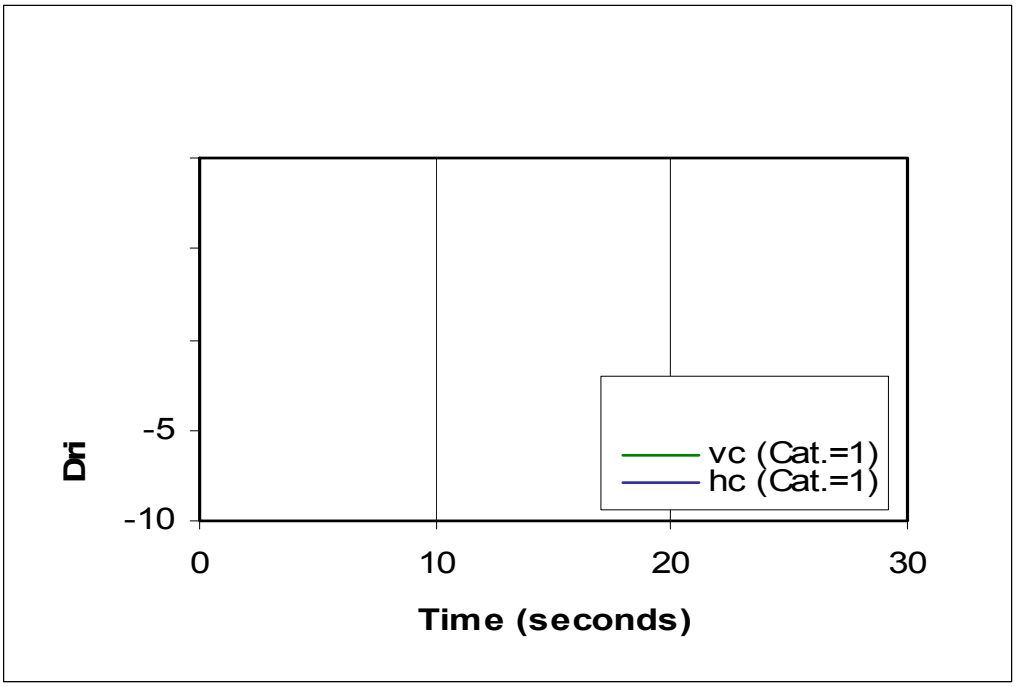

(a)

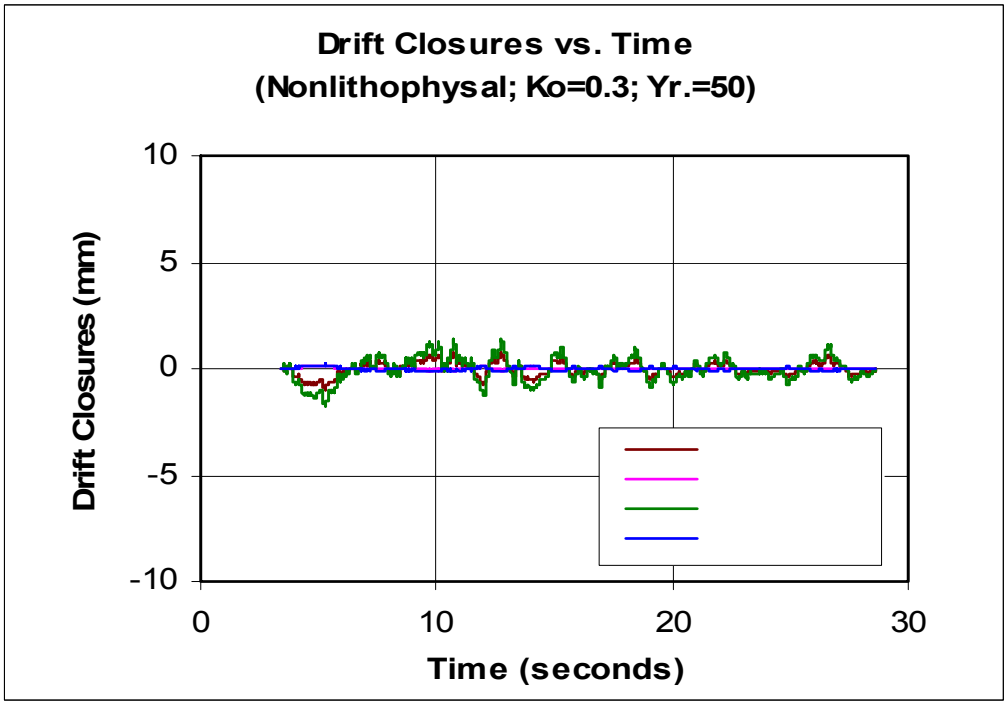

(b)

Figure 6-134 Time Histories of Closures of Exhaust Mains under Seismic Loads in Nonlithophysal Rock at (a) year 0; (b) Year 50.

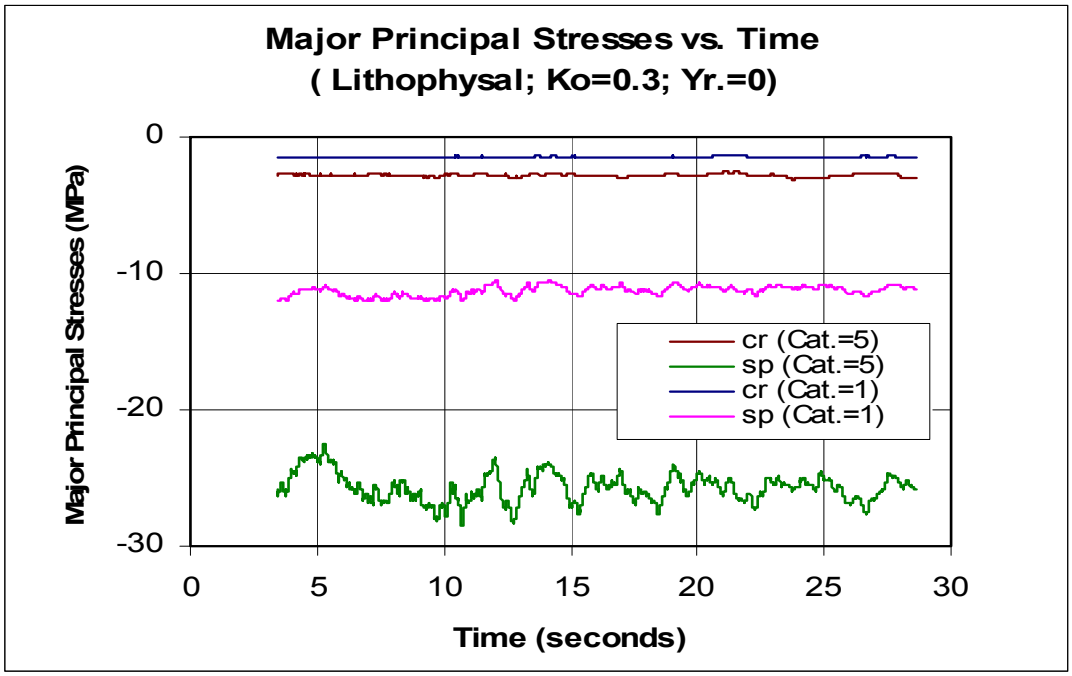

(a)

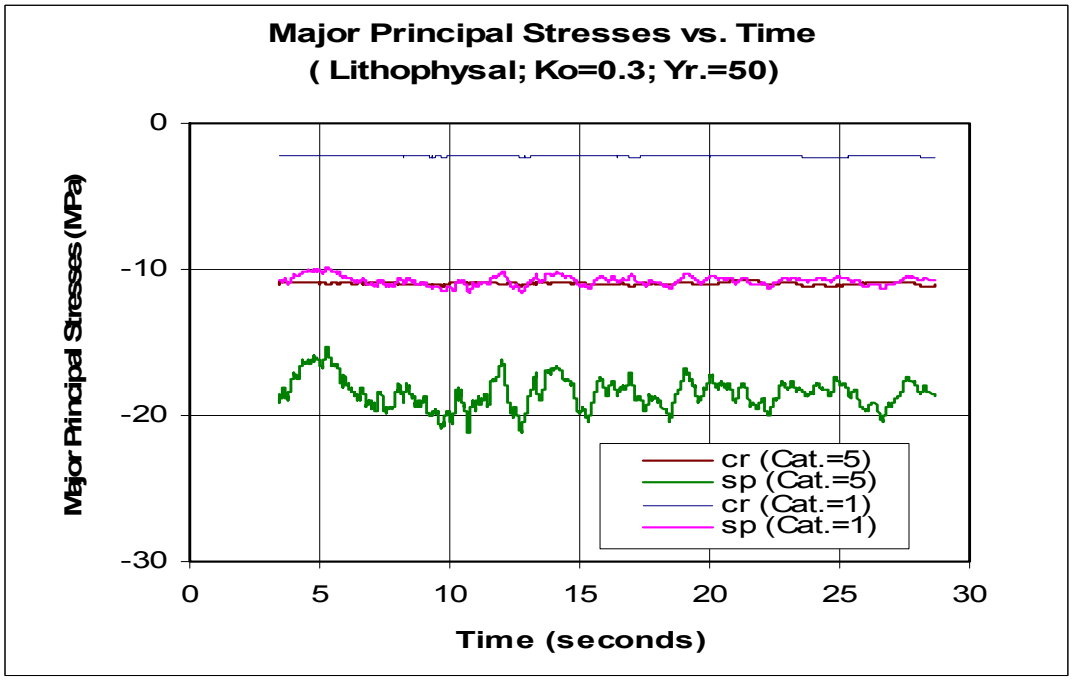

(b)

Figure 6-135 Time Histories of Major Principal Stresses near Crown and Springline of Exhaust Mains under In Situ, Thermal and Seismic Loads in Lithophysal Rock at (a) Year 0; (b) Year 50

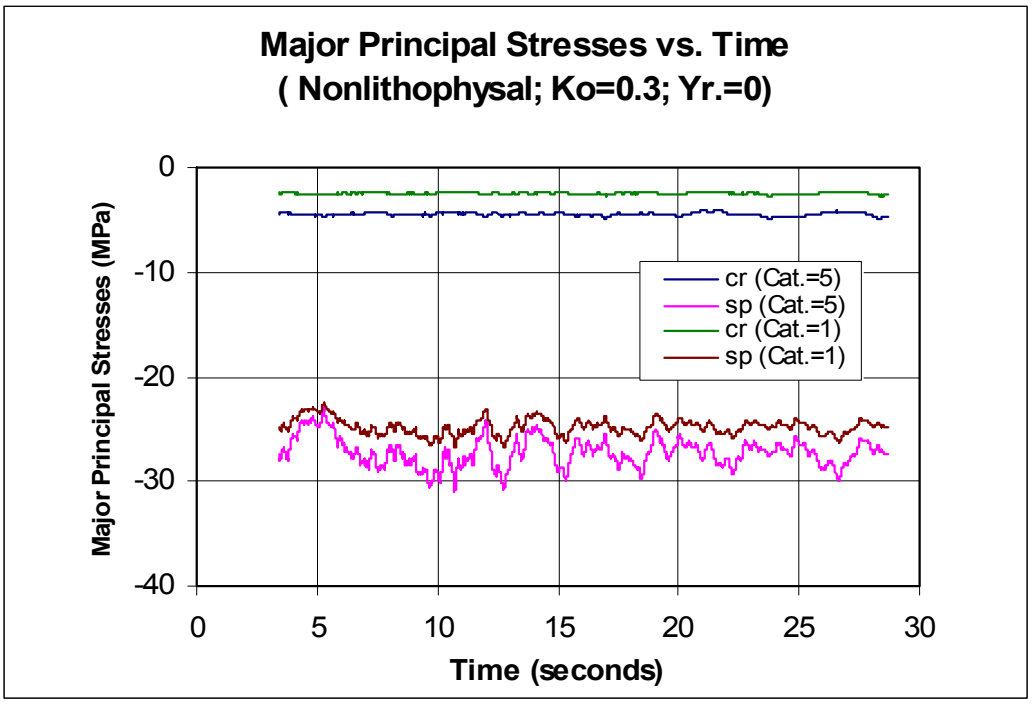

(a)

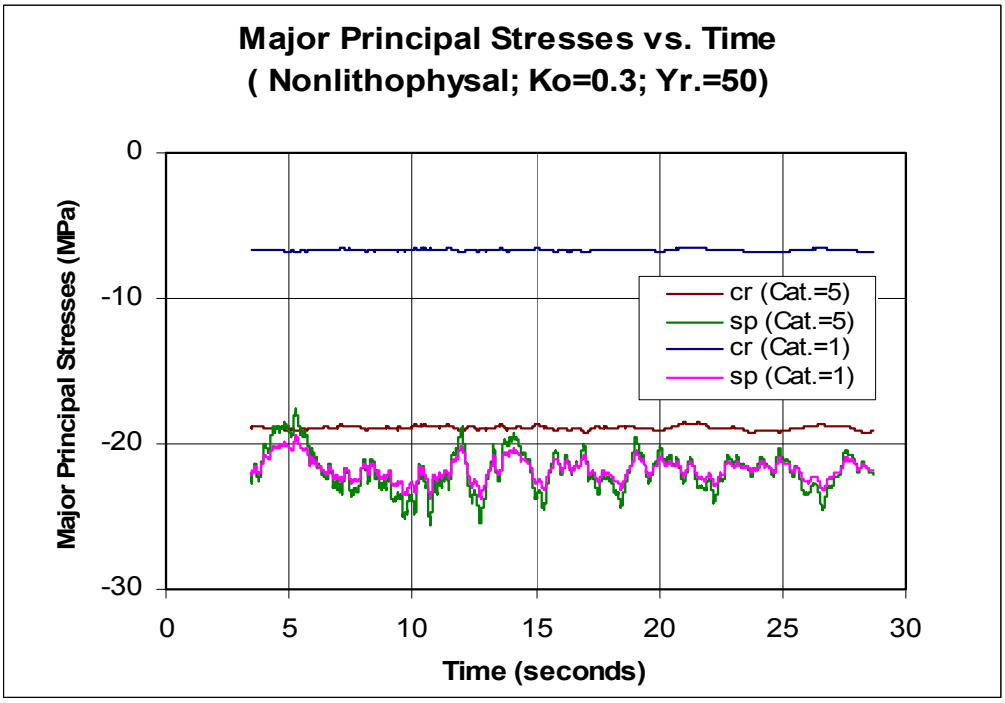

(b)

Figure 6-136 Time Histories of Major Principal Stresses near Crown and Springline of Exhaust Mains under Seismic Loads in Nonlithophysal Rock at (a) Year 0; (b) Year 50

6.5.3.3.4 Observation Drift

The observation drift was analyzed for seismic loading with an APE of 5 x 10^{-4} in both a typical cross-section and at the intersection between the observation drift and the exhaust main. The results are shown in Figure 6-137 to Figure 6-144. Seismic load causes insignificant increase in damage around the observation drift (compare Figure 6-137, Figure 6-141 and Figure 6-142 with Figure 6-61, Figure 6-65 and Figure 6-66), but there is no indication of large-scale instability. A preclosure level of ground motion could cause some rockfall resulting from shaking down of loosened blocks, but designed ground support will be sufficient to prevent most of such rockfall. The velocity histories in the tunnel crown (shown in Figure 6-139 are almost identical to the velocity histories of the incoming seismic wave (see Figure 6-1). There is no amplification of the velocities due to interaction of the wave with the excavations. The velocities indicate predominantly elastic response. The histories of the principal stress magnitudes (Figure 6-140) are recorded in the crown and the walls of the observation drift. Variation of the major principal stress in the crown of the observation drift is smaller than the variation of the major principal stress in the walls. The major principal stress in the crown of the tunnel is horizontal and is shielded by the tunnel from the seismic wave propagating vertically upward. Fluctuations of the major principal stresses in the drift walls, which are vertical, are direct consequence of the passage of the P-wave (see comparison between the history of the vertical component of the velocity in Figure 6-139 with histories of the major principal stresses in the walls shown in Figure 6-140). Seismic load causes some permanent stress redistribution that results in a small increase in the size of the plastic region (see comparison between Figure 6-141 and Figure 6-142 with Figure 6-65 and Figure 6-66).

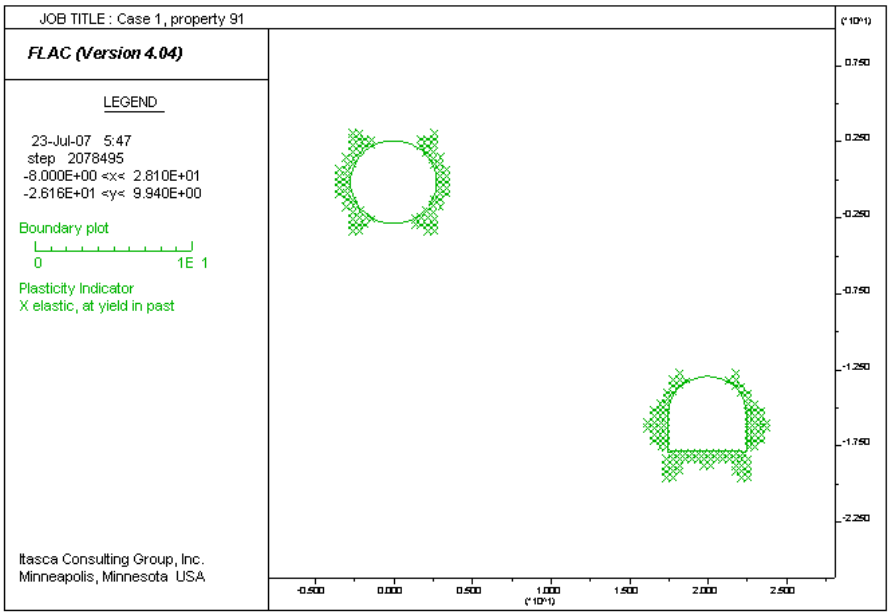

Figure 6-137 Potential Yield Zone around Observation Drift after Seismic Shaking

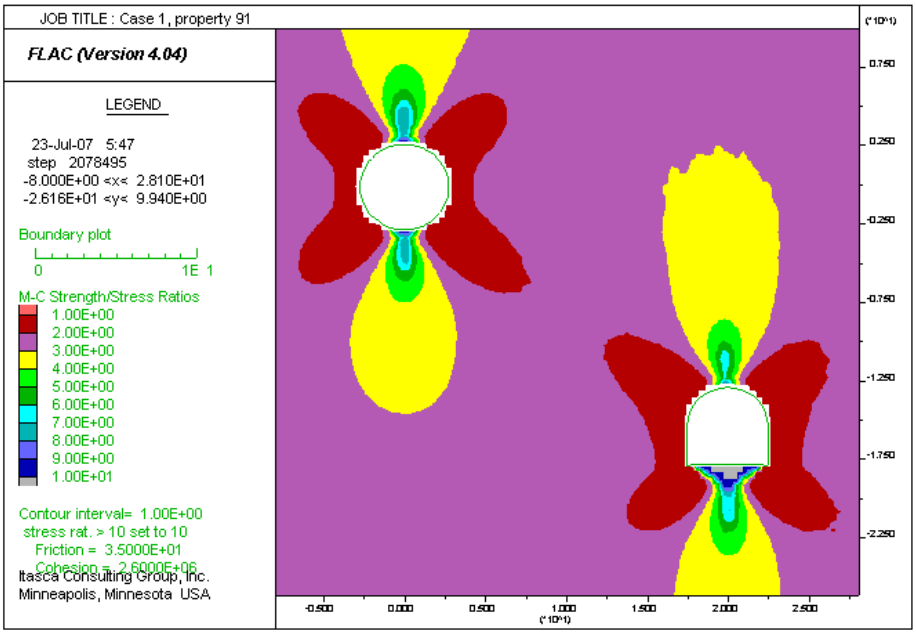

Figure 6-138 Factor of Safety around Observation Drift after Seismic Shaking

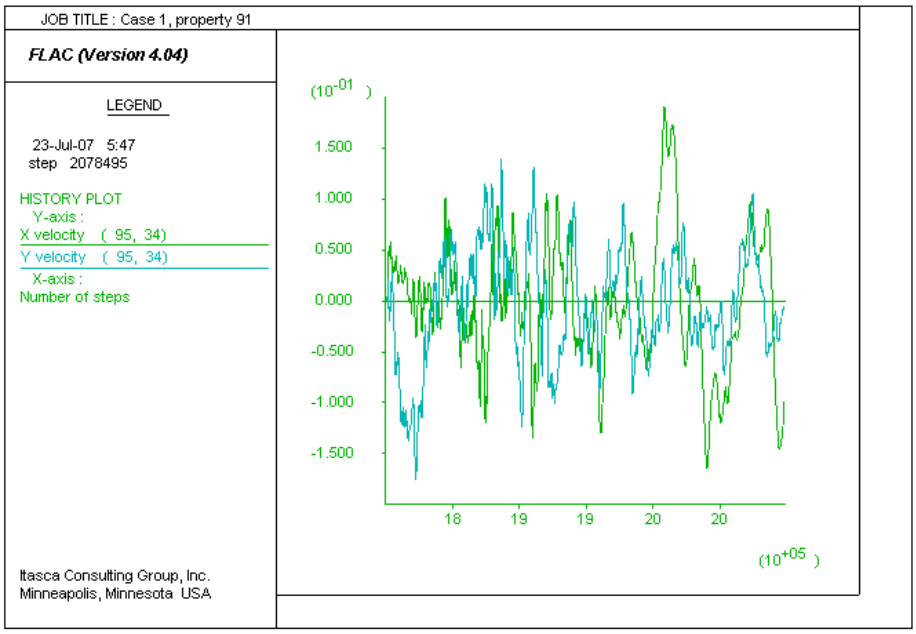

Figure 6-139 Velocity (m/sec) Histories of Point at Crown of Observation Drift during Seismic Shaking

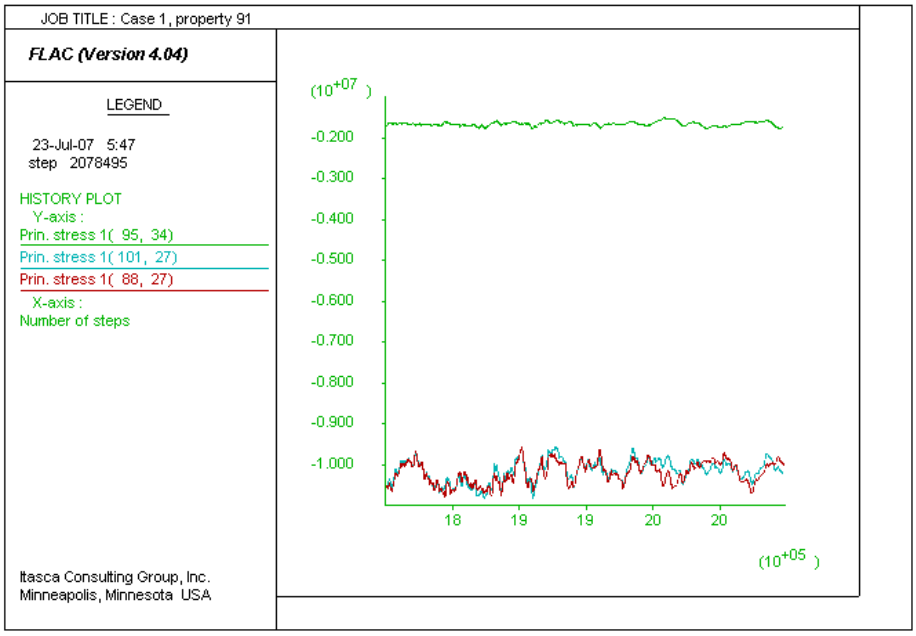

Figure 6-140 Stress (Pa) Histories of Points at the Crown and Left and Right walls of Observation Drift during Seismic Shaking

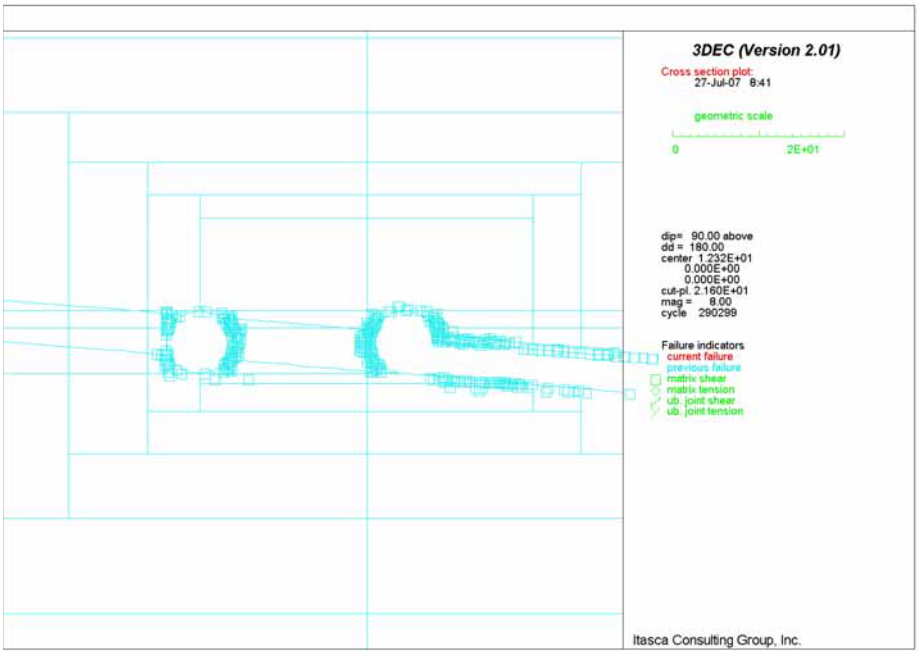

Figure 6-141 Potential Yield Zone in Intersection between Observation Drift and Exhaust Main in Vertical Section 1 after Seismic Shaking

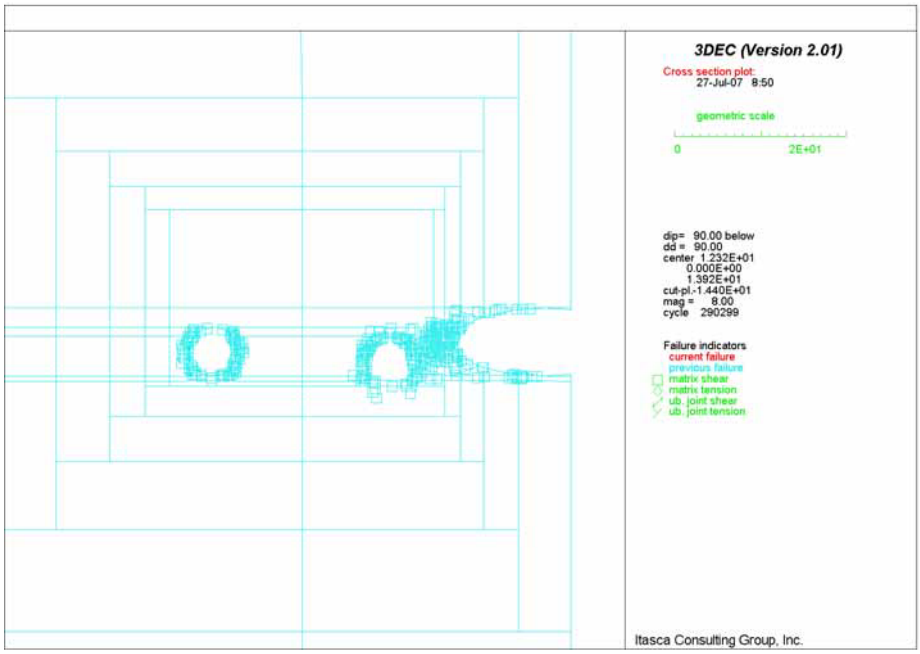

Figure 6-142 Potential Yield Zone in Intersection between Observation Drift and Exhaust Main in Vertical Section 2 after Seismic Shaking

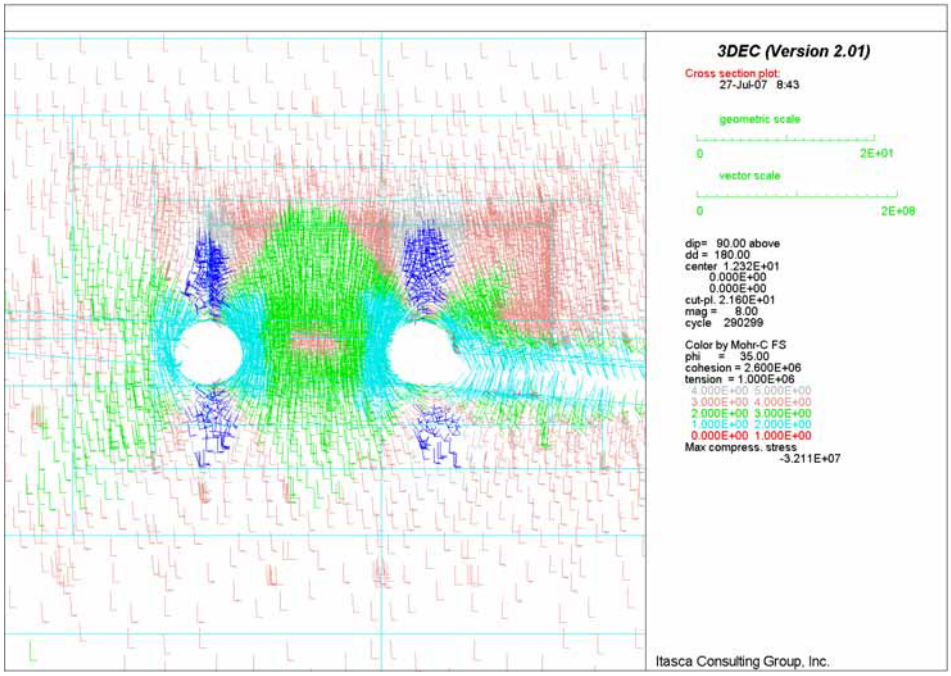

Figure 6-143 Factor of Safety in Intersection between Observation Drift and Exhaust Main in Vertical Section 1 after Seismic Shaking

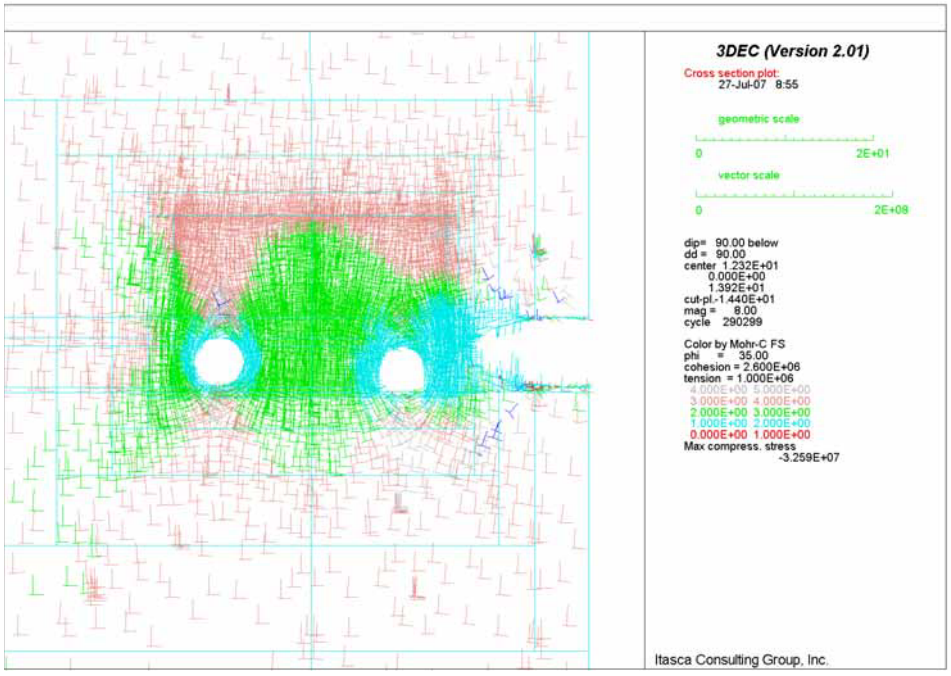

Figure 6-144 Factor of Safety in Intersection between Observation Drift and Exhaust Main in Vertical Section 2 after Seismic Shaking

6.5.3.3.5 TBM Launch Chamber

The results of the dynamic analysis of the TBM launch chamber, summarized in Figure 6-145 to Figure 6-148, are very similar to the results obtained for the observation drift. Preclosure seismic shaking (2,000-year return period) causes relatively small damage of the rock mass (Figure 6-145), but there is no indication of global instability of the launch chamber during or after the shaking. The velocity and stress histories at the points around the excavations are almost identical for the TBM launch chamber (see Figure 6-147 and Figure 6-148) and the observation drift (see Figure 6-139 and Figure 6-140).

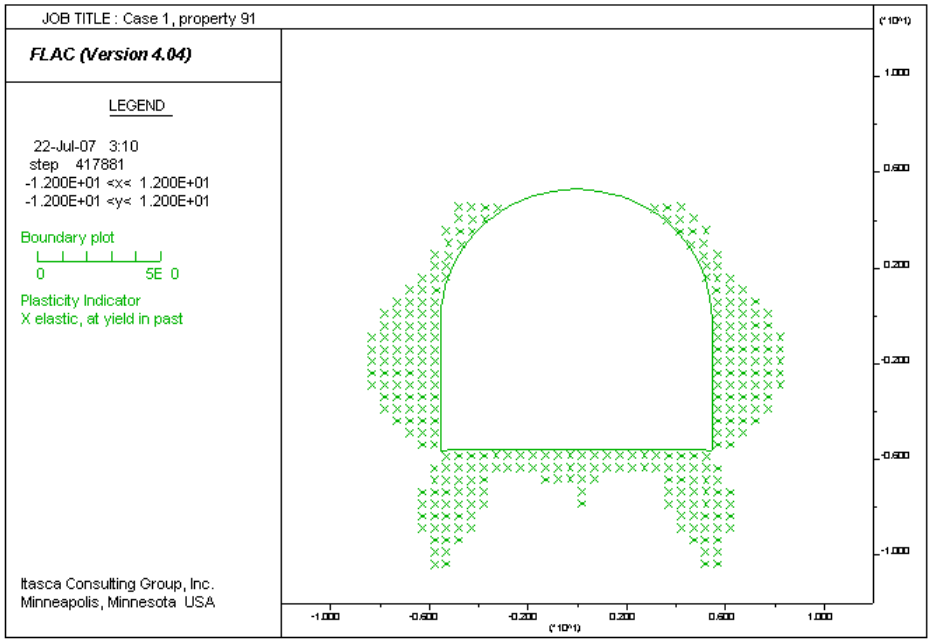

Figure 6-145 Potential Yield Zone around TBM Launch Chamber after Seismic Shaking

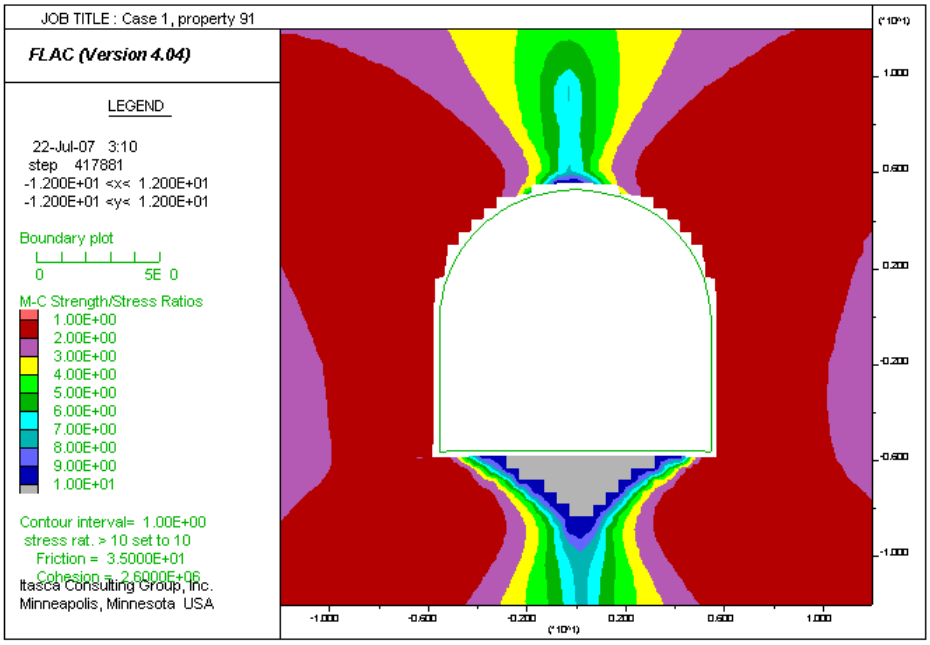

Figure 6-146 Factor of Safety around TBM Launch Chamber after Seismic Shaking

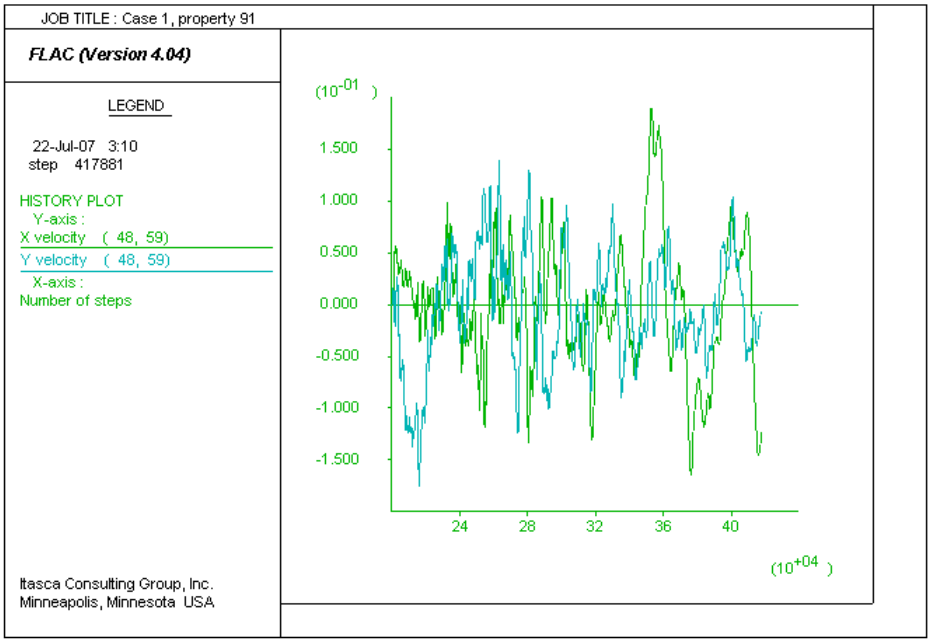

Figure 6-147 Velocity (m/sec) Histories of Point at Crown of TBM Launch Chamber after Seismic Shaking

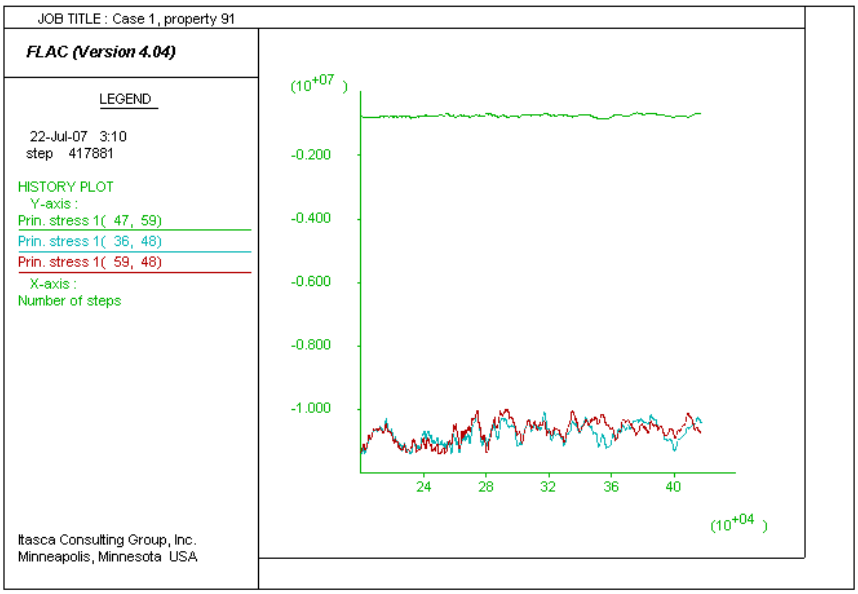

Figure 6-148 Stress (Pa) Histories at Three Points around TBM Launch Chamber after Seismic Shaking

6.5.3.3.6 North Portal

The results of dynamic analysis of stability of the North Portal under the seismic ground motion are shown in Figure 6-149 to Figure 6-154. The velocity histories recorded at the ground surface of the model (Figure 6-149) are almost identical to the input velocity histories of the design earthquake (Figure 6-1). This comparison is a proof that boundary conditions are implemented correctly in the model. The velocity histories recorded at the crown of the starter tunnel (Figure 6-150) indicate no additional amplification of velocity at the tunnel boundary and elastic model response to the seismic shaking.

Shaking due to the 2,000-year ground motion does not cause any plasticity in the model. Stress tensor fields colored by the major principal stress magnitude and factor-of-safety with respect to Mohr-Coulomb shear failure are shown (Figure 6-151 to Figure 6-154) at two states during dynamic simulation: after 21.46 seconds, and at the end of dynamic simulation. Ground shaking does not cause residual changes in the stress field, which is consistent with the observation that model behaves elastically. The factor of safety with respect to Mohr-Coulomb shear failure remained large in the entire model throughout the dynamic simulation.

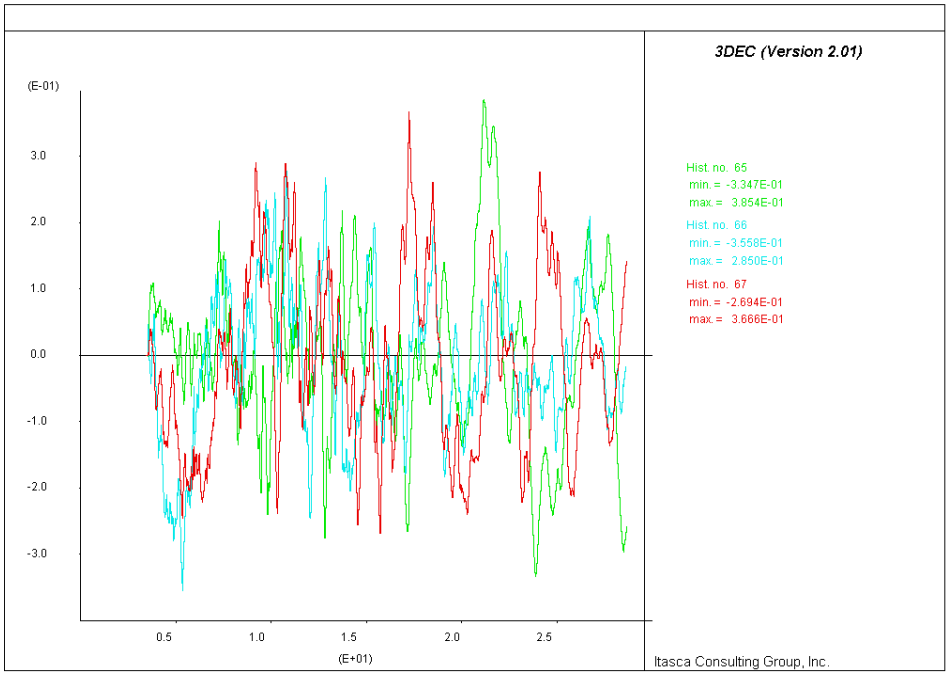

Note: Y axis-Velocity (m/sec); X axis-Time (sec)

Figure 6-149 Velocity Histories in X, Y, and Z Directions at Ground Surface

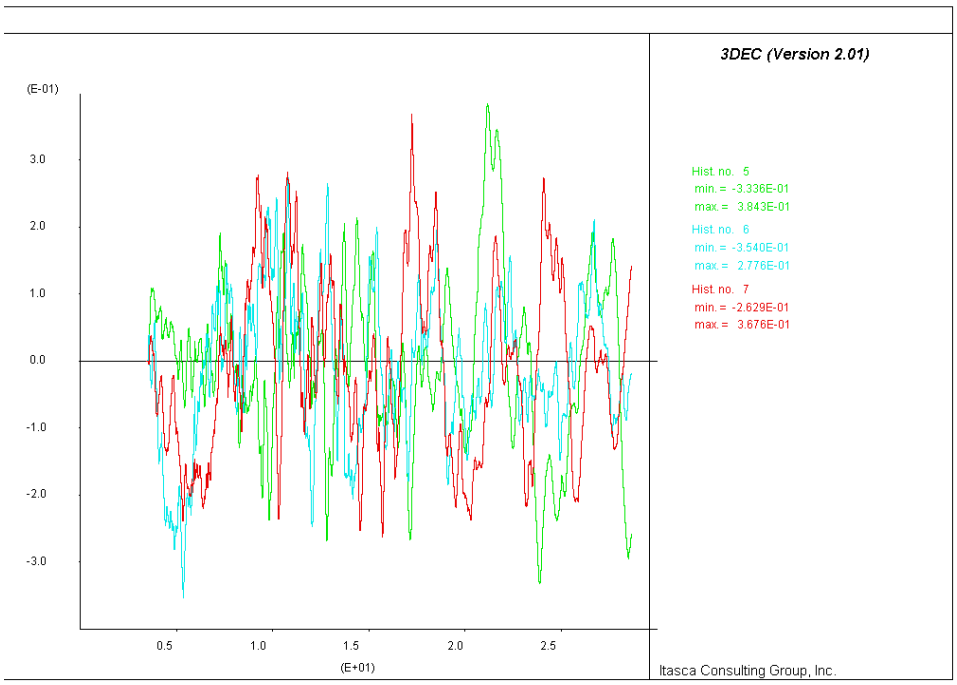

Note: Y axis-Velocity (m/sec); X axis-Time (sec)

Figure 6-150 Velocity Histories in X, Y, and Z Directions at Crown of Starter Tunnel

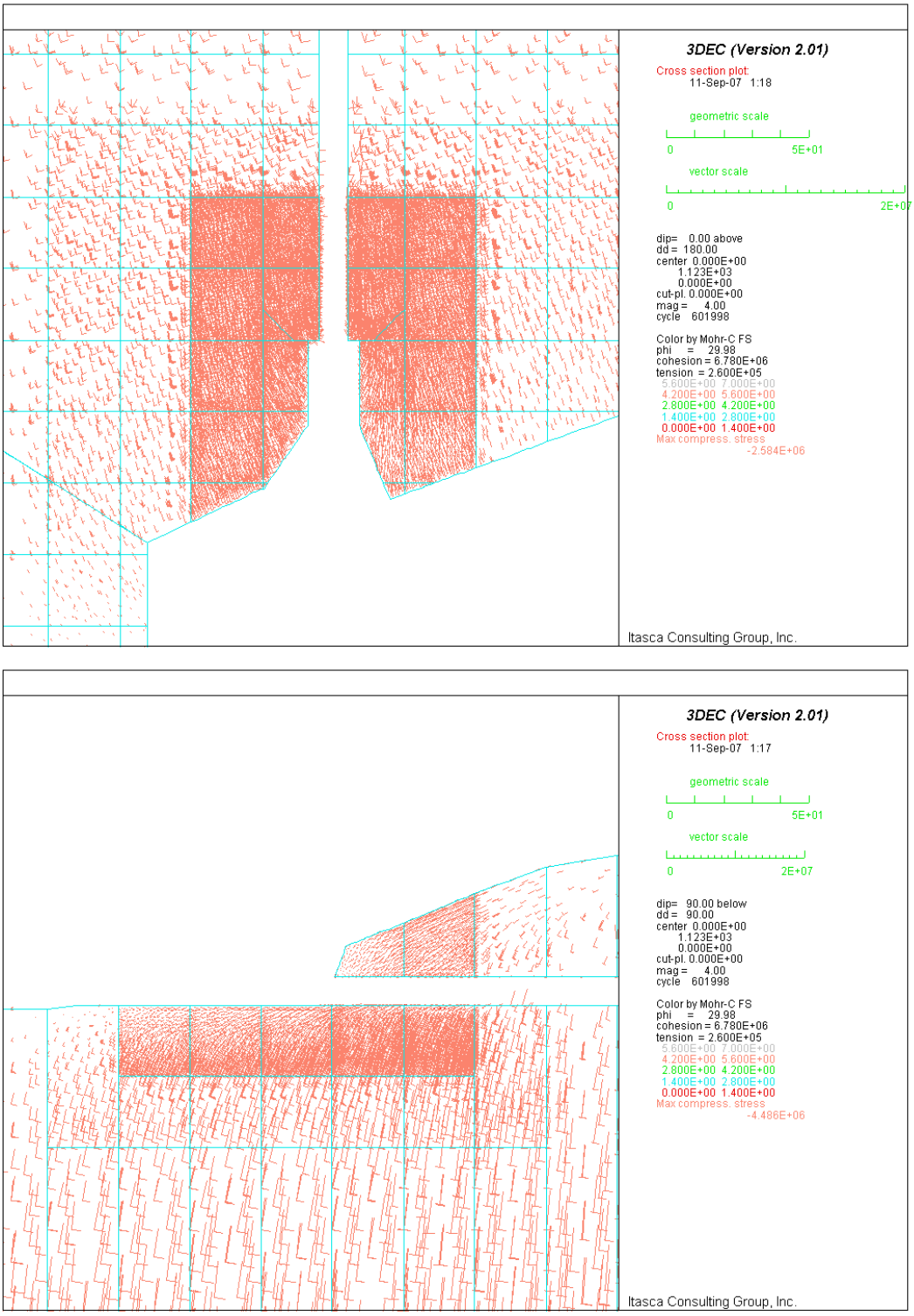

Figure 6-151 Factor of Safety after 21.46 Seconds of Ground Shaking: top) Horizontal Cross-section at Elevation 1123 m; and bottom) Longitudinal Cross-section L-L'

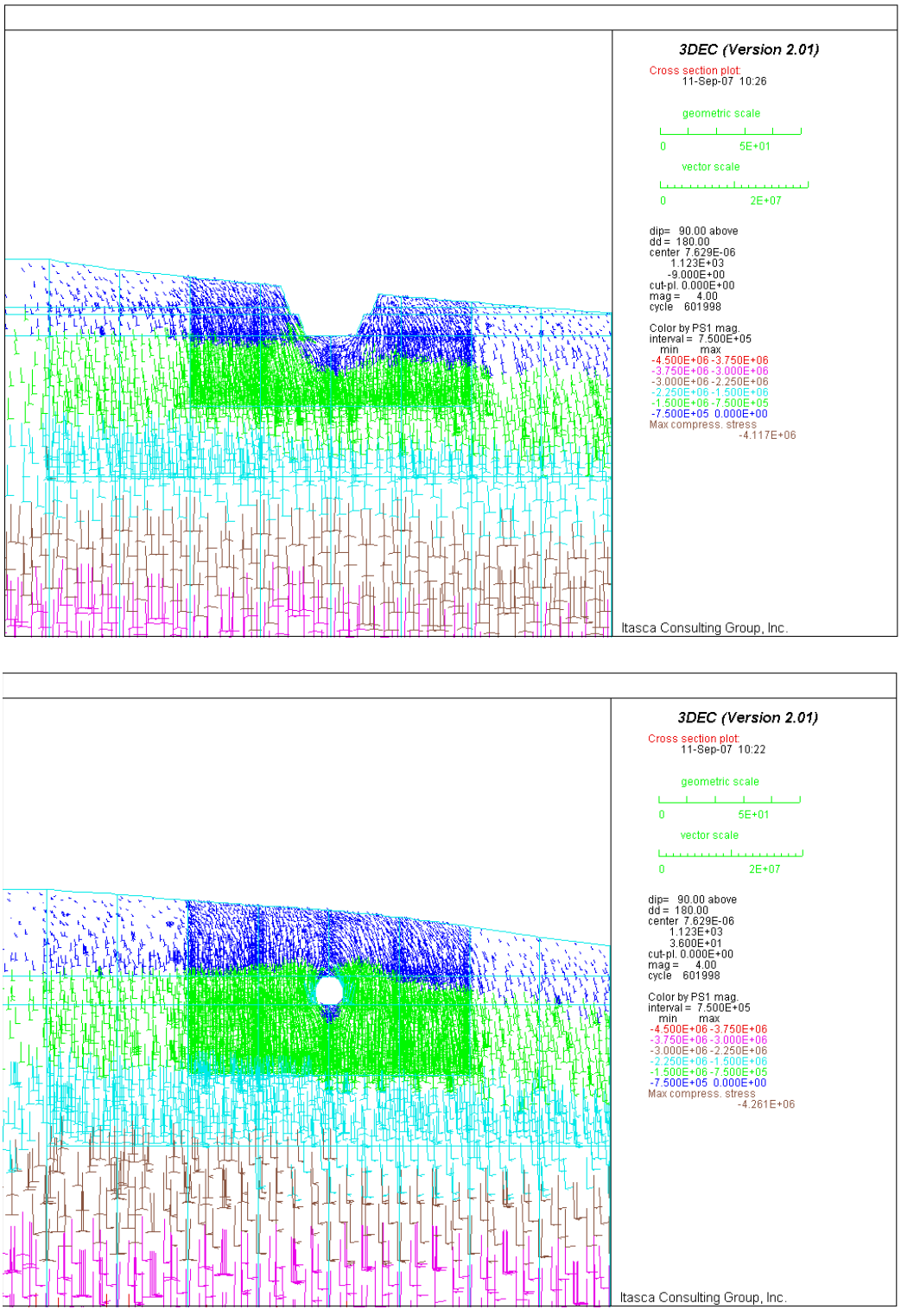

Figure 6-152 Major Principal Stresses after 21.46 Seconds of Ground Shaking for Cross-sections: a) C1-C1' and b) C2-C2'

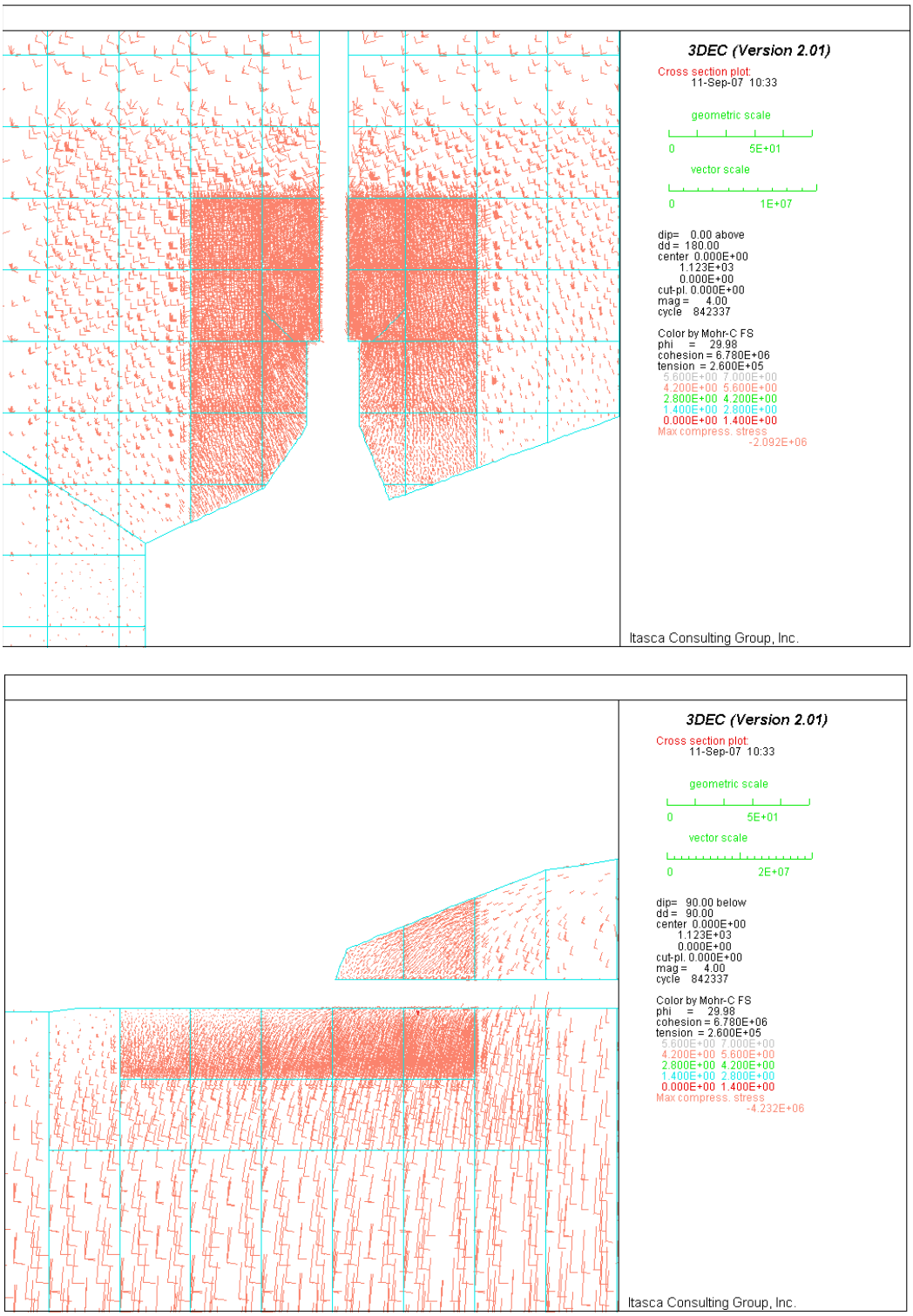

Figure 6-153 Factor of Safety at End of Ground Shaking: top) Horizontal Cross-section at Elevation 1123 m; and bottom) Longitudinal Cross-section L-L'

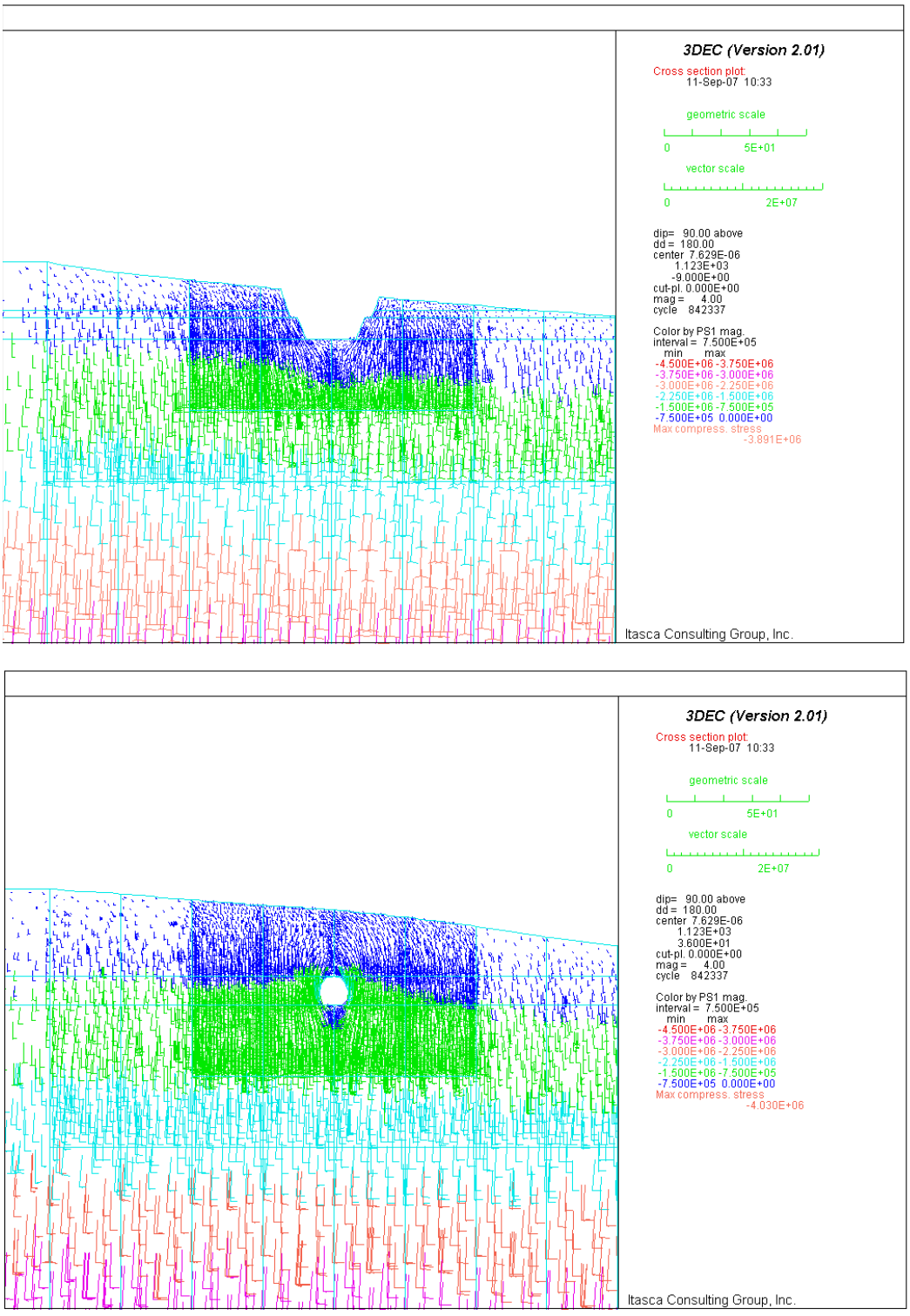

Figure 6-154 Major Principal Stresses at End of Ground Shaking for Cross-sections: top) C1-C1' and bottom) C2-C2'

6.5.3.3.7 Interburden Pillar between Shaft Access and Exhaust Mains

The results of dynamic simulation of the pillar for preclosure seismic ground motion of 2,000-year return period are shown in Figure 6-155 through Figure 6-159 . Seismic loading was applied to the model at the initial state, after excavation of the drifts, before heating (due to waste emplacement) began. The results of the thermomechanical analysis indicate that if the seismic load were applied to the model at any stage during 50 years, the difference in results of the dynamic analysis would be minimum or insignificant (see discussion in the first paragraph of Section 6.5.3.3.3 and comparing Figure 6-133(a) and Figure 6-133(b)).

The dynamic load causes insignificant additional yielding caused by stress oscillations (comparing Figure 6-156 and Figure 6-157 with Figure 6-82 and Figure 6-83). The contours of SF after seismic loading are almost the same as those due to in-situ stress loading (comparing Figure 6-158 and Figure 6-159 with Figure 6-80 and Figure 6-81). After completion of the dynamic simulation, the models for all simulated cases are stable. There is no indication of permanent stress redistribution or destressing of portions of rock mass indicating areas prone to rockfall. Velocity histories were recorded during the simulation at a number of points throughout the model. The histories near the center of the model are shown in Figure 6-155. These histories are almost identical to the velocity histories applied at the base of the model due to the vertically propagating seismic wave (see Figure 6-1). Thus, the model deforms elastically under seismic load. There is no indication of accumulation of irreversible, plastic deformation.

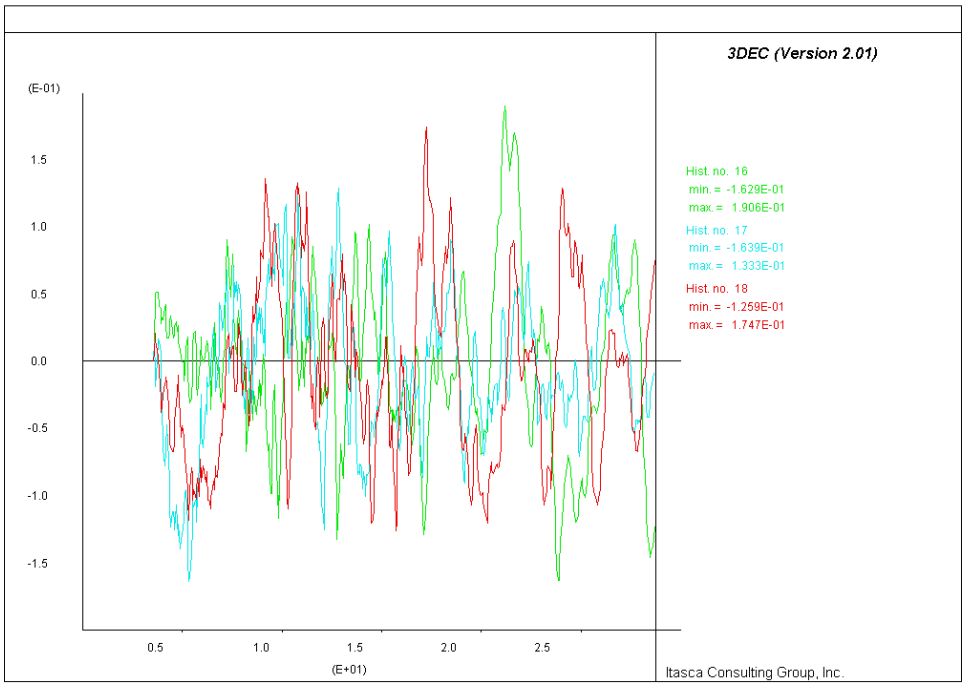

Note: Y axis-Velocity (m/sec); X axis- Time (sec)

Figure 6-155 Velocity Histories in X, Y, and Z Directions near Point 1 for Lith. Cat. 1 Rock at Interburden Area

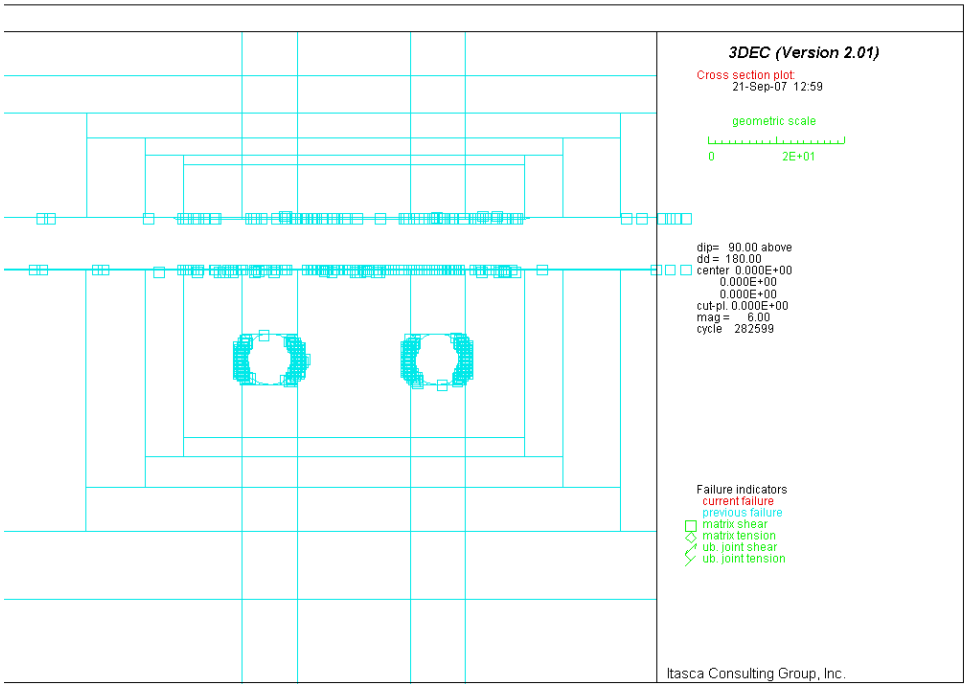

Figure 6-156 Potential Yield Zone in Vertical Section 1 for Lith. Cat. 1 Rock under In Situ and Seismic Loading at Interburden Area

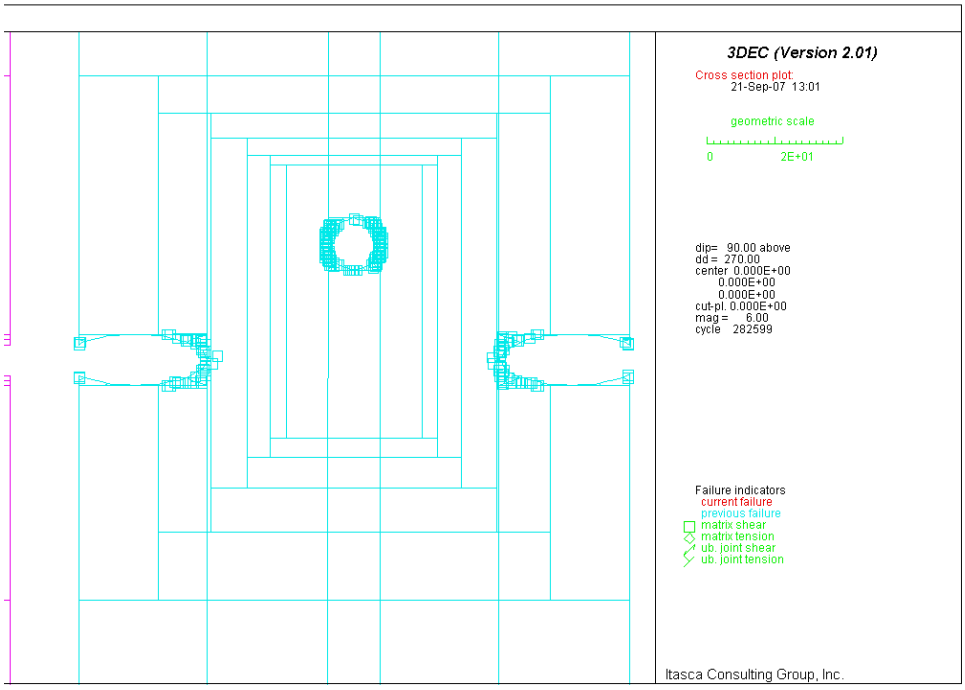

Figure 6-157 Potential Yield Zone in Vertical Section 2 for Lith. Cat. 1 Rock under In Situ and Seismic Loading at Interburden Area

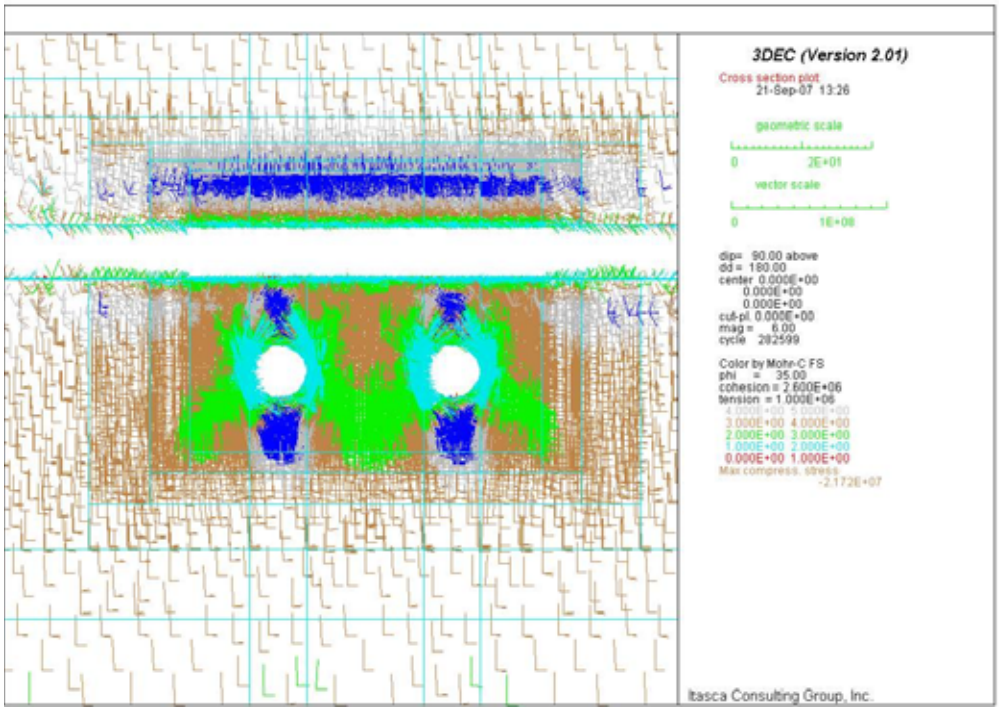

Figure 6-158 SF in Vertical Section 1 for Lith. Cat. 1 Rock under In Situ and Seismic Loading at Interburden Area

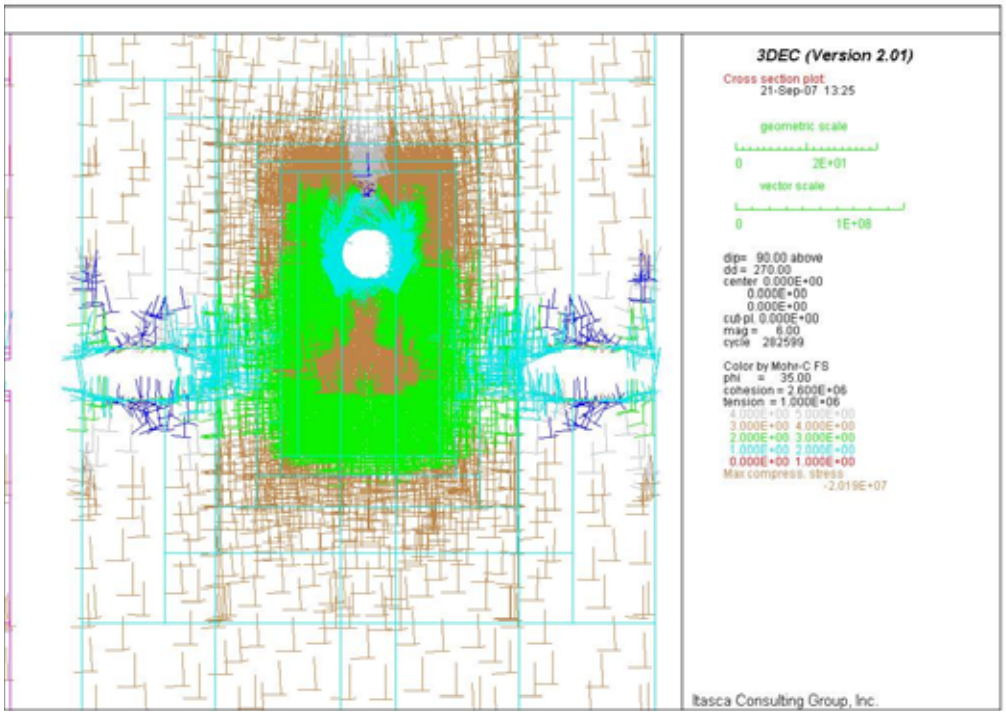

Figure 6-159 SF in Vertical Section 2 for Lith. Cat. 1 Rock under In Situ and Seismic Loading at Interburden Area

Based on the results of this section and those from Sections 6.5.3.1.7 and 6.5.3.2.4, it is indicated that the effect of the excavation of an overlying 7.62-m-diameter access drift and two underlying 7.62-m-diameter exhaust mains on the stability of 10-m high interburden pillar is minimum or insignificant.

6.5.3.4 Ground Reaction Curves

The Ground Reaction Curves (GRC) is often used for the analysis of ground support requirements or to examine the interaction between ground support components and rock. The visualization of GRC can serve as a check of the stability of unsupported non-emplacement drifts, and to quantify the potential load that may be induced in ground support components due to further ground convergence after ground support component installation. In this calculation, the GRC concepts are described in conjunction with presenting the results of the analysis of the access main in category 1 and 5 rock in the lithophysal and nonlithophysal units. This scenario was chosen for demonstration as it represents the worst-case rock mass scenario. The displacements developed around the excavation and resulting loads in the ground support are significantly greater than any other rock mass conditions for these drifts at Yucca Mountain.

Ground reaction curves for non-emplacement drifts with various rock categories and K_o values were generated using the FLAC models. Note that K_o of 1.0 was also used in the analysis of ground reaction curves. These curves are shown in Figure 6-160 and Figure 6-161 for the lithophysal and nonlithophysal rocks, respectively. For each point on a curve, a FLAC run was conducted by applying a pressure (or stress) on the drift wall to determine the relation between the applied pressure and the drift wall radial displacements. The applied pressure selected varied from zero to the in situ stress at the drift center, with five equal intervals. This resulted in a total of six points, or six FLAC runs, for each curve. Each point demonstrates the drift state of equilibrium at a specific level of pressure imposed by ground support.

As shown in Figure 6-160 and Figure 6-161 , the ground reaction curves are generally straight lines and all intersect with the displacement axis, indicating that the drifts are anticipated to be stable and self-supporting. The ground support function in these cases is merely retention of occasional loosened pieces of rock. The ground reaction curves for the non-emplacement drifts in category 1 lithophysal rock show stable conditions but the rock displacements are relatively large. To prevent any potential unstable conditions caused by excessive rock displacements, rock reinforcement by installing rock bolts quickly or using lining type support is necessary.

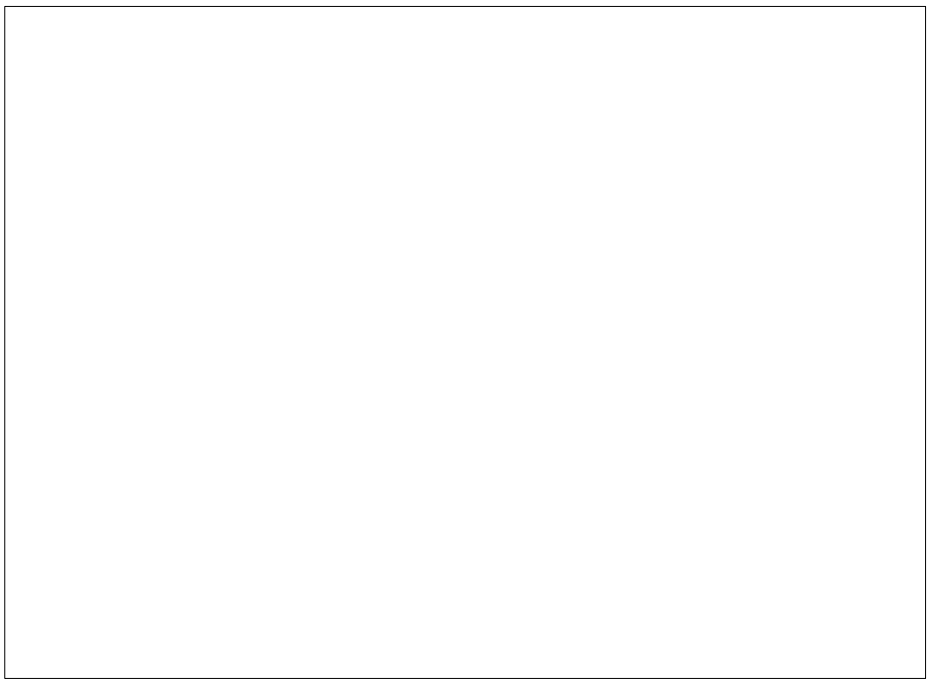

Figure 6-160 Ground Reaction Curves for Unsupported Access Mains: in Lithophysal Rock

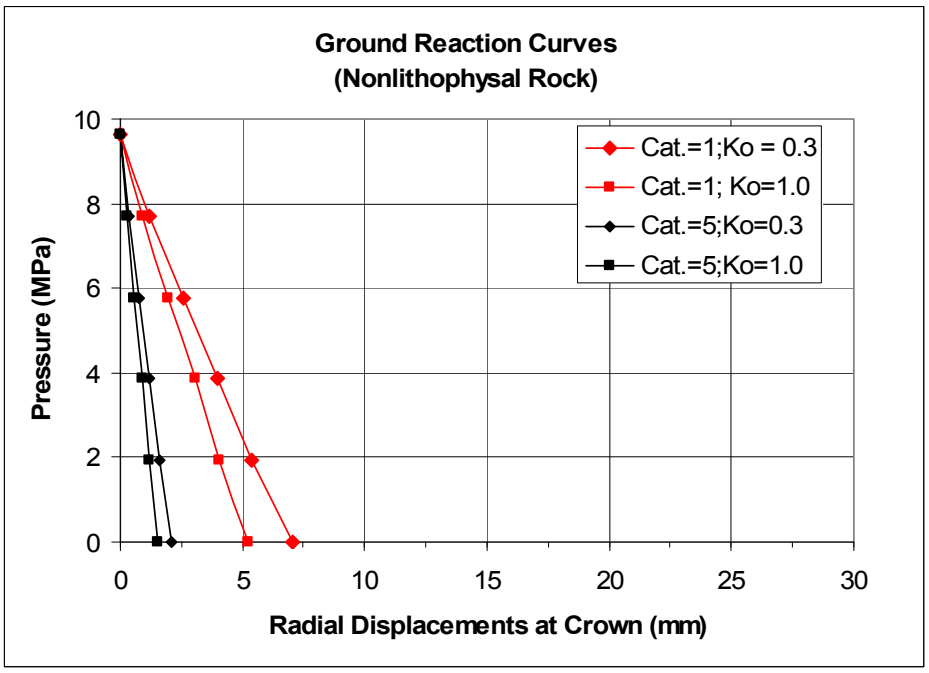

Figure 6-161 Ground Reaction Curves for Unsupported Access Mains in Nonlithophysal Rock

6.5.4 Ground Support Systems for Non-Emplacement Drifts

The ground support methods for non-emplacement drifts are selected based on the requirements of functions, performance, and service life of ground support system. As stated in Section 6.3, ground support system installed in non-emplacement drifts must ensure stable conditions for personnel and environmental safety during construction and the preclosure period, and be functional with planned maintenance in the accessible non-emplacement openings and little or no planned maintenance in the non-accessible non-emplacement areas during the operational life throughout the preclosure period of 100 years (Reference 2.2.28, Section 8.2.2.1).

6.5.4.1 Candidate Ground Support Systems

Based on the discussion and results presented in Sections 6.4.2 and 6.5.3, the ground support systems to be used in non-emplacement drifts are proposed as follows:

- For non-emplacement openings, which include access mains, exhaust mains, observation drift, test alcove, and TBM launch chambers: fully grouted rock bolts with heavy duty WWF.
- For intersections between access mains and turnouts and ramps: fully grouted bolts with steel fiber-reinforced shotcrete, and lattice girders as necessary for roof span control.
- For intersections between exhaust mains and emplacement drifts: the same ground support system as that for intersections between access mains and turnouts except that no shotcrete inside the emplacement drift.
- For emplacement drift turnouts: stainless steel friction-type rock bolts with stainless steel heavy duty WWF.

The fully grouted rock bolts with a typical length of 3 m, spaced at 1.25 m with heavy duty WWF, i.e., W4 x W4 with 100 mm center-to-center spacing, are designed to be used for ground support at typical non-emplacement openings, which include access mains, exhaust mains, observation drift, test alcove, TBM launch chambers and North Portal starter tunnel. It is noted that even though the stability analysis for test alcove was not performed, the same ground support system for the observation drift will apply to the test alcove since both of them have the same shape and dimension and are in the same PC facility area. Similarly, the same ground support system for access mains is considered adequate to be used for the ECRB Cross Drift in its future widening stage.

Stainless steel friction-type rock bolts with a typical length of 3 m, spaced at 1.25 m with stainless steel WWF, i.e., W4 x W4 with 75 mm center-to-center spacing, are designed to be used for ground support at emplacement drift turnouts.

In the intersection areas, in order to enhance the opening stability with large roof span, increased bolt length of about 5 m with 0.10 m thick steel fiber-reinforced shotcrete will be installed, and supplemented with lattice girder as necessary depending on rock mass quality and the associated roof span. Note that shotcrete is not designed to be used inside the emplacement drift since cementious materials are ruled out for use in emplacement drifts due to their potential adverse impact on the long-term waste isolation.

The same ground support system for the intersections will be applied to ramps except that the bolt length is 3 m long, even though ramps have the same shape and dimension as those of access and exhaust mains. The major reason is that ramps provide access either for men, materials, waste emplacement, or ventilation air. They begin at the interface with the portal and ends at interface with the access mains. Due to their important functions, especially the waste package transportation for North Ramp, it is desirable to supplement fully grouted bolts by shotcrete to enhance the ground support function. It should be noted that the designed ground support system for ramps may be only for North Ramp and may need to be changed for North Construction Ramp and South Ramp as fully grouted rock bolts with heavy duty WWF, with steel fiber-reinforced shotcrete installed on as-needed basis, depending on the rock mass condition and construction schedule.

For the ground support at North Portal, fully grouted rock bolts with fiber-reinforced shotcrete will be installed around the portal frontal and lateral faces. Rock bolts of 3 m long with 1.5 m spacing will be installed at the lateral faces of the portal whereas rock bolts of 5 m long with 1.5 m spacing will be applied at the frontal face. The portal face will be applied with shotcrete to a thickness of 0.1 m. Similar ground support design is expected for North Construction Portal and South Portal if their topographical and ground conditions, geometry, and construction method are similar.

Figure 6-162, Figure 6-163, and Figure 6-164 illustrate the ground support systems in access and exhaust mains, turnout departures, and turnouts, respectively.

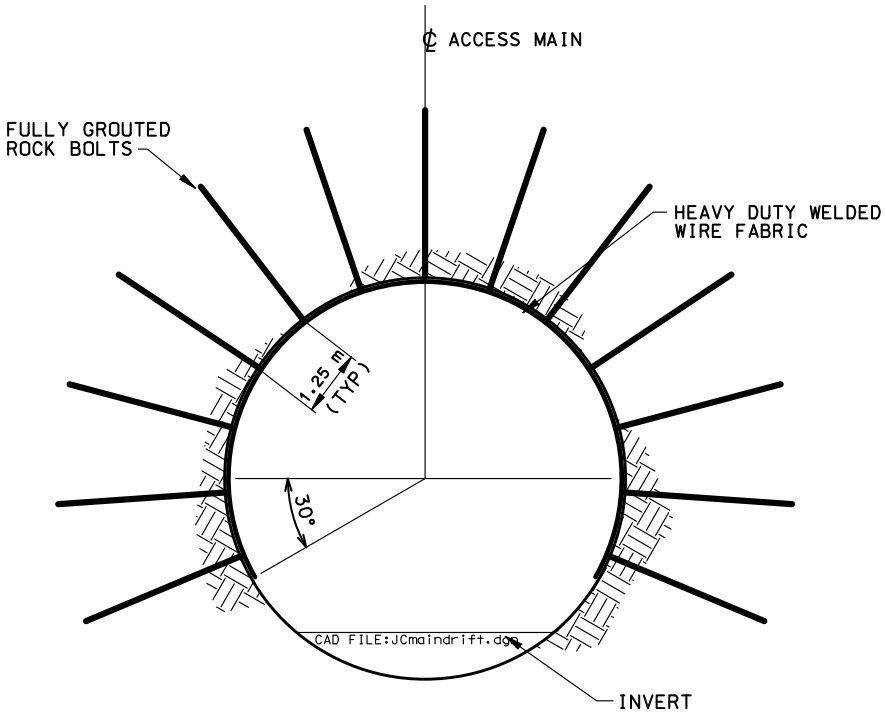

Note: Figure is not to scale; same ground support for exhaust mains.

Figure 6-162 Ground Support System in Access or Exhaust Mains

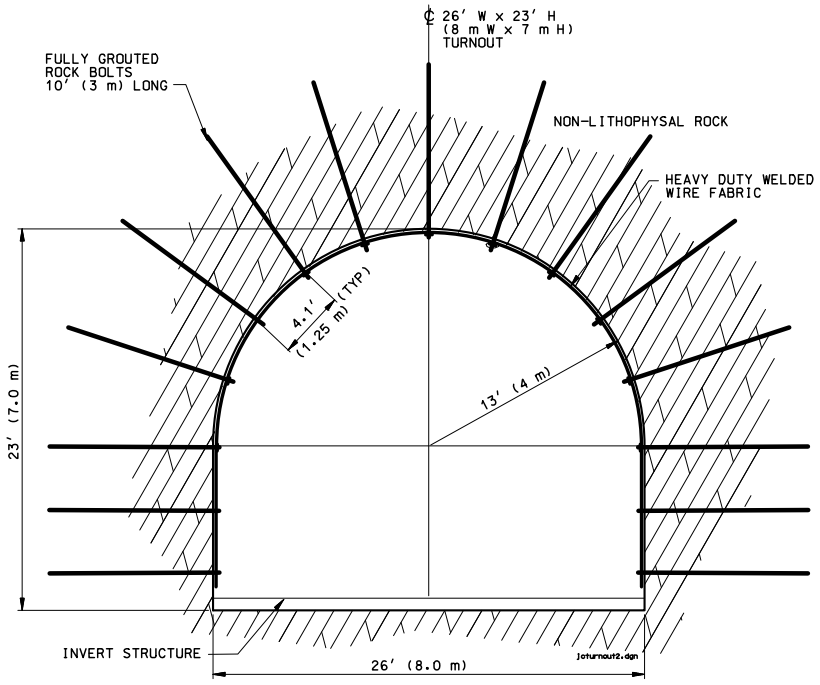

Note: Same ground support for lithophysal rock; figure is used to show ground support for modeling purpose and is not to scale and may not be the same as actual one.

Figure 6-163 Ground Support System in Turnout Departures

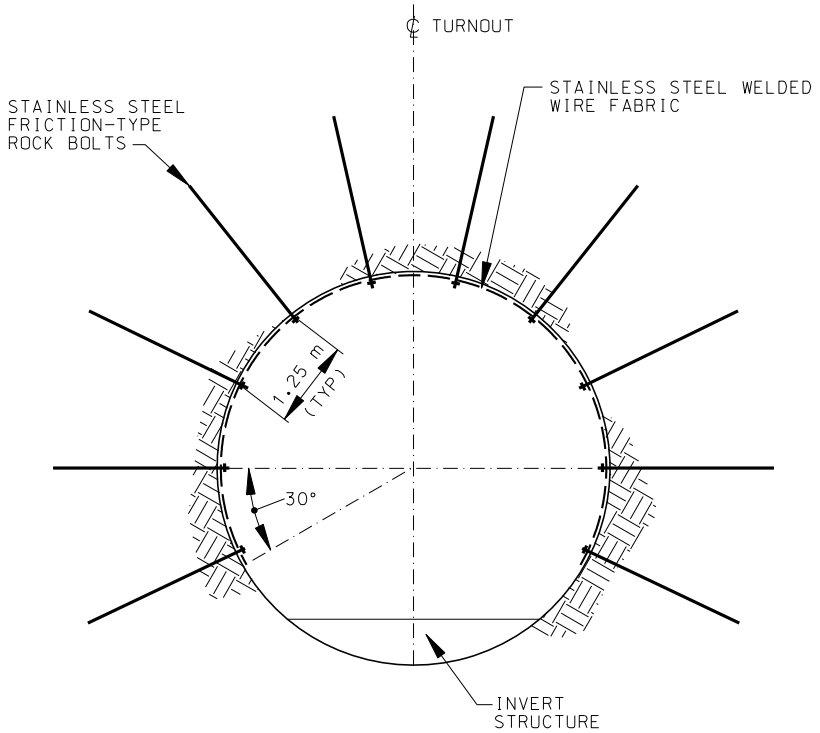

Note: figure is not to scale.

Figure 6-164 Ground Support System in Emplacement Drift Turnouts

6.5.4.2 Candidate Ground Support Materials

In order to make a proper selection of suitable ground support materials, it is important to know the service life in which these materials will be functional and understand under what kind of environment they will be subjected to during the service life.

As indicated in Section 6.3, in accessible non-emplacement openings, ground support will accommodate the maintenance. However, in the non-accessible non-emplacement areas, ground support will function without planned maintenance during the operational life, while providing for the ability to perform unplanned maintenance on as-needed basis.

Carbon steel including high-strength low-alloy steel is considered for all non-emplacement openings with the exception of emplacement drift turnouts. For ground support in emplacement drift turnouts, stainless steel is considered adequate in this potential high radiation environment due to the passage of the waste package loaded TEV.

Steel components that are manufactured based on the following standard specifications included in the American Society for Testing and Materials (ASTM) are expected to perform satisfactorily in the non-emplacement drift environment:

- ASTM A 36 *Standard Specification for Carbon Structural Steel* (Reference 2.2.9)
- ASTM A 242 *Standard Specification for High-Strength Low-Alloy Structural Steel* (Reference 2.2.11)
- ASTM A 588 *Standard Specification for High-Strength Low-Alloy Structural Steel with 50 ksi [345MPa] Minimum Yield Point to 4–in. [100–mm] Thick* (Reference 2.2.13)
- ASTM A 276 *Standard Specification for Stainless Steel Bars and Shapes* (Reference 2.2.12)
- ASTM F 432 *Standard Specification for Roof and Rock Bolts and Accessories* (Reference 2.2.14)
- ASTM A 82 *Standard Specification for Steel Wire, Plain, for Concrete Reinforcement* (Reference 2.2.10)

For cementitious materials to be used for grouted rock bolts, shotcrete or concrete, it is suggested to use a low pH grout and shotcrete/concrete mix, which will be developed with lesser amounts of portland cement and silica fume or to potentially use other types of grouts and cements which are of non-portland cement types. For information on material and properties and construction of shotcrete, the following documents are recommended:

- ACI 223 *Standard Practice for the Use of Shrinkage-Compensating Concrete* (Reference 2.2.3)
- ACI 506R *Guide to Shotcrete* (Reference 2.2.4)
- ACI 506.2 *Specification for Shotcrete* (Reference 2.2.5)

The typical dimension and material mechanical properties for fully grouted rock bolts, shotcrete and stainless steel friction-type rock bolts are listed in Table 6-3, Table 6-4, and Table 6-5 respectively.

The ground support system is designed to be functional with planned maintenance in the accessible non-emplacement openings and little or no planned maintenance in the non-accessible non-emplacement areas during the operational life. The accessible non-emplacement openings will be visually inspected by qualified personnel. Results of such a direct observation will be supplemented by a geotechnical instrumentation program designed to provide a field measure for drift closures, ground support loads, and potential overstressing zones. If necessary, adequate maintenance plans will be based on inspection results. For non-accessible non-emplacement openings, any necessary maintenance needs triggered by installation flaws, material defects, off-normal operational conditions, or unfavorable inspection results will be evaluated with a full consideration of the information gathered during the inspection and monitoring activities (Reference 2.2.31, Section 7).

6.5.4.3 Initial Ground Support Methods

Initial ground support is placed in close proximity to the advancing tunnel face for worker safety and prevention of equipment from damage due to rock fall until the permanent support system is installed. Note that initial ground support may also serve as the final ground support depending on its type and tunnel construction method. The initial ground support consists of friction-type rock bolts, such as Split Sets, and wire mesh based on industry standard materials (carbon steel). Rock bolts typically with a length of 1.5 m and a spacing of 1.5 m, installed in the crown (four bolts in each row), is considered adequate for the rock conditions anticipated but it may change depending on local ground condition and excavation method.

6.5.5 Stability of Supported Non-Emplacement Drifts

Based on the results presented in Section 6.5.3, a combination of static (in-situ stress), thermal (where applicable), and dynamic loads are not going to cause significant instability of the surrounding rock mass. The unsupported openings show overall stability due to the self-supporting capacity of the rock mass. Ground support is needed at localized areas as ESF experience shows.

The assessment of stability of supported non-emplacement drifts is presented in this section. The bolts and shotcrete were included in the models of the non-emplacement drifts, but the heavy-duty wire mesh was not. The dimensions and mechanical properties of the rock bolts and the shotcrete are listed in Table 6-3 through Table 6-5. The calculated loads in the ground support are the result of global deformation of the rock mass, subsequent to installation of the ground support. However, the purpose of the ground support is not to prevent or restrain the global deformation of the excavations, which are stable without any ground support, but to prevent local rock fall. The analysis of the ground support in the non-emplacement drifts was carried out mainly for the category 1 lithophysal rock mass, which is the poorest condition of rock mass quality at the repository level. The analysis of the ground support for North Portal was carried out for the category 1 rock in TCw unit.

6.5.5.1 Mechanical Properties of Fully Grouted Rock Bolts and Swellex Bolts

It is important to use appropriate material properties for modeling fully grouted bolts. Two key input parameters in the numerical approach are the bond stiffness (K_{bond}) and the bond shear strength (S_{bond}), which reflect the interaction between bolt and rock and control the bolt behavior. The bond stiffness of 8.68 x 10^8 N/m/m was estimated based on empirical correlation shown in Table 6-3. It is noted that the bond strength is a function of rock modulus; thus, the selection of properties should consider the host rock properties. Based on recommendation by Hutchinson and Diederichs (Reference 2.2.44, Figure 2.6.13), the bond strengths for grout with water/cement ratio of 0.4 are as follows: 260 kN/m for lithophysal category 1 rock (with Young's modulus of 1.9 GPa) and nonlithophysal category 1 rock (with Young's modulus of 10.59 GPa), and 300 and 305 kN/m for lithophysal and nonlithophysal category 5 rock, respectively (see detail in Table 6-3).

For the Swellex bolts to be used in emplacement drift turnouts, the appropriate values for bond stiffness and bond strength are estimated to be 3×10^8 N/m/m and 2.75×10^5 N/m, respectively (see detailed discussion in Section 6.7.1 of Reference 2.2.30).

6.5.5.2 In Situ Stress Loading Condition

6.5.5.2.1 Access and Exhaust Mains and Turnouts

The planned ground support for the access mains, exhaust mains and turnouts is analyzed using the FLAC code.

Figure 6-165 shows the displacements around supported access mains for lithophysal category 1 rock. The maximum vertical displacement at crown is 39.9 mm compared with 41.6 mm, which is shown in Table 6-13 for unsupported case. Figure 6-166 shows the axial load along fully grouted rock bolts around access mains for lithophysal category 1 rock. Note that the negative value in bolt load signifies tensile force in FLAC. The predicted largest axial force in the bolt is 84 kN/ meter of excavation. To account for the out-of-plane spacing by multiplying by 1.25; thus, the predicted largest axial force in the bolt is 105 kN, which is much smaller than the yield strength of fully grouted bolt, i.e., 264 kN (see Table 6-3). Figure 6-167 shows the axial load along fully grouted rock bolts around access mains for nonlithophysal category 1 rock. The predicted largest axial force in the bolt is 22 kN/ meter of excavation. To account for the out-of-plane spacing by multiplying by 1.25; thus, the predicted largest axial force in the bolt is 27.5 kN, which is much smaller than the yield strength of fully grouted bolt, i.e., 264 kN (see Table 6-3). Note that category 1 rock is the poorest rock mass category. For better rock mass such as categories 3 or 5 rock, the axial bolt forces will be much smaller. Figure 6-168 and Figure 6-169 show the SFs of supported openings for access and exhaust mains in lithophysal and non-lithophysal category 1 rock, respectively.

By comparing Figure 6-168 and Figure 6-169 with Figure 6-25 and Figure 6-28, it demonstrates an important point regarding the role of fully grouted rock bolt system in deep underground excavations. Ground support such as rock bolts should not be expected to arrest movement of the rock or reduce the rock mass stresses. Rather, it is there to support the loosened blocks that result from the slip and dilation of joint planes intersecting the excavation surface. It should be

noted that the same conclusions discussed above for access mains should apply to those of exhaust mains under in situ loading condition since the same rock properties and opening dimensions were used in numerical analysis for either opening.

Figure 6-170 and Figure 6-171 show the SFs of supported openings for turnouts in lithophysal and nonlithophysal category 1 rock, respectively.

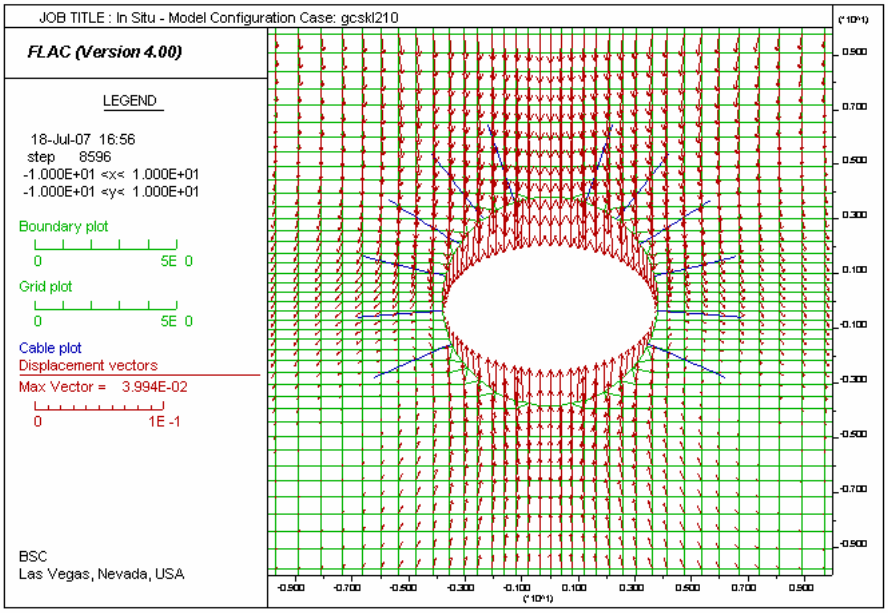

Figure 6-165 Displacements around Supported Access Main for Lith. Cat. 1 Rock

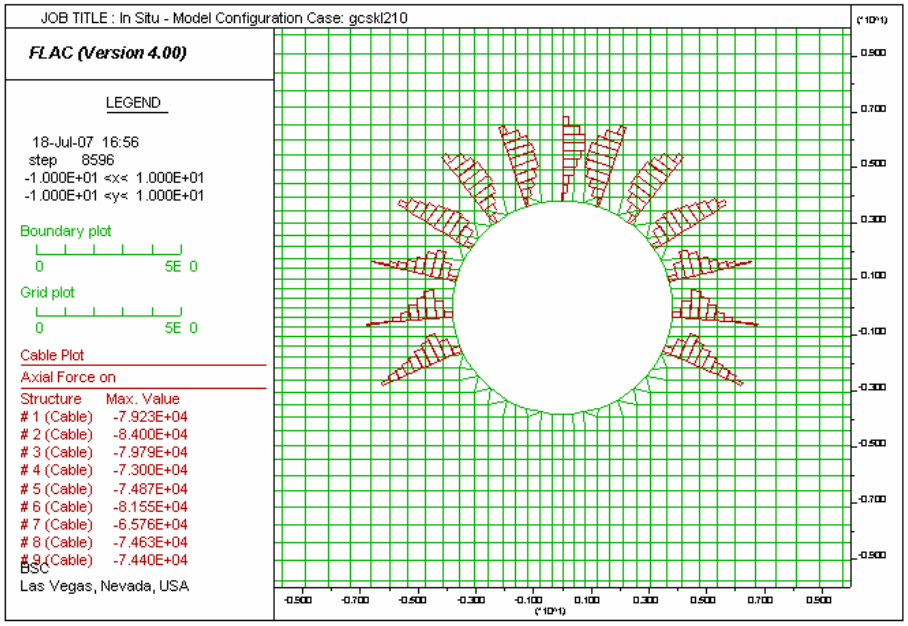

Figure 6-166 Axial Force (N) along Bolts at Access Main for Lith. Cat. 1 Rock

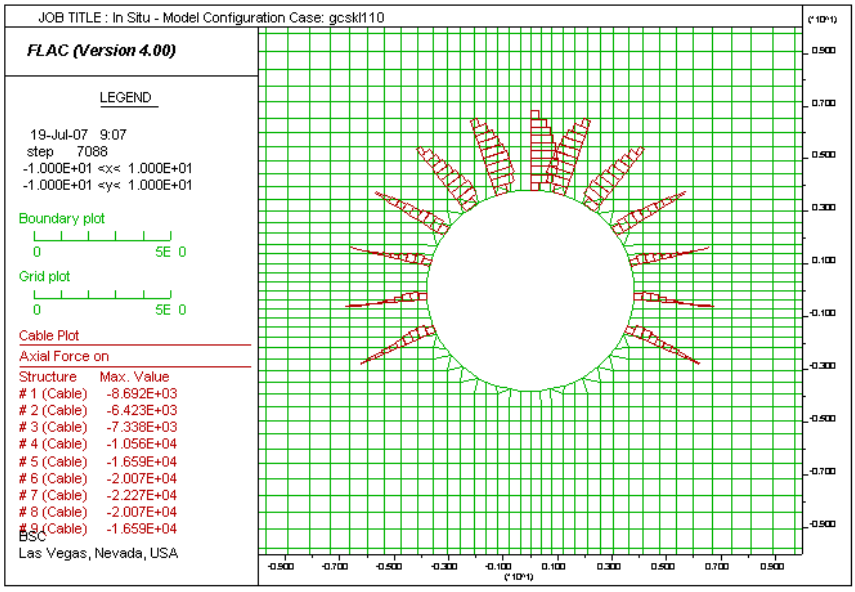

Figure 6-167 Axial Force (N) along Bolts at Access Main for Nonlith. Cat. 1 Rock

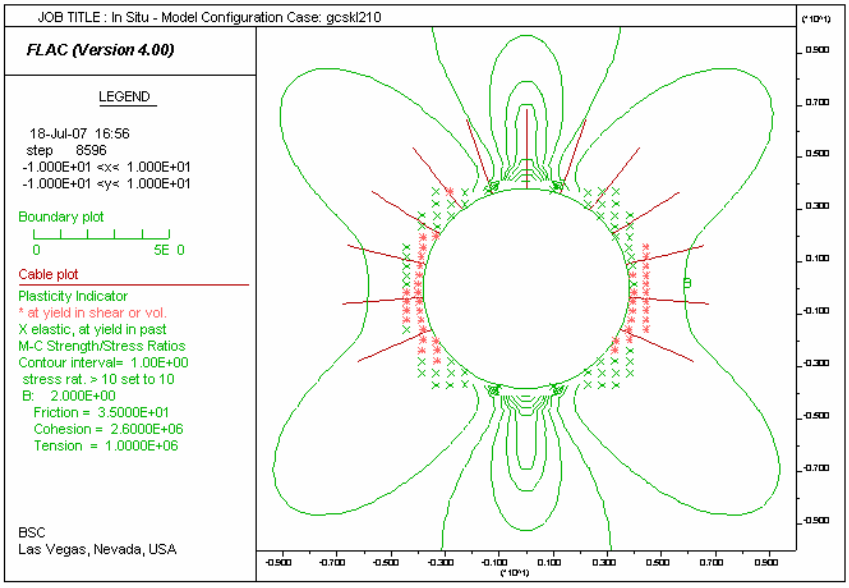

Figure 6-168 Contours of SF around Supported Access/Exhaust Main for Lith. Cat. 1 Rock

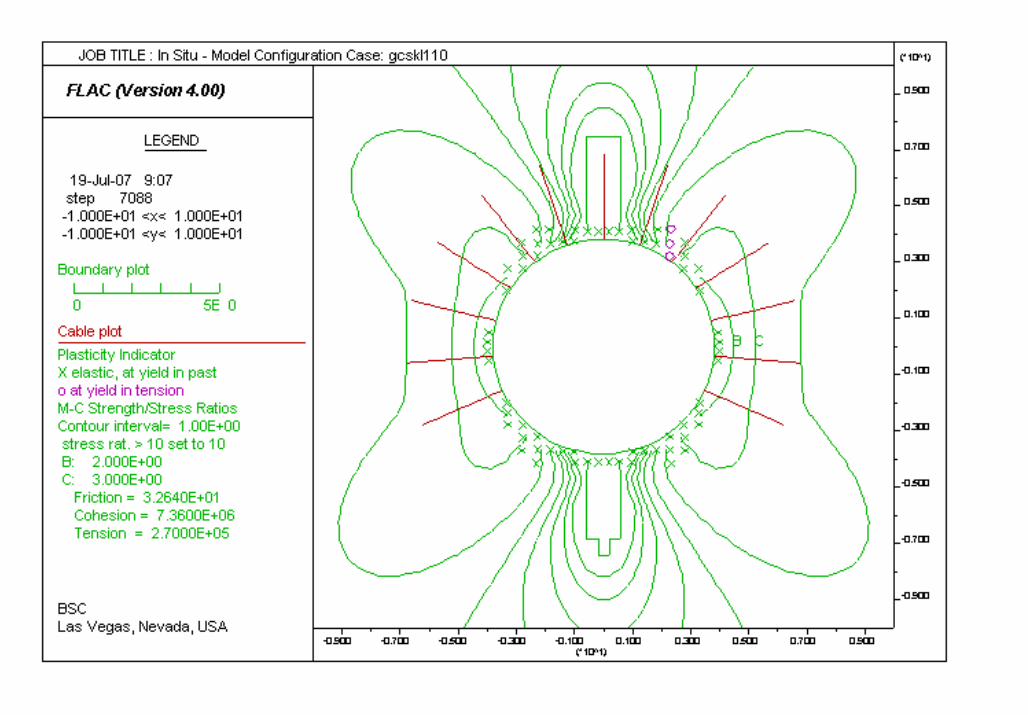

Figure 6-169 Contours of SF around Supported Access/Exhaust Main for N. Lith. Cat. 1 Rock

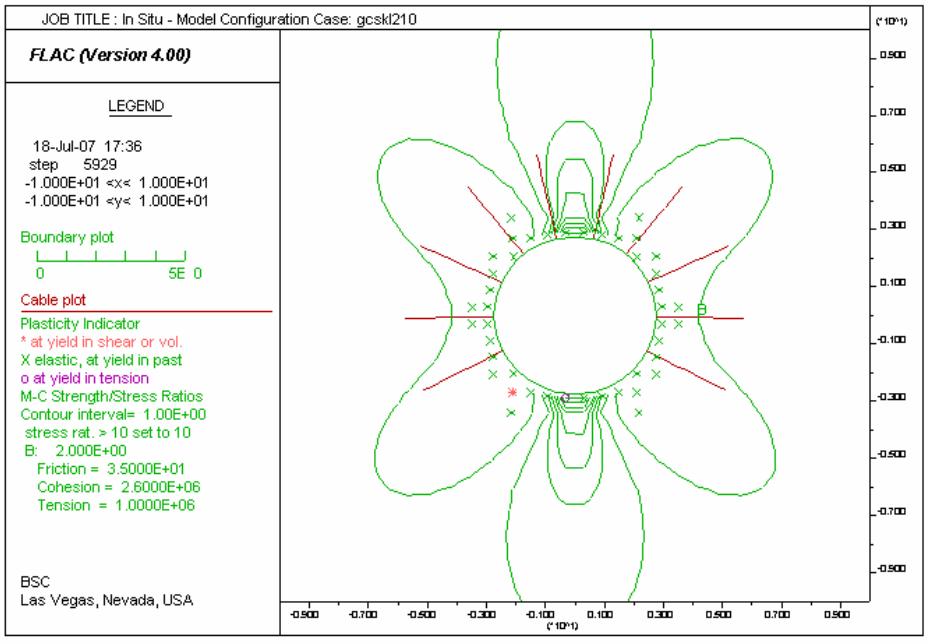

Figure 6-170 Contours of SF around Supported Turnout for Lith. Cat. 1 Rock

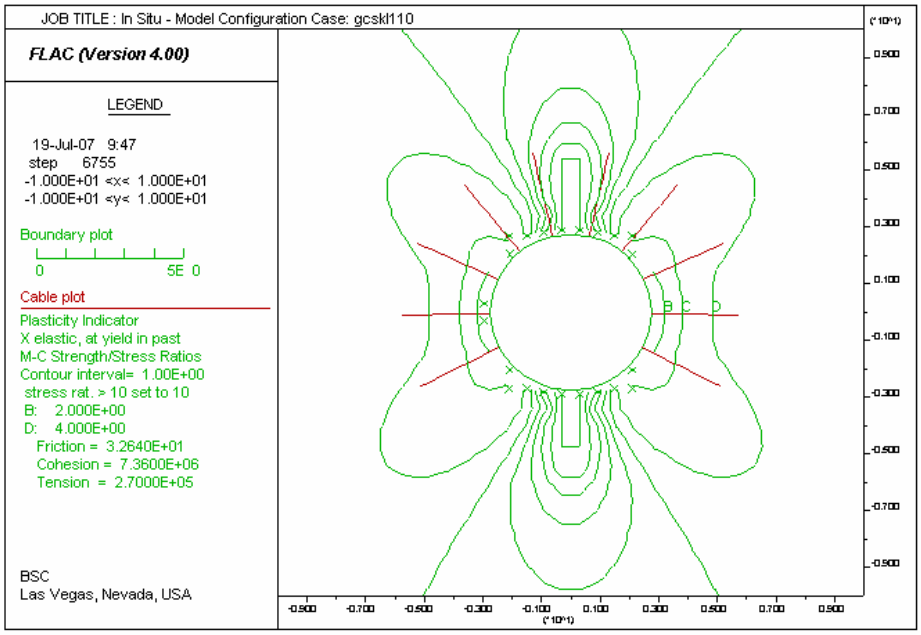

Figure 6-171 Contours of SF around Supported Turnout for N. Lith. Cat. 1 Rock

6.5.5.2.2 Intersections between Access Mains and Turnouts

The analysis of the ground support system in the access main intersections was carried out using 3DEC for the category 1 lithophysal rock mass, which is the poorest condition of rock mass quality at the repository level.

The elements of ground support are simulated in the numerical model, following the expected sequence of their installation during tunnel construction. The bolts will be installed at a certain distance behind the excavation face. From the three-dimensional model, which simulated the face advance, it is assumed that 60% of stress relaxation (Assumption 3.2.1) is completed before the bolts are installed (if the face advance is not explicitly considered). The bolts are loaded due to displacements caused by the remaining 40% of stress relaxation. The three-dimensional, simulation of the face advance and sequential installation of the bolts behind the face is a very time-consuming process.

The following are modeling steps performed during the analysis of the ground support in the intersection:

1. 60% of stress relaxation in the access main
2. Support of the access main with the grouted rock bolts and complete excavation of the access main
3. 60% of stress relaxation in the first turnout
4. Support of the first turnout with the grouted rock bolts and complete excavation of the first turnout
5. 60% of stress relaxation in the second turnout
6. Support of the second turnout with grouted rock bolts and complete excavation of the second turnout
7. Installation of the shotcrete in the intersection.

According to this construction sequence, it is clear that shotcrete in the intersection is not going to be loaded due to stress relaxation, which is caused by the excavation of the drifts under in-situ stresses. The shotcrete will be likely loaded by deformation due to time-dependent strength degradation or seismic loading subsequent to installation of the shotcrete. In order to examine the effect of sequential turnout excavation on the forces in the rock bolts already installed in the access main, the excavation of the second turnout was simulated following the expected sequence of face advance and bolt installation behind the advancing face.

The bolt forces in the view along the access main, due to 40% of stress relaxation after excavation of the access main, are shown in Figure 6-172. Locally, in the bolts installed around the crown, the forces reach 154 kN. This gives a SF of about 1.7 (264/154 = 1.7). In other words, the bolts have a reserve of at least 100 kN (i.e., 264 – 154 =110 > 100) to take the load by loosened, locally unstable blocks. However, the bolt forces below crown area are predominantly lower than 100 kN, which will have a SF of about 2.6 (264/100 = 2.64) with a load reserve of at least 150 kN (i.e., 264 – 100 =164 > 150).

The effect of excavation of the first turnout on the bolt forces in the access main is illustrated in Figure 6-173 and Figure 6-174. As expected, excavation of the turnout has the largest effect on the bolts already installed above the intersection. The maximum forces in the bolts between springline and the crown increase from approximately 150 kN (shown in Figure 6-172 after excavation of the access main) to about 240 kN. In the limited number of bolts that undergo the maximum force increase, the reserve available for additional load due to loosened blocks is 24 kN (i.e., 264 – 240 =24). A plot of the bolt forces in the plan view (Figure 6-174) indicates that the bolts that are additionally loaded due to excavation of the turnouts are located in the area above the intersection. The effect of the excavation of the turnout on the bolts in the access main rapidly decays as a function of distance in the plan view. That effect is illustrated in the plot (Figure 6-175) of the bolt forces after both intersections are excavated. The region of increased bolt forces above the first intersection does not expand (comparing Figure 6-174 and Figure 6-175). Forces in majority of the bolts within that region slightly increase due to excavation of the second turnout with the maximum bolt force still at about 240 kN. The exception are only several bolts at the very tip of the intersection, along the springline where the bolt axial force almost reaches the yield limit of 264 kN. Displacement vector fields shown in Figure 6-176 are in the vertical cross-section normal to the access main, through the center of the first intersection, for the model states before and after excavation of the second turnout. Any increase in displacements in this cross-section due to excavation of the second turnout is relatively small (shown at Figure 6-176(b)).

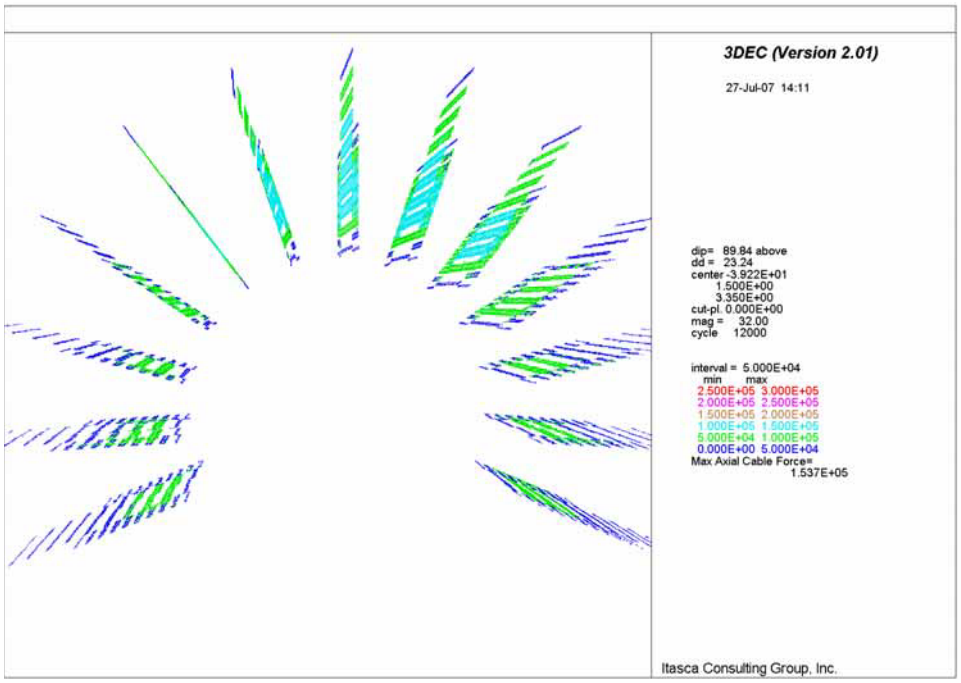

Figure 6-172 Axial Forces in Bolts (N) along the Access Main after Excavation

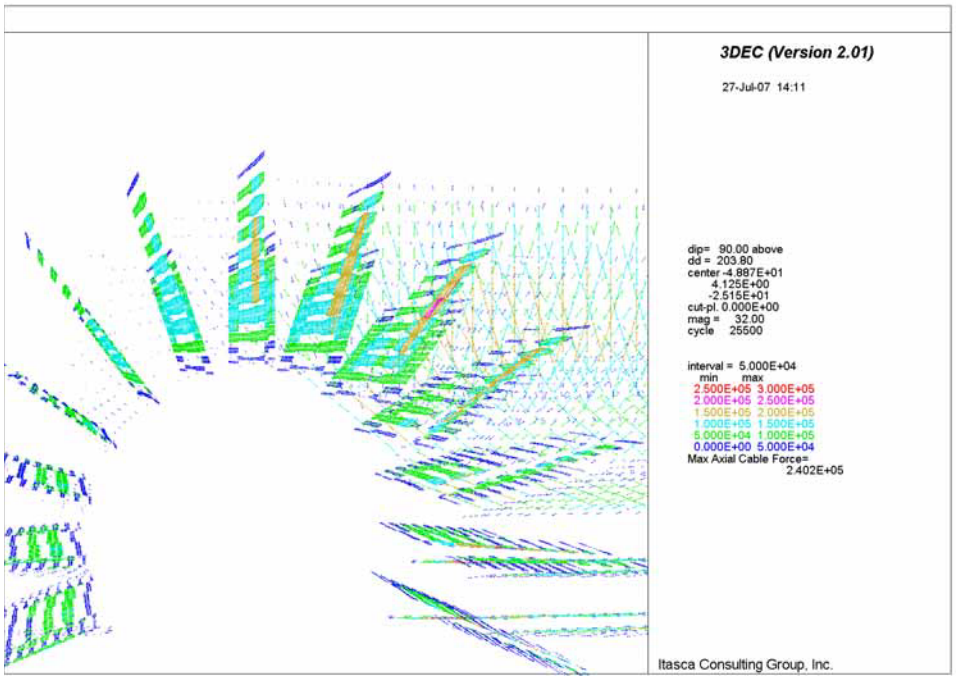

Figure 6-173 Axial Forces (N) in Bolts along the Access Main after Excavation of First Turnout

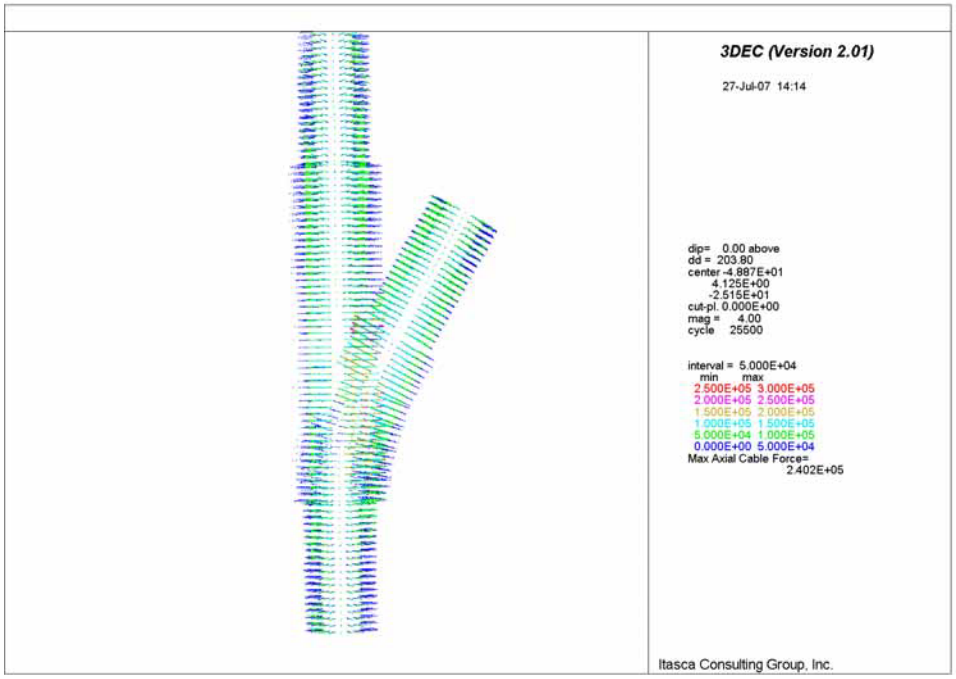

Figure 6-174 Plan View: Axial Forces (N) in Bolts along Access Main after Excavation of First Turnout

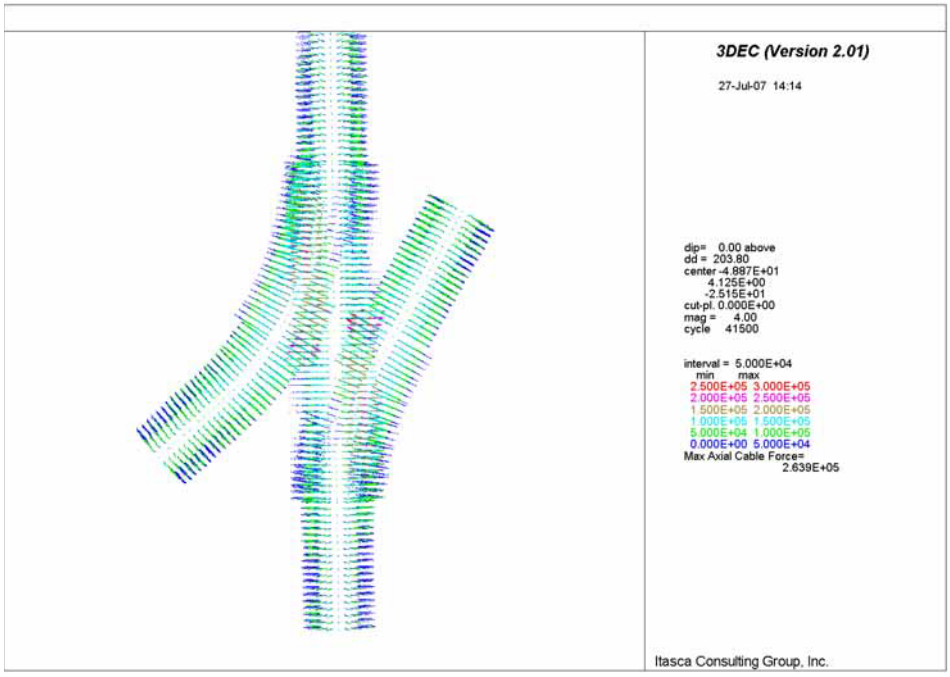

Figure 6-175 Plan View: Axial Forces (N) in Bolts along Access Main after Excavation of Both Turnouts

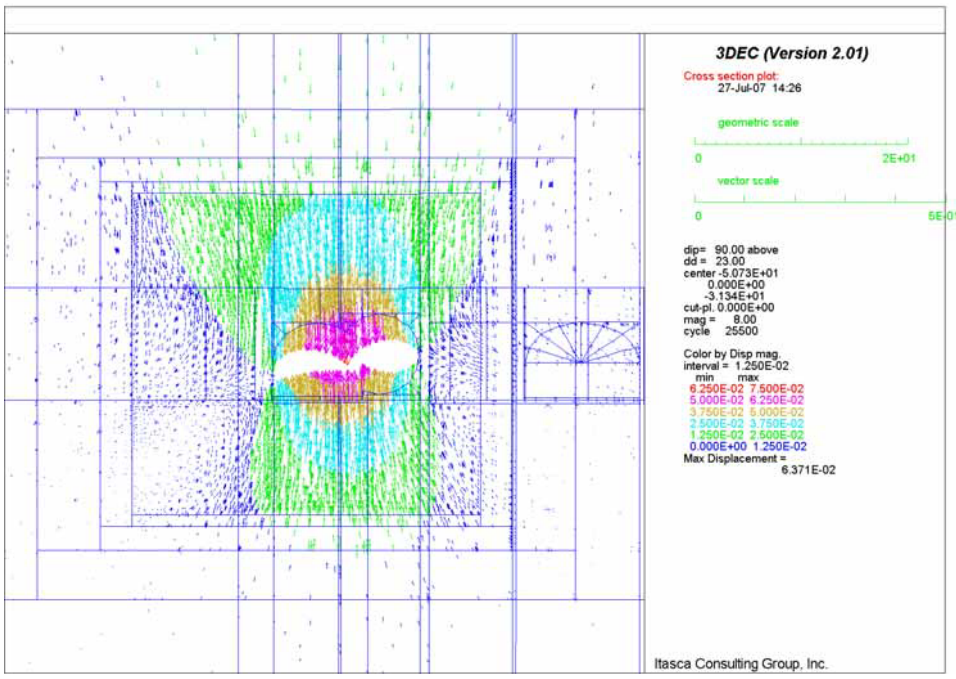

(a)

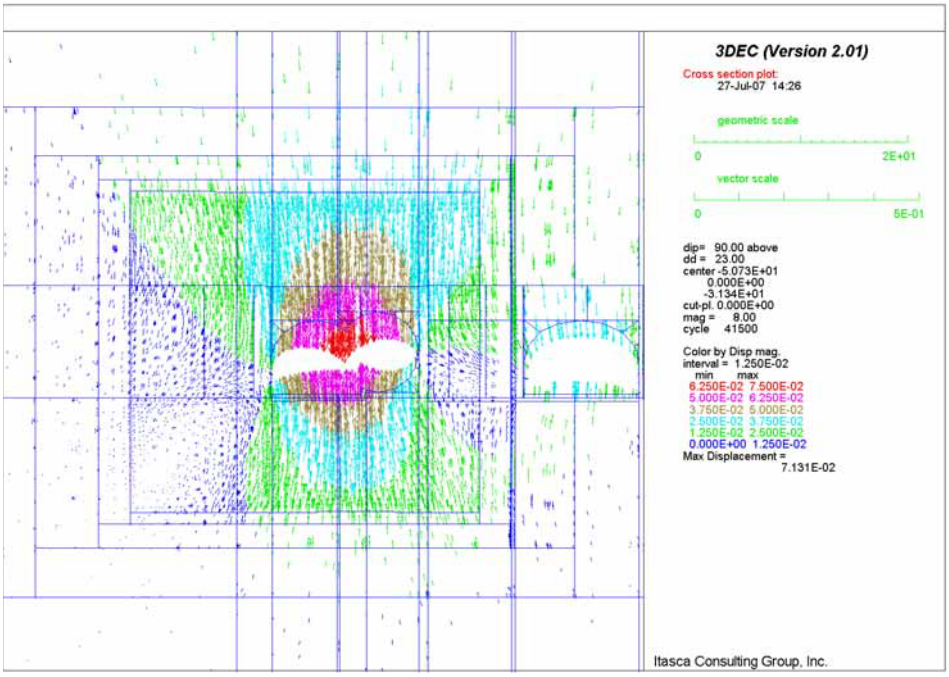

(b)

Figure 6-176 Displacement in Vertical Section 2 through First Intersection: a) before, b) after Excavation of Second Turnout

6.5.5.2.3 Intersections between Exhaust Mains and Emplacement Drifts

The ground support in the exhaust main is the same as the ground support used in the access main. The emplacement drifts will be supported by 3-m long Super Swellex rock bolts, at 1.25 m spacing, and Bernold-type perforated sheets (Reference 2.2.30, Section 6). The properties of the Super Swellex bolts used in the simulation of the ground support in the emplacement drift portion at the intersections between the exhaust main and the emplacement drifts are listed in Table 6-5. Bernold-type sheets were not included in the model. The ground support in the intersection (i.e., about 15-m length along the exhaust main and 5 m from the intersection into the emplacement drift) includes 5-m long rock bolts and 0.10-m thick steel-fiber reinforced shotcrete. Note that shotcrete was not applied inside the emplacement drift. The ground support analysis was carried out only for the intersection B, and using lithophysal rock mass category 1, as the most unfavorable conditions for the load in the ground support.

The loads in the bolts in the exhaust main after excavation of the exhaust main, looking along the exhaust main and in plan view, are shown in Figure 6-177 and Figure 6-178, respectively. With the exception of a few bolts affected by the local conditions, the maximum bolt force is around 150 kN. The forces in the bolts after excavation of both exhaust mains and the emplacement drifts are shown in Figure 6-179 through Figure 6-181. The maximum force increases to approximately 200 kN in the regions above the intersection. Those loads are within the limit of the elastic deformation of the bolts, which have yield strength of 264 kN, which gives a SF of 1.3. Note that the sign convention in 3DEC is that tensile force is positive.

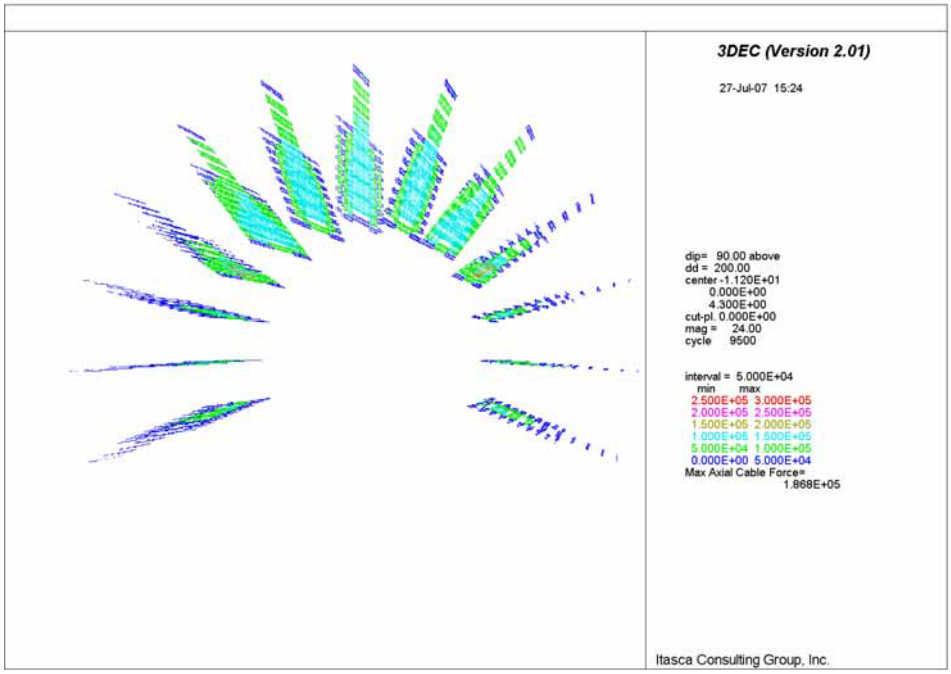

Figure 6-177 Axial Forces (N) in Bolts along Exhaust Main after Excavation

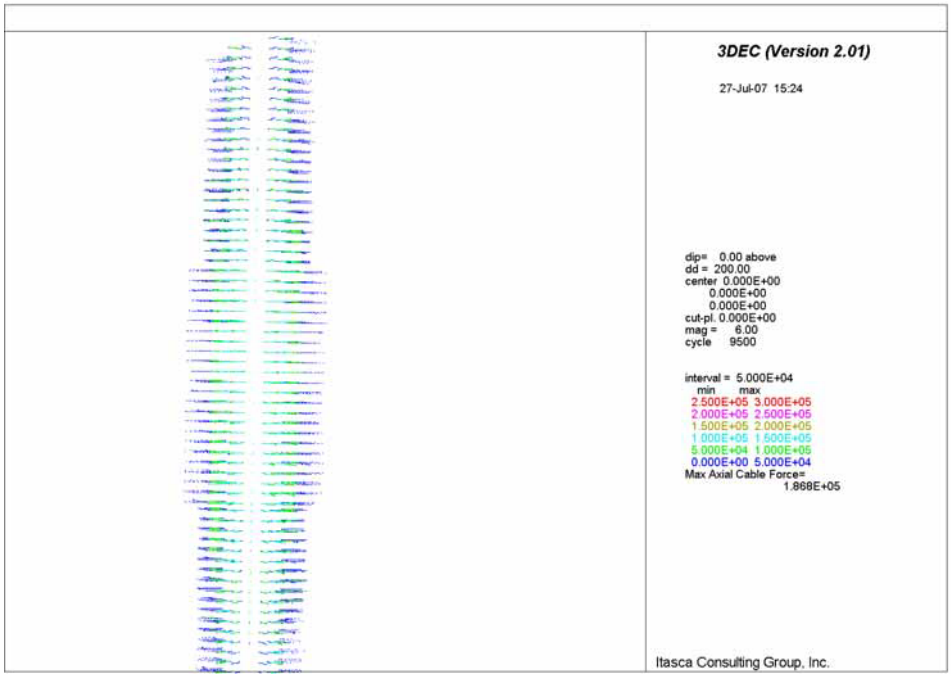

Figure 6-178 Plan View of Axial Forces (N) in Bolts along Exhaust Main after Excavation

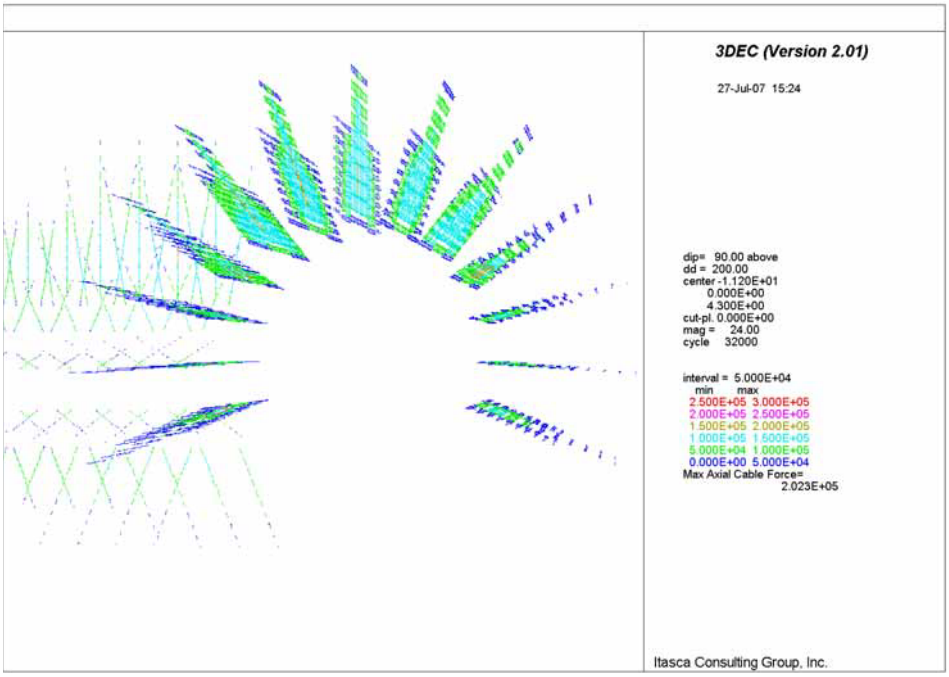

Figure 6-179 Axial Forces (N) in Bolts along Exhaust Main after Excavation of Exhaust Main and Emplacement Drift

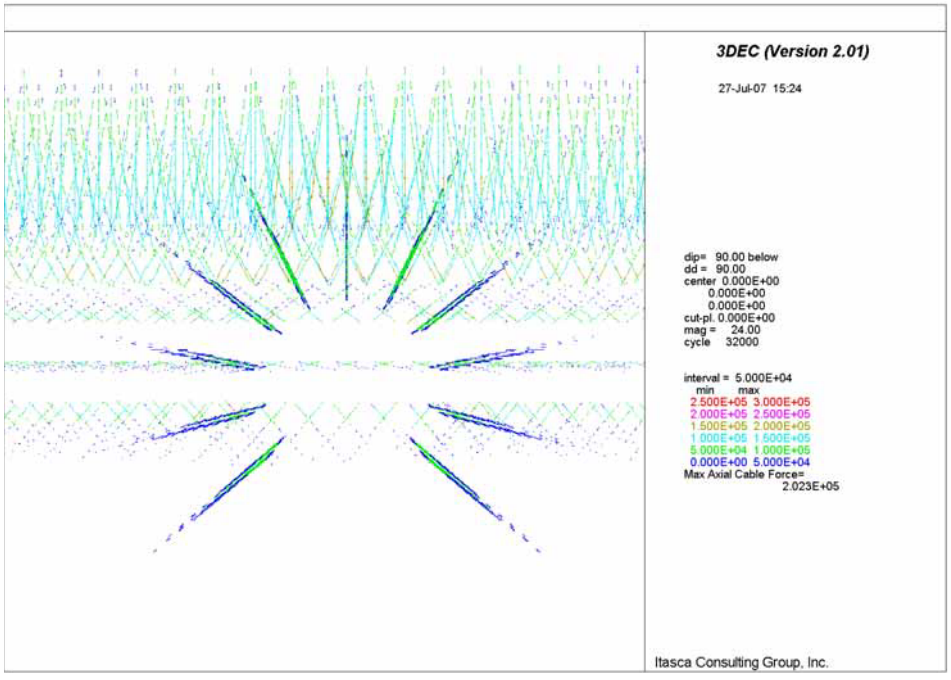

Figure 6-180 Axial Forces (N) in Bolts along Emplacement Drift after Excavation of Exhaust Main and Emplacement Drift

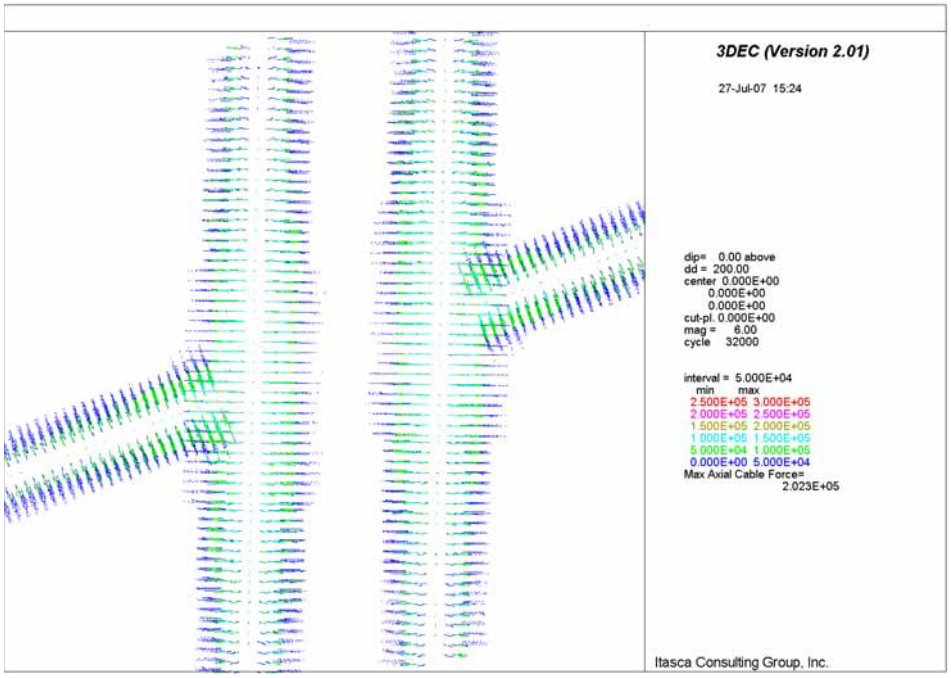

Figure 6-181 Plan View of Axial Forces (N) in Bolts along Exhaust Main after Excavation of Exhaust Main and Emplacement Drift

6.5.5.2.4 Observation Drift

The ground support for the observation drift and the intersection between the observation drift and the exhaust main is described in Section 6.5.4.1. The ground support will be used even though the numerical models show that the observation drift will be stable without any ground support (see Section 6.5.3.1.4). The used models are based on continuum theory and do not consider stability of the blocks created by joints in the walls and the crown of the drift. The used numerical models provide assessment of the global stability of the excavation. The designed ground support will prevent rockfall due to local instability.

The stability of the supported observation drift was numerically analyzed. The observation drift is planned to be excavated using the drill-and-blast method. Consequently, the ground relaxation due to excavation of the observation drift will be completed before the ground support inside the observation drift is installed.

Two different excavation sequences that have an effect on rockbolt loads were considered with regard to the sequence of drift excavation: in one case, the observation drift was excavated first; in the other, the emplacement drift was excavated first. The analysis has shown that the sequence of excavation has minor effect on the rockbolt forces. However, because the rockbolt forces are larger if the emplacement drift is excavated after excavation and support of the observation drift, the results in this section are presented for this case only.

The bolt forces after excavation of the emplacement drift ranging from 0.5 kN to 23 kN are shown in Figure 6-182. Note that the bolt forces in a two-dimensional model are presented per unit thickness of the model. The actual bolt forces can be obtained by multiplying values in the plot with spacing of the rows, which, in this case, is 1.25 m. These forces are insignificant considering the bolt yield strength of 264 kN.

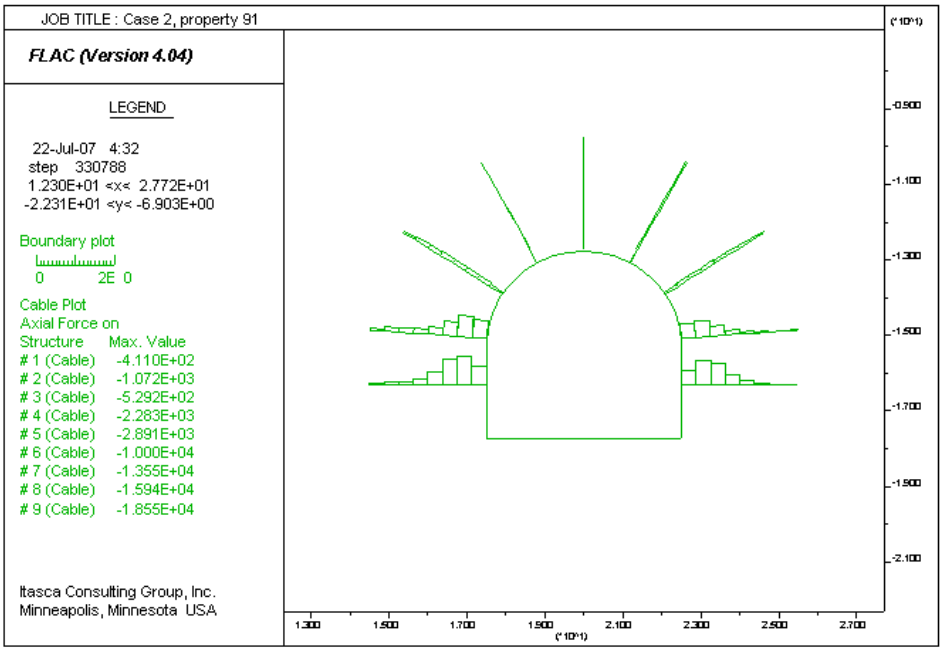

Figure 6-182 Bolt Forces (N) in Observation Drift after Excavation of Emplacement Drift

6.5.5.2.5 TBM Launch Chamber

The ground support system in the TBM launch chamber includes 3-m long grouted rockbolts and heavy-duty wire mesh. Only the grouted rockbolts are included in the numerical model. The analysis was carried out for the seismic load induced by the seismic event with a 2,000-yr return period. It is considered that the rockbolts will not take any load due to rock mass deformation caused by the relaxation of in situ stresses, as the TBM launch chamber will be excavated using the drill-and-blast method.

6.5.5.2.6 North Portal

Although it is demonstrated that the North Portal and the starter tunnel are stable under static and dynamic loading conditions, both excavations will be supported. The objective of the ground support is to prevent local instability.

For the North Portal modeling, shotcrete and rockbolt reinforcement have been considered (see Figure 6-183). Three different regions, denoted as a) Lateral surfaces, b) Frontal surface and c) Tunnel surface, can be distinguished in Figure 6-183.

The ground support is installed after complete relaxation of the in situ stresses due to excavation of the North Portal and the starter tunnel. Consequently, the ground support does not take any load under static conditions.

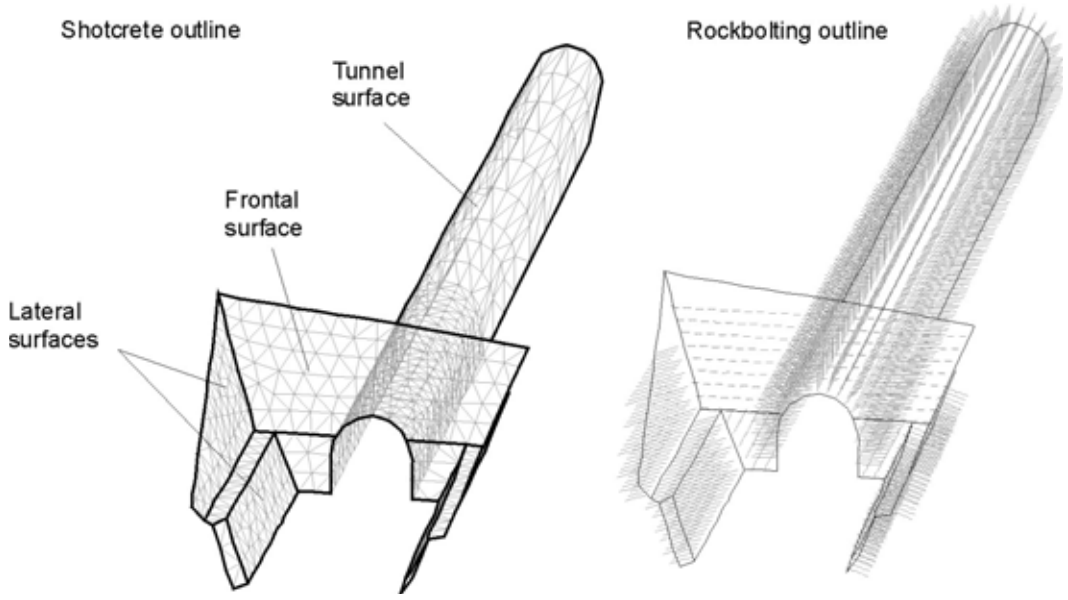

Figure 6-183 Isometric View of Shotcrete and Rockbolts in North Portal Model

6.5.5.3 Thermal Loading Condition

The thermal loading condition for supported non-emplacement drifts is only applied to intersections between exhaust mains and emplacement drifts, exhaust mains, observation drift, and intersection of observation drift with exhaust main.

6.5.5.3.1 Exhaust Mains and Observation Drift

Figure 6-184 shows the time histories of axial forces in fully grouted rock bolts for supported exhaust mains under in situ and thermal loading conditions in lithophysal and nonlithophysal category 1 rock units.

The results indicate that axial forces in the bolts are sensitive to the rock mass modulus. As can be seen from Figure 6-184, the bolts will be in tension throughout the operational time of 50 years for all cases except bolts near springline in the nonlithophysal rock. It should be noted that nonlithophysal category 1 rock is stronger than that of the lithophysal rock. For strong ground conditions, such as the nonlithophysal rock in this case, the bolts will be in tension when subjected to in situ load, and become in compression when the rock is heated up. In general, heating in rock is expected to reduce the tensile forces in bolts.

The maximum axial forces in the fully grouted bolts are predicted to be about 105 kN in tension for category 1 lithophysal rock and from about 10 kN in tension and about 26 kN in compression for nonlithophysal category 1 rock. These give a minimum factor of safety of 2.5 (264/105=2.5) (see Table 6-3).

Distributions of axial forces in fully grouted bolts are presented in Figure 6-185 and Figure 6-186 for lithophysal and nonlithophysal category 1 rocks, respectively. These forces are not uniformly distributed, and higher near the crown than near the springline. Under heating, some bolts in the nonlithophysal rock, especially near the springline, experience tension close to the drift surface and compression away from the surface. Comparing the axial forces under in situ loading condition (year=0) to those under combined in situ and thermal conditions (year=50), the maximum values in bolts are reduced, and change from negative (in tension) to positive (in compression) for bolts near springline in the nonlithophysal rock. It should be noted that the actual loads in bolts illustrated in Figure 6-185 and Figure 6-186 are equal to those shown in the figures times the bolt spacing of 1.25 m.

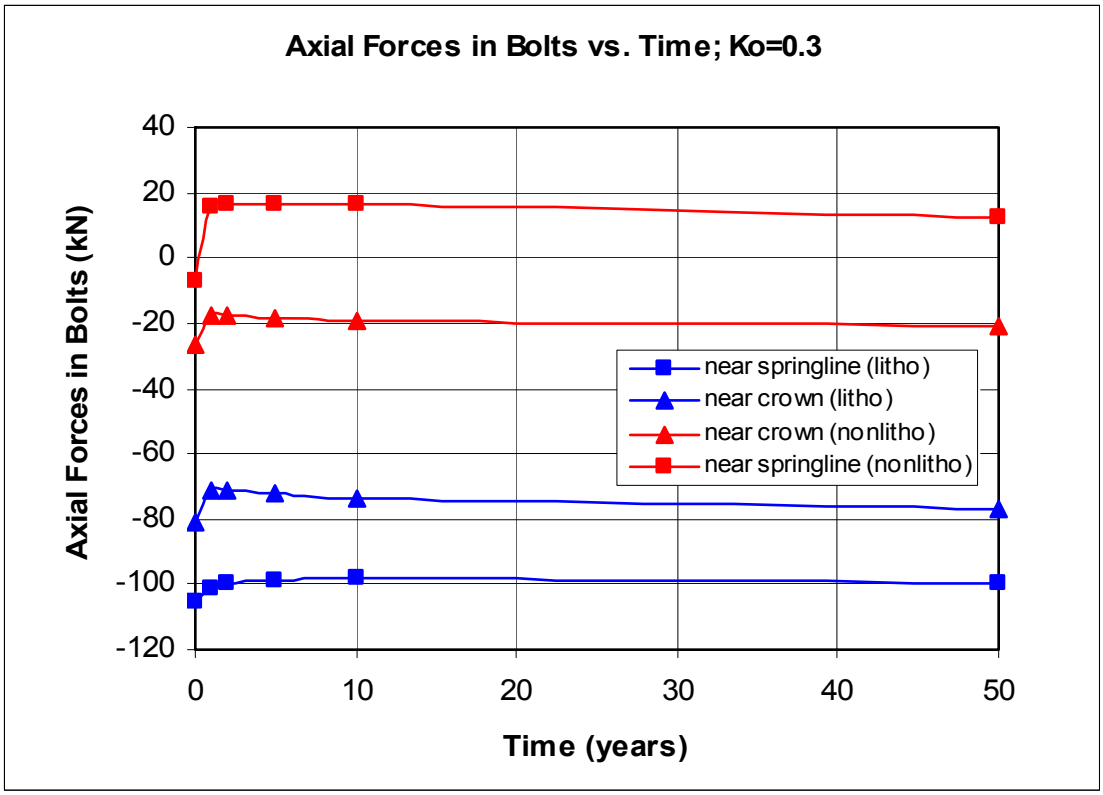

Figure 6-184 Axial Forces in Bolts Installed in Exhaust Mains in Lithophysal and Nonlithophysal Rock under In Situ and Thermal Loads and Ko=0.3.

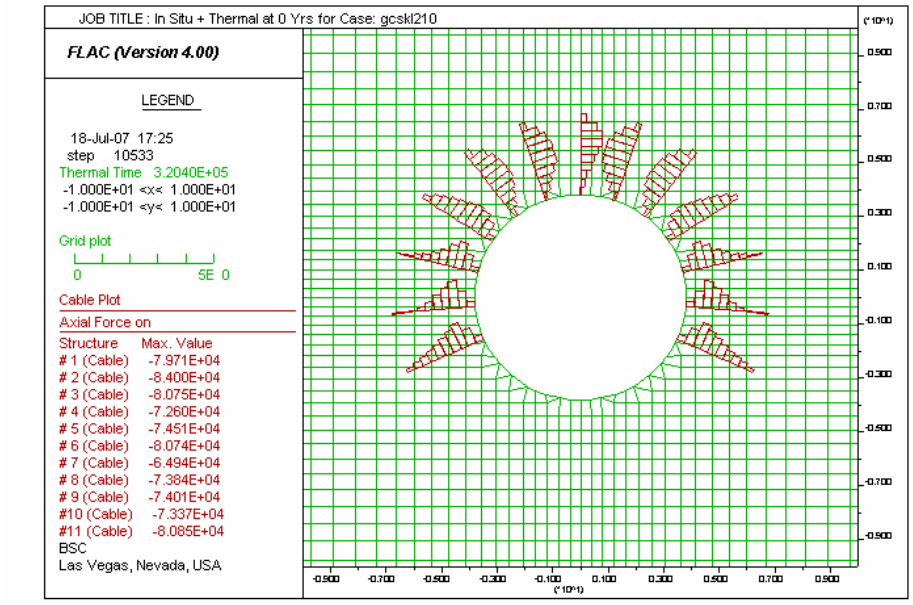

(a)

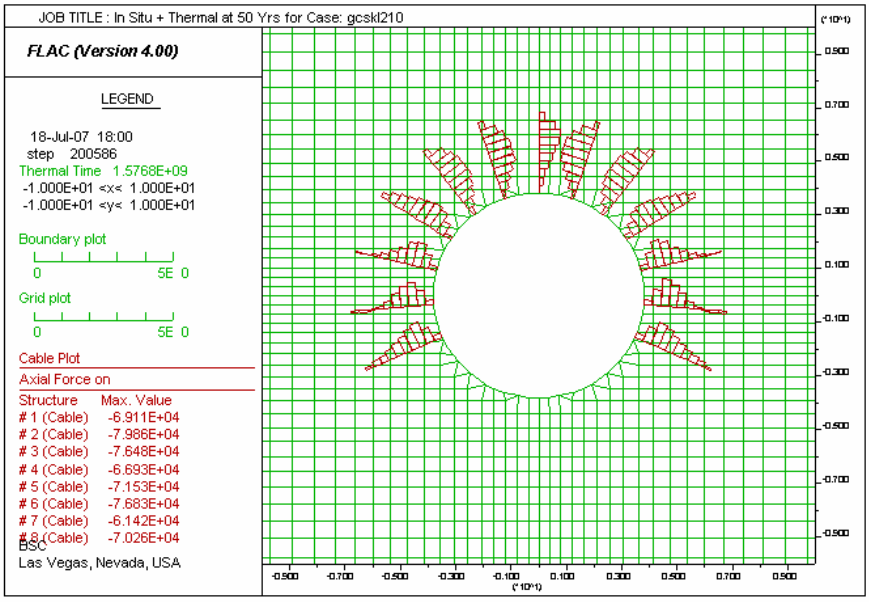

(b)

Figure 6-185 Distribution of Axial Forces (N) in Bolts Installed in Exhaust Mains in Lithophysal Rock under In Situ and Thermal Loads and Ko=0.3 at (a) Year 0; (b) Year 50.

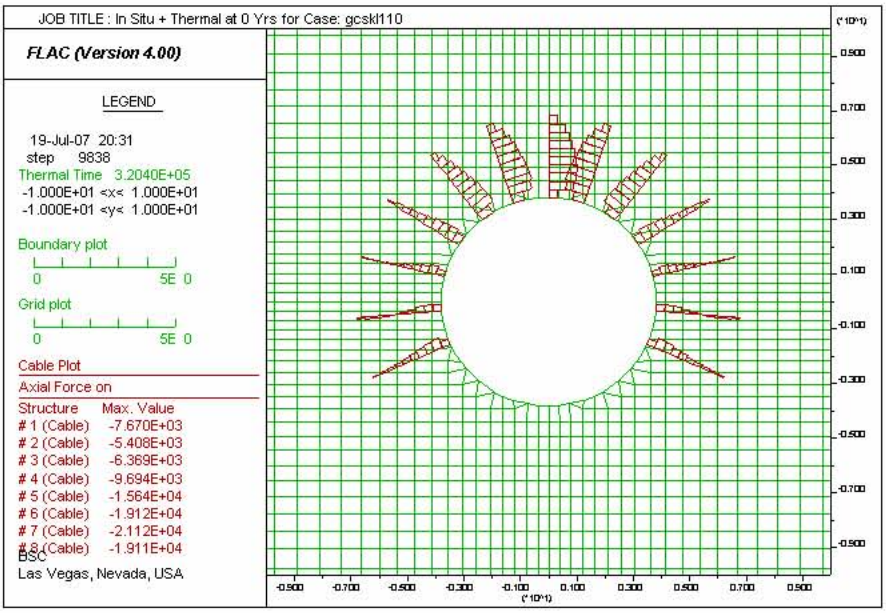

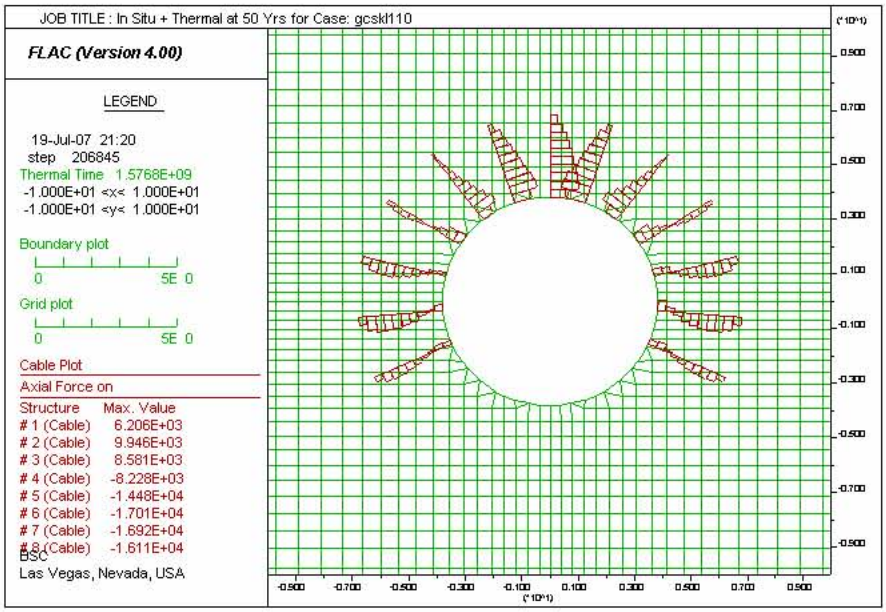

Figure 6-186 Distribution of Axial Forces (N) in Bolts Installed in Exhaust Mains in Nonlithophysal Rock under In Situ and Thermal Loads and Ko=0.3 at (a) Year 0; (b) Year 50

6.5.5.3.2 Intersections between Exhaust Mains and Emplacement Drifts

The axial forces in the bolts after 5 and 50 years of heating are shown in Figure 6-187 and Figure 6-188. Figure 6-189 shows the plan view of bolt forces after 50 years of heating. The predicted maximum force in the rock bolts is about 200 kN , at a SF of about 1.3, occurs after about 5 years of heating. The maximum force is about the same as the maximum force due to in situ loading (see Section 6.5.5.2.3) except that more bolts experience axial tension due to the thermal effects.

6.5.5.3.3 Intersection between Observation Drift and Exhaust Main

Thermal load causes an increase in bolt forces, as indicated in Figure 6-190, which shows the bolt forces after 50 years of heating (comparing with Figure 6-182). After 50 years of heating, the loads are well within the range of elastic deformation of the rockbolts. Figure 6-191 shows the extent of inelastic deformation predicted around the observation drift. The designed bolt length of 3 m appears to be sufficient to provide anchoring into the elastic (undamaged) rock.

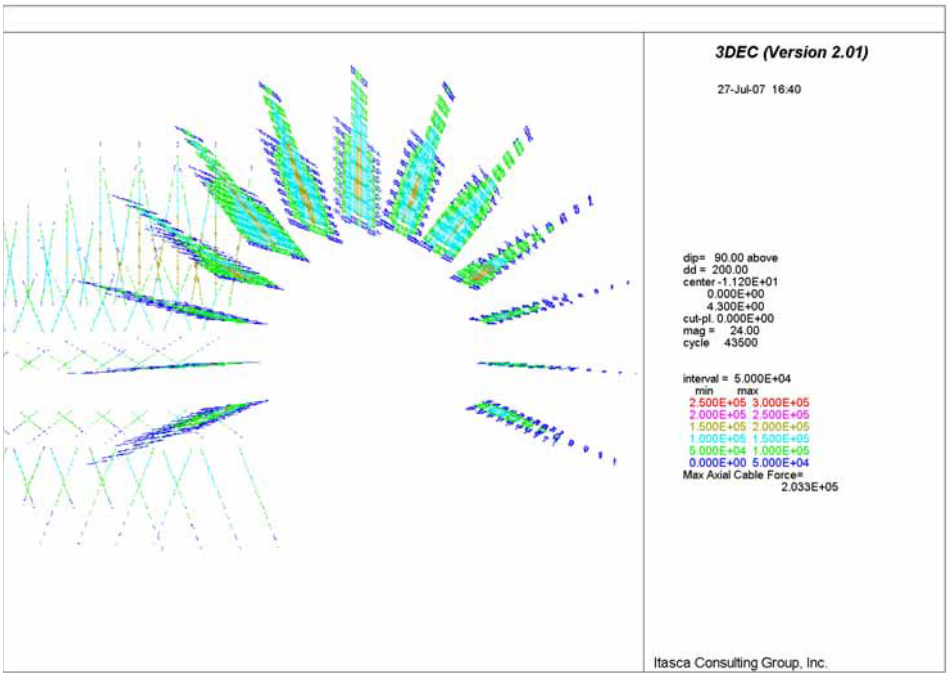

Figure 6-187 Intersection B: Forces (N) in Bolts along Exhaust Main after 5 Years of Heating

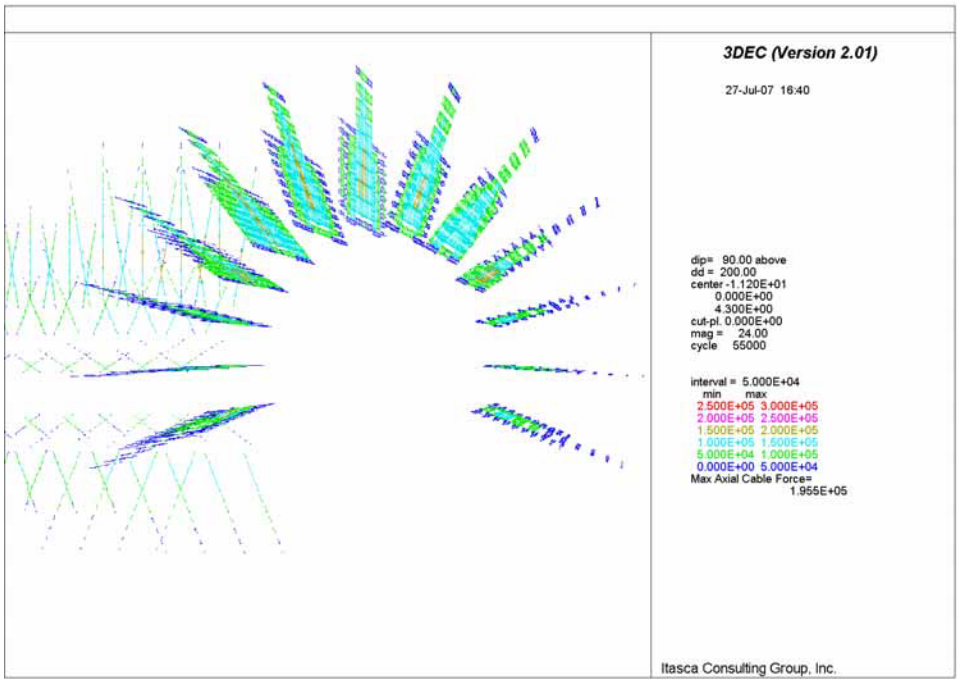

Figure 6-188 Intersection B: Forces (N) in Bolts along Exhaust Main after 50 Years of Heating

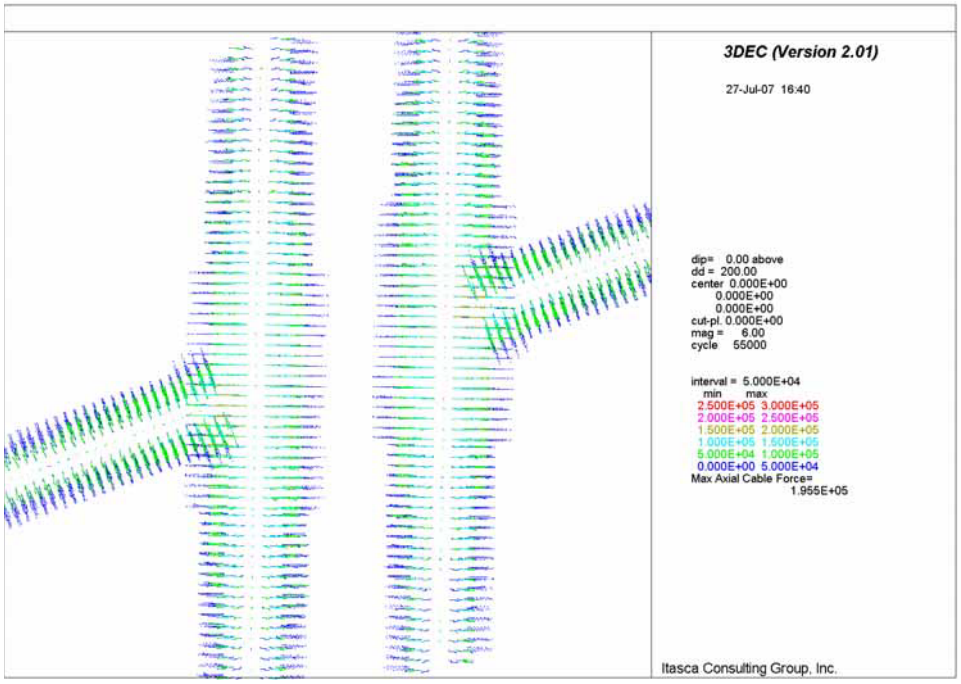

Figure 6-189 Plan view of Forces (N) in Bolts along Exhaust Main after 50 Years of Heating

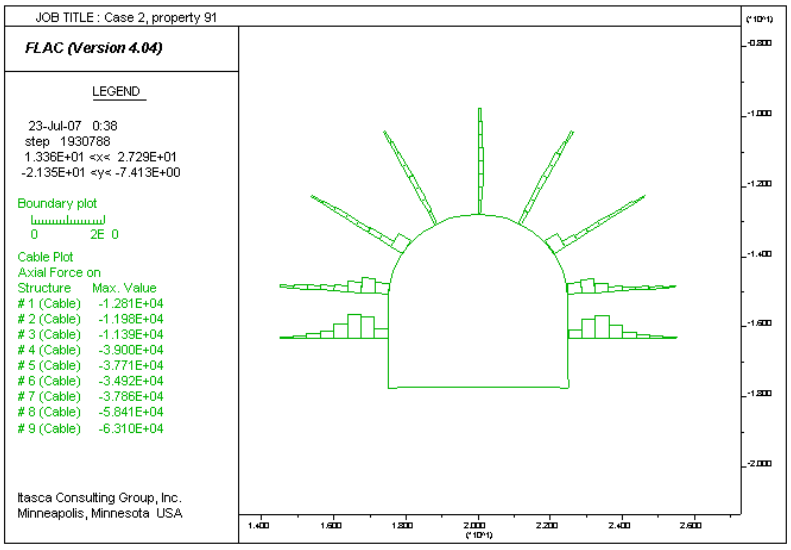

Figure 6-190 Bolt Forces (N) in Observation Drift after 50 Years of Heating

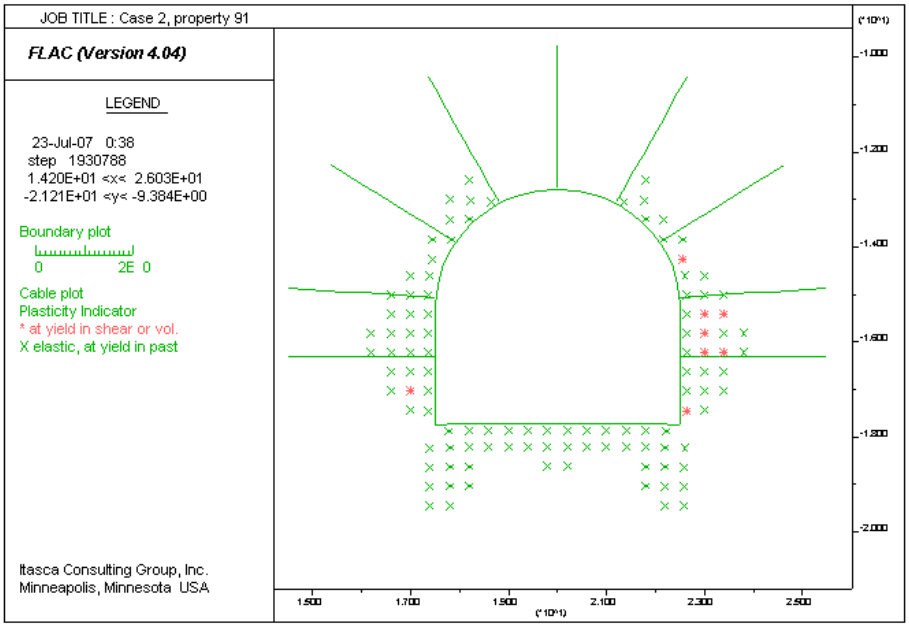

Figure 6-191 Potential Yield Zone around Observation Drift after 50 Years of Heating

6.5.5.4 Seismic Loading Condition

6.5.5.4.1 Access and Exhaust Mains and Turnouts

The stability condition of supported turnouts due to seismic loading are presented in this section. The bolt forces in Access Mains and Exhaust Mains due to seismic loading are discussed in the subsequent sections.

The bolt forces in turnouts under seismic loading are shown in Figure 6-192. The extent of the potential yield zone around the turnouts after seismic shaking is shown in Figure 6-193. The maximum bolt force due to seismic shaking is 104.2 kN (1.25m × 83.37 kN/m), much less than the bolt yield strength of 264 kN.

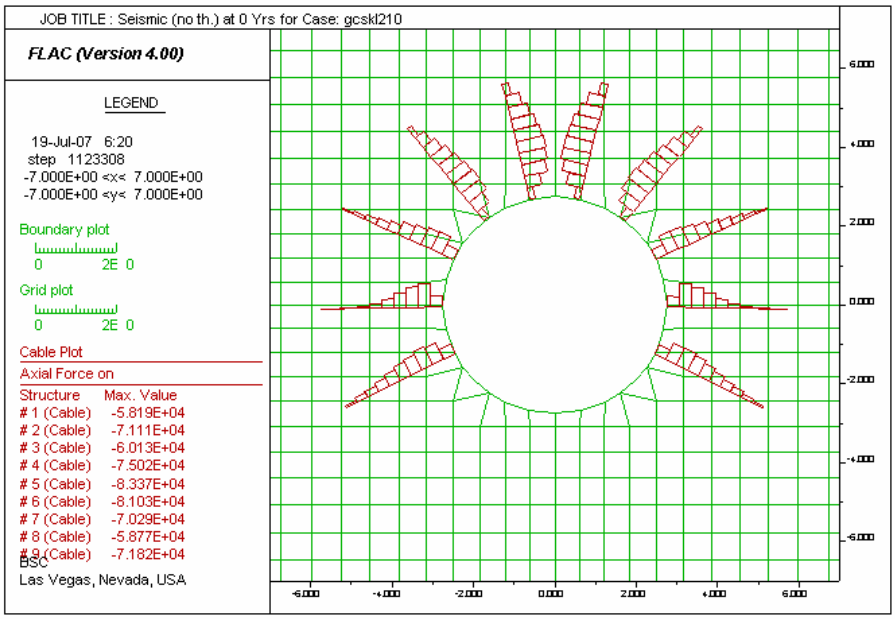

Figure 6-192 Axial Forces (N) in Bolts Installed in Turnouts in Lith. Cat. 1 Rock under Seismic Load

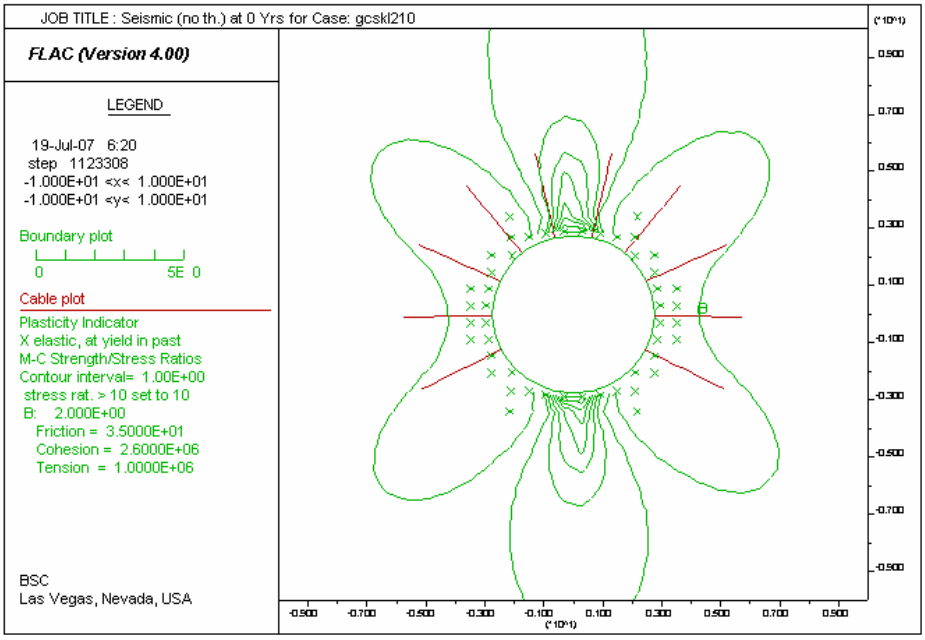

Figure 6-193 Contours of SF around Supported Turnout for Lith. Cat. 1 Rock under Seismic Load

6.5.5.4.2 Intersections between Access Mains and Turnouts

The intersection between Access Mains and Turnouts supported with rock bolts and shotcrete is simulated for dynamic loading due to earthquake with a 2,000-year return period. The shotcrete is represented in the model with shell elements, which can take axial and bending forces. The shell elements are generated to coincide with triangular faces of zones exposed on the walls of the excavations. The geometry of the shotcrete support is shown in the plan view in Figure 6-194 (together with the bolts), and in the view along the access main in Figure 6-195. Prior to seismic loading, the shotcrete carries no load; the forces in the bolts are as described in Section 6.5.5.2.2.

The unsupported intersection is stable after earthquake with a 2,000-year return period even using the category 1 lithophysal rock mass, the poorest quality rock mass (see Section 6.5.3.1.2). The increase in the permanent displacement is insignificant. Consequently, the residual load increase in the ground support after the seismic event predicted by this model is small. Figure 6-196, Figure 6-197 and Figure 6-198 show bolt forces along access mains before shaking, during shaking and at the end of shaking, respectively. The maximum transient bolt force increase to the yield level (264 kN) during seismic shaking. Knowing that steel is quite ductile (it can undergo substantial strain after yield before it breaks), it is not expected that earthquake with a 2,000-year return period will cause significant damage of the rockbolts in the intersections, even in the poorest quality rock mass (i.e., category 1, lithophysal rock mass). Note that in Figure 6-197 and Figure 6-198 several bolts, pulled out during the dynamic simulation, shown inside the access main, are yielding (indicated maximum force of 264 kN). These bolts are consequence of a local effect. All other bolts in the model behave elastically, with the maximum force less than 250 kN, i.e., a SF greater than 1.06. Majority of the bolts have maximum force less than 200 kN which corresponds to SF of 1.3.

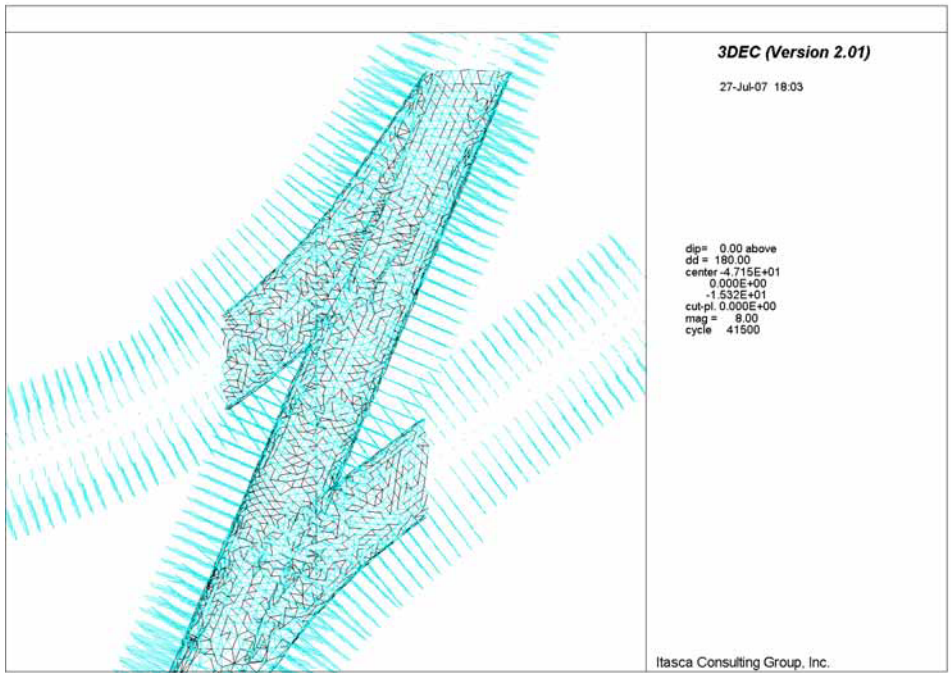

Figure 6-194 Plan View of Rock Bolts and Shotcrete at Intersection of Access Main and Turnout

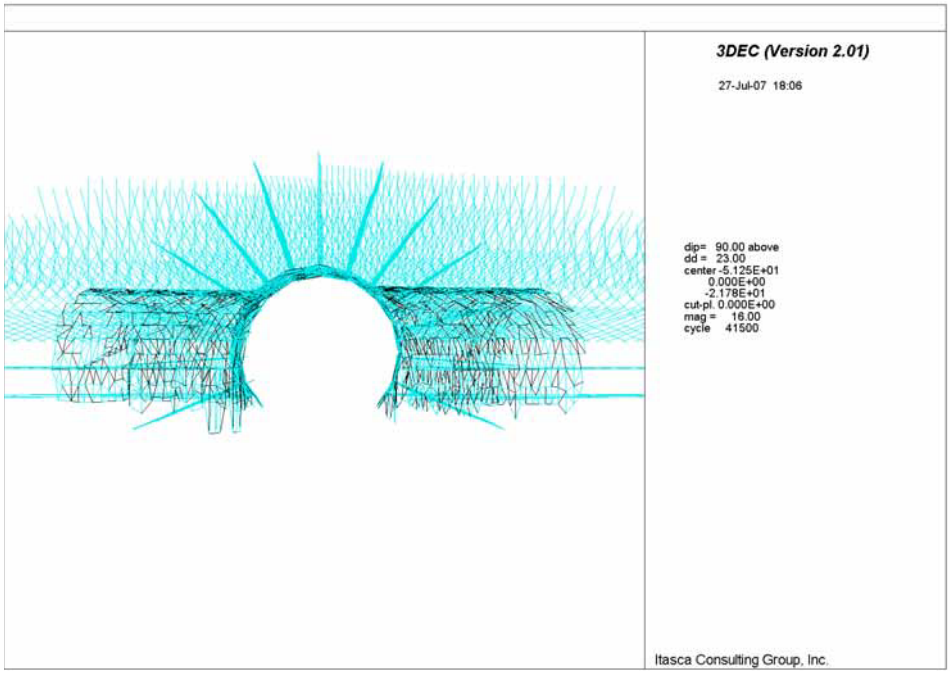

Figure 6-195 Perspective View along Access Main showing Geometry of Shotcrete

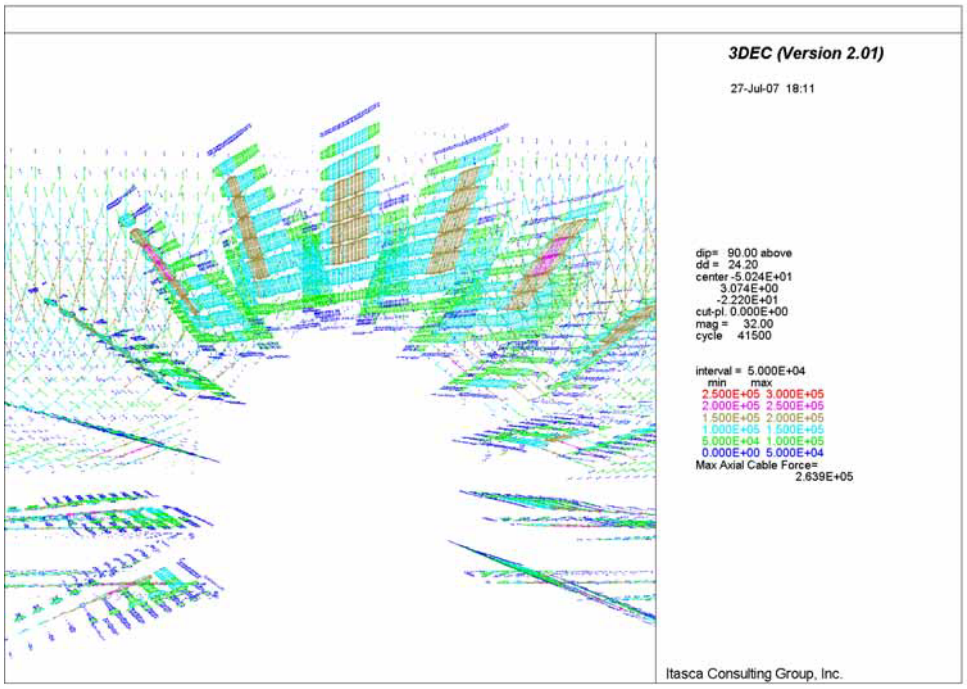

Figure 6-196 Axial Forces (N) in Bolts along Access Main before Seismic Shaking

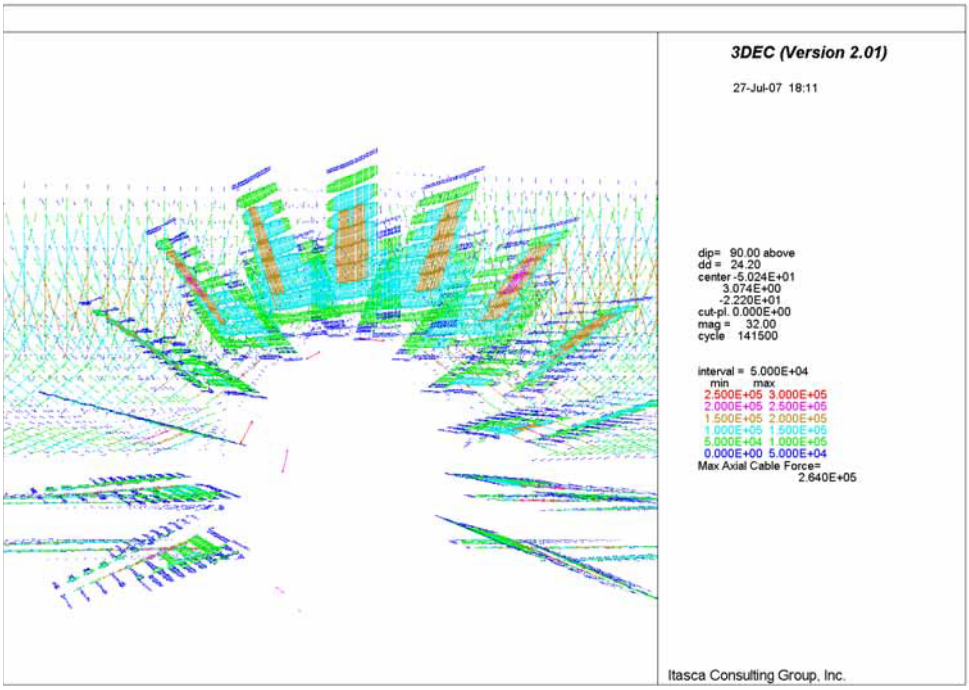

Figure 6-197 Axial Forces (N) in Bolts along Access Main after 14 seconds of Seismic Shaking

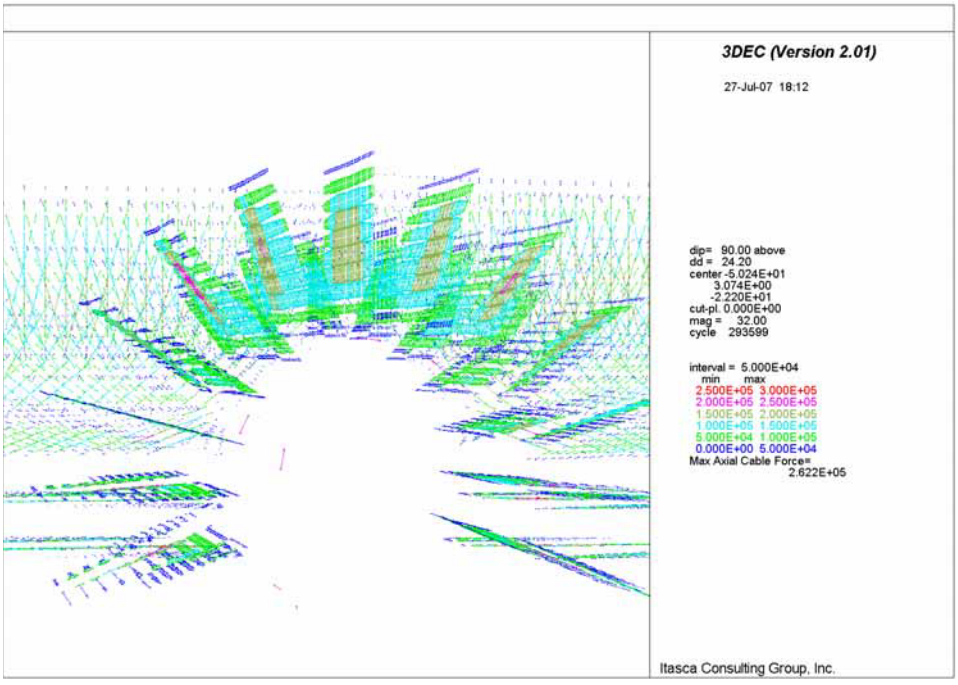

Figure 6-198 Axial Forces (N) in Bolts along Access Main at End of Seismic Shaking

6.5.5.4.3 Intersections between Exhaust Mains and Emplacement Drifts

For stability analysis of supported openings in intersections between exhaust mains and emplacement drifts, the maximum bolt forces, at the end of dynamic loading caused by ground motion with 2,000 year return period (applied after drift excavation and after heating of 50 years), are shown in Figure 6-199. The maximum increase in bolt forces compared to the static condition (in situ and thermal) is approximately 3 kN in the region above the intersection, resulting in a maximum bolt force of about 198 kN (comparing Figure 6-199 to Figure 6-188) with a SF of 1.33.

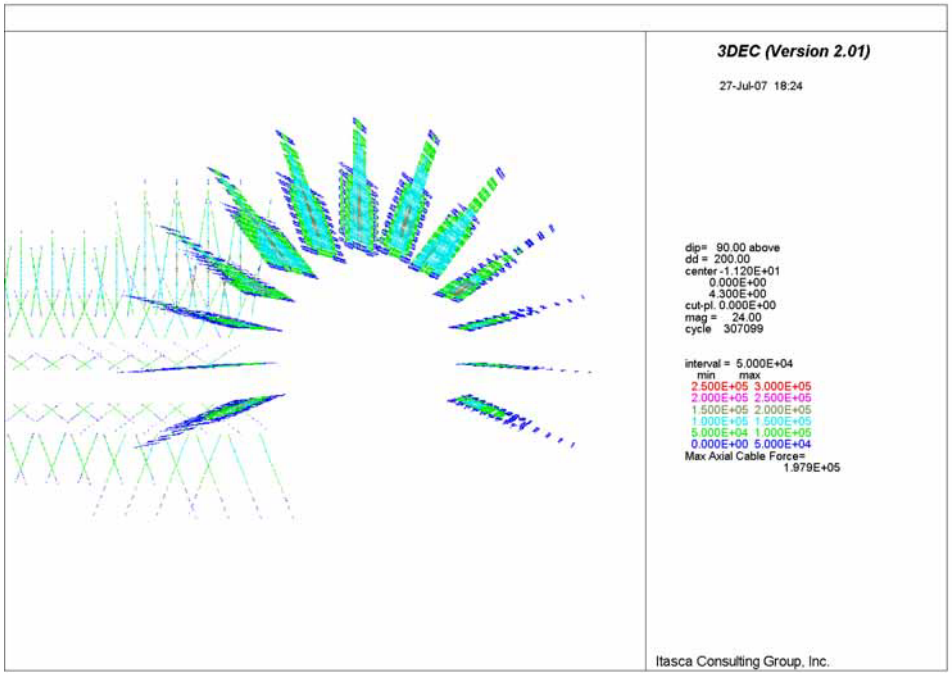

Figure 6-199 Forces (N) in Bolts along Exhaust Main at the end of Seismic Shaking

6.5.5.4.4 Observation Drift

The bolt forces in observation drift at the end of seismic shaking are shown in Figure 6-200. The extent of the potential yield zone around the observation drift after seismic shaking is shown in Figure 6-201. The maximum bolt force at the end of seismic shaking is 106.2 kN (1.25m × 84.99 kN/m), much less than the bolt yield strength of 264 kN.

The ground support in the intersection between observation drift and exhaust main was analyzed using a three-dimensional model. The predicted bolt forces after 50 years of heating and after seismic ground shaking are shown in different views in Figure 6-202 to Figure 6-206. The forces in the rockbolts installed in the exhaust main at the intersection with the observation drift are approximately 41 kN after seismic loading and thermal loading of 50 years. These loads are smaller than those predicted by the forces in the rockbolts at the intersection between the exhaust main and the emplacement drift (see Section 6.5.5.4.3). In the same time, the forces in the rockbolts in the observation drift in the intersection are quite small, less than 25 kN.

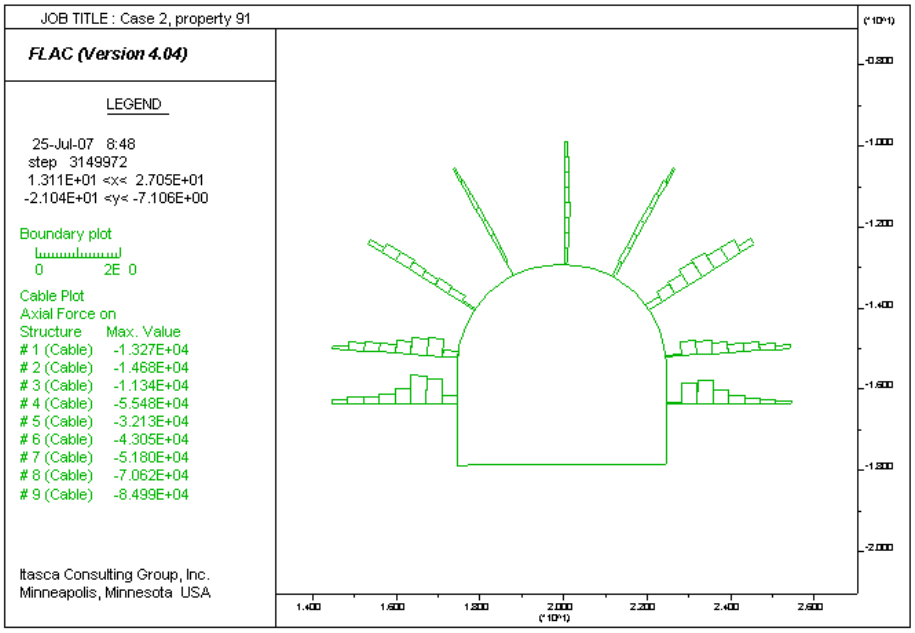

Figure 6-200 Bolt Forces (N) in Observation Drift after Seismic Shaking

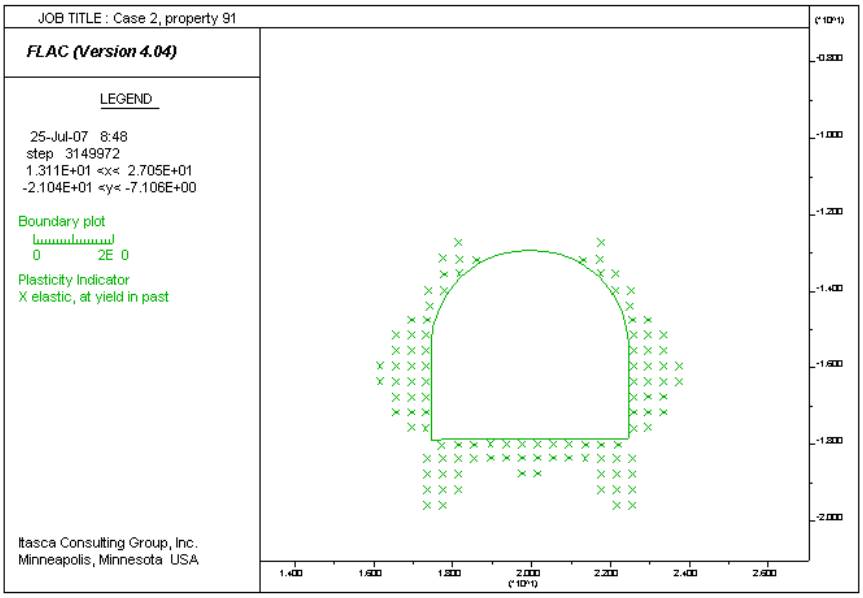

Figure 6-201 Potential Yield Zone around Observation Drift after Seismic Shaking

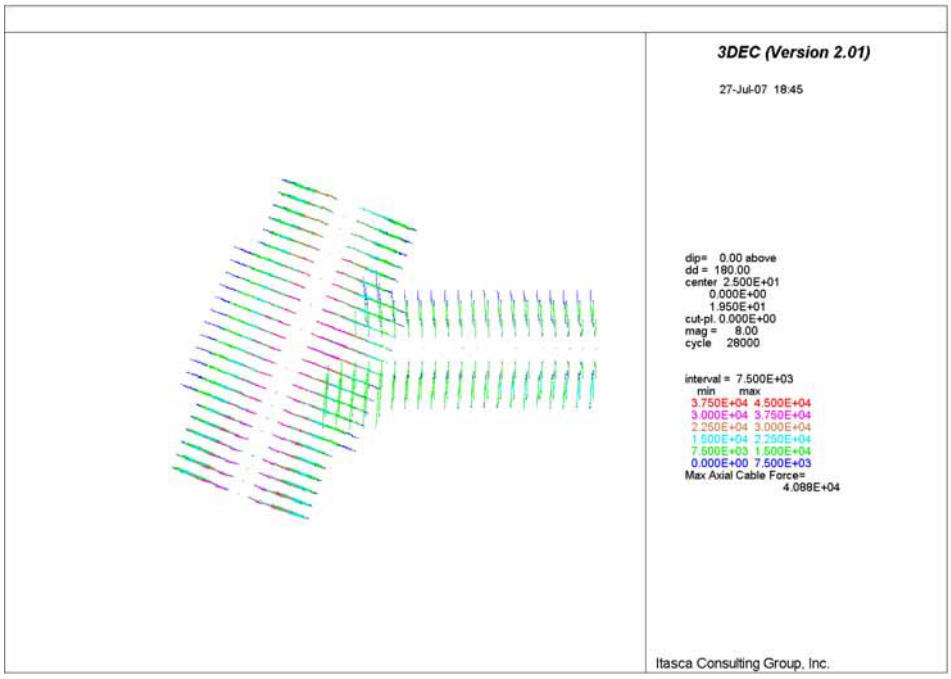

Figure 6-202 Plan View of Bolt Forces (N) in Intersection between Observation Drift and Exhaust Main after 50 Years of Heating

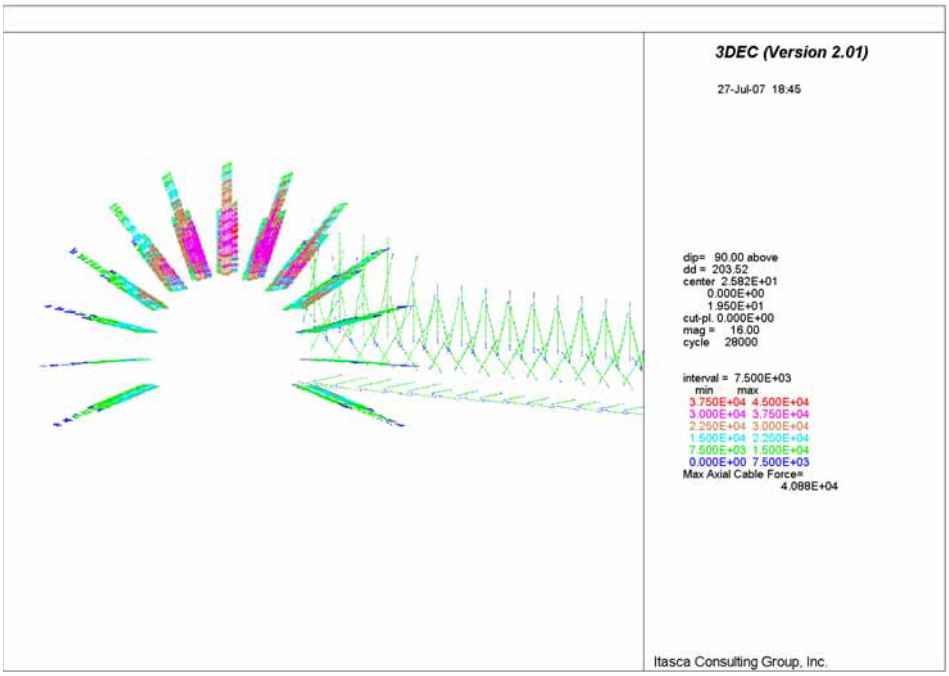

Figure 6-203 Bolt Forces (N) in Intersection between Observation Drift and Exhaust Main after 50 Years of Heating and Seismic Shaking – View along Exhaust Main

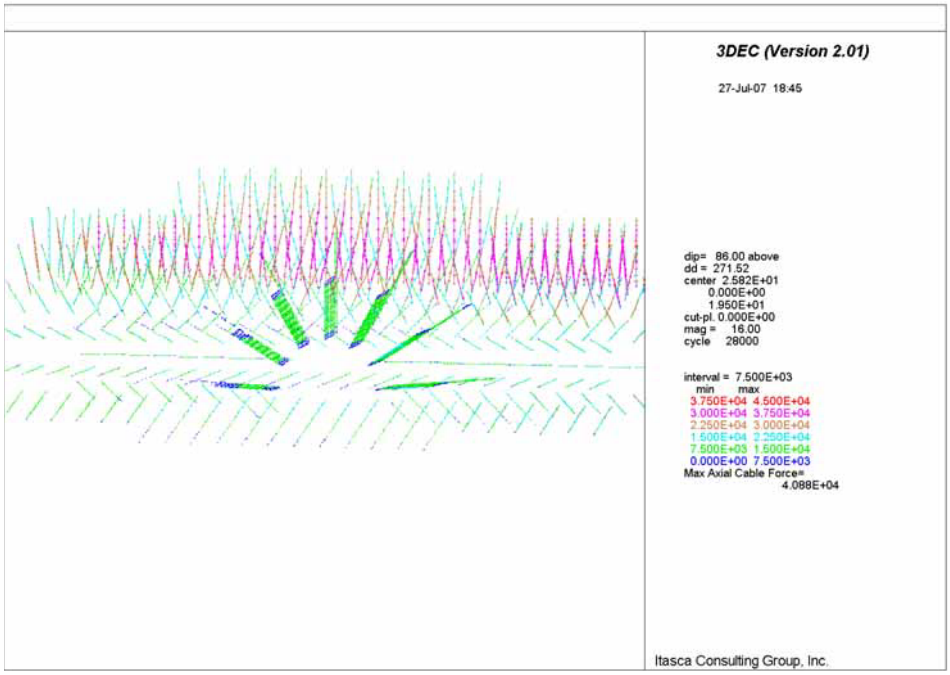

Figure 6-204 Bolt Forces (N) in Intersection between Observation Drift and Exhaust Main after 50 Years of Heating and Seismic Shaking – View along Observation Drift

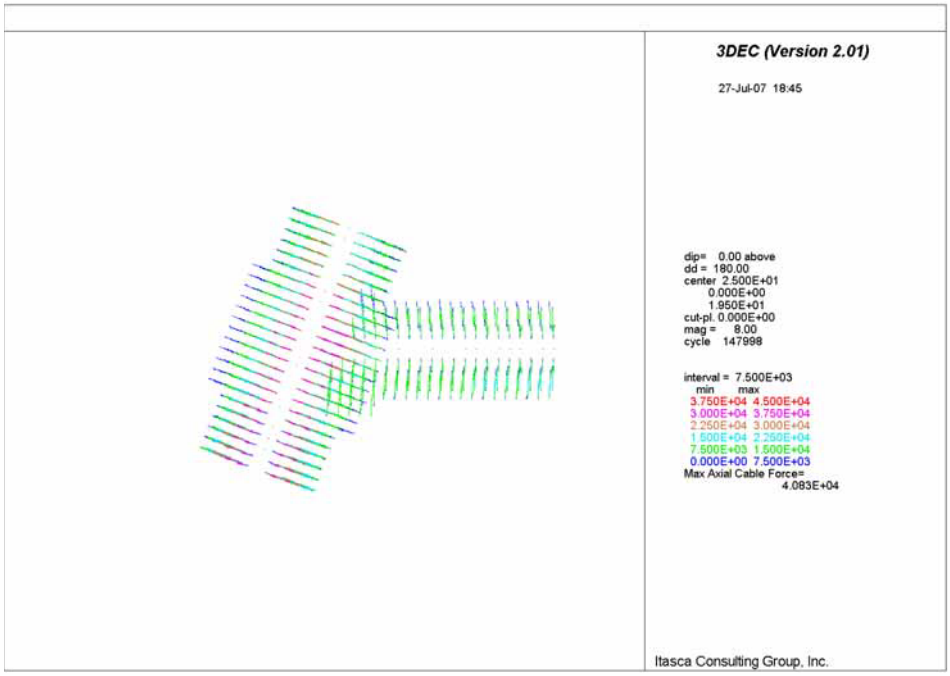

Figure 6-205 Plan View of Bolt Forces (N) in Intersection between Observation Drift and Exhaust Main after 15 Seconds of Seismic Shaking

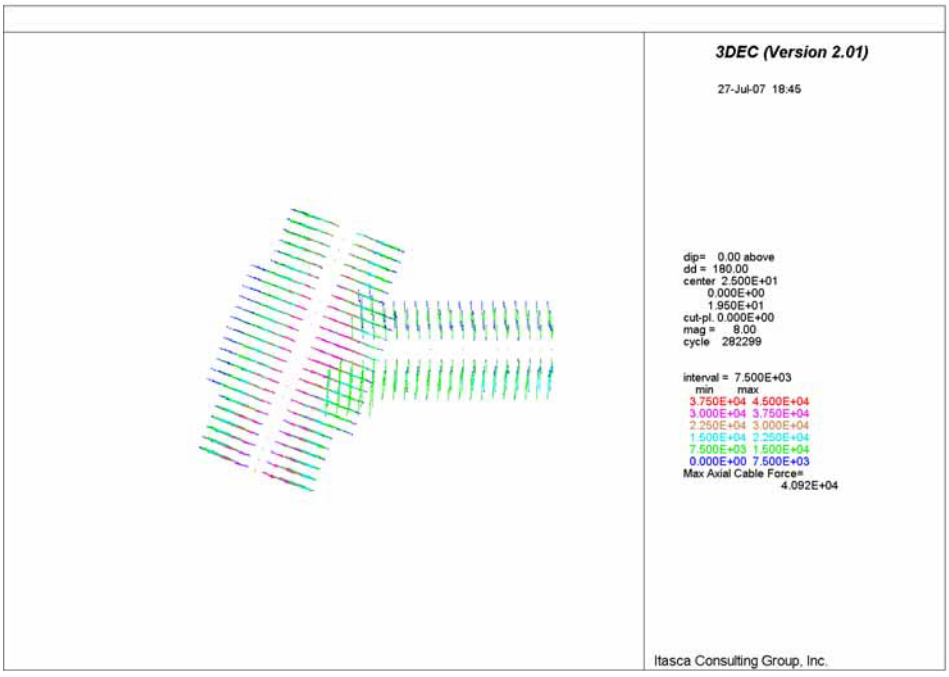

Figure 6-206 Plan View of Bolt Forces (N) in Intersection between Observation Drift and Exhaust Main at End of Seismic Shaking

6.5.5.4.5 TBM Launch Chamber

The forces in the rockbolts at the end of dynamic simulation, shown in Figure 6-207, are small relative to the yield strength of the rockbolts. Note that the values indicated in the figure need to be multiplied by the 1.25-m spacing of the bolt rows to obtain the forces in the bolts. Figure 6-208 indicates that the forces in the bolts installed in the wall (in the region of the largest damage of the rock mass) have a residual component in addition to transient oscillation after seismic loading. Figure 6-209 shows the potential yield zone around TBM launch chamber. It is predicted that no potential yield zones are developed in the crown but with most potential yield zones adjacent to the walls and to the floor. Note that the maximum axial forces in bolts at the end of dynamic simulation is about 36 kN (28.62 x 1.25 = 36, see Figure 6-207), which is much less than the yield strength of the bolts, i.e., 264 kN.

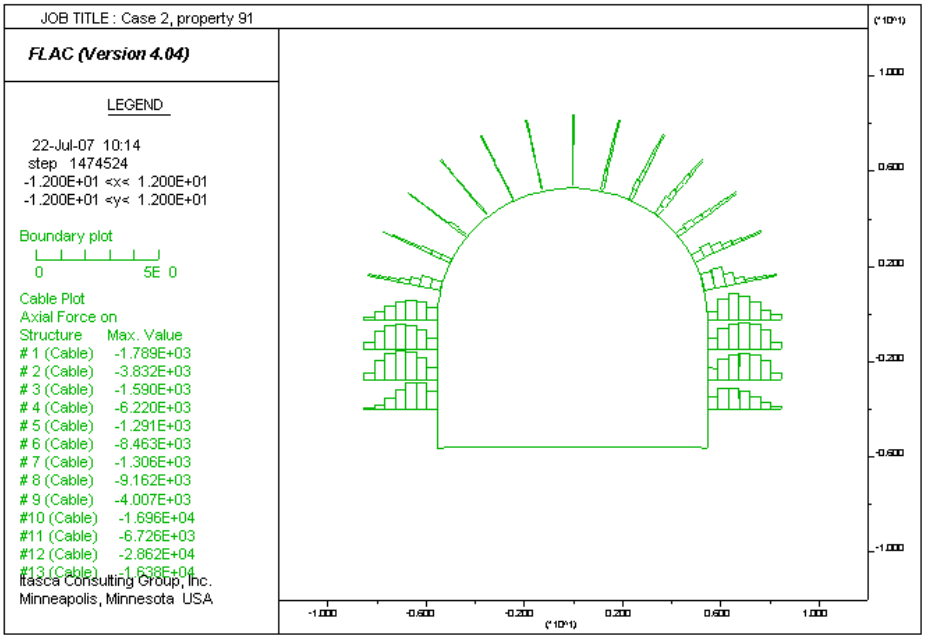

Figure 6-207 Bolt Forces (N) in TBM Launch Chamber after Seismic Shaking

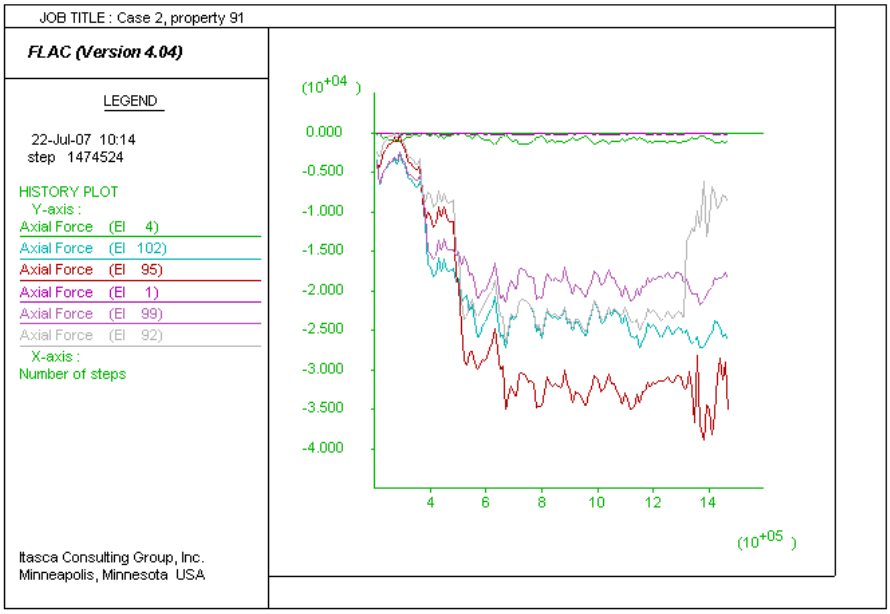

Figure 6-208 Histories of Forces (N) in Three Bolts in TBM Launch Chamber during Seismic Shaking

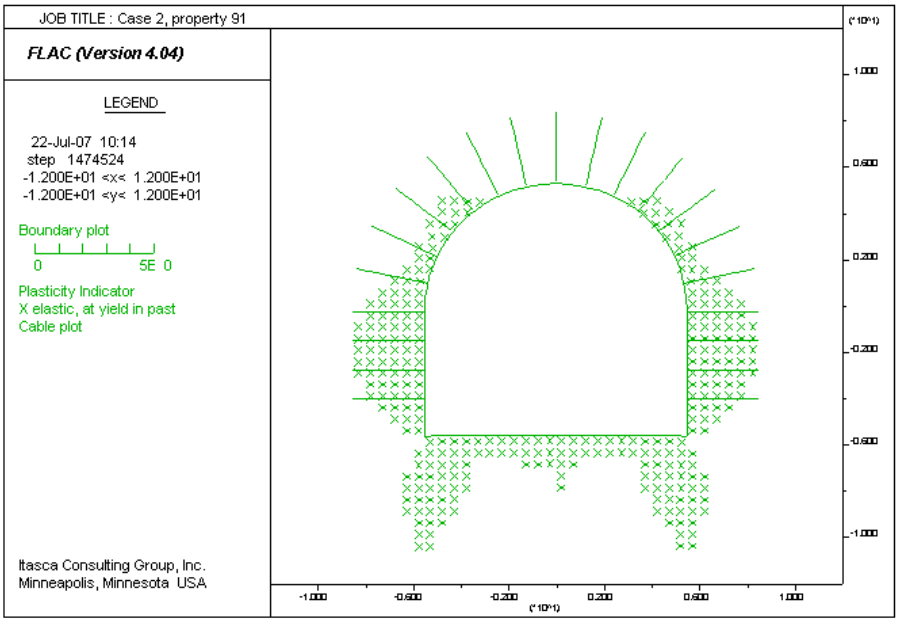

Figure 6-209 Potential Yield Zone around TBM Launch Chamber after Seismic Shaking

6.6 SENSITIVITY STUDY ON DRIFT STABILITY UNDER SEISMIC EVENT WITH APE OF 10^{-4}

The stability of non-emplacement drifts was analyzed in this calculation based on the seismic event of a 2,000-year return period, or annual probability exceedance (APE) of 5 x 10^{-4}. This section addresses the assessment of stability of non-emplacement drifts subjected to the seismic events with an APE of 10^{-4}.

Drift closures induced by seismic motions were calculated for unsupported exhaust mains in both the lithophysal and nonlithophysal category 1 rocks are presented in Figure 6-210(a) and Figure 6-210(b), respectively. The maximum closures due to seismic loadings are predicted to vary from less than 9 mm for the category 1 lithophysal rock to less than 5 mm for the category 1 nonlithophysal rock. Compared with the results subjected to the seismic events with an APE of 5 x 10^{-4} (see Figure 6-133 and Figure 6-134), the closures are slightly higher for the exhaust mains subjected to the seismic events with an APE of 10^{-4} but still not significant.

Time histories of the major principal stresses near crown and springline are shown in Figure 6-211(a) and Figure 6-211(b) for unsupported exhaust mains subjected to seismic loads and K_o of 0.3, in the lithophysal and nonlithophysal rocks, respectively. During seismic event, stresses fluctuate with seismic velocities for the lithophysal rock and the nonlithophysal rock. The magnitudes of fluctuation in stresses vary with locations. Near the crown of exhaust mains, the variations are small, while near the springlines, the changes are larger. The maximum fluctuation in the major principal stresses near the springline is predicted to vary from about 3 MPa for the category 1 lithophysal rock to about 6 MPa for the nonlithophysal category 1 rock Compared with the results subjected to the seismic events with an APE of 5 x 10^{-4} (see Figure 6-135 and Figure 6-136), the stresses are a little higher for the exhaust mains subjected to the seismic events with an APE of 10^{-4} but still not significant.

Based on the results of this sensitivity analysis, it can be predicted that the exhaust mains will be stable under seismic event with an APE of 10^{-4}. Seismic events with an APE of 10^{-4} do not become detrimental to drift stability or ground support. The stability condition of drifts predicted under seismic events with an APE of 5 x 10^{-4} generally holds for drifts under seismic events with an APE of 10^{-4}. Such a dynamic response is expected for all non-emplacement openings.

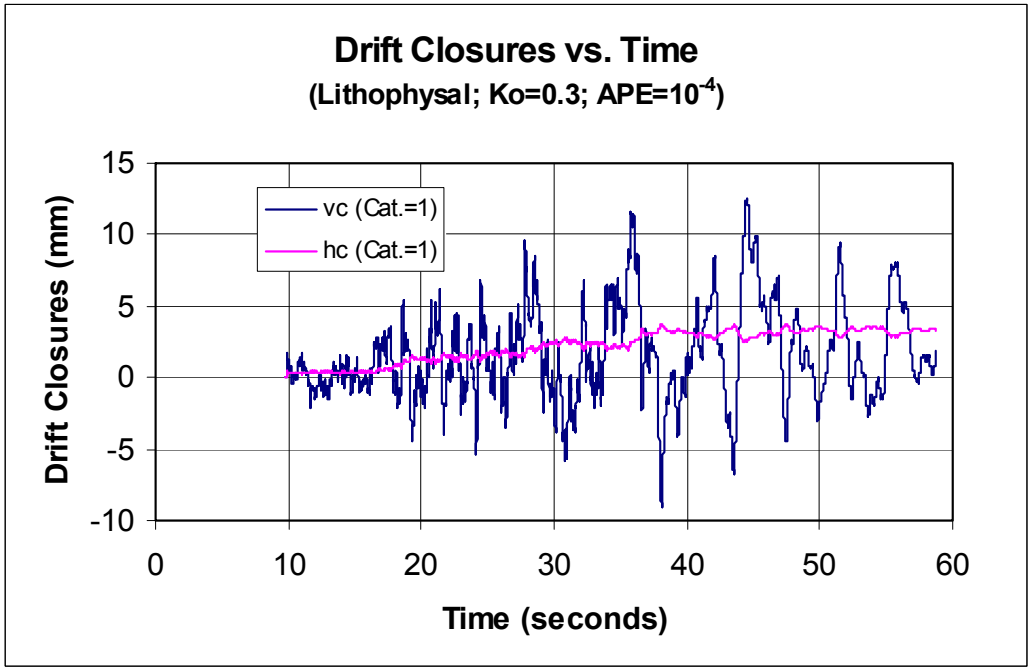

(a)

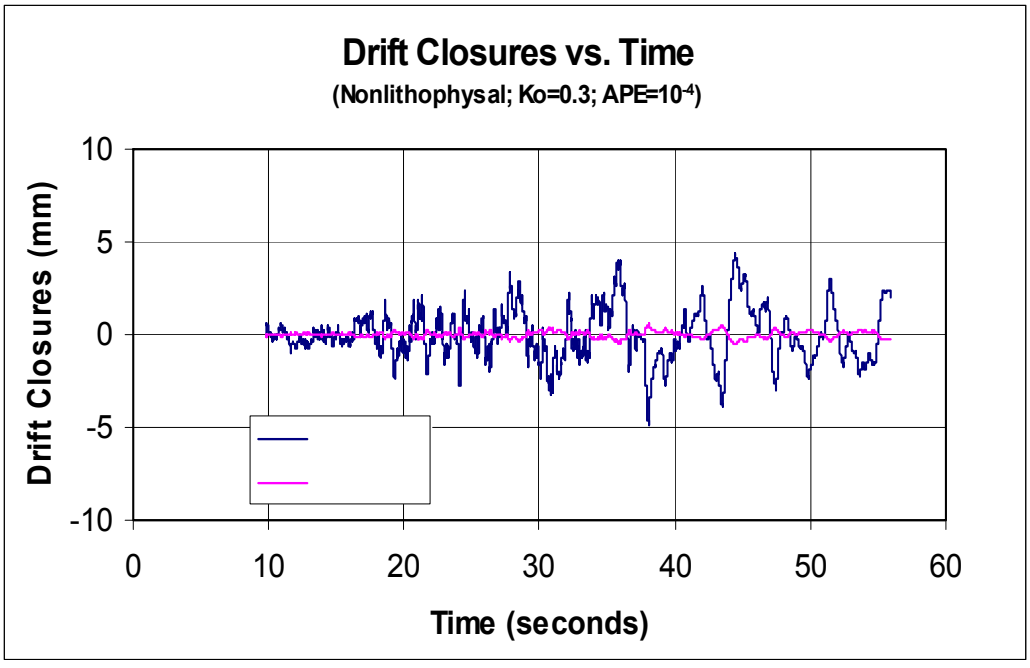

(b)

Figure 6-210. Time Histories of Closures of Exhaust Mains under Seismic Loads and Ko=0.3 in (a) Lithophysal and (b) Nonlithophysal Category 1 Rock

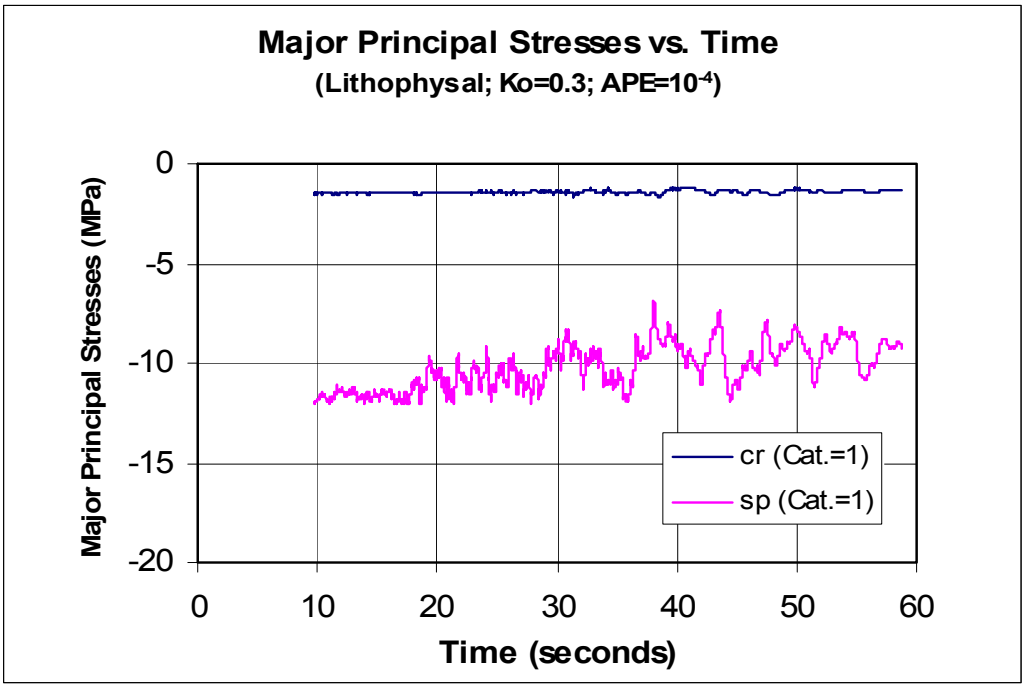

(a)

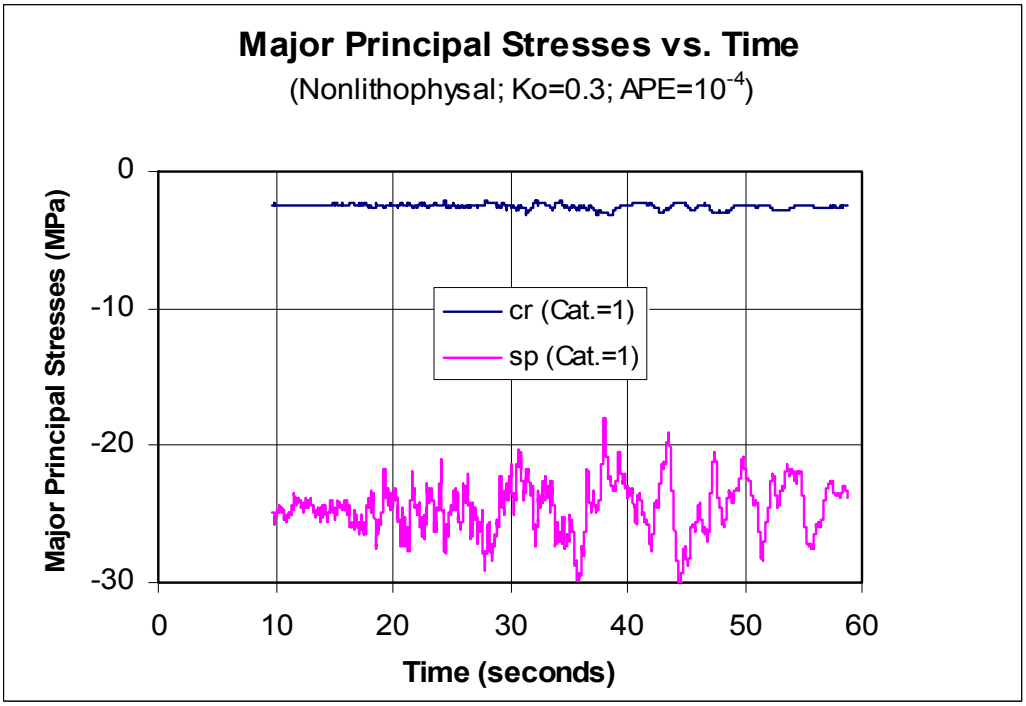

(b)

Figure 6-211. Time Histories of Major Principal Stresses near Crown and Springline of Exhaust Mains under In Situ, Thermal and Seismic Loads and Ko=0.3 in (a) Lithophysal and (b) Nonlithophysal Category 1 Rock

6.7 UNCERTAINTY DISCUSSION

There are uncertainties associated with this calculation. These uncertainties are discussed primarily in the following areas: empirical approach, numerical modeling methods, and input data.

6.7.1 Uncertainties with Empirical Approach

As discussed in Section 6.4, there are two empirical approaches adopted in this calculation for estimating the ground support need for openings at nonlithophysal rock in non-emplacement drifts, i.e., RMR and Q approaches.

For RMR approach, the ground support recommendation shown in Table 4-2 was based on a 10-m wide, horseshoe-shaped tunnel and mainly for conventional excavation method, i.e., not TBM operation. Since most tunnels or openings related to non-emplacement drifts are circular and will be excavated by TBM, therefore, there exist some uncertainties associated with the recommended ground support system based on RMR approach. In particular, the opening sizes for access and exhaust mains and turnouts are smaller than 10 m, which was the size based for Table 4-2. Therefore, the recommended ground support system based on RMR approach is considered very conservative.

For Q approach, the most important value for estimating the ground support need is the Q value. However, in order to derive the appropriate Q value, there are a number of steps to estimate various parameters as shown in Section 6.4.2, in which uncertainties are involved with each step. Moreover, in applying Q value to Figure 4-1, the corresponding bolt spacing and shotcrete thickness are estimated from ranges of values covered by various intervals. Again, uncertainties are associated with the selection of appropriate bolt spacing and shotcrete thickness.

Since uncertainties are associated with both empirical approaches, their use will provide us the design guidance. The final selection ground support system will depend on numerical analysis as well as the experience obtained from construction of ESF and ECRB.

6.7.2 Uncertainties with Numerical Modeling Method

For numerical analysis of stability of underground openings, there are two major modeling methods, i.e., continuous and discontinuum. In a continuum approach, the geologic features in the rock mass are “lumped” into the constitutive model that represents the overall equivalent effect of these features. In a discontinuum approach, fractures or lithophysae are modeled explicitly as interfaces or cavities.

The rock mass considered in this calculation contains many joints and voids. These discontinuities affect the behavior of non-emplacement drifts excavated in the discontinuous rock mass. Ideally, a discontinuum approach that explicitly simulates these discontinuities is preferred. In conventional mining or tunnel design, however, an equivalent continuum approach is most popular due to its simplicity and easy understanding of the results. In the continuum approach, the values of rock mass properties used are equivalent, meaning that the effect of discontinuities can be accounted for by choosing these property values. The continuum approach has been proved useful and reasonable through many years of industry practice.

In this calculation, two-dimensional FLAC is used to simulate any long tunnels compared with its dimension. 3DEC is used to simulate the intersection area, which is appropriate for three-dimensional layout configuration. FLAC is continuous approach whereas 3DEC is a discontinuum one. It is noted that for 3DEC approach used in this calculation, the joints between blocks are glued together to behave as a continuous one.

The ground support designs for the ESF and the ECRB tunnels were based primarily on the conventional continuum approach. The experiences from these tunnel designs and excavations indicate that the continuum approach is still applicable to the ground support design for non-emplacement drifts. Results from the continuum approach, such as rock deformation and stress, are considered equivalent to those that would be generated otherwise by using a discontinuum approach.

6.7.3 Uncertainties with Input Data

The uncertainties associated with input data for the numerical analyses are mainly involved in the following areas: material properties, overburden depth, and opening sizes.

The effect of the rock mass quality variability within the lithophysal and nonlithophysal units at the repository level was accounted for by considering different rock mass categories. As shown in Table 6-1 and Table 6-2 there are five rock mass categories for lithophysal and nonlithophysal rocks. The majority of computer simulations for unsupported openings in this calculation were carried out for category 1 rock (the poorest quality rock mass), category 3 rock (the medium quality rock mass), and category 5 rock (the strongest quality rock mass) both in lithophysal and nonlithophysal units. Stability analyses for supported openings were performed on category 1 rock (the poorest quality rock mass). Therefore, the stability of unsupported openings cover all rock conditions and the ground support design based on the poorest quality is conservative.

The average depth of RHH is assumed to be 400 m for all the model calculations. Although depth of non-emplacement drifts varies from drift to drift. The depths of emplacement drifts range from 215 to 450 m with the majority between 300 to 400 m (Assumption 3.2.3). As discussed in Assumption 3.2.3 that the emplacement drift stability results for the maximum value of 450 m would be similar to those for the bounding case of 400 m. The overburden depth of the majority of non-emplacement drifts are less than 400 m, use of a depth of 400 m for calculating in situ stress at the non-emplacement drift horizon is considered adequate for the purpose of this calculation.

There are several configurations in intersections between access mains and turnouts and between exhaust mains and emplacement drifts, with roof spans at openings varying from about 10 m to greater than 20 m. The intersection A at intersections between access mains and turnouts represents the critical conditions with respect to the maximum span of the roof and stress concentrations in the pillars compared with other similar intersections. The intersections B at intersections between exhaust mains and emplacement drifts represent intersection locations in the middle of the repository with large roof span whereas intersection C represents locations at the edge of the repository. Temperature changes at the edge of the repository (intersection C) are overpredicted by NUFT's two-dimensional results, resulting in conservative estimate of stress increase and more unfavorable stability conditions. Also, exhaust mains with the diameter of

7.62 m are used throughout the analysis, even though it is 5.5 m in Panel 1 of the repository. With large roof span, the larger stresses will be resulted, which will give conservative estimate on ground support system.

Based on the above discussion, the model layout in terms of locations and opening sizes should result in conservative results regarding the stability of non-emplacement drifts.

7 SUMMARY AND CONCLUSIONS

7.1 SUMMARY

The stability analyses of unsupported and supported non-emplacement drifts for the Yucca Mountain repository were performed in this calculation. The repository ground support design was based on both empirical approaches and analytical methods using acquired computer codes, and focused on the final support systems.

Empirical approaches using RMR value and Q index were used to estimate the ground support need for openings in the nonlithophysal rock. For analytical methods, both continuum and discontinuum modeling approaches were employed in the analyses of the rock mass behavior for both lithophysal and nonlithophysal rocks and in the evaluation of the stability of the openings.

The stability analyses were conducted for access mains, ramps, exhaust mains, turnouts, and intersections between main drifts with turnouts and emplacement drifts, observation drift, portals, and TBM launch chambers. The stability analysis of unsupported drifts at the interburden area between access drift to intake shaft #4 and two underlying exhaust mains was also performed.

The excavation effects (i.e., state of the stress change due to excavation), thermal effects (i.e., due to heat output from waste packages), and seismic effects (i.e., from potential earthquake events) were evaluated, and stress controlled modes of failure were examined for representing rock mass categories 1 and 5. The focus was on the category 1 rock because it is weaker than other categories of rock mass.

No credit or account was given for the initial or temporary ground support in modeling the final ground support systems for non-emplacement drifts in this analysis.

It should be noted that the results presented in this calculation are based on the adopted methods, input data and assumptions. If any input information is changed, the output information may vary. Also, as the design of ground support systems progresses, the evaluation of ground control for non-emplacement drifts will be updated as necessary.

7.2 STABILITY OF UNSUPPORTED NON-EMPLACEMENT DRIFTS

The results of stability analysis on unsupported access and exhaust mains indicate that, for the lithophysal category 1 rock, i.e., poorest rock mass category, a narrow zone adjacent to wall (about 1.0 m into wall) is shown with potential yield. For the lithophysal category 3 rock, i.e., median rock mass category, a very narrow zone adjacent to wall (about 0.4 m into wall) is shown with potential yield. At distance of about 1 m into wall, the SF increases to 2. For the lithophysal category 5 rock, i.e., highest rock mass category, only a few points near the crown are shown with potential yield. At distance of about 0.5 m into wall SF increases to 2. There is no indication of instability of the rock surrounding the unsupported access/exhaust mains and turnouts.

For unsupported intersection between access mains and turnouts, the 3DEC models predict similar deformation and stability conditions for intersections with large and small roof spans. The rock mass deformation around intersections will be predominantly elastic. The damage is expected to extend approximately 1 m from the drift walls into the rock mass, in the worst case, for the poorest quality rock mass. A relatively large displacement of about 70 mm predicted for the lithophysal rock mass, category 1, is a consequence of the very low Young's modulus used. There are no indications of loosening and instability of the rock mass in the crown for any of the analyzed cases. The roof in the intersections is shown to be stable, even at locations of the largest spans. The tips of the pillars between the access main and the turnouts will be damaged due to stress concentrations. The extent of this damage from the pillar tip will depend on the rock mass quality. Rounding of the pillars and additional ground support will resolve the problem of pillar instability.

Similar stability condition for intersections and pillars between exhaust mains and emplacement drifts as those at intersections at access mains are also obtained based on the computer results. The thermal stress changes are much larger in better quality and stiffer rock masses. The increase in the maximum major principal stress is about 25 MPa in category 5 of the lithophysal and nonlithophysal rock masses. However, the stress change does not change factor of safety with respect to the Mohr-Coulomb yield condition throughout the rock mass nor cause significant additional yielding of the rock mass. The extent of plastic deformation for intersections for different rock-mass categories remains practically unchanged after 50 years of heating. The results of dynamic analysis can be concluded that the seismic events with a mean annual probability exceedance of $5x10^{-4}$ does not cause significant, permanent change in the factor-of-safety with respect to the Mohr-Coulomb yield condition or increase the volume of the rock mass subject to tensile stresses. The average stresses in the pillar between the drifts are almost unchanged.

A sensitivity study was analyzed for unsupported exhaust mains in lithophysal and nonlithophysal category 1 rocks subjected to the seismic events with a mean annual probability of exceedance of 10^{-4}. The stability condition of drifts predicted under seismic events with an APE of 5×10^{-4} generally holds for drifts under seismic events with an APE of 10^{-4}. Such a dynamic response is expected for all non-emplacement openings.

For unsupported observation drift, excavations of the emplacement drift and the observation drift do not interact with each other. The predicted extent of the damage of the rock mass surrounding the observation drift and the emplacement drift is similar. There is a little more damage in the walls and the floor of the observation drift because of mechanically less-favorable shape. However, the factor-of-safety with respect to Mohr-Coulomb shear failure increases very quickly as a function of distance from the drift boundary; the factor-of-safety is larger than 2 only a couple of meters from the drift walls. It does not appear that the temperature change causes any additional damage around the observation drift. It also indicates that thermal loads do not affect the stability conditions of the rock mass around the intersection between the observation drift and the exhaust main.

The observation drift was analyzed for seismic loading due to a 2,000-yr return period ground motion in both typical cross-section and at the intersection between the observation drift and the

exhaust main. The results indicate that seismic load causes insignificant increase in damage around the observation drift, but there is no indication of large-scale instability.

For unsupported TBM launch chamber, due to the wider span (or height) of the launch chamber is approximately two times of the span of the observation drift, the depth of the damaged rock in the wall of the launch chamber is about 2 m, compared to the depth of about 1 m predicted in the wall of the observation drift. Outside the yielded region, the factor of safety to shear failure increases rapidly as a function of distance from the drift wall, indicating overall stability of the excavation.

The results of the dynamic analysis of the TBM launch chamber are similar to those obtained for the observation drift. Preclosure seismic shaking causes relatively small additional damage of the rock mass, but there is no indication of global instability of the launch chamber during or after the shaking.

The stability analysis for interburden pillar between access drift to intake shaft #4 and two underlying exhaust mains subjected to in-situ stress, thermal, and seismic loading has been performed. The results indicate that the effect of the excavation of an overlying 7.62-m-diameter access drift and two underlying 7.62-m-diameter exhaust mains on the stability of 10-m high interburden pillar is minimum or insignificant.

7.3 GROUND SUPPORT SYSTEM FOR NON-EMPLACEMENT DRIFTS

The ground support system designed for non-emplacement drifts is described as follows:

- For non-emplacement openings, which include access mains, exhaust mains, observation drift, test alcove, and TBM launch chambers: fully grouted rock bolts with heavy duty WWF.
- For intersections between access mains and turnouts, ramps and starter tunnels: fully grouted bolts with steel fiber-reinforced shotcrete, and lattice girders as necessary for roof span control.
- For intersections between exhaust mains and emplacement drifts: the same ground support system as that for intersections between access mains and turnouts except that no shotcrete inside the emplacement drift.
- For emplacement drift turnouts: stainless steel friction-type rock bolts with stainless steel heavy duty WWF.

The fully grouted rock bolts with a typical length of 3 m, spaced at 1.25 m with heavy duty WWF, i.e., W4 x W4 with 100 mm center-to-center spacing, are designed to be used for ground support at typical non-emplacement openings, which include access mains, exhaust mains, observation drift, test alcove, and TBM launch chambers. It is noted that the same ground support system for the observation drift will apply to the test alcove since both of them have the same shape and dimension and are in the same PC facility area. Similarly, the same ground support system for access mains is considered adequate to be used for the ECRB Cross Drift in its future widening stage.

Stainless steel friction-type rock bolts with a typical length of 3 m, spaced at 1.25 m with stainless steel WWF, i.e., W4 x W4 with 75 mm center-to-center spacing, are designed to be used for ground support at emplacement drift turnouts.

In the intersection areas, in order to enhance the opening stability with large roof span, increased bolt length of about 5 m with 0.10 m thick steel fiber-reinforced shotcrete will be installed, and supplemented with lattice girder as necessary depending on rock mass quality and the associated roof span. Note that shotcrete is not to be used inside the emplacement drift since cementious materials are ruled out for use in emplacement drifts due to their potential adverse impact on the long-term waste isolation.

It is noted that the same ground support system for the intersections will be applied to starter tunnel and ramps except that the bolt length is 3 m long. The designed ground support system for ramps may be only for North Ramp and may need to be changed for North Construction Ramp and South Ramp as fully grouted rock bolts with heavy duty WWF, with steel fiber-reinforced shotcrete installed on as-needed basis, depending on the rock mass condition and construction schedule.

For steel ground support components to be used in accessible openings of non-emplacement excavations and exhaust mains, carbon steel including high-strength low-alloy steel is considered. For ground support in emplacement drift turnouts, which are inaccessible non-emplacement openings, stainless steel friction-type rock bolts with stainless steel WWF are considered adequate. Note that exhaust mains can be maintained when deemed necessary since only temperatures will be higher compared with those at access mains but radiation level would be lower than that at turnouts which are the passage ways for the waste package-loaded TEV.

Candidate ground support components will be manufactured based on the proper ASTM standard specifications. For cementitious materials to be used for grouted rock bolts, shotcrete or concrete, a low pH grout and shotcrete/concrete mix or use of other types of grouts and cements made of non-portland cement types is proposed.

The ground support system is designed to be functional with planned maintenance in the accessible non-emplacement openings and little or no planned maintenance in the non-accessible non-emplacement areas during the operational life. For non-accessible non-emplacement openings, any necessary maintenance needs triggered by installation flaws, material defects, off-normal operational conditions, or unfavorable inspection results will be evaluated with a full consideration of the information gathered during the inspection and monitoring activities.

7.4 STABILITY OF SUPPORTED NON-EMPLACEMENT DRIFTS

For stability condition of supported non-emplacement openings, the computer models do not indicate formation of a failure mechanism, or the accumulation of residual displacement, which is a result of plastic deformation of the rock mass during shaking. However, the results do not imply that rockfall of any kind will not occur during an earthquake with 2,000 year return period. The limitation of this model is that it is formulated based on continuum mechanics. Consequently, it is not possible to simulate the formation of new or reopening of existing

fractures, which could form loosened blocks, resulting in a rockfall. The analysis implies that, if there is no ground support, the rockfall will be fairly limited and confined to the drift boundary.

To a large extent the load in the rock bolts is determined by the percentage of total relaxation completed at the moment of bolt installation, and by the stiffness and shear strength of the grout. Assuming 60% of stress relaxation (Assumption 3.2.1) due to a stand-off between the advancing face and installed rock bolts, the maximum forces in the bolts in the access main before excavation of the turnouts is predicted to be 154 kN. This gives a SF of about 1.7. In other words, the bolts have a reserve of at least 100 kN to take the load by loosened, locally unstable blocks. However, the majority of the bolts are loaded to less than 100 kN. Excavation of the turnouts results in an increase in load to less than 200 kN in the bolts above the turnouts. The bolts will remain elastic due to the loads generated by the convergence of the drifts for in-situ stresses. The forces in the rock bolt generated by the convergence of the drifts will act as an active force, as if the bolts are pre-tensioned. Seismic load has insignificant effect on the rock bolts. It appears that the shotcrete would be damaged during an earthquake with 2,000-year return period, but that damage (mostly tensile cracks) would be localized.

The stability condition of supported exhaust mains and their intersections are similar to those of access mains and the adjacent intersections. The maximum load in the bolts in the exhaust main after excavation of the exhaust main is around 150 kN, with exception of a few bolts affected by the local conditions. The maximum force in the bolts increases to approximately 200 kN in the regions above the intersection after excavation of both exhaust mains and the emplacement drifts. Those loads are well within the limit of the elastic deformation of the bolts, which have yield strength of 264 kN.

The forces in the bolts increase during the preclosure period due to heating. However, even using the conservative analysis, the predicted maximum force in the rock bolts is about 198 kN during the preclosure period, which is less than the yield strength. The maximum increase in bolt forces due to seismic loading compared to the static condition is approximately 3 kN in the region above the intersection, with the bolt load less than the yield strength. Note that the dynamic analysis of global stability of the intersections was carried out using the continuum models. In the simulations of intersections, the blocks were glued together to behave effectively as a continuum. Thus, the local stability of blocks created by joints around the excavation was not considered. However, such blocks will be of limited size and number and will be effectively supported by the designed ground support.

For supported observation drift under static loading, the forces in bolts are insignificant considering the bolt yield strength of 264 kN. Thermal load causes an increase in bolt forces, however, the loads are well within the range of elastic deformation of the rockbolts after 50 years of heating. The designed bolt length of 3 m appears to be sufficient to provide anchoring into the elastic (undamaged) rock. The maximum bolt force after seismic shaking is much less than the bolt yield strength of 264 kN.

For supported TBM launch chambers, the rockbolts do not take any load due to rock mass deformation caused by the relaxation of in situ stresses, as the launch chamber will be excavated using the drill-and-blast method. The forces in the rockbolts at the end of dynamic simulation are small relative to the yield strength of the rockbolts.

8 ATTACHMENT I LIST OF INPUT AND OUTPUT FILES

The list of input and output files for the numerical analyses for access mains, exhaust mains and turnouts are listed in this section. The list of input files for observation drift, TBM launch chamber, North portal, intersections between access mains and turnouts and between exhaust mains and emplacement drifts and between observation drift and exhaust main, and interburden pillar between shaft access and exhaust mains are listed here.

Directory of O:\RUD\GCNEDLA-2007\AccessMain\Litho_A\cat_1,3,5

properties.fis	3,823	7/14/2007	02:52p
hiszones_50.fis	1,235	5/15/2007	07:38p
makemovie.fis	3,408	5/15/2007	07:38p
driver.dat	1,784	5/15/2007	07:38p
relaxation.fis	2,152	5/15/2007	07:39p
seismic.dat	451	7/18/2007	03:24p
setup.fis	2,087	5/15/2007	07:39p
shake.fis	2,874	5/15/2007	07:39p
tunnel.dat	3,024	5/15/2007	07:39p
vel_hori_5e-4.tab	203,437	5/15/2007	07:39p
vel_vert_5e-4.tab	195,677	5/15/2007	07:39p
Acc_Main	962	8/9/2007	02:41p

12 File(s) 420,914 bytes

Directory of O:\RUD\GCNEDLA-2007\AccessMain\Litho_A\cat_1,5_grc

driver_grcll.dat	12,314	7/18/2007	04:56p
setup.fis	2,087	5/15/2007	07:39p
relaxation.fis	2,152	5/15/2007	07:39p
properties.fis	3,823	7/14/2007	02:52p
hiszones_50.fis	1,235	5/15/2007	07:38p
tunnel.dat	3,025	7/19/2007	04:05p

6 File(s) 24,636 bytes

Directory of O:\RUD\GCNEDLA-2007\AccessMain\Litho_A\cat_1,5_k=1.0_exv_output

relaxation.fis	2,152	5/15/2007	07:39p
hiszones_50.fis	1,235	5/15/2007	07:38p
properties.fis	3,823	7/14/2007	02:52p
driver.dat	1,189	7/20/2007	11:18a
setup.fis	2,087	5/15/2007	07:39p
Shortcut to flacw_sp.exe.lnk	402	07/20/2007	03:11p
tunnel.dat	3,024	5/15/2007	07:39p
gcuku210is.ini	2,873,707	7/20/2007	11:25a
gcuku210is.exv	3,017,595	7/20/2007	11:27a
gcuku250is.ini	2,873,707	7/20/2007	11:27a

gcuku250is.exv	3,009,435	7/20/2007	11:28a
ydisp_gcuku1_exv	787	7/20/2007	03:14p
ydisp_gcuku5_exv	787	7/20/2007	03:18p

13 File(s) 11,789,933 byte

Directory of O:\RUD\GCNEDLA-2007\AccessMain\Litho_A\cat_1_sup

properties.fis	3,823	7/14/2007	02:52p
boltprop.fis	1,642	5/15/2007	07:39p
driver.dat	624	5/25/2007	02:16p
hiszones_50.fis	1,235	5/15/2007	07:39p
makemovie.fis	3,408	5/15/2007	07:39p
bolt.dat	640	7/16/2007	10:22a
relaxation.fis	2,152	5/15/2007	07:39p
seismic.dat	228	5/25/2007	01:58p
setup.fis	2,087	5/15/2007	07:39p
shake.fis	2,872	5/15/2007	07:39p
tunnel_b.dat	3,041	5/15/2007	07:39p
vel_hori_5e-4.tab	203,437	5/15/2007	07:39p
vel_vert_5e-4.tab	195,677	5/15/2007	07:39p

13 File(s) 420,866 bytes

Directory of O:\RUD\GCNEDLA-2007\AccessMain\Litho_A\cat_1_sup_100%relax

makemovie.fis	3,408	5/15/2007	07:39p
boltprop.fis	1,642	5/15/2007	07:39p
driver.dat	624	7/19/2007	01:07p
hiszones_50.fis	1,235	5/15/2007	07:39p
bolt.dat	640	7/16/2007	10:22a
properties.fis	3,823	7/14/2007	02:52p
relaxation.fis	2,152	5/15/2007	07:39p
seismic.dat	228	5/25/2007	01:58p
setup.fis	2,087	5/15/2007	07:39p
shake.fis	2,872	5/15/2007	07:39p
tunnel_b.dat	3,043	6/2/2007	11:16a
vel_hori_5e-4.tab	203,437	5/15/2007	07:39p
vel_vert_5e-4.tab	195,677	5/15/2007	07:39p

13 File(s) 420,868 bytes

Directory of O:\RUD\GCNEDLA-2007\AccessMain\Nonlitho_A\cat_1,3,5

properties.fis	3,823	7/14/2007	02:52p
hiszones_50.fis	1,235	5/15/2007	07:39p
makemovie.fis	3,408	5/15/2007	07:39p
driver.dat	1,754	5/15/2007	07:39p
relaxation.fis	2,152	5/15/2007	07:39p
seismic.dat	451	7/19/2007	08:13a

setup.fis	2,087	5/15/2007	07:39p
shake.fis	2,874	5/15/2007	07:39p
tunnel.dat	3,024	5/15/2007	07:39p
vel_hori_5e-4.tab	203,437	5/15/2007	07:40p
vel_vert_5e-4.tab	195,677	5/15/2007	07:40p

11 File(s) 419,922 bytes

Directory of O:\RUD\GCNEDLA-2007\AccessMain\Nonlitho_A\cat_1,5_grc

properties.fis	3,823	7/14/2007	02:52p
hiszones_50.fis	1,235	5/15/2007	07:38p
driver_grcmn.dat	12,314	7/19/2007	10:36a
relaxation.fis	2,152	5/15/2007	07:39p
setup.fis	2,087	5/15/2007	07:39p
tunnel.dat	3,025	7/19/2007	05:01p

6 File(s) 24,636 bytes

Directory of O:\RUD\GCNEDLA-2007\AccessMain\Nonlitho_A\cat_1,5_k=1.0_exv_output

gcuku150is.ini	2,873,707	7/20/2007	11:25a
gcuku110is.exv	3,011,835	7/20/2007	11:25a
gcuku110is.ini	2,873,707	7/20/2007	11:24a
gcuku150is.exv	3,012,795	7/20/2007	11:27a
driver.dat	1,189	7/20/2007	11:22a
hiszones_50.fis	1,235	5/15/2007	07:38p
properties.fis	3,823	7/14/2007	02:52p
relaxation.fis	2,152	5/15/2007	07:39p
setup.fis	2,087	5/15/2007	07:39p
Shortcut to flacw_sp.exe.lnk	402	7/25/2007	12:14p
tunnel.dat	3,024	5/15/2007	07:39p
ydisp_gcuku1_exv	1,225	7/25/2007	12:17p
ydisp_gcuku5_exv	787	7/25/2007	12:17p

13 File(s) 11,787,968 bytes

Directory of O:\RUD\GCNEDLA-2007\AccessMain\Nonlitho_A\cat_1_sup

properties.fis	3,823	7/14/2007	02:52p
boltprop.fis	1,642	5/15/2007	07:40p
driver.dat	622	5/25/2007	02:18p
hiszones_50.fis	1,235	5/15/2007	07:40p
makemovie.fis	3,408	5/15/2007	07:40p
bolt.dat	640	7/16/2007	10:22a
relaxation.fis	2,152	5/15/2007	07:40p
seismic.dat	224	7/19/2007	08:01a
setup.fis	2,087	5/15/2007	07:40p
shake.fis	2,872	5/15/2007	07:40p

tunnel_b.dat	3,041	5/15/2007	07:40p
vel_hori_5e-4.tab	203,437	5/15/2007	07:40p
vel_vert_5e-4.tab	195,677	5/15/2007	07:40p

13 File(s) 420,860 bytes

Directory of O:\RUD\GCNEDLA-2007\AccessMain\Nonlitho_A\cat_1_sup_100%relax

properties.fis	3,823	7/14/2007	02:52p
boltprop.fis	1,642	5/15/2007	07:39p
driver.dat	624	7/19/2007	01:16p
hiszones_50.fis	1,235	5/15/2007	07:39p
makemovie.fis	3,408	5/15/2007	07:39p
bolt.dat	640	7/16/2007	10:22a
relaxation.fis	2,152	5/15/2007	07:39p
seismic.dat	228	7/19/2007	01:16p
setup.fis	2,087	5/15/2007	07:39p
shake.fis	2,872	5/15/2007	07:39p
tunnel_b.dat	3,043	6/2/2007	11:16a
vel_hori_5e-4.tab	203,437	5/15/2007	07:39p
vel_vert_5e-4.tab	195,677	5/15/2007	07:39p

13 File(s) 420,868 bytes

Directory of O:\RUD\GCNEDLA-2007\Data files_Itasca\3DEC_Data_files\1_Access-Turnout\Litho\cat_1

BLOCK.FIN	11,207	8/8/2007	09:38p
CONTACT.FIN	6,231	8/8/2007	09:38p
driver.dat	4,518	8/8/2007	09:38p
edgelength.fis	41,297	8/8/2007	09:38p
fixt.fis	720	8/8/2007	09:38p
functions.fis	27,046	8/8/2007	09:38p
geometry.fis	12,091	8/8/2007	09:38p
h1_18.vel	255,590	8/8/2007	09:38p
H2_18.vel	255,591	8/8/2007	09:38p
pillarStress.fis	1,005	8/8/2007	09:38p
plot.dat	1,345	8/8/2007	09:38p
plotfos.dat	6,968	8/8/2007	09:38p
plotplas.dat	413	8/8/2007	09:38p
print.dat	1,044	8/8/2007	09:38p
properties.fis	3,147	8/8/2007	09:38p
reset.fis	500	8/8/2007	09:38p
Shake.dat	1,404	8/8/2007	09:38p
States.dat	1,767	8/8/2007	09:38p
States.fis	961	8/8/2007	09:38p
times.fis	1,102	8/8/2007	09:38p
up_18.Vel	195,676	8/8/2007	09:38p

21 File(s) 829,623 bytes

Directory of O:\RUD\GCNEDLA-2007\Data files_Itasca\3DEC_Data_files\1_Access-Turnout\Litho\cat_1_10K_EQ

BLOCK.FIN	11,207	8/8/2007	09:37p
CONTACT.FIN	6,231	8/8/2007	09:37p
driver.dat	4,516	8/8/2007	09:37p
edgelength.fis	41,297	8/8/2007	09:37p
fixt.fis	720	8/8/2007	09:37p
functions.fis	27,046	8/8/2007	09:37p
geometry.fis	12,091	8/8/2007	09:37p
h1_19.vel	368,997	8/8/2007	09:37p
h2_19.vel	369,484	8/8/2007	09:37p
pillarStress.fis	1,005	8/8/2007	09:37p
plot.dat	1,345	8/8/2007	09:37p
plotfos.dat	6,968	8/8/2007	09:37p
plotplas.dat	413	8/8/2007	09:37p
print.dat	1,044	8/8/2007	09:37p
properties.fis	3,147	8/8/2007	09:37p
reset.fis	500	8/8/2007	09:37p
shake.dat	1,404	8/8/2007	09:37p
states.dat	1,767	8/8/2007	09:37p
States.fis	961	8/8/2007	09:37p
times.fis	1,102	8/8/2007	09:37p
Up_19.vel	368,522	8/8/2007	09:37p

21 File(s) 1,229,767 bytes

Directory of O:\RUD\GCNEDLA-2007\Data files_Itasca\3DEC_Data_files\1_Access-Turnout\Litho\cat_1_supported

BLOCK.FIN	11,207	8/8/2007	09:37p
CABLE.FIN	3,326	8/8/2007	09:37p
CONTACT.FIN	6,231	8/8/2007	09:37p
driver.dat	8,162	8/8/2007	09:37p
edgelength.fis	41,297	8/8/2007	09:37p
fixt.fis	720	8/8/2007	09:37p
functions.fis	27,046	8/8/2007	09:37p
geometry.fis	12,189	8/8/2007	09:37p
h1_18.vel	255,590	8/8/2007	09:38p
H2_18.vel	255,591	8/8/2007	09:38p
LINER.FIN	6,007	8/8/2007	09:38p
names1.fis	897	8/8/2007	09:38p
pillarStress.fis	1,005	8/8/2007	09:38p
plot.dat	1,323	8/8/2007	09:38p
plotcab.dat	3,467	8/8/2007	09:38p
plotplas.dat	415	8/8/2007	09:38p
print.dat	1,046	8/8/2007	09:38p
properties.fis	3,147	8/8/2007	09:38p

reset.fis	500	8/8/2007	09:38p
shake.dat	1,400	8/8/2007	09:38p
states.dat	1,767	8/8/2007	09:38p
States.fis	961	8/8/2007	09:38p
support.fis	29,694	8/8/2007	09:38p
times.fis	1,102	8/8/2007	09:38p
up_18.Vel	195,676	8/8/2007	09:38p

21 File(s) 869,766 bytes

Directory of O:\RUD\GCNEDLA-2007\Data files_Itasca\3DEC_Data_files\1_Access-Turnout\Litho\cat_3

BLOCK.FIN	11,207	8/8/2007	09:37p
CONTACT.FIN	6,231	8/8/2007	09:37p
driver.dat	4,516	8/8/2007	09:37p
edgelength.fis	41,297	8/8/2007	09:37p
fixt.fis	720	8/8/2007	09:37p
functions.fis	27,046	8/8/2007	09:37p
geometry.fis	12,091	8/8/2007	09:37p
h1_18.vel	255,590	8/8/2007	09:37p
H2_18.vel	255,591	8/8/2007	09:37p
pillarStress.fis	1,005	8/8/2007	09:37p
plot.dat	1,345	8/8/2007	09:37p
plotfos.dat	6,968	8/8/2007	09:37p
plotplas.dat	413	8/8/2007	09:37p
print.dat	1,044	8/8/2007	09:37p
properties.fis	3,147	8/8/2007	09:37p
reset.fis	500	8/8/2007	09:37p
shake.dat	1,404	8/8/2007	09:37p
states.dat	1,767	8/8/2007	09:37p
States.fis	961	8/8/2007	09:37p
times.fis	1,102	8/8/2007	09:37p
up_18.Vel	195,676	8/8/2007	09:37p

21 File(s) 829,621 bytes

Directory of O:\RUD\GCNEDLA-2007\Data files_Itasca\3DEC_Data_files\1_Access-Turnout\Litho\cat_5

BLOCK.FIN	11,207	8/8/2007	09:37p
CONTACT.FIN	6,231	8/8/2007	09:37p
driver.dat	4,516	8/8/2007	09:37p
edgelength.fis	41,297	8/8/2007	09:37p
fixt.fis	720	8/8/2007	09:37p
functions.fis	27,046	8/8/2007	09:37p
geometry.fis	12,091	8/8/2007	09:37p
h1_18.vel	255,590	8/8/2007	09:37p
H2_18.vel	255,591	8/8/2007	09:37p
pillarStress.fis	1,005	8/8/2007	09:37p
plot.dat	1,345	8/8/2007	09:37p

plotfos.dat	6,968	8/8/2007	09:37p
plotplas.dat	413	8/8/2007	09:37p
print.dat	1,044	8/8/2007	09:37p
properties.fis	3,147	8/8/2007	09:37p
reset.fis	500	8/8/2007	09:37p
shake.dat	1,404	8/8/2007	09:37p
states.dat	1,767	8/8/2007	09:37p
States.fis	961	8/8/2007	09:37p
times.fis	1,102	8/8/2007	09:37p
up_18.Vel	195,676	8/8/2007	09:37p

21 File(s) 829,621 bytes

Directory of O:\RUD\GCNEDLA-2007\Data files_Itasca\3DEC_Data_files\1_Access-Turnout\NonLitho\cat_1

BLOCK.FIN	11,207	8/8/2007	09:36p
CONTACT.FIN	6,231	8/8/2007	09:36p
driver.dat	4,517	8/8/2007	09:36p
edgelength.fis	41,297	8/8/2007	09:36p
fixt.fis	720	8/8/2007	09:36p
functions.fis	27,046	8/8/2007	09:36p
geometry.fis	12,091	8/8/2007	09:36p
h1_18.vel	255,590	8/8/2007	09:36p
H2_18.vel	255,591	8/8/2007	09:36p
pillarStress.fis	1,005	8/8/2007	09:36p
plot.dat	1,345	8/8/2007	09:36p
plotfos.dat	6,968	8/8/2007	09:36p
plotplas.dat	413	8/8/2007	09:36p
print.dat	1,044	8/8/2007	09:36p
properties.fis	3,147	8/8/2007	09:36p
reset.fis	500	8/8/2007	09:36p
shake.dat	1,404	8/8/2007	09:36p
states.dat	1,767	8/8/2007	09:36p
States.fis	961	8/8/2007	09:36p
times.fis	1,102	8/8/2007	09:36p
up_18.Vel	195,676	8/8/2007	09:37p

21 File(s) 829,622 bytes

Directory of O:\RUD\GCNEDLA-2007\Data files_Itasca\3DEC_Data_files\1_Access-Turnout\NonLitho\cat_1_10K_EQ

BLOCK.FIN	11,207	8/8/2007	09:35p
CONTACT.FIN	6,231	8/8/2007	09:35p
driver.dat	4,517	8/8/2007	09:35p
edgelength.fis	41,297	8/8/2007	09:35p
fixt.fis	720	8/8/2007	09:35p
functions.fis	27,046	8/8/2007	09:35p
geometry.fis	12,091	8/8/2007	09:35p

h1_19.vel	368,997	8/8/2007	09:35p
h2_19.vel	369,484	8/8/2007	09:35p
pillarStress.fis	1,005	8/8/2007	09:35p
plot.dat	1,345	8/8/2007	09:35p
plotfos.dat	6,968	8/8/2007	09:35p
plotplas.dat	413	8/8/2007	09:35p
print.dat	1,044	8/8/2007	09:35p
properties.fis	3,147	8/8/2007	09:35p
reset.fis	500	8/8/2007	09:35p
shake.dat	1,404	8/8/2007	09:35p
states.dat	1,767	8/8/2007	09:35p
States.fis	961	8/8/2007	09:35p
times.fis	1,102	8/8/2007	09:35p
Up_19.vel	368,522	8/8/2007	09:35p

21 File(s) 1,229,768 bytes

Directory of O:\RUD\GCNEDLA-2007\Data files_Itasca\3DEC_Data_files\1_Access-Turnout\NonLitho\cat_1_supported

BLOCK.FIN	11,207	8/8/2007	09:36p
CABLE.FIN	3,326	8/8/2007	09:36p
CONTACT.FIN	6,231	8/8/2007	09:36p
driver.dat	8,163	8/8/2007	09:36p
edgelength.fis	41,297	8/8/2007	09:36p
fixt.fis	720	8/8/2007	09:36p
functions.fis	27,046	8/8/2007	09:36p
geometry.fis	12,189	8/8/2007	09:36p
h1_18.vel	255,590	8/8/2007	09:36p
H2_18.vel	255,591	8/8/2007	09:36p
LINER.FIN	6,007	8/8/2007	09:36p
names1.fis	897	8/8/2007	09:36p
pillarStress.fis	1,005	8/8/2007	09:36p
plot.dat	1,323	8/8/2007	09:36p
plotcab.dat	3,467	8/8/2007	09:36p
plotplas.dat	415	8/8/2007	09:36p
print.dat	1,046	8/8/2007	09:36p
properties.fis	3,147	8/8/2007	09:36p
reset.fis	500	8/8/2007	09:36p
shake.dat	1,400	8/8/2007	09:36p
states.dat	1,767	8/8/2007	09:36p
States.fis	961	8/8/2007	09:36p
support.fis	29,694	8/8/2007	09:36p
times.fis	1,102	8/8/2007	09:36p
up_18.Vel	195,676	8/8/2007	09:36p

25 File(s) 869,767 bytes

Directory of O:\RUD\GCNEDLA-2007\Data files_Itasca\3DEC_Data_files\1_Access-Turnout\NonLitho\cat_3

BLOCK.FIN	11,207	8/8/2007	09:36p
CONTACT.FIN	6,231	8/8/2007	09:36p
driver.dat	4,517	8/8/2007	09:36p
edgelength.fis	41,297	8/8/2007	09:36p
fixt.fis	720	8/8/2007	09:36p
functions.fis	27,046	8/8/2007	09:36p
geometry.fis	12,091	8/8/2007	09:36p
h1_18.vel	255,590	8/8/2007	09:36p
H2_18.vel	255,591	8/8/2007	09:36p
pillarStress.fis	1,005	8/8/2007	09:36p
plot.dat	1,345	8/8/2007	09:36p
plotfos.dat	6,968	8/8/2007	09:36p
plotplas.dat	413	8/8/2007	09:36p
print.dat	1,044	8/8/2007	09:36p
properties.fis	3,147	8/8/2007	09:36p
reset.fis	500	8/8/2007	09:36p
shake.dat	1,404	8/8/2007	09:36p
states.dat	1,767	8/8/2007	09:36p
States.fis	961	8/8/2007	09:36p
times.fis	1,102	8/8/2007	09:36p
up_18.Vel	195,676	8/8/2007	09:36p

21 File(s) 829,622 bytes

Directory of O:\RUD\GCNEDLA-2007\Data files_Itasca\3DEC_Data_files\1_Access-Turnout\NonLitho\cat_5

BLOCK.FIN	11,207	8/8/2007	09:35p
CONTACT.FIN	6,231	8/8/2007	09:35p
driver.dat	4,517	8/8/2007	09:35p
edgelength.fis	41,297	8/8/2007	09:35p
fixt.fis	720	8/8/2007	09:35p
functions.fis	27,046	8/8/2007	09:35p
geometry.fis	12,091	8/8/2007	09:35p
h1_18.vel	255,590	8/8/2007	09:36p
H2_18.vel	255,591	8/8/2007	09:36p
pillarStress.fis	1,005	8/8/2007	09:36p
plot.dat	1,345	8/8/2007	09:36p
plotfos.dat	6,968	8/8/2007	09:36p
plotplas.dat	413	8/8/2007	09:36p
print.dat	1,044	8/8/2007	09:36p
properties.fis	3,147	8/8/2007	09:36p
reset.fis	500	8/8/2007	09:36p
shake.dat	1,404	8/8/2007	09:36p
states.dat	1,767	8/8/2007	09:36p
States.fis	961	8/8/2007	09:36p
times.fis	1,102	8/8/2007	09:36p
up_18.Vel	195,676	8/8/2007	09:36p

21 File(s) 829,622 bytes

Directory of O:\RUD\GCNEDLA-2007\Data files_Itasca\3DEC_Data_files\2_Exhaust-Emp.Drift\Litho(B)\cat_1

BLOCK.FIN	11,207	8/8/2007	09:26p
CABLE.FIN	3,326	8/8/2007	09:26p
CONTACT.FIN	6,231	8/8/2007	09:26p
dispver1.pcx	250,354	8/8/2007	09:27p
driver.dat	3,750	8/8/2007	09:26p
edgelength.fis	41,297	8/8/2007	09:27p
EQ_B_FOS_ver1.pcx	378,926	8/8/2007	09:27p
EQ_B_hist.pcx	165,560	8/8/2007	09:27p
EQ_B_plas_ver1.pcx	104,102	8/8/2007	09:27p
EQ_plas_HOR_B.pcx	154,759	8/8/2007	09:27p
fixt.fis	720	8/8/2007	09:27p
FOS_1yr.pcx	417,511	8/8/2007	09:27p
FOS_50yr.pcx	408,555	8/8/2007	09:27p
fos1_insitu.pcx	452,070	8/8/2007	09:27p
functions.fis	27,046	8/8/2007	09:27p
geometry.fis	12,292	8/8/2007	09:27p
h1_18.vel	255,590	8/8/2007	09:27p
H2_18.vel	255,591	8/8/2007	09:27p
inter.fis	4,745	8/8/2007	09:27p
LINER.FIN	6,007	8/8/2007	09:27p
names.fis	1,002	8/8/2007	09:27p
pillarStress.fis	1,005	8/8/2007	09:27p
plas_50yr.pcx	114,975	8/8/2007	09:27p
plashor.pcx	164,714	8/8/2007	09:27p
plasver1.pcx	108,219	8/8/2007	09:27p
plot.dat	1,345	8/8/2007	09:27p
plotplas.dat	413	8/8/2007	09:27p
princver1.pcx	402,407	8/8/2007	09:27p
print.dat	1,044	8/8/2007	09:27p
properties.fis	3,147	8/8/2007	09:27p
reset.fis	500	8/8/2007	09:27p
shake.dat	1,373	8/8/2007	09:27p
states.dat	1,767	8/8/2007	09:27p
States.fis	961	8/8/2007	09:27p
support.fis	29,694	8/8/2007	09:27p
temp_B.xls	36,864	8/8/2007	09:27p
temperature_1.dat	33,310	8/8/2007	09:27p
temperature_10.dat	33,310	8/8/2007	09:27p
temperature_2.dat	33,310	8/8/2007	09:27p
temperature_20.dat	33,310	8/8/2007	09:27p
temperature_3.dat	33,310	8/8/2007	09:27p
temperature_30.dat	33,310	8/8/2007	09:27p
temperature_5.dat	33,310	8/8/2007	09:27p
temperature_50.dat	33,310	8/8/2007	09:27p

temperatures.fis	806	8/8/2007	09:27p
times.fis	1,102	8/8/2007	09:27p
up_18.Vel	195,676	8/8/2007	09:27p

47 File(s) 4,293,133 bytes

Directory of O:\RUD\GCNEDLA-2007\Data files_Itasca\3DEC_Data_files\2_Exhaust-Emp.Drift\Litho(B)\cat_1_10K_EQ

BLOCK.FIN	11,207	8/8/2007	09:27p
CABLE.FIN	3,326	8/8/2007	09:27p
CONTACT.FIN	6,231	8/8/2007	09:27p
driver.dat	3,750	8/8/2007	09:27p
edgelength.fis	41,297	8/8/2007	09:27p
fixt.fis	720	8/8/2007	09:27p
functions.fis	27,046	8/8/2007	09:27p
geometry.fis	12,292	8/8/2007	09:27p
h1_19.vel	368,997	8/8/2007	09:28p
h2_19.vel	369,484	8/8/2007	09:28p
inter.fis	4,745	8/8/2007	09:28p
LINER.FIN	6,007	8/8/2007	09:28p
names.fis	1,002	8/8/2007	09:28p
pillarStress.fis	1,005	8/8/2007	09:28p
plot.dat	1,345	8/8/2007	09:28p
plotplas.dat	413	8/8/2007	09:28p
print.dat	1,044	8/8/2007	09:28p
properties.fis	3,147	8/8/2007	09:28p
reset.fis	500	8/8/2007	09:28p
shake.dat	1,373	8/8/2007	09:28p
states.dat	1,767	8/8/2007	09:28p
States.fis	961	8/8/2007	09:28p
support.fis	29,694	8/8/2007	09:28p
temperature_1.dat	33,310	8/8/2007	09:28p
temperature_10.dat	33,310	8/8/2007	09:28p
temperature_2.dat	33,310	8/8/2007	09:28p
temperature_20.dat	33,310	8/8/2007	09:28p
temperature_3.dat	33,310	8/8/2007	09:28p
temperature_30.dat	33,310	8/8/2007	09:28p
temperature_5.dat	33,310	8/8/2007	09:28p
temperature_50.dat	33,310	8/8/2007	09:28p
temperatures.fis	806	8/8/2007	09:28p
times.fis	1,102	8/8/2007	09:28p
Up_19.vel	368,522	8/8/2007	09:28p

34 File(s) 1,534,263 bytes

Directory of O:\RUD\GCNEDLA-2007\Data files_Itasca\3DEC_Data_files\2_Exhaust-Emp.Drift\Litho(B)\cat_1_supported

BLOCK.FIN	11,207	8/8/2007	09:28p
Cab_insitu_exhaust_36.pcx	137,768	8/8/2007	09:28p
Cab_insitu_exhaust_37.pcx	99,430	8/8/2007	09:28p
Cab_insitu_exhaust_38.pcx	148,931	8/8/2007	09:28p
Cab_insitu_exhaust_39.pcx	187,416	8/8/2007	09:28p
Cab_insitu_exhaust_40.pcx	142,521	8/8/2007	09:28p
Cab_ther_41.pcx	153,187	8/8/2007	09:28p
Cab_ther_42.pcx	152,676	8/8/2007	09:28p
Cab_ther_43.pcx	145,734	8/8/2007	09:28p
CABLE.FIN	3,326	8/8/2007	09:28p
CONTACT.FIN	6,231	8/8/2007	09:28p
driver.dat	7,198	8/8/2007	09:28p
edgelength.fis	41,297	8/8/2007	09:28p
fixt.fis	720	8/8/2007	09:28p
functions.fis	27,046	8/8/2007	09:28p
geometry.fis	12,292	8/8/2007	09:28p
h1_18.vel	255,590	8/8/2007	09:28p
H2_18.vel	255,591	8/8/2007	09:28p
inter.fis	4,745	8/8/2007	09:28p
LINER.FIN	6,007	8/8/2007	09:28p
names.fis	1,002	8/8/2007	09:28p
pillarStress.fis	1,005	8/8/2007	09:28p
plot.dat	1,345	8/8/2007	09:28p
plotplas.dat	413	8/8/2007	09:28p
print.dat	1,044	8/8/2007	09:28p
properties.fis	3,147	8/8/2007	09:28p
reset.fis	500	8/8/2007	09:28p
shake.dat	1,373	8/8/2007	09:28p
Shortcut to 3decw.exe.lnk	742	8/8/2007	09:28p
states.dat	1,767	8/8/2007	09:28p
States.fis	961	8/8/2007	09:28p
support.fis	29,694	8/8/2007	09:28p
temperature_1.dat	33,310	8/8/2007	09:28p
temperature_10.dat	33,310	8/8/2007	09:28p
temperature_2.dat	33,310	8/8/2007	09:28p
temperature_20.dat	33,310	8/8/2007	09:28p
temperature_3.dat	33,310	8/8/2007	09:28p
temperature_30.dat	33,310	8/8/2007	09:28p
temperature_5.dat	33,310	8/8/2007	09:28p
temperature_50.dat	33,310	8/8/2007	09:28p
temperatures.fis	806	8/8/2007	09:28p
times.fis	1,102	8/8/2007	09:28p
up_18.Vel	195,676	8/8/2007	09:28p

43 File(s) 2,305,970 bytes

Directory of O:\RUD\GCNEDLA-2007\Data files_Itasca\3DEC_Data_files\2_Exhaust-Emp.Drift\Litho(B)\cat_3

BLOCK.FIN	11,207	8/8/2007	09:28p
CABLE.FIN	3,326	8/8/2007	09:28p
CONTACT.FIN	6,231	8/8/2007	09:28p
driver.dat	3,750	8/8/2007	09:28p
edgelength.fis	41,297	8/8/2007	09:29p
fixt.fis	720	8/8/2007	09:29p
functions.fis	27,046	8/8/2007	09:29p
geometry.fis	12,292	8/8/2007	09:29p
h1_18.vel	255,590	8/8/2007	09:29p
H2_18.vel	255,591	8/8/2007	09:29p
inter.fis	4,745	8/8/2007	09:29p
LINER.FIN	6,007	8/8/2007	09:29p
names.fis	1,002	8/8/2007	09:29p
pillarStress.fis	1,005	8/8/2007	09:29p
plot.dat	1,345	8/8/2007	09:29p
plotplas.dat	413	8/8/2007	09:29p
print.dat	1,044	8/8/2007	09:29p
properties.fis	3,147	8/8/2007	09:29p
reset.fis	500	8/8/2007	09:29p
shake.dat	1,373	8/8/2007	09:29p
states.dat	1,767	8/8/2007	09:29p
States.fis	961	8/8/2007	09:29p
support.fis	29,694	8/8/2007	09:29p
temperature_1.dat	33,310	8/8/2007	09:29p
temperature_10.dat	33,310	8/8/2007	09:29p
temperature_2.dat	33,310	8/8/2007	09:29p
temperature_20.dat	33,310	8/8/2007	09:29p
temperature_3.dat	33,310	8/8/2007	09:29p
temperature_30.dat	33,310	8/8/2007	09:29p
temperature_5.dat	33,310	8/8/2007	09:29p
temperature_50.dat	33,310	8/8/2007	09:29p
temperatures.fis	806	8/8/2007	09:29p
times.fis	1,102	8/8/2007	09:29p
up_18.Vel	195,676	8/8/2007	09:29p

34 File(s) 1,134,117 bytes

Directory of O:\RUD\GCNEDLA-2007\Data files_Itasca\3DEC_Data_files\2_Exhaust-Emp.Drift\Litho(B)\cat_5

BLOCK.FIN	11,207	8/8/2007	09:29p
CABLE.FIN	3,326	8/8/2007	09:29p
CONTACT.FIN	6,231	8/8/2007	09:29p
driver.dat	3,750	8/8/2007	09:29p
edgelength.fis	41,297	8/8/2007	09:29p
fixt.fis	720	8/8/2007	09:29p
functions.fis	27,046	8/8/2007	09:29p
geometry.fis	12,292	8/8/2007	09:29p
h1_18.vel	255,590	8/8/2007	09:29p

H2_18.vel	255,591	8/8/2007	09:29p
inter.fis	4,745	8/8/2007	09:29p
LINER.FIN	6,007	8/8/2007	09:29p
names.fis	1,002	8/8/2007	09:29p
pillarStress.fis	1,005	8/8/2007	09:29p
plot.dat	1,345	8/8/2007	09:29p
plotplas.dat	413	8/8/2007	09:29p
print.dat	1,044	8/8/2007	09:29p
properties.fis	3,147	8/8/2007	09:29p
reset.fis	500	8/8/2007	09:29p
shake.dat	1,373	8/8/2007	09:29p
states.dat	1,767	8/8/2007	09:29p
States.fis	961	8/8/2007	09:29p
support.fis	29,694	8/8/2007	09:29p
temperature_1.dat	33,310	8/8/2007	09:29p
temperature_10.dat	33,310	8/8/2007	09:29p
temperature_2.dat	33,310	8/8/2007	09:29p
temperature_20.dat	33,310	8/8/2007	09:29p
temperature_3.dat	33,310	8/8/2007	09:29p
temperature_30.dat	33,310	8/8/2007	09:29p
temperature_5.dat	33,310	8/8/2007	09:29p
temperature_50.dat	33,310	8/8/2007	09:29p
temperatures.fis	806	8/8/2007	09:29p
times.fis	1,102	8/8/2007	09:29p
up_18.Vel	195,676	8/8/2007	09:29p

34 File(s) 1,134,117 bytes

Directory of O:\RUD\GCNEDLA-2007\Data files_Itasca\3DEC_Data_files\3_Pc_Drift(intersectionOD-EM)\Litho\cat_1

BLOCK.FIN	11,207	8/8/2007	09:30p
CONTACT.FIN	6,231	8/8/2007	09:30p
driver.dat	3,190	8/8/2007	09:30p
edgelength.fis	41,297	8/8/2007	09:30p
fixt.fis	720	8/8/2007	09:30p
functions.fis	27,318	8/8/2007	09:31p
geometry.fis	12,091	8/8/2007	09:31p
h1_18.vel	255,590	8/8/2007	09:31p
H2_18.vel	255,591	8/8/2007	09:31p
inter.fis	4,745	8/8/2007	09:31p
pillarStress.fis	1,005	8/8/2007	09:31p
plot.dat	1,345	8/8/2007	09:31p
plotplas.dat	413	8/8/2007	09:31p
print.dat	1,044	8/8/2007	09:31p
properties.fis	3,147	8/8/2007	09:31p
reset.fis	500	8/8/2007	09:31p
shake.dat	1,386	8/8/2007	09:31p

states.dat	1,767	8/8/2007	09:31p
States.fis	961	8/8/2007	09:31p
temperature_1.dat	33,310	8/8/2007	09:31p
temperature_10.dat	33,310	8/8/2007	09:31p
temperature_2.dat	33,310	8/8/2007	09:31p
temperature_20.dat	33,310	8/8/2007	09:31p
temperature_3.dat	33,310	8/8/2007	09:31p
temperature_30.dat	33,310	8/8/2007	09:31p
temperature_5.dat	33,310	8/8/2007	09:31p
temperature_50.dat	33,310	8/8/2007	09:31p
temperatures.fis	502	8/8/2007	09:31p
times.fis	1,102	8/8/2007	09:31p
up_18.Vel	195,676	8/8/2007	09:31p

30 File(s) 1,093,308 bytes

Directory of O:\RUD\GCNEDLA-2007\Data files_Itasca\3DEC_Data_files\3_Pc_Drift(intersectionOD-EM)\Litho\cat_1_supported

BLOCK.FIN	11,207	8/8/2007	09:31p
CABLE.FIN	3,326	8/8/2007	09:31p
CONTACT.FIN	6,231	8/8/2007	09:31p
driver.dat	5,665	8/8/2007	09:31p
edgelength.fis	41,297	8/8/2007	09:31p
fixt.fis	720	8/8/2007	09:31p
functions.fis	27,318	8/8/2007	09:31p
geometry.fis	12,091	8/8/2007	09:31p
h1_18.vel	255,590	8/8/2007	09:31p
H2_18.vel	255,591	8/8/2007	09:31p
inter.fis	4,745	8/8/2007	09:31p
LINER.FIN	6,007	8/8/2007	09:31p
pillarStress.fis	1,005	8/8/2007	09:31p
plot.dat	1,345	8/8/2007	09:31p
plotplas.dat	413	8/8/2007	09:31p
print.dat	1,044	8/8/2007	09:31p
properties.fis	3,147	8/8/2007	09:31p
reset.fis	500	8/8/2007	09:31p
shake.dat	1,386	8/8/2007	09:31p
states.dat	1,767	8/8/2007	09:31p
States.fis	961	8/8/2007	09:31p
support.fis	40,693	8/8/2007	09:31p
temperature_1.dat	33,310	8/8/2007	09:31p
temperature_10.dat	33,310	8/8/2007	09:31p
temperature_2.dat	33,310	8/8/2007	09:31p
temperature_20.dat	33,310	8/8/2007	09:31p
temperature_3.dat	33,310	8/8/2007	09:31p
temperature_30.dat	33,310	8/8/2007	09:31p
temperature_5.dat	33,310	8/8/2007	09:31p

temperature_50.dat	33,310	8/8/2007	09:31p
temperatures.fis	502	8/8/2007	09:31p
times.fis	1,102	8/8/2007	09:31p
up_18.Vel	195,676	8/8/2007	09:31p

33 File(s) 1,145,809 bytes

Directory of O:\RUD\GCNEDLA-2007\Data files_Itasca\3DEC_Data_files\3_Pc_Drift(intersectionOD-EM)\Litho\cat_3

BLOCK.FIN	11,207	8/8/2007	09:31p
CONTACT.FIN	6,231	8/8/2007	09:31p
driver.dat	3,188	8/8/2007	09:31p
edgelength.fis	41,297	8/8/2007	09:31p
fixt.fis	720	8/8/2007	09:31p
functions.fis	27,318	8/8/2007	09:31p
geometry.fis	12,091	8/8/2007	09:33p
h1_18.vel	255,590	8/8/2007	09:33p
H2_18.vel	114,688	8/8/2007	09:33p
inter.fis	4,745	8/8/2007	09:34p
pillarStress.fis	1,005	8/8/2007	09:34p
plot.dat	1,345	8/8/2007	09:34p
plotplas.dat	413	8/8/2007	09:34p
print.dat	1,044	8/8/2007	09:34p
properties.fis	3,147	8/8/2007	09:34p
reset.fis	500	8/8/2007	09:34p
shake.dat	1,386	8/8/2007	09:34p
states.dat	1,767	8/8/2007	09:34p
States.fis	961	8/8/2007	09:34p
temperature_1.dat	33,310	8/8/2007	09:34p
temperature_10.dat	33,310	8/8/2007	09:34p
temperature_2.dat	33,310	8/8/2007	09:34p
temperature_20.dat	33,310	8/8/2007	09:34p
temperature_3.dat	33,310	8/8/2007	09:34p
temperature_30.dat	33,310	8/8/2007	09:34p
temperature_5.dat	33,310	8/8/2007	09:34p
temperature_50.dat	33,310	8/8/2007	09:34p
temperatures.fis	502	8/8/2007	09:34p
times.fis	1,102	8/8/2007	09:34p
up_18.Vel	195,676	8/8/2007	09:34p

30 File(s) 952,403 bytes

Directory of O:\RUD\GCNEDLA-2007\Data files_Itasca\FLACDataFiles\Launch_Chamber\Litho\cat_1(no_ther)

degradation.dat	1,022	8/8/2007	07:29p
driver.dat	1,017	8/8/2007	07:29p
extract.fis	17,296	8/8/2007	07:29p
functions.fis	18,343	8/8/2007	07:29p

inter.fis	2,767	8/8/2007	07:29p
LaunchCham_Lith_cat1_eq.dat	209	8/8/2007	07:29p
plot.dat	731	8/8/2007	07:29p
print.dat	902	8/8/2007	07:29p
properties.fis	4,110	8/8/2007	07:29p
shake.dat	507	8/8/2007	07:29p
temperatures.fis	200	8/8/2007	07:29p
TIMES.FIS	1,102	8/8/2007	07:29p
tunnel.dat	1,898	8/8/2007	07:29p
vel_hori_5e-4.tab	203,437	8/8/2007	07:29p
vel_vert_5e-4.tab	195,677	8/8/2007	07:29p

15 File(s) 449,218 bytes

Directory of O:\RUD\GCNEDLA-2007\Data files_Itasca\FLACDataFiles\Launch_Chamber\Litho\cat_1_supported(no_ther)

degradation.dat	1,115	8/8/2007	07:29p
driver.dat	1,522	8/8/2007	07:29p
extract.fis	17,296	8/8/2007	07:29p
functions.fis	23,721	8/8/2007	07:29p
inter.fis	2,767	8/8/2007	07:29p
LaunchCham_Lith_cat1_S_eq.dat	209	8/8/2007	07:29p
plot.dat	731	8/8/2007	07:29p
print.dat	902	8/8/2007	07:29p
properties.fis	4,110	8/8/2007	07:29p
shake.dat	535	8/8/2007	07:29p
Str.fin	9,668	8/8/2007	07:29p
support.fis	5,068	8/8/2007	07:29p
temperatures.fis	200	8/8/2007	07:29p
TIMES.FIS	1,102	8/8/2007	07:29p
tunnel.dat	1,898	8/8/2007	07:29p
vel_hori_5e-4.tab	203,437	8/8/2007	07:29p
vel_vert_5e-4.tab	195,677	8/8/2007	07:29p

15 File(s) 469,958 bytes

Directory of O:\RUD\GCNEDLA-2007\Data files_Itasca\FLACDataFiles\Launch_Chamber\Litho\cat_3(no_ther)

degradation.dat	1,022	8/8/2007	07:29p
driver.dat	1,017	8/8/2007	07:29p
extract.fis	17,296	8/8/2007	07:29p
functions.fis	18,343	8/8/2007	07:29p
inter.fis	2,767	8/8/2007	07:29p
LaunchCham_Lith_cat3_eq.dat	209	8/8/2007	07:29p
plot.dat	731	8/8/2007	07:29p
print.dat	902	8/8/2007	07:29p
properties.fis	4,110	8/8/2007	07:30p
shake.dat	507	8/8/2007	07:30p

temperatures.fis	200	8/8/2007	07:30p
TIMES.FIS	1,102	8/8/2007	07:30p
tunnel.dat	1,898	8/8/2007	07:30p
vel_hori_5e-4.tab	203,437	8/8/2007	07:30p
vel_vert_5e-4.tab	195,677	8/8/2007	07:30p

15 File(s) 449,218 bytes

Directory of O:\RUD\GCNEDLA-2007\Data files_Itasca\FLACDataFiles\Launch_Chamber\NonLitho\cat_1(no_ther)

degradation.dat	1,022	8/8/2007	07:30p
driver.dat	1,018	8/8/2007	07:30p
extract.fis	17,296	8/8/2007	07:30p
functions.fis	18,343	8/8/2007	07:30p
inter.fis	2,767	8/8/2007	07:30p
LaunchCham_NonLith_cat1_eq.dat	210	8/8/2007	07:30p
plot.dat	731	8/8/2007	07:30p
print.dat	902	8/8/2007	07:30p
properties.fis	4,110	8/8/2007	07:30p
shake.dat	507	8/8/2007	07:30p
temperatures.fis	200	8/8/2007	07:30p
TIMES.FIS	1,102	8/8/2007	07:30p
tunnel.dat	1,898	8/8/2007	07:30p
vel_hori_5e-4.tab	203,437	8/8/2007	07:30p
vel_vert_5e-4.tab	195,677	8/8/2007	07:30p

15 File(s) 449,220 bytes

Directory of O:\RUD\GCNEDLA-2007\Data files_Itasca\FLACDataFiles\Launch_Chamber\NonLitho\cat_1_supported(no_ther)

degradation.dat	1,115	8/8/2007	07:30p
driver.dat	1,523	8/8/2007	07:30p
extract.fis	17,296	8/8/2007	07:30p
functions.fis	23,721	8/8/2007	07:30p
inter.fis	2,767	8/8/2007	07:30p
LaunchCham_NonLith_cat1_S_eq.dat	210	8/8/2007	07:30p
plot.dat	731	8/8/2007	07:30p
print.dat	902	8/8/2007	07:30p
properties.fis	4,110	8/8/2007	07:30p
shake.dat	535	8/8/2007	07:30p
Str.fin	9,668	8/8/2007	07:30p
support.fis	5,068	8/8/2007	07:30p
temperatures.fis	200	8/8/2007	07:30p
TIMES.FIS	1,102	8/8/2007	07:30p
tunnel.dat	1,898	8/8/2007	07:30p
vel_hori_5e-4.tab	203,437	8/8/2007	07:30p
vel_vert_5e-4.tab	195,677	8/8/2007	07:30p

17 File(s) 469,960 bytes

Directory of O:\RUD\GCNEDLA-2007\Data files_Itasca\FLACDataFiles\Launch_Chamber\NonLitho\cat_3(no_ther)

degradation.dat	1,022	8/8/2007	07:30p
driver.dat	1,018	8/8/2007	07:30p
extract.fis	17,296	8/8/2007	07:30p
functions.fis	18,343	8/8/2007	07:30p
inter.fis	2,767	8/8/2007	07:30p
LaunchCham_NonLith_cat3_eq.dat	210	8/8/2007	07:30p
plot.dat	731	8/8/2007	07:30p
print.dat	902	8/8/2007	07:30p
properties.fis	4,110	8/8/2007	07:30p
shake.dat	507	8/8/2007	07:30p
temperatures.fis	200	8/8/2007	07:30p
TIMES.FIS	1,102	8/8/2007	07:30p
tunnel.dat	1,898	8/8/2007	07:30p
vel_hori_5e-4.tab	203,437	8/8/2007	07:30p
vel_vert_5e-4.tab	195,677	8/8/2007	07:30p

15 File(s) 449,220 bytes

Directory of O:\RUD\GCNEDLA-2007\Data files_Itasca\FLACDataFiles\ObservationDrift\Litho\cat_1

degradation.dat	1,474	8/8/2007	07:30p
degradation_standard.dat	1,474	8/8/2007	07:30p
driver.dat	1,949	8/8/2007	07:30p
extract.fis	17,296	8/8/2007	07:30p
functions.fis	23,637	8/8/2007	07:30p
inter.fis	2,767	8/8/2007	07:30p
plot.dat	731	8/8/2007	07:30p
print.dat	902	8/8/2007	07:30p
properties.fis	4,110	8/8/2007	07:30p
shake.dat	536	8/8/2007	07:30p
temperature_1.dat	33,310	8/8/2007	07:30p
temperature_10.dat	33,310	8/8/2007	07:30p
temperature_2.dat	33,310	8/8/2007	07:30p
temperature_20.dat	33,310	8/8/2007	07:30p
temperature_3.dat	33,310	8/8/2007	07:30p
temperature_30.dat	33,310	8/8/2007	07:30p
temperature_5.dat	33,310	8/8/2007	07:30p
temperature_50.dat	33,310	8/8/2007	07:30p
temperatures.fis	200	8/8/2007	07:30p
TIMES.FIS	1,102	8/8/2007	07:30p
tunnel.dat	1,901	8/8/2007	07:30p
tunnel_standard.dat	1,896	8/8/2007	07:30p
vel_hori_5e-4.tab	203,437	8/8/2007	07:30p

vel_vert_5e-4.tab	195,677	8/8/2007	07:30p

24 File(s) 725,536 bytes

Directory of O:\RUD\GCNEDLA-2007\Data files_Itasca\FLACDataFiles\ObservationDrift\Litho\cat_1_supported

degradation.dat	1,472	8/8/2007	07:31p
driver.dat	2,494	8/8/2007	07:31p
extract.fis	17,296	8/8/2007	07:31p
functions.fis	23,968	8/8/2007	07:31p
inter.fis	2,767	8/8/2007	07:31p
plot.dat	731	8/8/2007	07:31p
print.dat	902	8/8/2007	07:31p
properties.fis	4,110	8/8/2007	07:31p
shake.dat	535	8/8/2007	07:31p
Str.fin	9,668	8/8/2007	07:31p
support.fis	5,053	8/8/2007	07:31p
temperature_1.dat	33,310	8/8/2007	07:31p
temperature_10.dat	33,310	8/8/2007	07:31p
temperature_2.dat	33,310	8/8/2007	07:31p
temperature_20.dat	33,310	8/8/2007	07:31p
temperature_3.dat	33,310	8/8/2007	07:31p
temperature_30.dat	33,310	8/8/2007	07:31p
temperature_5.dat	33,310	8/8/2007	07:31p
temperature_50.dat	33,310	8/8/2007	07:31p
temperatures.fis	200	8/8/2007	07:31p
TIMES.FIS	1,102	8/8/2007	07:31p
tunnel.dat	1,898	8/8/2007	07:31p
vel_hori_5e-4.tab	203,437	8/8/2007	07:31p
vel_vert_5e-4.tab	195,677	8/8/2007	07:31p

24 File(s) 737,790 bytes

Directory of O:\RUD\GCNEDLA-2007\Data files_Itasca\FLACDataFiles\ObservationDrift\Litho\cat_1_supported

degradation.dat	1,474	8/8/2007	07:31p
driver.dat	1,949	8/8/2007	07:31p
extract.fis	17,296	8/8/2007	07:31p
functions.fis	23,637	8/8/2007	07:31p
inter.fis	2,767	8/8/2007	07:31p
plot.dat	731	8/8/2007	07:31p
print.dat	902	8/8/2007	07:31p
properties.fis	4,110	8/8/2007	07:31p
shake.dat	536	8/8/2007	07:31p
temperature_1.dat	33,310	8/8/2007	07:31p
temperature_10.dat	33,310	8/8/2007	07:31p
temperature_2.dat	33,310	8/8/2007	07:31p
temperature_20.dat	33,310	8/8/2007	07:31p
temperature_3.dat	33,310	8/8/2007	07:31p

temperature_30.dat	33,310	8/8/2007	07:31p
temperature_5.dat	33,310	8/8/2007	07:31p
temperature_50.dat	33,310	8/8/2007	07:31p
temperatures.fis	200	8/8/2007	07:31p
TIMES.FIS	1,102	8/8/2007	07:31p
tunnel.dat	1,898	8/8/2007	07:31p
vel_hori_5e-4.tab	203,437	8/8/2007	07:31p
vel_vert_5e-4.tab	195,677	8/8/2007	07:31p

22 File(s) 722,196 bytes

Directory of O:\RUD\GCNEDLA-2007\Data files_Itasca\FLACDataFiles\ObservationDrift\NonLitho\cat_1

degradation.dat	1,474	8/8/2007	07:31p
driver.dat	1,953	8/8/2007	07:31p
extract.fis	17,296	8/8/2007	07:31p
functions.fis	23,637	8/8/2007	07:31p
inter.fis	2,767	8/8/2007	07:31p
plot.dat	731	8/8/2007	07:31p
print.dat	902	8/8/2007	07:31p
properties.fis	4,110	8/8/2007	07:31p
shake.dat	536	8/8/2007	07:31p
Shortcut to flacw_sp.exe.lnk	924	8/8/2007	07:31p
temperature_1.dat	33,310	8/8/2007	07:31p
temperature_10.dat	33,310	8/8/2007	07:31p
temperature_2.dat	33,310	8/8/2007	07:31p
temperature_20.dat	33,310	8/8/2007	07:31p
temperature_3.dat	33,310	8/8/2007	07:31p
temperature_30.dat	33,310	8/8/2007	07:31p
temperature_5.dat	33,310	8/8/2007	07:31p
temperature_50.dat	33,310	8/8/2007	07:31p
temperatures.fis	200	8/8/2007	07:31p
TIMES.FIS	1,102	8/8/2007	07:31p
tunnel.dat	1,898	8/8/2007	07:31p
vel_hori_5e-4.tab	203,437	8/8/2007	07:31p
vel_vert_5e-4.tab	195,677	8/8/2007	07:31p

23 File(s) 723,124 bytes

Directory of O:\RUD\GCNEDLA-2007\Data files_Itasca\FLACDataFiles\ObservationDrift\NonLitho\cat_1_supported

degradation.dat	1,472	8/8/2007	07:31p
driver.dat	2,498	8/8/2007	07:31p
extract.fis	17,296	8/8/2007	07:31p
functions.fis	23,968	8/8/2007	07:31p
inter.fis	2,767	8/8/2007	07:31p
plot.dat	731	8/8/2007	07:31p
print.dat	902	8/8/2007	07:31p

properties.fis	4,110	8/8/2007	07:31p
shake.dat	535	8/8/2007	07:31p
Shortcut to flacw_sp.exe.lnk	938	8/8/2007	07:31p
Str.fin	9,668	8/8/2007	07:31p
support.fis	5,053	8/8/2007	07:31p
temperature_1.dat	33,310	8/8/2007	07:31p
temperature_10.dat	33,310	8/8/2007	07:31p
temperature_2.dat	33,310	8/8/2007	07:31p
temperature_20.dat	33,310	8/8/2007	07:32p
temperature_3.dat	33,310	8/8/2007	07:32p
temperature_30.dat	33,310	8/8/2007	07:32p
temperature_5.dat	33,310	8/8/2007	07:32p
temperature_50.dat	33,310	8/8/2007	07:32p
temperatures.fis	200	8/8/2007	07:31p
TIMES.FIS	1,102	8/8/2007	07:32p
tunnel.dat	1,898	8/8/2007	07:32p
vel_hori_5e-4.tab	203,437	8/8/2007	07:32p
vel_vert_5e-4.tab	195,677	8/8/2007	07:32p

25 File(s) 738,732 bytes

Directory of O:\RUD\GCNEDLA-2007\Data files_Itasca\FLACDataFiles\ObservationDrift\NonLitho\cat_3

degradation.dat	1,474	8/8/2007	07:32p
driver.dat	1,953	8/8/2007	07:32p
extract.fis	17,296	8/8/2007	07:32p
functions.fis	23,637	8/8/2007	07:32p
inter.fis	2,767	8/8/2007	07:32p
plot.dat	731	8/8/2007	07:32p
print.dat	902	8/8/2007	07:32p
properties.fis	4,110	8/8/2007	07:32p
shake.dat	536	8/8/2007	07:32p
Shortcut to flacw_sp.exe.lnk	924	8/8/2007	07:32p
temperature_1.dat	33,310	8/8/2007	07:32p
temperature_10.dat	33,310	8/8/2007	07:32p
temperature_2.dat	33,310	8/8/2007	07:32p
temperature_20.dat	33,310	8/8/2007	07:32p
temperature_3.dat	33,310	8/8/2007	07:32p
temperature_30.dat	33,310	8/8/2007	07:32p
temperature_5.dat	33,310	8/8/2007	07:32p
temperature_50.dat	33,310	8/8/2007	07:32p
temperatures.fis	200	8/8/2007	07:32p
TIMES.FIS	1,102	8/8/2007	07:32p
tunnel.dat	1,898	8/8/2007	07:32p
vel_hori_5e-4.tab	203,437	8/8/2007	07:32p
vel_vert_5e-4.tab	195,677	8/8/2007	07:32p

23 File(s) 723,124 bytes

Directory of O:\RUD\GCNEDLA-2007\ExhaustMain\Litho_A\cat_1,3,5

properties.fis	3,823	7/14/2007	02:49p
hiszones_50.fis	1,235	5/15/2007	07:40p
initemp.fis	392	5/15/2007	07:41p
makemovie.fis	3,408	5/15/2007	07:41p
driver.dat	1,849	7/18/2007	04:05p
relaxation.fis	2,152	5/15/2007	07:41p
seismic.dat	451	7/18/2007	03:24p
setup.fis	2,077	5/25/2007	03:20p
shake.fis	2,871	5/15/2007	07:41p
temphis_50.tab	945	5/15/2007	02:13p
thermal_50.dat	1,628	5/15/2007	07:41p
thermoprop.fis	3,679	5/15/2007	03:11p
tunnel.dat	3,024	5/15/2007	07:41p
vel_hori_5e-4.tab	203,437	5/15/2007	07:41p
vel_vert_5e-4.tab	195,677	5/15/2007	07:41p
seismic_50.dat	455	7/24/2007	12:16p
driver_50.dat	1,852	7/24/2007	12:17p

17 File(s) 428,955 bytes

Directory of O:\RUD\GCNEDLA-2007\ExhaustMain\Litho_A\cat_1_G10k

thermal_50.dat	1,628	5/15/2007	07:41p
vel_hori_1e-4.tab	373,597	6/30/2003	10:41a
temphis_50.tab	945	5/15/2007	02:13p
thermoprop.fis	3,679	5/15/2007	03:11p
hiszones_50.fis	1,235	5/15/2007	07:40p
initemp.fis	392	5/15/2007	07:41p
makemovie.fis	3,408	5/15/2007	07:41p
relaxation.fis	2,152	5/15/2007	07:41p
vel_vert_1e-4.tab	373,120	6/30/2003	10:40a
tunnel.dat	3,024	5/15/2007	07:41p
setup.fis	2,077	5/25/2007	03:20p
seismic.dat	389	6/20/2007	01:31p
shake.fis	2,871	6/20/2007	01:34p
properties.fis	3,823	7/14/2007	02:52p
driver.dat	655	7/19/2007	05:53p

15 File(s) 772,995 bytes

Directory of O:\RUD\GCNEDLA-2007\ExhaustMain\Litho_A\cat_1_sup

thermal_50.dat	1,628	5/15/2007	07:41p
boltprop.fis	1,642	5/15/2007	07:41p
hiszones_50.fis	1,235	5/15/2007	07:41p
initemp.fis	392	5/15/2007	07:41p
makemovie.fis	3,408	5/15/2007	07:41p

relaxation.fis	2,152	5/15/2007	07:41p
shake.fis	2,871	5/15/2007	07:41p
thermoprop.fis	3,679	5/15/2007	04:06p
tunnel_b.dat	3,041	5/15/2007	07:41p
vel_hori_5e-4.tab	203,437	5/15/2007	07:41p
vel_vert_5e-4.tab	195,677	5/15/2007	07:41p
driver.dat	645	5/25/2007	02:52p
temphis_50.tab	947	5/25/2007	02:53p
seismic.dat	378	5/25/2007	02:54p
setup.fis	2,077	5/25/2007	03:22p
properties.fis	3,823	7/14/2007	02:52p
bolt.dat	640	7/16/2007	10:22a

17 File(s) 427,672 bytes

Directory of O:\RUD\GCNEDLA-2007\ExhaustMain\Litho_A\k=1.0\cat_1,5

properties.fis	3,823	7/14/2007	02:52p
hiszones_50.fis	1,235	5/15/2007	07:41p
initemp.fis	392	5/15/2007	07:41p
makemovie.fis	3,408	5/15/2007	07:41p
driver.dat	1,225	7/19/2007	01:38p
relaxation.fis	2,152	5/15/2007	07:41p
seismic.dat	783	7/19/2007	01:44p
setup.fis	2,077	5/25/2007	03:23p
shake.fis	2,871	5/15/2007	07:41p
temphis_50.tab	1,023	5/15/2007	07:41p
thermal_50.dat	1,628	5/15/2007	07:41p
thermoprop.fis	3,679	5/15/2007	04:08p
tunnel.dat	3,024	5/15/2007	07:41p
vel_hori_5e-4.tab	203,437	5/15/2007	07:41p
vel_vert_5e-4.tab	195,677	5/15/2007	07:42p

15 File(s) 426,577 bytes

Directory of O:\RUD\GCNEDLA-2007\ExhaustMain\Nonlitho_A\cat_1,3,5

makemovie.fis	3,408	5/15/2007	07:41p
thermoprop.fis	3,679	5/15/2007	04:08p
hiszones_50.fis	1,235	5/15/2007	07:41p
initemp.fis	392	5/15/2007	07:41p
driver.dat	1,821	5/15/2007	04:07p
relaxation.fis	2,152	5/15/2007	07:41p
shake.fis	2,871	5/15/2007	07:41p
temphis_50.tab	1,023	5/15/2007	07:41p
thermal_50.dat	1,628	5/15/2007	07:41p
tunnel.dat	3,024	5/15/2007	07:41p
vel_hori_5e-4.tab	203,437	5/15/2007	07:41p
vel_vert_5e-4.tab	195,677	5/15/2007	07:42p

setup.fis	2,077	5/25/2007	03:23p
properties.fis	3,823	7/14/2007	02:52p
seismic.dat	451	7/19/2007	08:24a
seismic_50.dat	455	7/24/2007	12:27p
driver_50.dat	1,824	7/24/2007	12:28p

17 File(s) 428,977 bytes

Directory of O:\RUD\GCNEDLA-2007\ExhaustMain\Nonlitho_A\cat_1_G10k

properties.fis	3,823	7/14/2007	02:52p
hiszones_50.fis	1,235	5/15/2007	07:40p
initemp.fis	392	5/15/2007	07:41p
makemovie.fis	3,408	5/15/2007	07:41p
driver.dat	655	7/19/2007	06:25p
relaxation.fis	2,152	5/15/2007	07:41p
seismic.dat	389	7/19/2007	06:26p
setup.fis	2,077	5/25/2007	03:20p
shake.fis	2,871	6/20/2007	01:34p
temphis_50.tab	945	5/15/2007	02:13p
thermal_50.dat	1,628	5/15/2007	07:41p
thermoprop.fis	3,679	5/15/2007	03:11p
tunnel.dat	3,024	5/15/2007	07:41p
vel_hori_1e-4.tab	373,597	6/30/2003	10:41a
vel_vert_1e-4.tab	373,120	6/30/2003	10:40a

16 File(s) 772,995 bytes

Directory of O:\RUD\GCNEDLA-2007\ExhaustMain\Nonlitho_A\cat_1_sup

thermal_50.dat	1,628	5/15/2007	07:41p
boltprop.fis	1,642	5/15/2007	07:41p
hiszones_50.fis	1,235	5/15/2007	07:41p
initemp.fis	392	5/15/2007	07:41p
makemovie.fis	3,408	5/15/2007	07:41p
relaxation.fis	2,152	5/15/2007	07:41p
shake.fis	2,871	5/15/2007	07:41p
thermoprop.fis	3,679	5/15/2007	04:06p
tunnel_b.dat	3,041	5/15/2007	07:41p
vel_hori_5e-4.tab	203,437	5/15/2007	07:41p
vel_vert_5e-4.tab	195,677	5/15/2007	07:41p
temphis_50.tab	947	5/25/2007	02:53p
setup.fis	2,077	5/25/2007	03:22p
properties.fis	3,823	7/14/2007	02:52p
bolt.dat	640	7/16/2007	10:22a
driver.dat	645	7/19/2007	07:22p
seismic.dat	378	7/19/2007	07:22p

16 File(s) 427,672 bytes

Directory of O:\RUD\GCNEDLA-2007\Turnout\Litho_A\cat_1,3,5

properties.fis	3,823	7/14/2007	02:52p
hiszones_50.fis	659	3/20/2007	10:08p
makemovie.fis	3,408	5/15/2007	07:38p
driver.dat	1,756	7/18/2007	04:25p
relaxation.fis	2,152	5/15/2007	07:39p
seismic.dat	451	7/18/2007	03:24p
setup.fis	2,087	5/15/2007	07:39p
shake.fis	2,874	5/15/2007	07:39p
tunnel.dat	3,024	5/15/2007	07:39p
vel_hori_5e-4.tab	203,437	5/15/2007	07:39p
vel_vert_5e-4.tab	195,677	5/15/2007	07:39p

11 File(s) 419,348 bytes

Directory of O:\RUD\GCNEDLA-2007\Turnout\Litho_A\cat_1_sup

shake.fis	2,872	5/15/2007	07:39p
hiszones_50.fis	659	3/20/2007	10:08p
makemovie.fis	3,408	5/15/2007	07:39p
relaxation.fis	2,152	5/15/2007	07:39p
setup.fis	2,087	5/15/2007	07:39p
boltprop.fis	1,592	3/20/2007	10:08p
tunnel_b.dat	3,041	5/15/2007	07:39p
vel_hori_5e-4.tab	203,437	5/15/2007	07:39p
vel_vert_5e-4.tab	195,677	5/15/2007	07:39p
seismic.dat	228	5/25/2007	01:58p
bolt.dat	630	6/22/2007	04:32p
properties.fis	3,823	7/14/2007	02:52p
driver.dat	623	7/18/2007	04:28p

13 File(s) 420,229 bytes

Directory of O:\RUD\GCNEDLA-2007\Turnout\Nonlitho_A\cat_1,3,5

vel_hori_5e-4.tab	203,437	5/15/2007	07:39p
makemovie.fis	3,408	5/15/2007	07:38p
relaxation.fis	2,152	5/15/2007	07:39p
setup.fis	2,087	5/15/2007	07:39p
shake.fis	2,874	5/15/2007	07:39p
tunnel.dat	3,024	5/15/2007	07:39p
hiszones_50.fis	659	3/20/2007	10:08p
vel_vert_5e-4.tab	195,677	5/15/2007	07:39p
properties.fis	3,823	7/14/2007	02:52p
driver.dat	1,756	7/19/2007	08:36a
seismic.dat	451	7/19/2007	08:37a

11 File(s) 419,348 bytes

Directory of O:\RUD\GCNEDLA-2007\Turnout\Nonlitho_A\cat_1_sup

properties.fis	3,823	7/14/2007	02:52p
boltprop.fis	1,592	3/20/2007	10:08p
driver.dat	623	7/19/2007	08:40a
hiszones_50.fis	659	3/20/2007	10:08p
makemovie.fis	3,408	5/15/2007	07:39p
bolt.dat	630	6/22/2007	04:32p
relaxation.fis	2,152	5/15/2007	07:39p
seismic.dat	228	6/22/2007	05:30p
setup.fis	2,087	5/15/2007	07:39p
shake.fis	2,872	5/15/2007	07:39p
tunnel_b.dat	3,041	5/15/2007	07:39p
vel_hori_5e-4.tab	203,437	5/15/2007	07:39p
vel_vert_5e-4.tab	195,677	5/15/2007	07:39p

11 File(s) 420,229 bytes

Volume in drive O is New Volume
Volume Serial Number is 683C-0946

Directory of O:\RUD\GCNEDLA-2007\4_North_Portal\final_run

09/27/2007	08:17a	<DIR> .
09/15/2007	02:43p	<DIR> ..
09/11/2007	05:10p	879 [0]_3DEC_Slope_[MASTER].dat
09/11/2007	05:10p	4,865 [1]_3DEC_Slope_[Block_Def].dat
09/11/2007	05:10p	5,656 [2]_3DEC_Slope_[Block_Zon].dat
09/27/2007	08:09a	6,177 [3]_3DEC_Slope_[Run_Consol].dat
09/11/2007	05:10p	17,368 [4]_3DEC_Slope_[Run_Excav].dat
09/11/2007	05:10p	10,858 [5]_3DEC_Slope_[Run_Seismic].dat
09/11/2007	05:10p	11,207 BLOCK.FIN
09/11/2007	05:10p	0 Fish_functions_[1].fis
09/11/2007	05:10p	0 Fish_functions_[2].fis
09/11/2007	05:10p	10,703 Fish_functions_[3].fis
09/11/2007	05:10p	0 Fish_functions_[4].fis
09/11/2007	05:10p	1,327 Fish_functions_[5].fis
09/11/2007	05:10p	27,318 functions.fis
09/11/2007	05:10p	255,590 H1_18.vel
09/11/2007	05:10p	255,591 H2_18.vel
09/11/2007	05:10p	24,426 New_topo_[3DEC_file].dat
09/11/2007	05:10p	3,147 properties.fis
09/11/2007	05:10p	195,676 UP_18.Vel
09/27/2007	08:17a	134 file_list_North_Portal

19 File(s) 830,922 bytes
2 Dir(s) 62,044,430,336 bytes free

Volume in drive O is New Volume
Volume Serial Number is 683C-0946

Directory of O:\RUD\GCNEDLA-2007\5_Pillar_btwn_AccessShaft_EM\Pillar

```
09/27/2007  08:22a    <DIR>          .
09/27/2007  08:21a    <DIR>          ..
09/26/2007  01:33a            11,207 BLOCK.FIN
09/26/2007  01:32a             6,231 CONTACT.FIN
09/26/2007  01:33a             4,283 driver_ther_eq.dat
09/26/2007  01:33a            41,297 edgelength.fis
09/26/2007  01:33a               720 fixt.fis
09/26/2007  01:33a            27,046 functions.fis
09/26/2007  01:33a            12,091 geometry.fis
09/26/2007  01:33a           255,590 h1_18.vel
09/26/2007  01:33a           255,591 H2_18.vel
09/26/2007  01:32a             4,840 inter.fis
09/26/2007  01:33a             1,005 pillarStress.fis
09/26/2007  01:33a               413 plotplas.dat
09/26/2007  01:33a             1,044 print.dat
09/26/2007  01:33a             3,147 properties.fis
09/26/2007  01:33a                48 rerun.dat
09/26/2007  01:33a               500 reset.fis
09/26/2007  01:33a             1,767 states.dat
09/26/2007  01:32a               961 States.fis
09/26/2007  01:33a            33,310 temperature_1.dat
09/26/2007  01:33a            33,310 temperature_10.dat
09/26/2007  01:33a            33,310 temperature_2.dat
09/26/2007  01:33a            33,310 temperature_20.dat
09/26/2007  01:33a            33,310 temperature_3.dat
09/26/2007  01:33a            33,310 temperature_30.dat
09/26/2007  01:33a            33,310 temperature_5.dat
09/26/2007  01:33a            33,310 temperature_50.dat
09/26/2007  01:33a               806 temperatures.fis
09/26/2007  01:33a             1,102 times.fis
09/26/2007  01:33a           195,676 UP_18.Vel
09/27/2007  08:22a               145 file_list_Pillar
              30 File(s)      1,091,990 bytes
               2 Dir(s)  62,043,688,960 bytes free
```